University of Windsor
Scholarship at UWindsor

Electronic Theses and Dissertations

2015

New Materials and Methods for the Fabrication of Large-Area Stretchable Electronics

Heather Lynn Filiatrault,
University of Windsor

Follow this and additional works at: http://scholar.uwindsor.ca/etd

Recommended Citation
Filiatrault,, Heather Lynn, "New Materials and Methods for the Fabrication of Large-Area Stretchable Electronics" (2015). *Electronic Theses and Dissertations.* Paper 5622.

This online database contains the full-text of PhD dissertations and Masters' theses of University of Windsor students from 1954 forward. These documents are made available for personal study and research purposes only, in accordance with the Canadian Copyright Act and the Creative Commons license—CC BY-NC-ND (Attribution, Non-Commercial, No Derivative Works). Under this license, works must always be attributed to the copyright holder (original author), cannot be used for any commercial purposes, and may not be altered. Any other use would require the permission of the copyright holder. Students may inquire about withdrawing their dissertation and/or thesis from this database. For additional inquiries, please contact the repository administrator via email (scholarship@uwindsor.ca) or by telephone at 519-253-3000ext. 3208.

New Materials and Methods for the Fabrication of Large-Area Stretchable Electronics

By

Heather Lynn Filiatrault

A Dissertation
Submitted to the Faculty of Graduate Studies
through the Department of **Chemistry and Biochemistry**
in Partial Fulfillment of the Requirements for
the Degree of **Doctor of Philosophy** at the
University of Windsor

Windsor, Ontario, Canada

2015

© 2015 Heather Lynn Filiatrault

New Materials and Methods for the Fabrication of Large-Area Stretchable Electronics

by

Heather Filiatrault

APPROVED BY:

_____

W.S. Kim, External Examiner
Simon Fraser University

_____

A. Hubberstey
Department of Biological Sciences

_____

H. Eichhorn
Department of Chemistry & Biochemistry

_____

B. Mutus
Department of Chemistry & Biochemistry

_____

T. Carmichael, Advisor
Department of Chemistry & Biochemistry

February 6, 2015

Declaration of Co-Authorship / Previous Publication

I. Co-Authorship Declaration

I hereby declare that this dissertation incorporates material that is result of joint research, as follows: This dissertation incorporates the outcome of the research undertaken in Dr. Tricia Carmichael's research group. In all cases, the key ideas, primary contributions, experimental designs, data analysis and interpretation, were performed by the author under the guidance of the Dr. Tricia Carmichael. I acknowledge all my colleagues listed as co-authors on manuscripts for assistance with raw data acquisition (Rachel A. Boutette, Danny M.J. Mansour, and Gyllian C. Porteous) and R. Stephen Carmichael for assistance with data analysis, photography and equipment setup. I acknowledge Dr. Heng-Yong Nie for collecting AFM images of samples for Chapters 2, 3, and 5. I acknowledge Brad Kobe for collecting SEM images for Chapters 2, 3, and 5, Rebecca Jacklin for acquiring SEM images for Chapter 2 and Dr. Todd Simpson for acquiring SEM images for Chapter 6. I acknowledge my colleague Dr. Gregory J.E. Davidson for conceptualizing and initiating the project discussed in Chapter 4. I acknowledge Dr. John Trant of Elizabeth Gillies' Group for synthesizing the IIR-g-PEO used in the emissive layers of Chapter 5. I acknowledge Dr. Natalie Suhan, Lorenzo Ferrari, Dr. Conrad Siegers and Dr. Gregory Davidson of Lanxess, Inc. for supplying the IIR sheets used in Chapter 6.

I am aware of the University of Windsor Senate Policy on Authorship and I certify that I have properly acknowledged the contribution of other researchers to my dissertation, and have obtained written permission from each of the co-author(s) to include the above material(s) in my dissertation.

I certify that, with the above qualification, this dissertation, and the research to which it refers, is the product of my own work.

II. Declaration of Previous Publication

This dissertation includes one original paper that has been previously published/submitted for publication in peer reviewed journals. The remaining four chapters are in preparation for publication as follows:

Dissertation Chapter	Publication title/full citation	Publication status
Chapter 2	Filiatrault, H.L.; Boutette, R.A.; Carmichael, R.S.; Carmichael, T.B. "A Self-Assembled, Low-Cost Microstructured Layer for Extremely Stretchable Gold Films" (ACS Applied Materials and Interfaces)	In Preparation
Chapter 3	Filiatrault, H.L.; Mansour, D.M.J.; Carmichael, T.B. "Highly Stretchable Gold Films on Elastomeric Substrates Coated with a Poly(Vinyl Alcohol) Interlayers"	In Preparation
Chapter 4	Filiatrault, H. L.; Porteous, G. C.; Carmichael, R. S.; Davidson, G. J. E.; Carmichael, T. B. Stretchable Light-Emitting Electrochemical Cells Using an Elastomeric Emissive Material. Advanced Materials 2012, 24 (20), 2673-2678.	Published
Chapter 5	Filiatrault, H.L.; Mansour, D.M.J.; Carmichael, R.S.; Trant, J.F.; Gillies, E.R.; Carmichael, T.B. "Light-Emitting Electrochemical Cells with IIR-g-PEO Elastomeric Matrices for Improved Mixing with Ionic Transition Metal Complex Emitters"	In Preparation
Chapter 6	Filiatrault, H.L.; Vohra, A.; Mansour, D.M.J.; Boutette, R.A.; Carmichael, R.S.; Carmichael, T.B. "Methods to Enable the Fabrication of Conductive Metal Films on Butyl Rubber Substrates"	In Preparation

I certify that I have obtained a written permission from the copyright owner(s) to include the above published material(s) in my dissertation. I certify that the above material describes work completed during my registration as graduate student at the University of Windsor.

I declare that, to the best of my knowledge, my dissertation does not infringe upon anyone's copyright nor violate any proprietary rights and that any ideas, techniques, quotations, or any other material from the work of other people included in my dissertation, published or otherwise, are fully acknowledged in accordance with the standard referencing practices. Furthermore, to the extent that I have included copyrighted material that surpasses the bounds of fair dealing within the meaning of the Canada Copyright Act, I certify that I have obtained a written permission from the copyright owner(s) to include such material(s) in my dissertation.

I declare that this is a true copy of my dissertation, including any final revisions, as approved by my dissertation committee and the Graduate Studies office, and that this dissertation has not been submitted for a higher degree to any other University or Institution.

Abstract

This dissertation addresses three main challenges towards the fabrication of large-area stretchable electronic devices. First, we replaced expensive photolithography techniques with low-cost methods to achieve highly stretchable gold films on elastomers. Second, we enabled the fabrication of large-area stretchable pixels through the incorporation of stretchable elastomers in the emissive layer of light-emitting devices. Third, we made progress towards the inception of air-stable large-area stretchable electronics by developing methods to deposit conductive metal films on new highly impermeable stretchable substrates.

Chapter 2 describes the deposition of a low-cost, microstructured glue interlayer on an elastomeric substrate to enable the fabrication of gold films with high stretchability for use as device interconnects and strain sensors. The microstructured glue interlayer is low-cost, commercially available and green and can be deposited by benchtop fabrication processes eliminating the need for expensive photolithographic patterning techniques to achieve stretchable metal geometries.

Chapter 3 expands upon the work of Chapter 2 to develop a poly(vinyl alcohol) polymer interlayer whose tunable mechanical properties affect the crack propagation in overlying metal films. When the polymer is dry, it is a brittle film that cracks under strain and causes metal films to fail electrically at low elongations. After exposure to water condensation the polymer interlayer softens and a wrinkled topography develops which enables gold films to stretch to 75% elongation before failure occurs.

Chapter 4 reports the development of an elastomeric emissive material capable of withstanding strains up to 27% before light emission is no longer observed. This is the first example of a room-temperature stretchable large-area light-emitting device.

Chapter 5 builds upon the work of Chapter 4 by incorporating graft copolymers with increased air and moisture permeability into the emissive layer. We demonstrate that the graft copolymers provide greater device stability than the elastomer reported in Chapter 3 and can sustain repeated cyclic strains without influencing the peak radiance.

Chapter 6 presents methods to enable the deposition of conductive metal films on elastomers with high impermeability to water and oxygen. This is the first step to realizing commercial stretchable electronic devices capable of ambient operation.

Acknowledgements

First and foremost I would like to thank my parents, Pierrette and Joseph Filiatrault for supporting me throughout my education and for all the sacrifices that they have made so that I can have all the opportunities I've had in my life. I'd like to thank my sister, Brandi Filiatrault for always being there for me and listening to my long-winded tales. I'd like to thank my grandfather, Pierre Filiatrault for his motivational support. Thank you as well to my entire extended family for their support and encouragement.

I would like to thank my supervisor, Dr. Tricia Carmichael for providing me with the opportunity to work in her laboratory as an inexperienced undergraduate student and for her continued support throughout my doctorate degree. I truly appreciate all of the freedom you afforded me in pursuing new projects and your considered direction through the challenges that arose. Your guidance throughout my time in your laboratory has taught me so much on how to conduct research, how to write scientifically and how to present findings in a unique way.

I would like to thank Dr. Gregory Davidson for mentoring me as an undergraduate student and for demonstrating to me how to conceptualize projects and what questions to ask when conducting experiments. I would like to thank Steve Carmichael for capturing photographs and videos of my electronic devices and for helpful discussions on circuits and light-emitting devices.

I would like to thank my colleagues for making my time in the laboratory so enjoyable, I know I have made lifelong friends out of many of you and I wouldn't be where I am today without your support. Thank you to Dr. Ronan San Juan for always being a source of positivity, willing to help me in any way that you could. I would like to thank Dr. Michael Miller for his dependable knowledge and counsel, and for useful discussions into the challenges I faced on many projects. Thank you to Akhil Vohra for always listening to whatever ideas or thoughts I had to get out of my head, giving invaluable advice and for being the spy-turned-BFF. Thank you to my officemate Michael-Anthony Ferrato for embracing the term and day-to-day banter. Chen Yiting, xie xie for always bringing a smile to my face and for teaching me Mandarin. Thank you to Stanley Amyotte for always providing me with a different perspective on life. Thank you to Gyllian Porteous for exposing me to new things (glass blowing) and sharing travel advice. Thank you to all of the undergraduate students that allowed me to mentor then through the course of their undergraduate dissertations: I learned a lot about research and teaching through those experiences. I would like to especially thank the undergraduate students that contributed significantly to the projects presented in this dissertation: Gyllian Porteous, Danny Mansour, Rachel Boutette and Brittany Ives. I could not have

achieved what I did without your countless hours of sample preparation and assistance in device testing. Thank you to all of my current and former colleagues of the Carmichael Lab for your contributions to my dissertation.

I would like to thank the entire community that makes up the Department of Chemistry and Biochemistry. You have all had a profound impact on my time here. Thank you to Dr. Christopher Allan, Lee-Anne Fochesato, Dr. Jillian Hatnean, Dr. Elizabeth Viljoen and Dr. Jonathan Dube for your support and for the many memories we have shared over the course of our studies together. Thank you to the Curry gang: Dr. Giorgio Baggi, Alex Stirk, Pablo Martinez-Bulit, Katharina Kreß and Akhil Vohra. We shared so many experiences together and I'm sad to see it come to an end. Thank you to the members of the soccer team (FC60) and the softball team (The Isotopes) for so many fond memories. Thank you to my friends Laura Renaud, Monique Pirillo, Katie Cha and Andrea Staruch for moral support.

Thank you to all of the support staff that have helped me on countless occasions: Marlene Bezaire, Cathy Wilson and Beth Kickham. Thank you to all of the professors that I had the pleasure of learning from for their involvement in making the Department the unique place that it is. Thank you to the staff at Surface Science Western and the Nanofab at UWO (Ross Davidson, Brad Kobe, Rebecca Jacklin, Dr. Heing-Yong Nie and Dr. Todd Simpson) for assistance in SEM and AFM imaging. Thank you to Lorenzo Ferrrari, Dr. Gregory Davidson, Dr. Conrad Siegers, and Dr. Natalie Suhan at Lanxess for your unique perspectives and insights. I feel very privileged to have taken part in an industry collaboration and for the opportunities I was afforded in attending workshops and giving knowledge transfer presentations.

Finally I would like to thank my committee members: Dr. Bulent Mutus, Dr. Holger Eichhorn, and Dr. Andrew Hubberstey for their feedback at all of my committee meetings and for the guidance they have provided over the course of my degree and thank you to Dr. Woo Soo Kim for agreeing to be my external examiner. I am appreciative of the critiques and suggestions you will provide that will improve this body of work.

Table of Contents

List of Figures

List of Supplementary Figures

List of Tables

List of Abbreviations

%	percent
%T	percent transmittance
&	and
~	approximately
<	less than
>	greater than
°C	degree Celsius
µ	micro-
A	amp
Å	angstrom
AFM	atomic force microscopy
AgNW	silver nanowire
AuNP	gold nanoparticle
Avg	average
B-IIR	black-filled isobutylene-co-isoprene rubber
bpy	bipyridyl
cc	cubic centimeter
CNT	carbon nanotube
CVD	chemical vapor deposition
DC	direct current
DI	deionized
DMSO	dimethyl sulfoxide
DPPS	diphenylphosphinostyrene
dtb	di-tertbutyl
ε	strain
e-beam	electron beam
ECD	electrochemical doping
ED	electrodynamic
EDL	electric double layer
EGaIn	eutectic gallium-indium
EQE	external quantum efficiency
Etot	total energy emitted over lifetime
eV	electron volt
FIB	focused ion beam
FOTS	trichloro(1-H,1-H,2-H,2-H-perfluorooctyl)silane
g	gram
GF	gauge factor

GPa	gigapascal
h or hr	hour
HOMO	highest-occupied molecular orbital
Hz	Hertz
IIR	isobutylene-co-isoprene rubber
IIR-g-PEO	isobutylene-co-isoprene rubber with graft poly(ethylene oxide) side chains
ILED	inorganic light-emitting diode
iTMC	ionic transition metal complex
ITO	indium tin oxide
k	kilo-
L	liter
LEC	light-emitting electrochemical cell
LED	light-emitting diode
λ_{max}	wavelength of maximum absorbance or emission
LUMO	lowest-unoccupied molecular orbital
m	meter
m	milli-
Mpa	megapascal
N	Newton
n	nano
n-doped	negatively-doped
n-type	negative-type
OLED	organic light-emitting device
p	pico-
P3AT	poly(3-alkylthiophene)
P3BT	poly(3-butylthiophene)
P3DDT	poly(3-dodecylthiophene)
P3HT	poly(3-hexylthiophene)
Pa	Pascal
PC	polycarbonate
PCBM	(6,6)-phenyl-C_{61}-butyric acid methyl ester
PDMS	poly(dimethyl siloxane)
p-doped	positively-doped
PEDOT:PSS	poly(3,4-ethylenedioxythiophene):poly(4-styrenesulphonic acid)
PEN	poly(ethylenenaphthalate)
PEO	poly(ethylene oxide)
PF_6	hexafluorophosphate
Phr	per hundred parts rubber

PIB	poly(isobutylene)
p-i-n	positvely-doped semiconductor and negatively-doped semiconductor separated by an intrinsic undoped region
PLEC	polymer light-emitting electrochemical cell
PLED	polymer light-emitting diode
PMMA	poly(methyl methacrylate)
PS	polystyrene
psig	pounds per square inch
PTFE	polytetrafluoroethylene
p-type	positive-type
PUA	poly(urethane acrylate)
PVA	poly(vinyl alcohol)
PVAc	poly(vinyl acetate)
QCM	quartz crystal microbalance
R/R_0	normalized resistance
R_0	initial resistance
R1/5	20% of the maximum radiance
RH	relative humidity
RMS	root mean squared
rpm	rotations per minute
R_s	sheet resistance
R_{var}	variable resistor
s or sec	second
SEM	scanning electron microscopy
SPR	surface plasmon resonance
SY	Super Yellow
$t_{1/2}$	time for radiance to decay to half of maximum
$t_{1/5}$	time for radiance to decay to one fifth of maximum
Tg	glass transition temperature
THF	tetrahydrofuran
T-IIR	transparent isobutylene-co-isoprene rubber
Tm	melting temperature
t_{on}	turn-on time
UV	ultraviolet
UV-vis	ultraviolet-visible
V	volt
v/v	volume/volume ratio
V_T	total voltage drop

Ω	ohm
W	watt
Ω/sq or Ω/□	ohm per square
w/w	weight ratio
W-IIR	white-filled isobutylene-co-isoprene rubber
wt%	weight percent

1. Chapter 1

Introduction

1.1 Stretchable Electronic Devices

Stretchable electronics enable new applications such as wearable electronics, biointegratable electronics and electronics that can inflate or conform to non-planar surfaces due to the soft elastomeric nature of the substrates upon which they are built. Traditional electronics are rigid, boxy and bulky making their integration with humans and moving robotic parts challenging. Traditional biomedical sensors must be strapped to the skin and the wearer is very conscious of their presence due to the bulk and weight of the device. The soft, light-weight and conformal nature of stretchable electronics opens the door to the seamless incorporation of sensors on the human body: Soft, light-weight, thin polymers with patterned metal circuits can be applied to the chest of babies like an adhesive bandage to monitor temperature, heart rate and movement while the babies sleep and transmit the information wirelessly to the parents' mobile phones in order to monitor for sudden infant death syndrome.[1] Contact lenses with metal circuitry are now being developed at University of Washington to detect glucose levels in tears to provide live-feedback to patients suffering from diabetes.[2] Stretchable electronics are also being incorporated into biomedical diagnostic tools to render surgeries less invasive and faster: Soft, inflatable balloon catheters decorated with stretchable patterned metal circuits can be used to sense damaged areas of the heart and perform local ablations combining the functions of "mapping and zapping" all in one tool to treat a variety of cardiac conditions.[3] Similarly, smart surgical gloves with patterned metal circuits in the glove fingertips allow surgeons to detect changes in temperature and electrical potential for direct assessment of tissue during surgery.[4] The field of biomedical science is not the only area benefitting from advances in stretchable electronics: Stretchable light-emitting displays,[5],[6],[7],[8],[9],[10],[11] stretchable solar cells[12],[13],[14],[15] and stretchable batteries[16],[17] will enable the commercialization of consumer goods with new form factors such as computers rendered shatter-proof through the incorporation of components made entirely of stretchable thin films and soft rubbery materials, light-emitting wallpapers that can conform to non-planar surfaces, and solar cells integrated into clothing that can charge personal electronic devices in your pockets.

There are two general approaches to creating stretchable electronic devices: The first approach relies on connecting rigid device islands with stretchable interconnects. In this approach all of the strain is absorbed by the interconnect while the device islands themselves do not experience significant strain. The interconnects must maintain high conductivity under applied strain. Metals and semiconductors are the optimal interconnect material for high conductivity; these materials however, are generally hard and brittle failing at low strains. In order to impart stretchability to rigid metal and semiconductor materials, new geometrical arrangements have been designed to convert tensile strain into planarization or out-of-plane bending which is more easily tolerated by the conductive materials. The second approach to fabricating stretchable electronics focuses on the fabrication of large-area stretchable devices. In order to achieve large-area devices every component of the device - electrodes, active layers, and interconnects - must be able to tolerate tensile strain. These devices are realized by developing new classes of inherently stretchable materials for incorporation into device components. The following sections will explore in greater detail the two approaches to rendering materials stretchable and discuss their applications as device interconnects and in large-area stretchable electronics.

1.1.1. Geometrical Arrangements of Rigid Materials

Metals and semiconductors are used ubiquitously in rigid electronic devices as interconnects and circuit elements owing to their high conductivity. In order to implement these materials into stretchable electronic devices, they must maintain conductivity over large strains (> 10%). Free-standing metal films fail at small strains due to elongation of the metal in one direction and thinning in the transverse direction resulting in the formation of a single neck which causes ruptures in the metal film and completely disrupts conductivity at only a few percent elongation.[18] Bonding metal films to compliant substrates delocalizes the strain in the metal film which creates multiple necking sites and allows the film to deform to larger strains before cracks interrupt conductivity (Figure 1.1).[19] Lacour et al. demonstrated that thin films of gold on poly(dimethyl siloxane) (PDMS) substrates can be stretched to 22% before electrical failure occurs.[20] Gold films on PDMS can also endure repeated cyclic strains of 20% up

to 250,000 times thanks to the presence of tribranched microcracks which open and close upon stretch and release cycles.[21] Crack propagation in metal films under tensile strain causes the resistance in the film to increase by several orders of magnitude and often the crack propagation is uncontrolled and irreproducible. Researchers have therefore sought ways to eliminate or minimize crack formation in semiconductor and metal films in order to develop interconnects that exhibit very small changes in resistance as a function of strain. The following sections will explore methods to avoid crack formation in rigid materials on compliant substrates by laying out the materials into new architectures and geometries that support strain. Additionally, a new approach to controlling crack propagation through metal films on compliant microstructured substrates will be detailed.

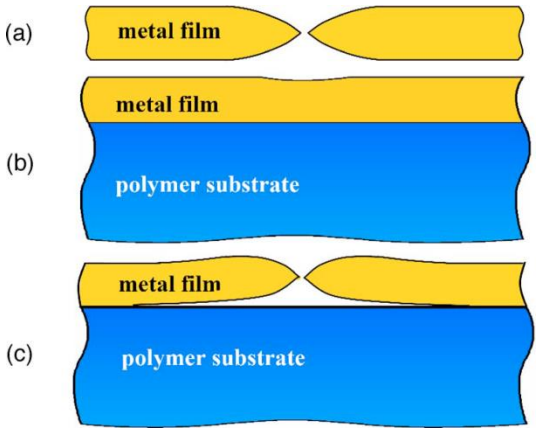

Figure 1.1. Comparison of strain effects on free-standing metal films and metal films bonded to a polymer substrate (a) Free-standing metal film under tensile load forms a single neck and ruptures. (b) Metal film bound to polymer substrate experiences delocalized strain preventing the formation of a single neck. (c) Metal film with poor adhesion to polymer substrate delaminates from substrate and experiences strain localization and ruptures. Adapted with permission from reference 19.

1.1.1.1. Buckling and Pop-ups

One method to increase the elongation at electrical failure of metal films on elastomers is to deposit the metal onto a pre-strained elastomeric substrate such that when the pre-strain is released, the metal film is subjected to compressive strains causing it to buckle. The presence of buckles converts tensile strain to bending strain which is more easily supported by metal films. Lacour et al. demonstrated that by pre-straining a PDMS

substrate to 25% prior to depositing 20 nm of gold, followed by release of the pre-strain enables gold films to remain conductive up to 100% before electrical failure occurs.[22] Buckled gold films with a period of 8.4 μm and amplitude 1.2 μm were prepared by the deposition of 20 nm-thick gold films on PDMS substrates prestrained to 15% followed by relaxation of the prestrain (Figure 1.2).[23] The buckled gold films can also be subjected to repetitive stretching cycles of 15% strain with little change in resistance making them ideal candidates for stretchable interconnects. The high peak-to-valley amplitude of buckled metal films renders it difficult to subsequently deposit thin films on top of the gold electrode and thus negates their use as device electrodes unless the entire device is fabricated on the pre-stretched substrate and released together.

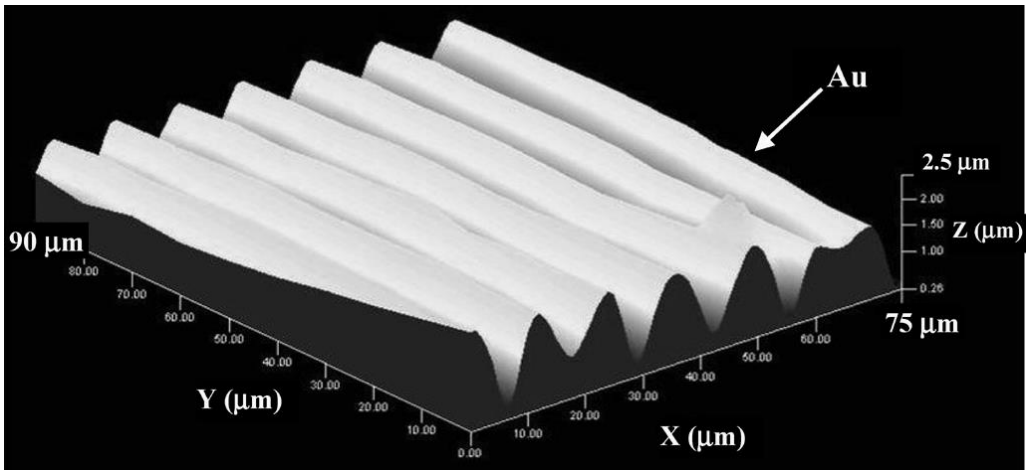

Figure 1.2. 3-dimensional profile of a buckled gold film on PDMS after release from 15% prestrain. Adapted with permission from reference 23.

While application of uniaxial prestrain to the elastomeric substrate prior to metal deposition enables elongation in the direction of prestrain, Görrn et al. demonstrated that radially prestraining PDMS substrates prior to metal deposition followed by release of prestrain allows for biaxial stretching. Samples that were radially prestretched prior to metal deposition were able to support uniaxial stretching in any direction to more than the amount of prestrain and biaxial stretching up to the prestrain amount.[24]

When the metal or semiconductor film is bound to the elastomer only at the extremities, release of the prestrain allows the metal film to pop-up in the centre where there is no adhesion resulting in the formation of arc-shaped bridges.[25],[26] These pop-up

architectures can be fabricated with metals and thin films of silicon (Figure 1.3) enabling their application as interconnects in stretchable light-emitting displays (LEDs)[5],[6] (where all of the strain is absorbed by planarization of the bridge and the pixels themselves are rigid and do not deform) and hemispherical eye-ball cameras[27]. This approach can be rather expensive as it relies on photolithography to pattern the metal interconnects and the rigid device islands.

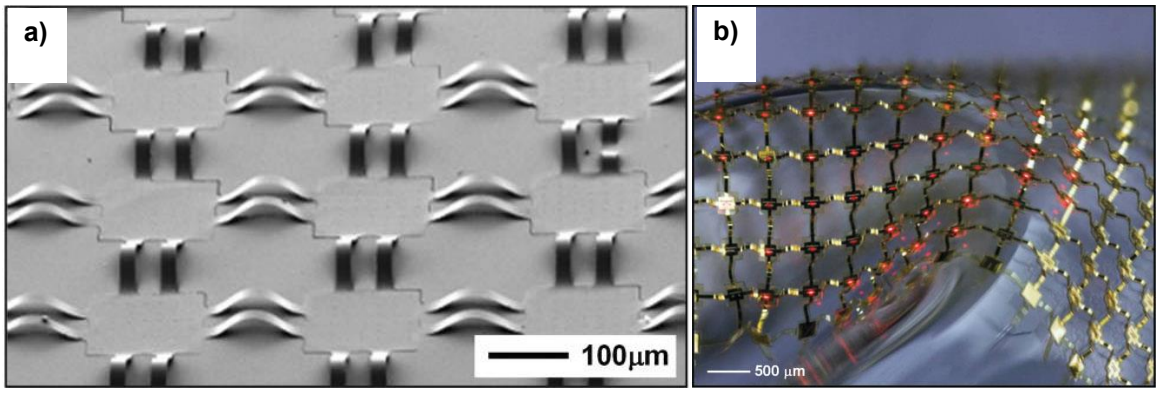

Figure 1.3. (a) SEM image of a stretchable silicon pop-up membrane bonded to the elastomeric substrate at the square contact pads. (b) Passive matrix, stretchable display based on an array of inorganic LEDs in a non-coplanar mesh configuration on a PDMS substrate. Adapted with permission from references 5 and 26.

1.1.1.2. Serpentines

Rather than create buckles or out-of-plane bridges in metal films, in-plane patterning of the metal film can be used to create high elongations at failure in rigid materials. Much in the way that a metal spring uncoils, a tortuous or serpentine wire patterned in the plane of an elastomeric substrate can twist out of plane to accommodate the elongation via straightening of the wire, significantly reducing the strain experienced in the film.[28]

Gray et al. demonstrated that gold wires patterned in a horseshoe geometry were able to withstand elongations of 54% before electrical failure occurred and they were able to be stretched repetitively to 25% several hundred times (Figure 1.4).[29] At 50% strain, the tortuous wires were nearly linear and further strain was accommodated by deformation of the metal film which resulted in imminent failure.

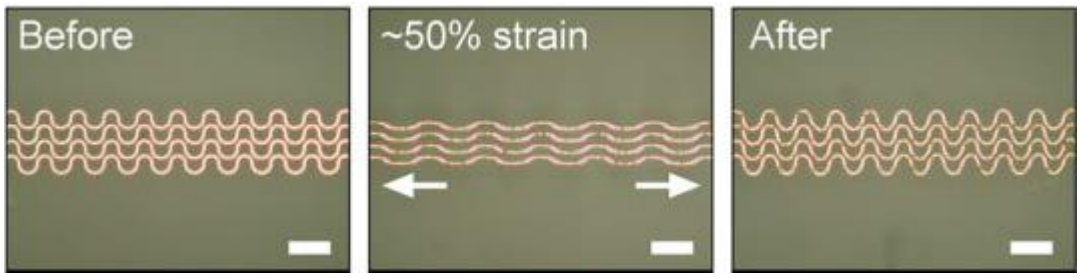

Figure 1.4. Optical micrographs of tortuous wires a) before application of strain b) at ~ 50% strain c) after release of strain. Adapted with permission from reference 29.

Xu et al. reported the fabrication of a "self-similar" pattern of serpentines in which the metal lines making up the serpentine array are serpentine themselves (2 levels of serpentines) (Figure 1.5).[30] As strain is applied to the substrate, the second level of serpentines unravels by bending and twisting. Once the 2nd level is fully extended the 1st level begins unravelling allowing for strains up to 300%. Stretching of self-serpentine copper wires can attain 321% elongation where analogous conventional serpentines connected by straight metal segments fail at 134%. These self-similar serpentines were employed as interconnects in an array of lithium ion batteries on an elastomeric substrate.

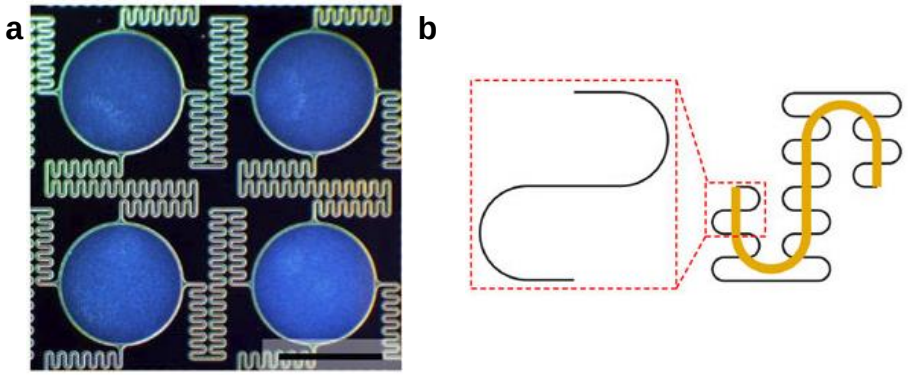

Figure 1.5. Stretachable battery array with self-similar serpentine interconnects. (a) Optical images of Al electrode pads and self-similar interconnects on a Si wafer. (b) Illustration of 'self-similar' serpentine geometries used for the interconnects (black: 1st level serpentine; yellow: 2nd level serpentine). Adapted with permission from reference 30.

The serpentine approach can be combined with pre-strain to enhance elastic stretchability by two times through the combination of buckle planarization with the unraveling of the serpentines.[31] The main drawback of the serpentine strategy is that it

relies on high-cost fabrication methods such as photolithography and the surface area of the serpentine wire is limited. The serpentine method is not exclusive to vapor deposited metal films. Park et al. demonstrated that air-sprayed films of silver nanowires deposited onto horseshoe shaped PDMS substrates exhibited smaller changes in resistance upon stretching compared to analogous films deposited onto flat PDMS.[32] This type of approach eliminates the need for high-cost photolithography techniques to generate metal serpentine patterns. The following section will describe other methods researchers have developed to move away from high-cost photolithography techniques in order to achieve low-cost, large-area stretchable metal films.

1.1.1.3. Alternative Approach to Stretchable Metal Films: Engineered Cracking

While the approaches highlighted above focused on minimizing or avoiding cracking in rigid metal films upon application of strain, an alternative method to making stretchable electronics involves *controlling* the crack propagation through metal films in order to delay the merging of cracks and enhance the elongation at failure of metal films. Alteration of the crack propagation in metal films on elastomers occurs through the introduction of patterned reliefs on the surfaces of the elastomeric substrate which localize strain and produce multiple crack nucleation sites. Multiple crack nucleation sites are desirable because they alleviate strain in the metal film surrounding the crack. When a crack propagates into a relaxed region of the metal film it ceases to propagate leading to the formation of numerous shallow cracks which do not propagate along the full width of the metal film.[33]

Gold films deposited onto smooth, unpatterned elastomers exhibit cracking upon application of linear strain. The propagation of cracks and stretchability of gold films on elastomeric substrates is related to the initial morphology of the gold film. Three typical morphologies exhibited by gold films on PDMS substrates are buckles, microcracks or smooth surfaces. Buckled topographies, which result from compressive stress, initially exhibit a low resistivity that increases linearly up to a critical strain (typically 10 – 20%) due to the continuous propagation of cracks along the surface of the metal film which completely disrupts the conductive pathway. While the resistance of microcracked films is initially higher than that of buckled films, the microcracks provide strain relief by

allowing the gold film to elastically deform by twisting and deflecting out of plane[34] allowing these gold films to remain conductive up to 60% elongation.[35] Graudejus et al. determined that the morphology of gold films obtained by e-beam metal deposition on PDMS depends on six factors: gold thickness, deposition temperature, elastic modulus of PDMS, adhesion layer thickness, surface treatment of PDMS, and mechanical prestrain of the substrate.[36] The complexity of the interplay between the variables responsible for microcrack formation makes it difficult to reproducibly achieve gold films with the desired microcrack morphology.[35] In order to achieve controlled crack propagation in metal films researchers have begun to investigate the use of patterned topographies on the surface of the elastomeric substrate.

Mandlik et al. have demonstrated that the introduction of a topographic pyramidal nanopattern, created by curing the PDMS against a photolithographic master, creates multiple crack nucleation sites in the overlying gold film and inhibits crack propagation as strain is increased.[35] At strains of 25% the resistance of the gold film only changes by a factor of 1.6x. Similarly, Robinson et al. demonstrated that silver films deposited onto a microstructured silicone substrate could sustain cyclic strains of 20% over 1000 times without electrical failure.[37] Scanning electron microscopy of the silver film confirmed that cracks were localized about the micropillars and that micropillars create multiple sites for crack nucleation (Figure 1.6). The main drawback of these examples is that they still rely on photolithography to create the lithographic master upon which PDMS is cured.

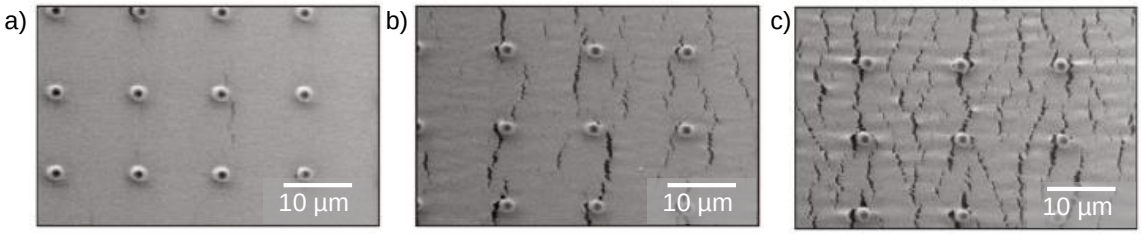

Figure 1.6. SEM images of silver ink conductor surfaces while under applied uniaxial strain on patterned PDMS: (a) unstretched; (b) stretched 10%; (c) stretched 20%. Adapted with permission from reference 37.

Lambricht et al. demonstrated a lithography-free approach to creating a rough patterned topography by curing PDMS against sand-blasted masters.[33] As with the previous examples, the presence of the rough substrate creates multiple sites for crack nucleation and the cracks entering relaxed zones of the metal film experience arrested development allowing gold films to remain conductive to higher elongations at failure than analogous gold films deposited onto smooth substrates. Through a combination of pre-strain and surface roughness, 500 nm-thick gold films maintained conductivity up to 100% elongation. This method is fast, inexpensive and allows for high throughput.

1.1.2. Inherently Stretchable Materials

While geometrical arrangements of metals and semiconductors enable the fabrication of stretchable interconnects, the fabrication of large-area stretchable devices requires that every layer of the device supports stretchability, from the electrodes to the active layer to the interconnects. This demand requires the development of new stretchable materials as the conventional inorganic materials that make up electronic devices are brittle and do not support stretching. Research into the fabrication of inherently stretchable materials has led to the development of composites of nanomaterials embedded in elastomers for stretchable device interconnects,[7] stretchable transparent electrodes[10],[38],[39],[40],[41] and stretchable photodetectors[42],[43]; gel materials doped with conductive pastes and electrolytes for stretchable solid state batteries[16]; liquid metals that have self-healing properties for use as stretchable antennas[44],[45],[46] and in self-healing stretchable circuits[47]; and semiconducting polymers for use as active layers in stretchable solar cells[14],[48], stretchable light-emitting devices,[9],[10] and as stretchable transparent electrodes[15],[49]. The following sections will explore some of these materials, their properties and their function in stretchable electronic devices in greater detail.

1.1.2.1. Stretchable Polymer Materials

Stretchable, conductive polymer films have the potential to replace conventional brittle transparent electrode materials such as indium-tin oxide (ITO) whose brittle nature and high processing temperatures prohibit its use in stretchable electronics. The high sheet resistance of the conductive polymer poly(3,4-ethylenedioxythiophene):polystyrene

sulfonate (PEDOT:PSS) (10^5 Ω/sq) previously limited its application as a transparent electrode, however Bao and coworkers found that by incorporating additives such as dimethyl sulfoxide (DMSO) and the fluorosurfactant Zonyl, the sheet resistance of PEDOT:PSS could be decreased to 240 Ω/sq at 97% transparency.[15] The increase in conductivity was attributed to increased phase separation between the conductive PEDOT chains and the insulating PSS chains which created longer conductive channels of PEDOT. Multilayer deposition of PEDOT:PSS layers enabled the production of films with 46 Ω/sq sheet resistance and 82% transparency which approaches the values of ITO.[15] Films of PEDOT:PSS deposited onto pre-strained PDMS were able to maintain conductivity when stretched to the value of the prestrain demonstrating their superior mechanical properties over ITO. Bao and co-workers investigated the mechanical properties of PEDOT:PSS films on PDMS substrates without prestrain and found that PEDOT:PSS films could retain conductivity up to 188% elongation and were reversibly stretchable to 30% strain[49]. Therefore, there is much promise in using conductive polymers as a replacement for ITO as the stretchable transparent electrode in optoelectronic devices. Lipomi et al. demonstrated the first large-area stretchable solar cell with semiconducting polymers in two of the device layers, the anode and the active layer.[14] PEDOT:PSS was spin coated onto pre-strained PDMS followed by deposition of a blend of the semiconductor poly(3-hexylthiophene) (P3HT) and (6,6)-phenyl-C_{61}-butyric acid methyl ester (PCBM), materials commonly used in bulk heterojunction solar cells. The top electrode consisted of a drop of EGaIn liquid metal. Devices that were pre-strained to 27% could accommodate repetitive strains up to 27% elongation.[14] Semiconducting polymers can also be incorporated into stretchable light-emitting devices and these materials will be discussed in greater detail in Section 1.3.4.

Previous research on organic electronic devices has primarily focused on maximizing the optoelectronic performance of active layer materials, however the dawn of stretchable electronics forces researchers to consider the conformability and ductility of materials. While Lipomi et al. demonstrated that P3HT had stretchable functionality when deposited on pre-strained substrates, analogous devices fabricated without prestrain exhibited cracking in the P3HT layer.[14] Therefore, less brittle semiconducting polymers are required for stretchable electronic devices. In semiconducting polymers stretchability

often comes at the expense of conductivity. P3HT belongs to the family of poly(3-alkylthiophene) (P3ATs) polymers which are semiconducting polymers used in organic bulk heterojunction solar cells. It has been found that increasing the length of the alkyl side chain decreases the Young's Modulus from 2.08 GPa to 0.09 GPa for the polymer film going from poly(3-butylthiophene) (P3BT) to poly(3-dodecylthiophene) (P3DDT) however this comes at the expense of the electronic performance: Bulk heterojunction solar cells fabricated with blends of P3AT and PCBM showed that blends containing longer dodecyl side chains on the P3AT backbone have power conversion efficiencies that are half as large as those of analogous devices with hexyl side chains in the unstretched state.[50] It was also shown that films with higher Young's Modulus crack at lower percent elongations than those with lower Young's Modulus indicating a correlation between tensile modulus and brittleness in semiconducting polymer films on compliant substrates. Figure 1.7 shows photographs of devices under 10% strain with cracks visible in the P3HT:PCBM layer while the film of P3DDT:PCBM with the lower Young's modulus was crack-free.

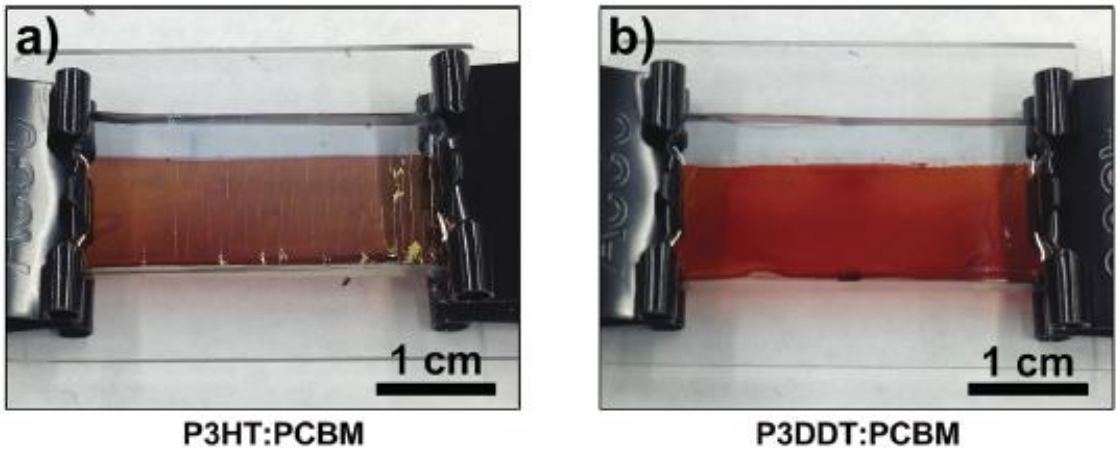

Figure 1.7. Photograph of (a) P3HT:PCBM and (b) P3DDT:PCBM under 10% strain. Adapted with permission from reference 50.

Savagatrup et al. found that there is a "sweet-spot" of A=heptyl for P3AT at which point the film possesses superior mechanical compliance without compromising the electronic performance of the bulk heterojunction solar cell compared to analogous devices made with the shorter chain P3HT semiconducting polymer.[51] This study

demonstrates that there is extensive work that can be done in molecular design of semiconducting polymers to maximize both the electronic properties and the mechanical properties.

1.1.2.2. Liquid Metals in Stretchable Electronic Devices

Liquid metals are attractive candidates for stretchable electronic devices because their liquid nature allows them to deform under applied strain. A common liquid metal used in stretchable electronics is EGaIn which is liquid at room-temperature (Tm = 15.5 °C), highly conductive (3.4×10^4 Scm^{-1}),[52] and non-toxic. The liquid nature of EGaIn allows it to be used as a conformal, non-damaging electrode in metal-molecule-metal-junctions,[53] stretchable solar cells,[14] and rigid and flexible light-emitting electrochemical devices[54],[55]. Free-standing liquid metal drops have the advantage of fast processing and simple deposition as they can be pipetted directly onto the active layer of devices, however for the fabrication of practical, commercial devices EGaIn needs to be encased.

EGaIn forms a gallium oxide skin under ambient conditions and this oxide skin gives EGaIn its unique rheological properties: when the skin envelops the liquid core it acts as an elastic material, whereas rupture of the skin enables the EGaIn to flow. This feature allows EGaIn to be injected into microfluidic channels: Pressure applied at the inlet of the channel is sufficient to rupture the skin and fill the channel; subsequent reformation of the native oxide layer allows the formation of stable structures when the applied pressure is removed. Analogous channels filled with mercury (a metal that does not possess a native oxide) do not form stable structures; when the inlet pressure returns to ambient, the mercury withdraws from the channel leaving it empty. These EGaIn filled microchannels have sufficient flow to maintain electrical conductivity under applied strain allowing them to be used as stretchable interconnects[56] and reversibly deformable, mechanically tunable antennas[44],[46]. Additionally, the EGaIn filled microchannels are self-healing: antennas maintained electrical conductivity even after being cut with a razor blade. Confinement of EGaIn within a microfluidic channel will allow for fully enclosed stretchable electronic devices with liquid metal electrodes.

The self-healing nature of EGaIn can also be used to heal electronic devices such as multilayered circuits. White and co-workers doped electrolyte layers of a multilayered circuit with EGaIn microspheres in order to provide internal autonomous healing to the device. When cracks propagated through the film the EGaIn microspheres ruptured, pouring liquid metal into the crack which restored the electrical pathway and autonomously healed the circuit (Figure 1.8).[47]

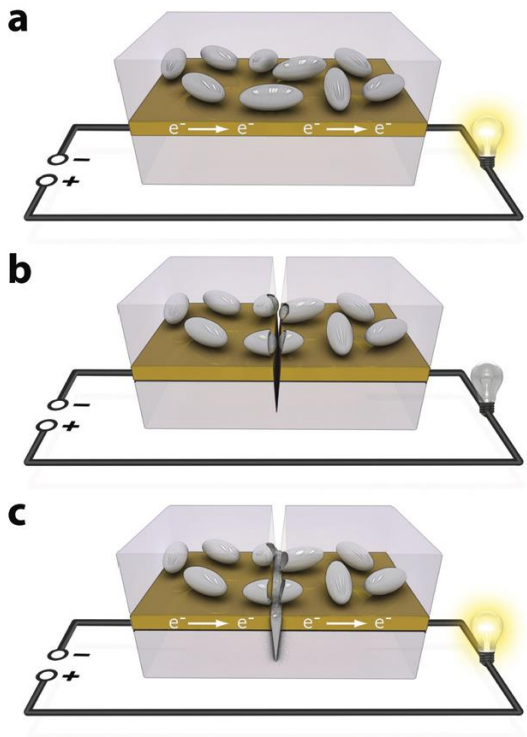

Figure 1.8. Demonstration of the autonomic conductivity restoration concept in a multilayered microelectronic device: (a) Microencapsulated liquid metal dispersed in a dielectric material and deposited on a conductive line on an elastomeric substrate. (b) Elongation causes a crack to form simultaneously interrupting electron transport and rupturing the capsules. (c) The liquid metal flows to the damaged area, restoring conductivity. Adapted with permission from reference 47.

1.2. Stretchable Substrates

1.2.1. Poly(dimethyl siloxane) Substrates

PDMS is the most commonly used elastomeric substrate in stretchable electronics owing to its commercial availability, moldability, optical transparency and biocompatibility. PDMS is comprised of a backbone of alternating silicon and oxygen atoms whereupon each silicon atom in the backbone bears two methyl groups. The repeat unit of PDMS is -[$SiO(CH_3)_2$]-. PDMS is cross-linked by mixing two liquid components, the base and the curing agent, followed by curing in air between 20°C and 150°C. The silicon hydride groups present in the curing agent react with the vinyl groups in the base via a platinum-catalyzed hydrosilylation reaction. When PDMS is cured against a smooth surface, flat substrates are obtained which are employed in the fabrication of stretchable electronic devices.

In addition to flat PDMS substrates, PDMS can be molded into stamps and microchannels by casting the prepolymer against a master patterned by photolithography. Molding PDMS against a master generates the negative relief of the master on the surface of the PDMS. PDMS microchannels have applications in microfluidic devices[57] and in stretchable electronics to confine liquid metals for the fabrication of self-healing antennas[44],[46] as demonstrated in Section 1.1.2.2.

1.2.1.1. Surface Modification of PDMS Substrates

The native surface of PDMS has a low surface free energy of 19.8 mN/m.[58] The hydrophobic surface of PDMS results in water contact angles of 116 ± 1°. Silanol groups (Si-OH) can be generated at the surface of PDMS through air or oxygen plasma treatment which oxidizes the methyl groups.[59] Long exposure to air plasma results in a glassy SiO_x layer which cracks spontaneously or after mechanical strain is applied.[60] Generation of silanol groups at the surface of PDMS allows for chemical modification of the surface through silane coupling. Miller et al. demonstrated that oxidized PDMS could be chemically modified through treatment with 3-aminopropyltriethoxysilane to activate the PDMS for electroless metal deposition.[61] Microcontact printing a chemical ink onto

the APTES-functionalized PDMS substrate enables selective deactivation of the surface effectively controlling where metal deposits during electroless metal deposition. Patterned copper wires deposited using this process remained conductive up to 52%.

1.2.1.2. PDMS as a Substrate in Stretchable Electronics

PDMS has many of the desirable properties for a substrate in stretchable electronic devices. The high optical transparency of PDMS enables its application in stretchable displays and stretchable solar cells where light is required to enter or exit the device. Additionally, PDMS is a soft material that is stretchable at room temperature enabling its use as a substrate for electronic skins which must be capable of deforming with the moving joints of the human body or robotic parts. PDMS is biocompatible and can thus be used in biomedical applications as implants or sensors such as in electronic balloon catheters that sense damaged areas of the heart.[3] In addition to its biocompatibility, PDMS is also permeable to oxygen and moisture enabling its application as a smart contact lens bearing metal electrodes to sense changes in corneal pressure and detect glaucoma.[62]

While high permeability is beneficial for health monitoring applications such as smart contact lenses, it is a severe limitation in the area of stretchable electronics where oxygen and moisture have deleterious effects on device performance. Many organic electronic materials are sensitive to oxygen and moisture and metals such as silver and copper undergo oxidation under ambient conditions. Therefore devices fabricated on PDMS substrates will require additional encapsulation layers to protect the organic layers from oxygen and moisture. The current challenge in stretchable electronics is the development of stretchable encapsulation layers for stretchable electronic devices.

1.2.2. Butyl Rubber Substrates

There is a need to develop stretchable barrier layers to encapsulate and seal stretchable electronic devices from water and moisture permeation or alternatively, to develop new elastomeric substrates with higher inherent moisture and gas impermeability. Butyl rubber (IIR), a copolymer of isobutylene and isoprene (Figure 1.9), is an elastomer that

possesses high oxygen and moisture impermeability. The high impermeability of IIR to oxygen and moisture stems from the polymer's high density (0.917 g/cm^3) and the presence of methyl chains on the rubber backbone that reduce the free volume in the polymer and limit diffusion of small molecules through the polymer. The fractional free volume of IIR (0.026) is almost three times lower than that of PDMS (0.071).[63] Additionally, IIR has low temperature flexibility, heat resistance and chemical resistance which are desirable properties for stretchable electronic substrate materials.

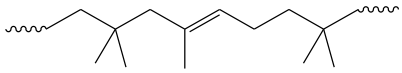

Figure 1.9. Chemical structure of isobutylene-co-isoprene.

Traditionally IIR has been used in tire applications such as inner liners, sidewalls, inner tubes and curing bladders which accounts for ~ 90% of current butyl rubber usage. IIR also has applications in the pharmaceutical industry where it is used in seals and septa. Additionally it is employed in adhesives and in chewing gum. While IIR has the ideal moisture and oxygen impermeability properties required for use as a substrate in stretchable electronics, there are no literature examples of its application in this area. There are three main hurdles which must be overcome to enable the application of IIR as a substrate in stretchable electronic devices: conception of molding methods for the production of IIR sheets with low surface roughness, development of transparent butyl rubber for photovoltaic and lighting and display applications, and surface modification of IIR for deposition of adhesion layers and patterning wettability for solution-based electrode deposition. The following sections will discuss how these criteria have been met in order to make IIR a suitable substrate for stretchable electronic applications.

1.2.2.1. Fabrication of Smooth Butyl Rubber Substrates

Stretchable electronic devices are often comprised of thin films of organic and inorganic materials. Often times the active component of a light-emitting device or photovoltaic device can be as thin as 100 nm which means that any protrusions from the substrate or electrodes that is greater than 100 nm threatens to penetrate through the

active layer thin film material leading to current leakage and electrical shorts. For this reason it is imperative that smooth IIR substrates be used as substrates in stretchable electronic devices.

In order to create cross-linked sheets of IIR, the base polymer is mixed with a curing agent and some particulate filler, which reduces the free volume in the cured sheets and increases the rubber's impermeability to oxygen and moisture. Lanxess Inc. has developed IIR materials with carbon black fillers (B-IIR) for use in tire innerliners and white IIR (W-IIR) peroxide curable rubber materials which contain calcinated clay as the filler. The mixed IIR formulations containing base polymer, curing agent and fillers are cured at elevated temperatures by pressing the mixed formulation in a metal mold which results in rough surfaces. Molding black-filled IIR (B-IIR) against Teflon sheets facilitates removal of cured rubber sheets from the mold, however the rough template of the Teflon sheets causes RMS roughness values of 108.42 ± 9.95 nm in the B-IIR sheets. Carmichael and coworkers developed a method to obtain smooth sheets of B-IIR by molding the rubber against a smooth silicon wafer template coated with a thin PDMS release layer. The low surface free energy of PDMS creates a release layer from which the cured rubber is easily removed. The resultant B-IIR sheet has a much lower RMS roughness of 13.56 ± 1.88 nm.[64]

1.2.2.2. Fabrication of Transparent Butyl Rubber Substrates

The second criterion to employing butyl rubber in stretchable electronic devices is the formulation of a transparent butyl rubber substrate. Light-emitting devices and photovoltaic devices require transparent substrates in order for light to exit/enter the device. Traditional butyl rubber formulations such as B-IIR and W-IIR contain fillers such as carbon black and calcinated clay in order to reduce the free volume in the rubber and increase the impermeability to oxygen and moisture. These fillers also have the effect of rendering the resultant rubber sheets colored and opaque. Lanxess Inc. has developed an IIR formulation free of fillers to enable the fabrication of transparent IIR sheets (T-IIR). The formulation consists of brominated butyl rubber modified with diphenylphosphinostyrene (DPPS) (Figure 1.10) to generate an ionomer which can then be peroxide cured with no additional fillers.[65] The lack of fillers causes T-IIR to have

slightly higher oxygen permeation rates of 216 ± 4 cc-mm/(m^2-day) compared to those of B-IIR or W-IIR whose oxygen permeation rates are 138.6 ± 9.9 cc-mm/(m^2-day) and 104.2 ± 8.8 cc-mm/(m^2-day) respectively.[66] The oxygen permeation rates of T-IIR are still much lower than those of PDMS which were above the detection limit of the instrument.

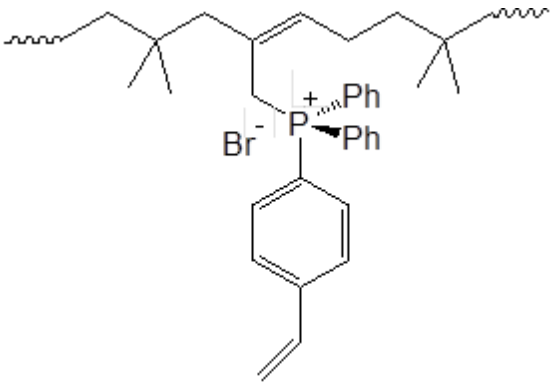

Figure 1.10. Chemical structure of diphenylphosphinostyrene-modified rubber used in the production of T-IIR.

Molding T-IIR between two Teflon sheets produces rubber sheets with RMS roughness values of 167.47 ± 2.93 nm. The high RMS roughness results in scattering of light and a low optical transparency of 17% at 630 nm. By molding T-IIR against a smooth template of PDMS on silicon wafer, the RMS roughness can be decreased to 6.59 ± 0.51 nm with an optical transparency of 84% at 630 nm. Molding against glass slides produced a RMS roughness of 44.36 nm indicating the importance of having a smooth template with low surface free energy to facilitate removal of the cured rubber.

1.2.2.3 Surface Modification of Butyl Rubber Substrates

Butyl rubber has a low surface free energy resulting in a native hydrophobic surface with water contact angles of 95.5 ± 2.3°.[66] In order for butyl rubber to be used in stretchable electronics applications methods were developed to make the surface more hydrophilic to enable deposition of thin films from aqueous solution and chemical modification of the surface through treatment with organosilanes. The first step to creating a more hydrophilic surface is treatment with oxygen plasma. Oxygen plasma effectively lowers the water contact angles from 95.5 ± 2.3° to 47.8 ± 3.2°.[66] Swabbing

with isopropanol removes chain scission products leaving a heterogeneous mixture of oxidized functional groups at the surface[67] giving a water contact angle of 74.6 ± 1.7°. Additional surface treatment with $SiCl_4$ vapor produces silicon dioxide on the surface of IIR through adsorption and hydrolysis of $SiCl_4$ which further lowers the water contact angle to < 20° for $SiCl_4$ treated T-IIR.[66] The hydroxyl-terminated SiO_2 layer can be further chemically modified through reaction with organosilanes to generate the desired functional groups at the surface of IIR (Figure 1.11).[68] For instance, Vohra et al. demonstrated that reaction of the oxidized T-IIR surface with trichloro(1-H,1-H,2-H,2-H-perfluorooctyl)silane (FOTS) decreases the permeation rate of oxygen through T-IIR to 162 ± 6 cc-mm/m^2-day.[66]

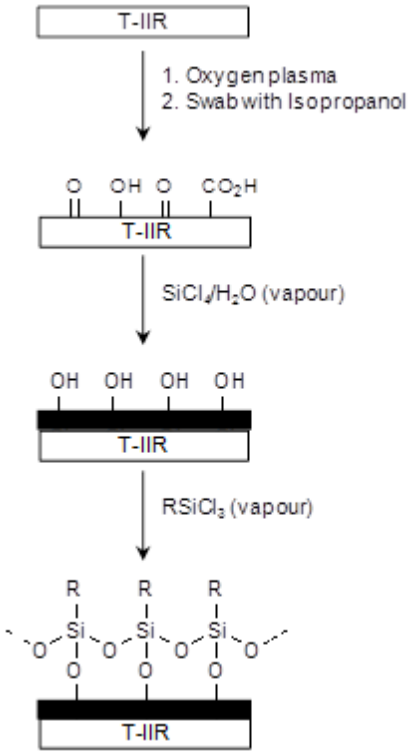

Figure 1.11. Schematic illustration of the surface modification of T-IIR and subsequent formation of an organosilane SAM. Adapted with permission from reference 64.

1.3. Light-Emitting Electrochemical Cells

Despite the numerous advances in the field of stretchable electronics, one of the largest challenges that remains is the fabrication of large-area stretchable light-emitting devices for lighting and signage applications. The reason light-emitting devices are so challenging to render stretchable is because the inorganic materials that comprise the light-emitting layer are crystalline, brittle materials. Even in organic light-emitting devices, several hurdles exist to rendering the devices stretchable: Most notably, organic light-emitting devices (OLEDs) rely on multilayer stacks of charge injection, charge transport and emissive recombination layers for light-emission to occur, each of which must be rendered stretchable in order for the entire device to perform under applied strain. In comparison to OLEDs, light-emitting electrochemical cells (LECs) possess a simpler single-layer architecture in which all functionality of charge injection, charge transport and emissive recombination exists within a single layer. The first example of such a single-layer polymer LEC (PLEC) was reported by Pei and co-workers in 1995 based on a semiconducting polymer mixed with an electrolyte composed of lithium salt and ion conducting polymer.[69] Under an applied voltage bias, the ions migrate to the electrodes to facilitate electron and hole injection into the semiconducting polymer. As the electrons and holes propagate towards the center of the device an exciton is formed which results in light emission. Shortly after this discovery, Maness et al.[70] and Lee et al.[71] reported single-layer light-emitting devices based on ruthenium ionic transition metal complexes (iTMC). The charged nature of the iTMC eliminated the need for added electrolytes and was thus the first report of a single-layer light-emitter based on a single component. While the original PLEC and iTMC devices differ in the constituents that produce light-emission they operate under the same mechanisms due to the ionic nature of the emissive layer. The following sections will outline the models of LEC operating mechanisms.

1.3.1. Device Operating Mechanism

In general, there are two competing models to describe the operating mechanism of LECs, the electrodynamic model[72],[73],[74],[75] and the electrochemical doping model[69],[76],[77],[78],[79],[80],[81],[82], and evidence exists to support each model. Both models agree that the injection barrier of electrons and holes at the electrodes is reduced by separation of ions in the light-emitting layer under application of a voltage bias.

In the electrodynamic model, application of a potential leads to the migration and accumulation of ions at the electrodes causing electric double layers (EDLs) to form. The formation of EDLs causes a drop in the electric potential at the electrodes and promotes charge injection into the emissive layer. In the bulk of the device there is a field-free region where the cations and anions of the iTMC remain closely associated with one another and the electronic current is diffusion-dominated (Figure 1.12a). Light-emission occurs from the field-free region of the device.

In the electrochemical doping model, accumulation of ions also leads to the formation of EDLs at the electrodes however only to the extent required to form ohmic contacts. The ECD model also states that in the bulk, positively doped (p-doped) and negatively doped (n-doped) regions develop in the emissive layer due to injection of electrons and holes at the cathode and anode respectively. The counter ions migrate to neutralize the local charge. Over time, the doped regions grow until a p-i-n junction forms between them, where i is the intrinsic undoped region (Figure 1.12b). Charge recombination is favored in the intrinsic region due to the applied potential drop.

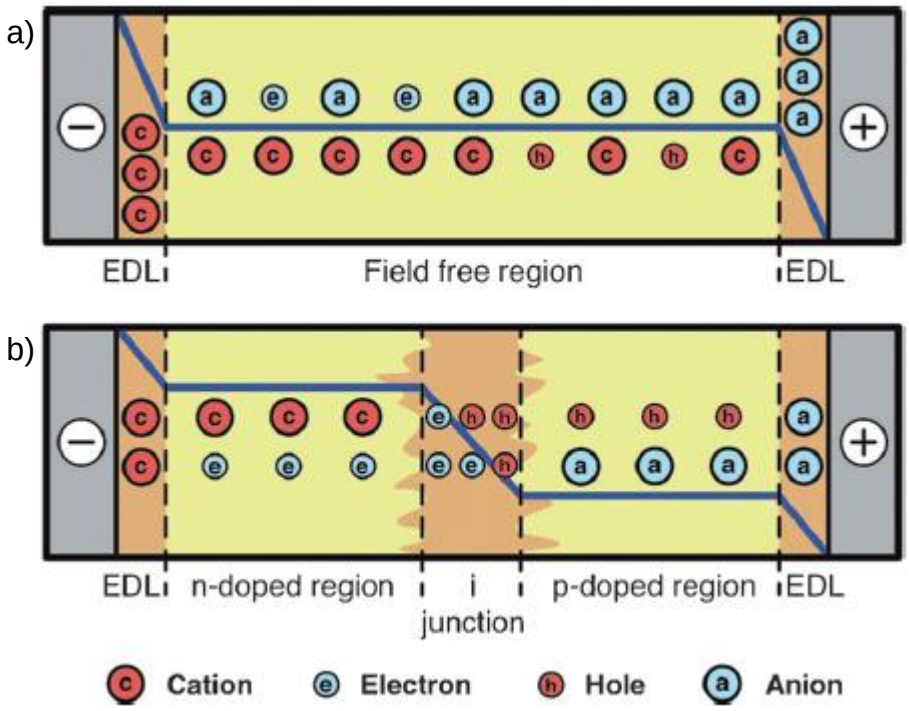

Figure 1.12. Illustration of potential profile and electronic and ionic charge ditribution in a LEC during steady-state operation for the (a) ED model and (b) ECD model. Adapted with permission from reference 83.

Recent studies suggest that the ECD model and the ED model are not mutually exclusive but rather extreme cases of what may occur in LECs depending on the rate of charge injection into the emissive layer. Van Reenen et al. demonstrated through simulations that when injection into LECs is limited (rate of injection is low), two large EDLs form in agreement with the ED model however when injection into LECs occurs at a fast rate, ohmic contacts are formed and the rest of the potential is dropped over a p-n junction in the bulk consistent with the ECD model.[83] Their simulations were substantiated through the fabrication of planar LECs with gold contacts which were capable of forming ohmic contacts and operated in accordance with the ECD model. Analogous devices with oxidized aluminum contacts had limited injection resulting in device operation following the ED model.

1.3.2. Figures of Merit

In order to quantitatively compare the performance of LECs with different emissive materials researchers must rely upon a standard set of figures of merit. The commonly used figures of merit to quantify LEC performance are:

- *Maximum radiance*: The maximum radiance of the device is the measure of the maximum amount of light emitted in Watts.
- *Turn-on time (t_{on})*: the amount of time it takes for the device to reach its maximum radiance. Typical turn-on times in LECs can range from a few seconds to several hours depending on the constitution of the emissive layer and the operating conditions. Many factors are known to influence the turn-on time of devices most notably the mobility of the counter-anion in the light-emitting layer, the voltage at which the device is driven and the presence of insulating or ion-conducting additives.
- *External quantum efficiency (EQE)*: a measure of the amount of photons emitted per electron injected.
- *Lifetime*: There are two values typically reported for device lifetime. The lifetime can be reported as the time it takes for the device radiance to decay to one half of the maximum value ($t_{1/2}$) or as the time it takes for device radiance to decay to one fifth of the maximum value ($t_{1/5}$).
- *Total Energy Emitted (E_{tot})*: calculated by integrating the area under the radiance curve from t=0 (onset of voltage bias application) to t=1/5 for a light-emitting area of 3 mm^2.

1.3.3. Types of LECs

There are two types of LECs: polymer LECs (PLECs) and ionic transition metal complex (iTMC) LECs. While the light-emitting components of each type of device differ, their overall operation mechanism is the same. The following sections will provide a brief overview of the components of the light-emitting layers of PLECs and iTMC LECs.

1.3.3.1. Polymer LECs

PLECs were first reported in 1995 by Pei and coworkers and consist of semiconducting conjugated polymers mixed with solid electrolytes.[69] Upon application of a voltage bias, electrons are injected into the lowest-unoccupied molecular orbital (LUMO) of the semiconducting polymer and holes are injected into the highest occupied molecular orbital (HOMO) of the semiconducting polymer at the cathode and anode respectively. The injection of electrons and holes is facilitated by the migration of mobile ions from the electrolyte. Injection of electrons and holes results in the formation of p-type carriers and n-type carriers at the anode and cathode respectively. The p-type carriers propagate towards the cathode and the n-type carriers propagate towards the anode forming a p-i-n junction when they meet. It is in the intrinsic junction region where the electrons and holes recombine to form neutral pairs which radiatively decay to the ground state. Typically, salts such as $LiCF_3$ are employed in the electrolyte along with an ion-transport polymer such as poly(ethylene oxide) (PEO). The ions from the salt not only reduce the barrier to charge injection by forming EDLs at the electrode but also provide charge balance to the p-doped and n-doped regions of the emissive layer.

PLECs have been fabricated with a number of conjugated polymers such as poly(*p*-phenylene)s, poly(phenylene vinylene)s, polyfluorenes and polythiophenes and a variety of emission colors have been produced.[84] As these emissive layers are comprised of multiple components they experience some degree of phase separation. In order to reduce the amount of phase separation in the system researchers have tried several approaches including the addition of bipolar surfactants[85], the use of new electrolytes such as crown ether/lithium salt complexes[86] or ionic liquids[87],[88],[89], and implementing ion-transporting side groups to the semiconducting polymer such as oligo(ethylene oxide) side chains in order to reduce the amount of PEO required and to compatibilize the components[90],[91].

1.3.3.2. iTMC LECs

Ionic transition metal complex LECs differ from PLECs in that the light-emitter itself is ionic, eliminating the need for additional electrolytes. This enables the fabrication of single-component emissive layers thus eliminating phase separation. Seminal work on iTMC LECs focused primarily on $Ru(bpy)_3^{2+}$ as the light-emitter. The charge on the iTMC is compensated for by mobile counter anions that migrate towards the anode and facilitate hole injection under applied voltage bias. Researchers have found that the size and dielectric constant of the mobile counter anion affects the turn-on time of the device: For instance $Ru(dtb\text{-}bpy)_3^{2+}$ LECs exhibit faster turn-on times as the size of the counter ion is decreased from PF_6 to BF_4.[92] Under applied voltage bias, the Ru^{2+} species is oxidized to Ru^{3+} at the anode and at the cathode the Ru^{2+} is reduced to Ru^{+}. The charges hop from Ru-centre to Ru-centre until recombination of the Ru^{3+} and Ru^{+} produces two Ru^{2+} species, one in the excited state and one in the ground state. Relaxation of the Ru^{2+} to the ground state results in the emission of a photon.

Although iTMC emitters can be incorporated into LECs as a single component system, researchers have investigated the effect of dispersing the iTMC in a non-conductive polymer matrix in order to improve film quality and increase device yield. Dispersing the Ru-iTMC in poly(methyl methacrylate) (PMMA) or poly(styrene) (PS) led to increased device lifetimes ($t_{1/2}$) of 900 hours and 1100 hours compared to pristine films which had lifetimes of 700 hours.[93] When PEO is employed as the polymer matrix it acts as both a film processing aid and as a polymer electrolyte to facilitate ion migration through the emissive layer. Indeed, Ru-iTMC devices incorporating PEO polymer matrices exhibit faster turn-on times of 30 seconds compared to pristine devices which require 1.5 - 2.5 minutes to reach maximum radiance.[94]

The color of light emission in iTMC LECs can be tuned by altering the ligand or the metal centre of the iTMC, thus altering the HOMO-LUMO gap. For instance $Ru(dtb\text{-}bpy)_3^{2+}$ emits light at 630 nm while incorporation of an esterified bipyridine ligand red shifts the emission to 690 nm.[95] In 2004, Slinker et al. reported the iTMC LEC based on an $Ir(ppy)_2(dtb\text{-}bpy)^{+}$ which exhibits a maximum emission at 560 nm.[96] The high ligand field-splitting energy of iridium allows for higher color tunability and complexes with

emissions ranging from blue to red have been reported.[97] While iridium-based LECs possess slower turn-on times, faster times can be achieved through the addition of ionic liquids or salts to enhance the ion mobility in the emissive layer.[98]

1.3.4. Stretchable Device Architectures

Since the initial reports of LECs in the mid-1990s, it took nearly 15 years for the first flexible version of a LEC to be demonstrated Fang et al.[99] During the course of this dissertation, Pei and co-workers reported the first stretchable LEC based on an electroluminescent polymer blend sandwiched between two nanocomposite carbon nanotube (CNT) stretchable electrodes.[10] When the device was heated above the glass transition temperature of the CNT-polymer composite electrodes the device could be deformed. With this technology, Pei and coworkers were able to fabricate a LEC that was stretchable up to 45% elongation when heated to 70°C.

In 2013, Pei and co-workers demonstrated that by replacing the shape memory polymer of the substrate/composite material for a composite based on silver nanowires (AgNWs) embedded in a room-temperature stretchable polyurethane acrylate (PUA) elastomer enabled the fabrication of PLECs that could sustain strains as large as 120% with continued light-emission at room temperature.[9] The emissive layer of these devices was based on a blend of the yellow light-emitting polymer Super Yellow (SY) (phenyl substituted poly(1,4-phenylene vinylene)) with ion conducting polymer additives and salt. While devices exhibited light emission up to 120% elongation (Figure 1.13), the electroluminescent performance trailed off quickly at strains above 40% elongation due to damage to the SY and PEDOT polymer layers.

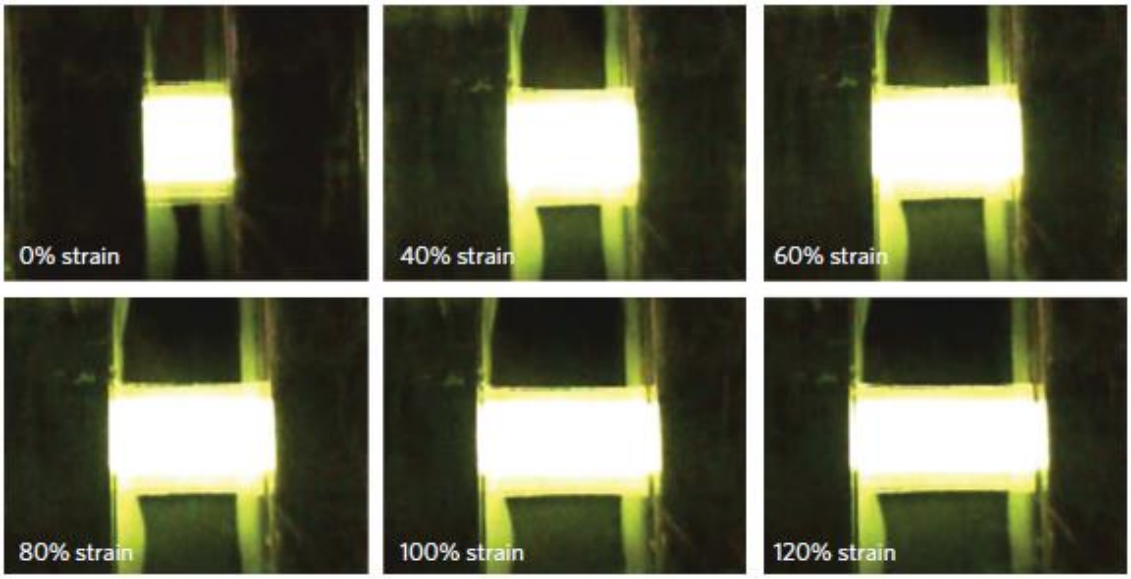

Figure 1.13. Photographs of a Super Yellow PLEC (original light-emitting area, 5.0 x 4.5 mm^2) biased at 14 V at specified strains. Adpated with permission from reference 9.

1.3.5. Sensitivity to Moisture and Oxygen

One of the main challenges remaining in the fabrication of commercial products based on LECs is their sensitivity to water and oxygen. Moisture has a detrimental effect on the iTMC materials due to ligand exchange of water for bpy in the excited state forming the hypothesized quencher molecule $Ru(bpy)_2(H_2O)_2^{2+}$.[100] Slinker et al. used Raman spectroscopy to identify an oxo-bridged dimer that quenches luminescence in $Ru(bpy)_3^{2+}$ devices.[101] When devices were run in alternating vacuum and oxygen-rich environments the current remained steady while the radiance decreased with each successive introduction of oxygen. Luminescence recovered slightly upon reapplication of vacuum (Figure 1.14). The active elements of PLECs are also sensitive to ambient air and therefore the majority of PLEC devices are fabricated and tested in inert atmosphere. Edman and co-workers demonstrated that PLEC devices operated in ambient atmosphere suffer from delamination of the metal cathode due to generation and expansion of hydrogen gas created by the reduction of water at the interface between the electrode and the emissive layer.[102]

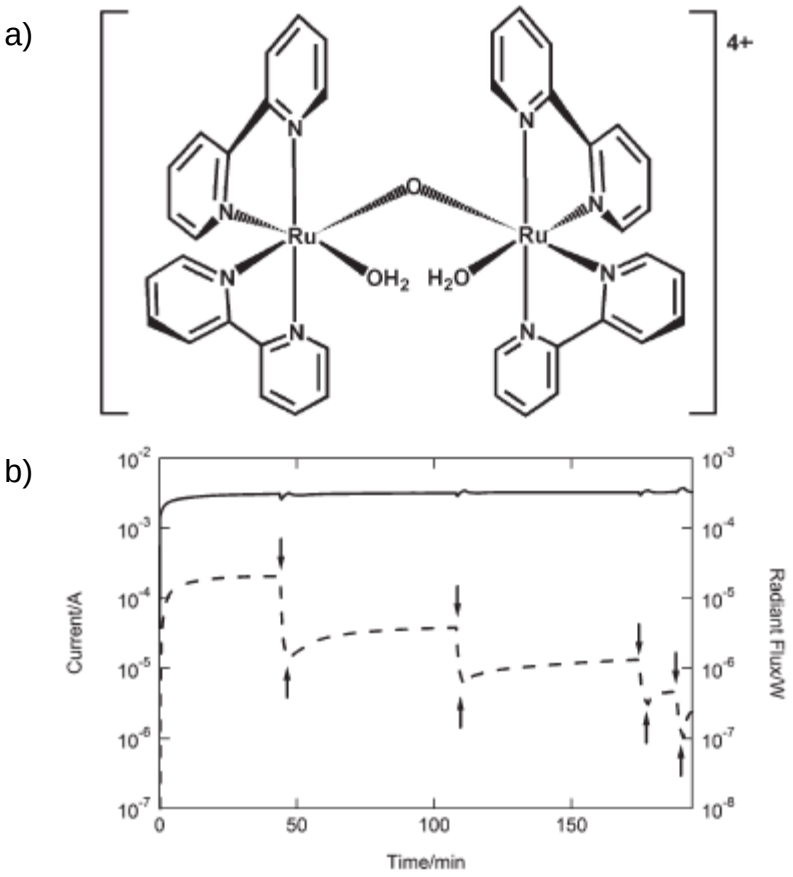

Figure 1.14. **(**a) Structure of the oxo-bridged dimer quencher species $[Ru(bpy)_2(H_2O)]_2O^{4+}$. (b) Current (solid line) and radiant flux (dotted lines) of an ITO/$Ru(bpy)_3^{2+}(PF_6^-)_2$/Au device operating at 3 V under alternating vacuum and oxygen-rich environments. The downward arrows indicate the time when oxygen was introduced into the system while the upward arrows indicate where the vacuum was restored. Adapted with permission from reference 101.

The sensitivity of LEC devices requires their operation in inert conditions or the development of encapsulation layers in order to prevent oxygen and moisture diffusion into the device. Edman and co-workers demonstrated that through the encapsulation of LECs with a glass slide and UV-curable epoxy it was possible to achieve uninterrupted lifetimes of 490 hours at high brightness.[102] Encapsulation with glass is not compatible with stretchable device technologies and this poses the additional challenge of developing stretchable barrier and encapsulating layers. Pei and co-workers acknowledge that in order for fully stretchable commercial OLED displays to be realized one of the requirements is the development of rubbery sealing materials for encapsulation.[9]

1.4. Dissertation Objectives

1.4.1. Altering the Cracking Mechanism of Metal Films on Elastomers

The first section of the dissertation aims to alter the crack propagation in metal films on compliant substrates to achieve ultrahigh elongation at electrical failure. Ultrahigh stretchable gold films that exhibit small changes in resistance with applied strain have applications in stretchable electronic devices as interconnects and electrodes while gold films that are more sensitive to applied strain and experience larger changes in resistance have applications as human motion and robotic strain sensors. As-deposited gold films on PDMS substrates fail electrically at strains of ~23% due to large cracks that propagate the full width of the film and eliminate the conductive pathway.[20] Recent approaches to alter the crack propagation through metal films on elastomer have relied on photolithography to generate a photolithographic master from which the elastomeric substrate can be molded, creating a microstructured relief on the surface of the elastomer which introduces multiple sites for crack nucleation allowing overlying metal films to achieve higher strains before electrical failure occurs. The microstructured relief alters the crack propagation in metal films enabling the fabrication of gold films that can be stretched repeatedly to 20% with high reproducibility. We seek to eliminate the need for photolithography while creating a beneficial cracking pattern that enables ultrahigh elongations of the metal film.

First, we investigate a solution-based approach to depositing aqueous emulsions of poly(vinyl acetate) (PVAc) glue onto elastomeric substrates to create a microstructured topography. By shifting to solution deposited polymers to create the rough topography we will reduce the fabrication cost of preparing metal films with ultrahigh stretchability by eliminating the need for photolithography. White glue has the additional benefits of being commercially available, low-cost and biodegradable. We investigate the effect of emulsion concentration on the change in resistance and demonstrate applications of the gold films as interconnects and human motion strain sensors. This research is presented in Chapter 2.

Second, we examine a water-soluble poly(vinyl alcohol) (PVA) polymer interlayer to demonstrate that the mechanical properties of the interlayer dictate the crack propagation through gold films. PVA is a water soluble polymer that swells in the presence of moisture and whose Young's Modulus is affected by relative humidity. We investigate the effects of relative humidity and thus the mechanical properties of the interlayer on the elongation at failure of gold. This study provides insights into the properties of the polymer interlayer required to achieve ultrahigh stretchability of gold films. Much like the work in Chapter 2, this approach to creating ultrahigh stretchable gold films is also free of lithography and is low-cost. This research is presented in Chapter 3.

1.4.2. Development of Elastomeric Emissive Layers for Large-Area Stretchable Electronics

Imagine light-emitting wallpaper that can be unrolled and laminated to walls, light-therapy treatments fabricated from soft rubbery materials that can be adhered directly to your skin, and signage that conforms to non-planar surfaces. The advent of stretchable electronics brings us closer to these types of products becoming a reality. Traditional organic light-emitting devices are comprised of a multilayer stack responsible for charge injection, charge transport and emissive recombination. In order to render these devices stretchable each thin film in the multilayer stack must be rendered stretchable which presents a challenge. In contrast, light-emitting electrochemical cells benefit from a simple device architecture where all functions of charge injection, charge transport and emissive recombination occur in a single layer. This simplifies the device architecture as now only one material must be rendered stretchable.

Up until 2010, only rigid LECs fabricated on glass had been reported. During the course of this dissertation, research into the area of stretchable electronics exploded. Pei and co-workers reported the first large-area stretchable polymer light-emitting electrochemical cell in 2011 that could be stretched to 45% when heated to 70°C.[10] Later in 2013, Pei and co-workers demonstrated a room temperature stretchable light-emitting device capable of emitting light up to 120% elongation.[9] As discussed in

Section 1.3.3. there are two types of LECs, polymer LECs and iTMC LECs. We aimed to develop stretchable LECs based on iTMC LECs.

First, we investigated the commercially available elastomer PDMS as the polymer matrix in an iTMC LEC. We fabricated rigid devices to characterize the optoelectronic properties of LECs and compared the properties to conventional iTMC LECs fabricated with glassy poly(methyl methacrylate) polymers blended in the emissive layer. We tested the mechanical properties of the LECs by fabricating LECs on stretchable substrates with thin metal anodes and a liquid metal cathode and subjecting the devices to repetitive strains of 15%. In Chapter 4, we report the first example of a room temperature stretchable light-emitting electrochemical cell based on an ionic transition metal light-emitter dispersed in an elastomeric matrix. Room-temperature stretchability is a crucial feature to enable compatibility with the human body.

Second, we investigated isobutylene-co-isoprene rubber (IIR) elastomers as the polymer matrix in iTMC LECs. We were motivated to create stretchable LECs with long lifetimes and high stability. IIR has high oxygen and moisture impermeability combined with high stretchability making it an ideal candidate for the fabrication of LECs with high stability. We investigated the phase separation between the IIR polymer matrix and the iTMC and investigated graft copolymers of IIR with poly(ethylene oxide) side chains to assist in mixing of the IIR polymer with the iTMC light emitter. We varied the molecular weight of the PEO polymer in the side chains to determine the impact of PEO content on device operation. We fabricated rigid LECs and compared their stability to the LECs fabricated in Chapter 4. We performed preliminary studies on the mechanical properties of the LECs by fabricating them on stretchable substrates and subjecting them to repetitive strains of 15%. This work is presented in Chapter 5.

1.4.3. Developing Methods to Enable the Fabrication of Conductive Metal Films on Butyl Rubber Substrates

In order prevent moisture and oxygen from penetrating into the device causing deleterious effects to device stability and performance, organic electronics require barrier and encapsulation layers. In stretchable electronic devices this requirement is especially

challenging because these additional encapsulation layers must be able to stretch with the rest of the device. Our approach to fabricating stable electronic devices involves combining water and oxygen barrier properties with stretchability in new elastomeric substrate materials in order to circumvent the need for additional barrier layers. We investigated isobutylene-co-isoprene rubber as a substrate in the fabrication of electronic devices due to its high water and oxygen impermeability.

The first step to fabricating stretchable electronic devices involves the fabrication of stretchable metal wires on the substrate in order to create circuits and device electrodes. Traditional methods to deposit metal onto elastomeric substrates involve the use of physical vapor deposition methods such as e-beam metal deposition. We demonstrate that when metal is deposited onto IIR by e-beam metal deposition, non-conductive films form due to the penetration of metal atoms into the surface of IIR resulting in a non-conductive gold/IIR composite. In order to circumvent damage to the IIR layer during e-beam metal deposition we deposited thin polymer films that protect the IIR substrate during metal deposition, allowing conductive films to be deposited onto IIR. We deposited the polymer interlayers by spin coating aqueous polymer solutions onto IIR prior to metallization. We investigate the electrical properties of the resultant gold films under strain to determine their viability as interconnects in stretchable electronic devices. This work is presented in Chapter 6.

1.5. References

[1] D.-H. H. Kim, N. Lu, R. Ma, Y.-S. S. Kim, R.-H. H. Kim, S. Wang, J. Wu, S. M. Won, H. Tao, A. Islam, K. J. Yu, T.-i. I. Kim, R. Chowdhury, M. Ying, L. Xu, M. Li, H.-J. J. Chung, H. Keum, M. McCormick, P. Liu, Y.-W. W. Zhang, F. G. Omenetto, Y. Huang, T. Coleman, J. A. Rogers, *Science* **2011**, *333*, 838-843.

[2] H. Yao, A. J. Shum, M. Cowan, I. Lähdesmäki, B. A. Parviz, *Biosensors and Bioelectronics* **2011**, *26*, 3290-3296.

[3] D.-H. H. Kim, N. Lu, R. Ghaffari, Y.-S. S. Kim, S. P. Lee, L. Xu, J. Wu, R.-H. H. Kim, J. Song, Z. Liu, J. Viventi, B. de Graff, B. Elolampi, M. Mansour, M. J. Slepian, S. Hwang, J. D. Moss, S.-M. M. Won, Y. Huang, B. Litt, J. A. Rogers, *Nature Materials* **2011**, *10*, 316-323.

[4] Y. Ming, P. B. Andrew, L. Nanshu, S. Yewang, L. Rui, C. Huanyu, A. Abid, H. Yonggang, A. R. John, *Nanotechnology* **2012**, *23*, 344004.

[5] S.-I. Park, Y. Xiong, R.-H. Kim, P. Elvikis, M. Meitl, D.-H. Kim, J. Wu, J. Yoon, C.-J. Yu, Z. Liu, Y. Huang, K.-c. Hwang, P. Ferreira, X. Li, K. Choquette, J. A. Rogers, *Science* **2009**, *325*, 977-981.

[6] S.-I. I. Park, Y. Xiong, R.-H. H. Kim, P. Elvikis, M. Meitl, D.-H. H. Kim, J. Wu, J. Yoon, C.-J. J. Yu, Z. Liu, Y. Huang, K.-c. C. Hwang, P. Ferreira, X. Li, K. Choquette, J. A. Rogers, *Science* **2009**, *325*, 977-981.

[7] T. Sekitani, H. Nakajima, H. Maeda, T. Fukushima, T. Aida, K. Hata, T. Someya, *Nature materials* **2009**, *8*, 494-499.

[8] M. S. White, M. Kaltenbrunner, E. D. Glowacki, K. Gutnichenko, G. Kettlgruber, I. Graz, S. Aazou, C. Ulbricht, D. A. M. Egbe, M. C. Miron, Z. Major, M. C. Scharber, T. Sekitani, T. Someya, S. Bauer, N. S. Sariciftci, *Nature Photonics* **2013**, *7*, 811-816.

[9] J. Liang, L. Li, X. Niu, Z. Yu, Q. Pei, *Nature Photonics* **2013**, *7*, 817-824.

[10] Z. Yu, X. Niu, Z. Liu, Q. Pei, *Advanced materials* **2011**, *23*, 3989-3994.

[11] J. Liang, L. Li, K. Tong, Z. Ren, W. Hu, X. Niu, Y. Chen, Q. Pei, *ACS Nano* **2014**, *8*, 1590-1600.

[12] D. J. Lipomi, Z. Bao, *Energy & Environmental Science* **2011**, *4*, 3314-3328.

[13] D. J. Lipomi, H. Chong, M. Vosgueritchian, J. Mei, Z. Bao, *Solar Energy Materials and Solar Cells* **2012**, *107*, 355-365.

[14] D. J. Lipomi, B. C. Tee, M. Vosgueritchian, Z. Bao, *Advanced Materials* **2011**, *23*, 1771-1775.

[15] M. Vosgueritchian, D. J. Lipomi, Z. Bao, *Advanced Functional Materials* **2012**, *22*, 421-428.

[16] M. Kaltenbrunner, G. Kettlgruber, C. Siket, R. Schwödiauer, S. Bauer, *Advanced materials* **2010**, *22*, 2065-2067.

[17] G. Kettlgruber, M. Kaltenbrunner, C. M. Siket, R. Moser, I. M. Graz, R. Schwodiauer, S. Bauer, *Journal of Materials Chemistry A* **2013**, *1*, 5505-5508.

[18] D. W. Pashley, *Proceedings of the Royal Society of London A* **1960**, 255, 218-231.

[19] Y. Xiang, T. Li, Z. Suo, J. J. Vlassak, *Applied Physics Letters* **2005**, *87*, 161910.

[20] S. P. Lacour, S. Wagner, Z. Huang, S. Suo, *Applied Physics Letters* **2003**, *82*, 2404.

[21] I. M. Graz, D. P. J. Cotton, S. P. Lacour, *Applied Physics Letters* **2009**, *92*, 071902.

[22] J. Jones, S. P. Lacour, S. Wagner, Z. Suo, *Journal of Vacuum Science & Technology A* **2004**, *22*, 1723-1725.

[23] S. P. Lacour, J. Jones, Z. Suo, S. Wagner, *Electron Device Letters, IEEE* **2004**, *25*, 179-181.

[24] P. Gorrn, W. Cao, S. Wagner, *Soft Matter* **2011**, *7*, 7177-7180.

[25] Y. Sun, W. M. Choi, H. Jiang, Y. Y. Huang, J. A. Rogers, *Nature Nanotechnology* **2006**, *1*, 201-207.

[26] D.-H. Kim, J. Xiao, J. Song, Y. Huang, J. A. Rogers, *Advanced Materials* **2010**, *22*, 2108-2124.

[27] H. C. Ko, M. P. Stoykovich, J. Song, V. Malyarchuk, W. M. Choi, C.-J. Yu, J. B. Geddes Iii, J. Xiao, S. Wang, Y. Huang, J. A. Rogers, *Nature* **2008**, *454*, 748-753.

[28] T. Li, Z. Suo, S. P. Lacour, S. Wagner, *Journal of Materials Research* **2005**, *20*, 3274-3277.

[29] D. S. Gray, J. Tien, C. S. Chen, *Advanced Materials* **2004**, *16*, 393-397.

[30] S. Xu, Y. Zhang, J. Cho, J. Lee, X. Huang, L. Jia, J. A. Fan, Y. Su, J. Su, H. Zhang, *Nature communications* **2013**, *4*, 1543.

[31] Z. Yihui, W. Shuodao, L. Xuetong, A. F. Jonathan, X. Sheng, S. Young Min, C. Ki-Joong, Y. Woon-Hong, L. Woosik, N. Sharaf Nafees, L. Bingwei, Y. Lan, H.

Keh-Chih, A. R. John, H. Yonggang, *Advanced Functional Materials* **2014**, *24*, 2028-2037.

[32] J. S. Park, M. Rezaei, W. S. Kim, *Advanced Engineering Materials* **2014**, *16*, 905-908.

[33] N. Lambricht, T. Pardoen, S. Yunus, *Acta Materialia* **2013**, *61*, 540547.

[34] S. P. Lacour, D. Chan, S. Wagner, T. Li, Z. Suo, *Applied Physics Letters* **2006**, *88*, 204103.

[35] P. Mandlik, S. P. Lacour, J. W. Li, S. Y. Chou, S. Wagner, *Electron Device Letters, IEEE* **2006**, *27*, 650-652.

[36] O. Graudejus, P. Görrn, S. Wagner, *ACS Applied Materials & Interfaces* **2010**, *2*, 1927-1933.

[37] A. P. Robinson, I. Minev, I. M. Graz, S. P. Lacour, *Langmuir : the ACS journal of surfaces and colloids* **2011**, *27*, 4279-4284.

[38] J. Liang, L. Li, K. Tong, Z. Ren, W. Hu, X. Niu, Y. Chen, Q. Pei, *ACS Nano* **2014**, *8*, 1590-1600.

[39] F. Xu, Y. Zhu, *Advanced Materials* **2012**, *24*, 5117-5122.

[40] W. Hu, R. Wang, Y. Lu, Q. Pei, *Journal of Materials Chemistry C* **2014**, *2*, 1298-1305.

[41] W. Hu, X. Niu, L. Li, S. Yun, Z. Yu, Q. Pei, *Nanotechnology* **2012**, *23*, 344002.

[42] C. Yan, J. Wang, X. Wang, W. Kang, M. Cui, C. Y. Foo, P. S. Lee, *Advanced Materials* **2014**, *26*, 943-950.

[43] J. Wang, C. Yan, W. Kang, P. S. Lee, *Nanoscale* **2014**, *6*, 10734-10739.

[44] M. Kubo, X. Li, C. Kim, M. Hashimoto, B. J. Wiley, D. Ham, G. M. Whitesides, *Advanced Materials* **2010**, *22*, 2749-2752.

[45] M. D. Dickey, R. C. Chiechi, R. J. Larsen, E. A. Weiss, D. A. Weitz, G. M. Whitesides, *Advanced Functional Materials* **2008**, *18*, 1097-1104.

[46] J.-H. So, J. Thelen, A. Qusba, G. J. Hayes, G. Lazzi, M. D. Dickey, *Advanced Functional Materials* **2009**, *19*, 3632-3637.

[47] B. J. Blaiszik, S. L. B. Kramer, M. E. Grady, D. A. McIlroy, J. S. Moore, N. R. Sottos, S. R. White, *Advanced Materials* **2012**, *24*, 398-401.

[48] S. Savagatrup, A. D. Printz, T. F. O'Connor, A. V. Zaretski, D. J. Lipomi, *Chemistry of Materials* **2014**, *26*, 3028-3041.

[49] D. J. Lipomi, J. A. Lee, M. Vosgueritchian, B. C. Tee, J. A. Bolander, Z. Bao, *Chemistry of Materials* **2012**, *24*, 373382.

[50] S. Savagatrup, A. S. Makaram, D. J. Burke, D. J. Lipomi, *Advanced Functional Materials* **2014**, *24*, 1169-1181.

[51] S. Savagatrup, A. D. Printz, D. Rodriquez, D. J. Lipomi, *Macromolecules* **2014**, *47*, 1981-1992.

[52] D. Zrnic, D. S. Swatik, *Journal of the Less-Common Metals* **1969**, *18*, 67-68.

[53] R. C. Chiechi, E. A. Weiss, M. D. Dickey, G. M. Whitesides, *Angewandte Chemie-International Ediion.* **2008**, *47*, 142-144.

[54] F. G. Gao, A. J. Bard, *Journal of the American Chemical Society* **2000**, *122*, 7426-7427.

[55] M. S. Miller, J. C. O'Kane, A. Niec, R. S. Carmichael, T. B. Carmichael, *ACS Applied Materials & Interfaces* **2013**, *5*, 10165-10172.

[56] H.-J. Kim, C. Son, B. Ziaie, *Applied Physics Letters* **2008**, *92*, 011904.

[57] J. C. McDonald, G. M. Whitesides, *Accounts of Chemical Research* **2002**, *35*, 491-499.

[58] M. J. Owen, *Why Silicones Behave Funny*, Dow Corning Corporation, **2005**.

[59] H. Hillborg, J. F. Ankner, U. W. Gedde, G. D. Smith, H. K. Yasuda, K. Wikström, *Polymer* **2000**, *41*, 6851-6863.

[60] H. Hillborg, U. W. Gedde, *Dielectrics and Electrical Insulation, IEEE Transactions on* **1999**, *6*, 703-717.

[61] M. S. Miller, G. J. E. Davidson, B. J. Sahli, C. M. Mailloux, T. B. Carmichael, *Advanced Materials* **2008**, *20*, 59-64.

[62] H. Cong, T. Pan, *Advanced Functional Materials* **2008**, *18*, 1912-1921.

[63] L. K. Massey, *Plastics Design Library: Permeability Properties of Plastics and Elastomers - A Guide to Packaging and Barrier Materials*, Elsevier Science & Technology Books, **2003**.

[64] A. Vohra, H. L. Filiatrault, N. Suhan, C. Siegers, G. J. E. Davidson, L. Ferrari, T. B. Carmichael, *unpublished work* **2011**.

[65] L. Ferrari, N. Suhan, T. B. Carmichael, C. Siegers, PCT/CA2013/001035, **2014**.

[66] T. B. Carmichael, A. Vohra, L. Ferrari, N. Suhan, PCT/CA2013/001047, **2014**.

[67] G. S. Ferguson, M. K. Chaudhury, H. A. Biebuyck, G. M. Whitesides, *Macromolecules* **1993**, *26*, 5870-5875.

[68] A. Vohra, H. L. Filiatrault, N. Suhan, C. Siegers, L. Ferrari, T. B. Carmichael, *unpublished work* **2014**.

[69] Q. B. Pei, G. Yu, C. Zhang, Y. Yang, A. J. Heeger, *Science* **1995**, *269*, 1086-1088.

[70] K. M. Maness, R. H. Terrill, T. J. Meyer, R. W. Murray, R. M. Wightman, *Journal of the American Chemical Society* **1996**, *118*, 10609-10616.

[71] J. K. Lee, D. S. Yoo, E. S. Handy, M. F. Rubner, *Applied Physics Letters* **1996**, *69*, 1686-1688.

[72] J. C. deMello, N. Tessler, S. C. Graham, R. H. Friend, *Physical Review B* **1998**, *57*, 12951-12963.

[73] J. C. deMello, J. J. M. Halls, S. C. Graham, N. Tessler, R. H. Friend, *Physical Review Letters* **2000**, *85*, 421-424.

[74] J. C. deMello, *Physical Review B* **2002**, *66*, 235210.

[75] J. D. Slinker, J. A. DeFranco, M. J. Jaquith, W. R. Silveira, Y.-W. Zhong, J. M. Moran-Mirabal, H. G. Craighead, H. D. Abruna, J. A. Marohn, G. G. Malliaras, *Nature Materials* **2007**, *6*, 894-899.

[76] Q. B. Pei, Y. Yang, G. Yu, C. Zhang, A. J. Heeger, *Journal of the American Chemical Society* **1996**, *118*, 3922-3929.

[77] D. J. Dick, A. J. Heeger, Y. Yang, Q. B. Pei, *Advanced Materials* **1996**, *8*, 985-987.

[78] D. L. Smith, *Journal of Applied Physics* **1997**, *81*, 2869-2880.

[79] M. Buda, G. Kalyuzhny, A. J. Bard, *Journal of the American Chemical Society* **2002**, *124*, 6090-6098.

[80] H. Rudmann, S. Shimada, M. F. Rubner, *Journal of Applied Physics* **2003**, *94*, 115-122.

[81] Y. Hu, J. Gao, *Journal of the American Chemical Society* **2011**, *133*, 2227-2231.

[82] P. Matyba, K. Maturova, M. Kemerink, N. D. Robinson, L. Edman, *Nature materials* **2009**, *8*, 672-676.

[83] S. van Reenen, P. Matyba, A. Dzwilewski, R. A. J. Janssen, L. Edman, M. Kemerink, *Journal of the American Chemical Society* **2010**, *132*, 13776-13781.

[84] S. Qingjiang, Y. Li, P. Qibing, *Journal of Display Technology* **2007**, *3*, 211-224.

[85] Y. Cao, G. Yu, A. J. Heeger, C. Y. Yang, *Applied Physics Letters* **1996**, *68*, 3218-3220.

[86] Y. Cao, Q. B. Pei, M. R. Andersson, G. Yu, A. J. Heeger, *Journal of the Electrochemical Society* **1997**, *144*, L317-L320.

[87] S. Panozzo, M. Armand, O. Stephan, *Applied Physics Letters* **2002**, *80*, 679-681.

[88] T. Ouisse, O. Stephan, M. Armand, J. C. Lepretre, *Journal of Applied Physics* **2002**, *92*, 2795-2802.

[89] T. Ouisse, M. Armand, Y. Kervella, O. Stephan, *Applied Physics Letters* **2002**, *81*, 3131-3133.

[90] Y. Yang, Q. B. Pei, *Journal of Applied Physics* **1997**, *81*, 3294-3298.

[91] Q. B. Pei, Y. Yang, *Journal of the American Chemical Society* **1996**, *118*, 7416-7417.

[92] H. Rudmann, S. Shimada, M. F. Rubner, *Journal of the American Chemical Society* **2002**, *124*, 4918-4921.

[93] H. Rudmann, M. F. Rubner, *Journal of Applied Physics* **2001**, *90*, 4338-4345.

[94] C. H. Lyons, E. D. Abbas, J. K. Lee, M. F. Rubner, *Journal of the American Chemical Society* **1998**, *120*, 12100-12107.

[95] E. S. Handy, A. J. Pal, M. F. Rubner, *Journal of the American Chemical Society* **1999**, *121*, 3525-3528.

[96] J. D. Slinker, A. A. Gorodetsky, M. S. Lowry, J. J. Wang, S. Parker, R. Rohl, S. Bernhard, G. G. Malliaras, *Journal of the American Chemical Society* **2004**, *126*, 2763-2767.

[97] R. D. Costa, E. Orti, H. J. Bolink, F. Monti, G. Accorsi, N. Armaroli, *Angewandte Chemie-International Edition* **2012**, *51*, 8178-8211.

[98] J. D. Slinker, C. Y. Koh, G. G. Malliaras, M. S. Lowry, S. Bernhard, *Applied Physics Letters* **2005**, *86*, 173506.

[99] J. Fang, P. Matyba, L. Edman, *Advanced Functional Materials* **2009**, *19*, 2671-2676.

[100] D. L. Pile, A. J. Bard, *Chemistry of Materials* **2005**, *17*, 4212-4217.

[101] J. D. Slinker, J.-S. Kim, S. Flores-Torres, J. H. Delcamp, H. D. Abruna, R. H. Friend, G. G. Malliaras, *Journal of Materials Chemistry* **2007**, *17*, 76-81.

[102] A. Asadpoordarvish, A. Sandstrom, S. Tang, J. Granstrom, L. Edman, *Applied Physics Letters* **2012**, *100*, 193508.

2. Chapter 2

A Self-Assembled, Low-Cost Microstructured Layer for Extremely Stretchable Gold Films

2.1. Introduction

The fabrication of electronic devices on soft, elastomeric substrates has opened the way to entirely new and exciting applications for electronics. Stretchable light-emitting devices are the building blocks for foldable and expandable display screens, electronics-integrated clothing, and wallpaper-like lighting. Other devices can be worn on the body, such as smart surgical gloves that sense temperature and electrical potentials[1] and wearable health monitors that acquire and wirelessly transmit electrophysiological data[2]. A step further leads to devices that can be integrated inside the body, such as stretchable balloon catheters that can "map and zap" damaged areas of the heart[3]. These diverse stretchable electronics applications have a common feature: Each application requires robust conductive materials for use as device electrodes and interconnects that maintain electrical conductivity during stretching. Metals are the materials of choice due to their high conductivity (the resistivity of gold at 20°C is 2.44×10^{-8} Ωm)[4]; however, the ability of metal films on elastomers to remain conductive during stretching is limited due to cracks that propagate across the metal film as it is elongated and interrupt the conductive pathway. Here, we describe a simple, low-cost approach to create a microstructured layer on the silicone elastomer polydimethylsiloxane (PDMS) that can be coated with gold. This microstructure provides numerous sites of strain localization when this structure is stretched, resulting in the initiation of numerous microcracks. Interactions between these microcracks prevent long-range crack propagation, which better preserves the conduction pathway at high strains. We demonstrate the use of these extremely stretchable gold films as stretchable device interconnects and wearable strain sensors.

Stretchable conductors are essential to all stretchable electronic devices, where they are used as device interconnects and contacts. The challenge with developing useful stretchable conductors is the trade-off that often occurs between stretchability and high conductivity. For example, composites of conductive carbon nanotubes,[5] carbon black,[6] or metallic particles embedded in a rubbery matrix,[7] sheets of graphene on PDMS,[8] and films of conducting polymers on PDMS[9] retain their conductivity to high

elongations, but the inherently high resistivity of these systems limits their utility as circuit interconnects and electrodes. The obvious way to increase the conductivity is to use metal films, which are ubiquitous as conductive elements in conventional rigid devices and circuits. Although freestanding metal films fracture at a few percent tensile strain, adhering a metal film to a compliant substrate such as PDMS can suppress the strain localization that is responsible for necking and rupture of freestanding films. Gold films on PDMS can adopt two possible topographies that result from either compressive or tensile stress during deposition of the gold film. Buckled topographies, which result from compressive stress, initially exhibit a low resistivity that increases linearly up to a critical strain (typically 10 – 20%).[10] The resistance increases dramatically beyond this critical strain. The second type of topography is thought to result from tensile stress of the gold film during deposition. These films do not exhibit buckles; rather, SEM reveals the appearance of tribranched, Y-shaped microcracks.[11],[12] The initial resistance of this film type is higher than that of the buckled type, but these structures remain conductive to high strains (60%) due to the formation of a network of microcracks that preserves an interconnected network of gold ligaments for electrical conduction. An understanding of the conditions necessary to selectively prepare gold films with either buckled or tribranch cracked topographies puzzled researchers until a recent report by Graudejus et al. revealed the complexity of this fabrication process by elucidating a number of pertinent variables, such as the gold film thickness, strength of adhesion of the gold to PDMS, deposition temperature, adhesion layer thickness, etc., that operate together to determine the gold film topography.[13]

The complex interplay of the fabrication parameters that determines the topography of gold films deposited on PDMS, and hence the elongation at electrical failure, makes the implementation of these gold/PDMS structures as interconnects and contacts in stretchable devices challenging. Thus, there is a need for gold films on elastomers that function at higher elongations while delivering highly reproducible resistance changes with stretching. Two methods that have been extensively investigated to increase the elongation to which gold/PDMS structures remain conductive rely on altering the configuration of the gold film: First, stretching the PDMS substrate before gold

deposition and then releasing the pre-stretch compresses the gold film, configuring it into a wavy structure. Stretching these structures flattens the waves, and conductivity persists to the pre-stretch elongation, up to 100%.[14] These structures can be stretched uniaxially; biaxial pre-stretching creates a random pattern of buckles in the gold film that enables radial stretching up to 40%.[15] Second, gold films configured into serpentine wire patterns on PDMS act like helical springs when the gold/PDMS structure is elongated. Serpentine gold wires accommodate elongation by twisting out of plane, which allows conductivity to persist to elongations of 70-100%, depending on the dimensions of the serpentine.[16] This approach requires lithographic patterning, and the limited surface areas of the serpentine films make them useful as device interconnects rather than electrodes. A third approach to achieving highly stretchable gold films that has received less attention uses topographical features on the surface of the underlying PDMS to localize the microcracks that form in the gold during stretching, which better preserves the conduction pathway when the sample is elongated compared to analogous gold films on flat PDMS. Geometrical patterns of topographical features such as nanoscale pyramids[17] or micron-scale circular pillars[18] can be fabricated by molding PDMS against lithographically-fabricated masters. The resistance, R, of a thin gold film deposited on a PDMS substrate bearing an array of protruding nanoscale pyramids on the surface, for example, increases to ~1.6 x the initial resistance (R_0) at 25% elongation, whereas the resistance of a gold film on flat PDMS climbs to ~4.3R_0 at the same elongation.[17] Although both of these studies demonstrate the potential of using topography to boost performance by strain localization, the use of lithography to create the topographical patterns is not suitable for low-cost manufacturing, which is often a concern with high-volume, lightweight electronics. One method to avoid the use of lithography uses rough polycarbonate substrates produced by sandblasting as masters to prepare PDMS substrates with rough surfaces.[19] The random peaks and valleys on the PDMS surface provide numerous sites of strain localization, which is where microcracks initiate. These microcracks continue to nucleate at larger deformations compared to flat PDMS substrates, resulting in a non-percolating crack pattern due to an entangling interaction of the microcracks. Gold films on rough PDMS substrates remain conductive to 40% elongation, at which point R is ~1000R_0.

Here, we report a low-cost, bottom-up and organic solvent-free approach to creating topographical features on a PDMS substrate that provide numerous sites of strain localization. Our method uses low-cost spin-coating to deposit an aqueous emulsion of poly(vinyl acetate) (PVAc)– common, commercially available white school glue diluted in water – onto an oxidized PDMS surface. The resulting surface consists of a self-assembled, random array of clustered PVAc globules, which can be uniformly coated with gold by e-beam evaporation. The resulting PDMS/glue/gold layered structures remain highly conductive to 60% elongation.

2.2. Experimental Section

2.2.1. Materials

Poly(dimethylsiloxane) (PDMS) (Sylgard 184) was obtained from Dow Corning, Midland, MI. All other chemicals were obtained from Sigma-Aldrich and were used as received. Elmer's Glue-All was obtained from Elmer's Products, Inc (Westerville, Ohio).

2.2.2. Preparation of PDMS Substrates

PDMS (Dow Corning Sylgard 184) was prepared by mixing prepolymer with curing agent in a 10:1 w:w ratio and stirring, followed by degassing under vacuum. The prepolymer mixture was cured in a polystyrene Petri dish to obtain PDMS samples with smooth surfaces.

2.2.3. Oxidation of PDMS Substrates

PDMS substrates were treated with air plasma at medium discharge setting for 10 seconds at an air pressure of 10 psig (flow rate of 32 mL/min). (Harrick Plasma PDC32-G coupled to a PlasmaFlo gas flow mixer).

2.2.4. Glue Interlayer Deposition on PDMS

Glue solutions were prepared by diluting Glue-All in water at room temperature until dissolved. Three emulsion concentrations were employed: 1:1 v/v water:glue, 3:1 v/v

water:glue and 5:1 v/v water:glue. Oxidized PDMS substrates were spin coated with the glue solution at 1000 rpm for 1 minute followed by 2000 rpm for 1 minute (Laurell Technologies WS-400A-6NPP). We estimated the surface coverage of the glue diluations on PDMS by calculating the area occupied by clusters measuring ≥ 10 μm in diameter in a 500 x magnificiation SEM image with a total area of 150 μm x 150 μm.

2.2.5. Metal Deposition on PDMS

An e-beam evaporator was used to deposit 30 Å titanium, followed by 250 Å gold, onto PDMS/glue substrates at a rate of 0.3 Å/s and 1 Å/s respectively, under high vacuum (10^{-6} mbar).

2.2.6. Strain Sensor Fabrication

The 3:1 v/v water:glue emulsion was spin coated onto an oxidized 1.5 cm x 3.5 cm piece of PDMS followed by e-beam metal deposition of a 30-Å-thick titanium adhesion layer and 250-Å-thick gold. These gold films were mounted to a Band-Aid for use as a human motion strain sensor using PDMS pre-polymer as the adhesive (Sylgard 184, Dow Corning) followed by curing for one hour. To facilitate connection to the sourcemeasure unit, strips of aluminum foil were glued to each extremity of the gold-coated PDMS/glue samples using a conductive silicone paste which was allowed to set overnight (Effective Shielding, West Chester PA).

2.2.7. Characterization

Optical characterization was performed using an Olympus BX51 microscope equipped with an Olympus Q-Color3 digital camera. A micro-vice stretcher (S. T. Japan, USA, Inc.) was mounted to the microscope stage and samples were clamped in the stretcher to obtain microscope images of stretched samples. Scanning electron microscopy was carried out on a Hitachi S-4500 scanning electron microscope. Samples were stretched manually and secured with copper tape to the specimen stage. Prior to imaging, stretched samples and non-metallized samples of glue on PDMS were coated with 3-5 nm Au using a Hummer VI sputtering system to prevent charging. Atomic force microscopy was

carried out using the dynamic force mode of a Park Systems XE-100 AFM. A silicon cantilever with a nominal spring constant of 40 N/m, resonant frequency of 300 kHz and tip radius of 10 nm was used. Images were collected from three spots on each sample in an area of 40 μm × 40 μm. For electrical characterization, gallium-indium eutectic (EGaIn) (~0.01 mL) was first deposited by syringe to the corners (for sheet resistance measurements) or ends (for resistance measurements) of the gold surface to facilitate electrical contact. A Keithley 2601A Sourcemeter and LabTracer software applied a voltage sweep of -0.5 V to 0.5 V with a 10 ms delay, and 101 data points of current were measured. Data sets consisted of three samples, and the average was reported. For electrical measurements under strain, samples were clamped in a micro-vice stretcher (S.T. Japan, USA, Inc.) and stretched in 5% increments while the resistance was measured. PDMS/glue/gold samples used in interconnect studies were mounted in the microvice stretcher with EGaIn drops providing soft contact to electrical probes. The gold wire was connected in series to the Keithley sourcemeter and a green LED. The LED was driven at a current bias of 20 mA. Strain sensors on Band-aids were adhered to the thumb and resistance was measured by applying a 1 V DC bias and measuring the current response as a function of bending strain. For video S2.1, the strain sensor was connected to a breadboard and an Arduino Uno singleboard controller in order to control which LEDs light up due to changes in resistance in the sensor. The code to program the Arduino was adapted from: http://arduinobasics.blogspot.ca/2011/05/arduino-uno-flex-sensor-and-leds.html (Available in Supplementary Information). The Arduino's analog-to-digital converter converts the input voltage (from 0-5V) to a digital value between 0 and 1023. The digital values dictate the output corresponding to an LED numbered from 4-13 which controls which LEDs turn on.

2.3. Results and Discussion

2.3.1. Characterization of Microstructured Glue Films on PDMS

White school glue is a synthetic thermoplastic adhesive consisting of an emulsion of PVAc in water, along with proprietary additives to stabilize the emulsion. We diluted white glue with water to three different concentrations (1:1, 3:1, and 5:1 v/v water:glue)

to reduce the viscosity of the glue and the concentration of colloidal PVAc particles in the suspension. Dark-field optical micrographs of liquid films of the three glue concentrations show the globules suspended in water; the largest visible globules are ~ 2-3 μm in diameter (Figure S2.1). We spin-coated each of the three formulations onto PDMS substrates oxidized for 10 s in an air plasma to enable wetting. Scanning electron microscopy (SEM) and tapping-mode atomic force microscopy (AFM) reveal that the glue emulsion forms a microstructured coating on the PDMS surface that consists of clustered globules of PVAc (Figure 2.1). The density of these globules depends on the concentration of glue in the emulsion. At the highest concentration of glue (PDMS/glue$_{1:1}$), the surface of the PDMS substrate is homogeneously covered in densely packed glue globules that range in diameter from ~8 μm to < 1 μm (Figure 2.1a, b). The RMS roughness of this coating is 350.5 nm ± 21.87 nm. SEM cross sections (Figure S2.2a) reveal that the glue$_{1:1}$ coating is continuous and ~ 2-3.5 μm in thickness. Increasing the water:glue ratio to 3:1 and 5:1 produces surfaces that are not uniformly coated in glue globules. Using 3:1 water:glue (PDMS/glue$_{3:1}$) produces a surface comprised of individual and clustered globules of PVAc glue randomly distributed over the PDMS surface (Figure 2.1c, d). The largest clusters are ~ 40-60 μm in diameter which exceeds the scanning range of the AFM instrument. The largest individual clusters within the instrument range were measured to be ~ 30 μm in diameter and ~ 3 - 4 μm in height (Figure S2.3a, b). Reducing the concentration of the glue further to 5:1 water:glue (PDMS/glue$_{5:1}$) produces a surface comprised of sparsely populated PVAc clusters that are smaller than those of PDMS/glue$_{3:1}$ (Figure 2.1e, f) with the largest clusters having a diameter of ~ 40 μm and height of ~ 2 - 3 μm (Figure S2.3c, d). SEM cross sections show that glue$_{3:1}$ and glue$_{5:1}$ coatings are not as uniform in thickness as glue$_{1:1}$; instead, these surfaces consist of clusters of PVAc globules separated by regions of either bare PDMS or a thin (~ 0.4 μm) polymer coating (Figure S2.2c, d). Whereas the PVAc globules in the glue$_{1:1}$ coating cover 100% of the PDMS surface, we estimate that the coverage of the glue$_{3:1}$ and glue$_{5:1}$ coatings is lower, at ~ 44% and ~ 17%, respectively.

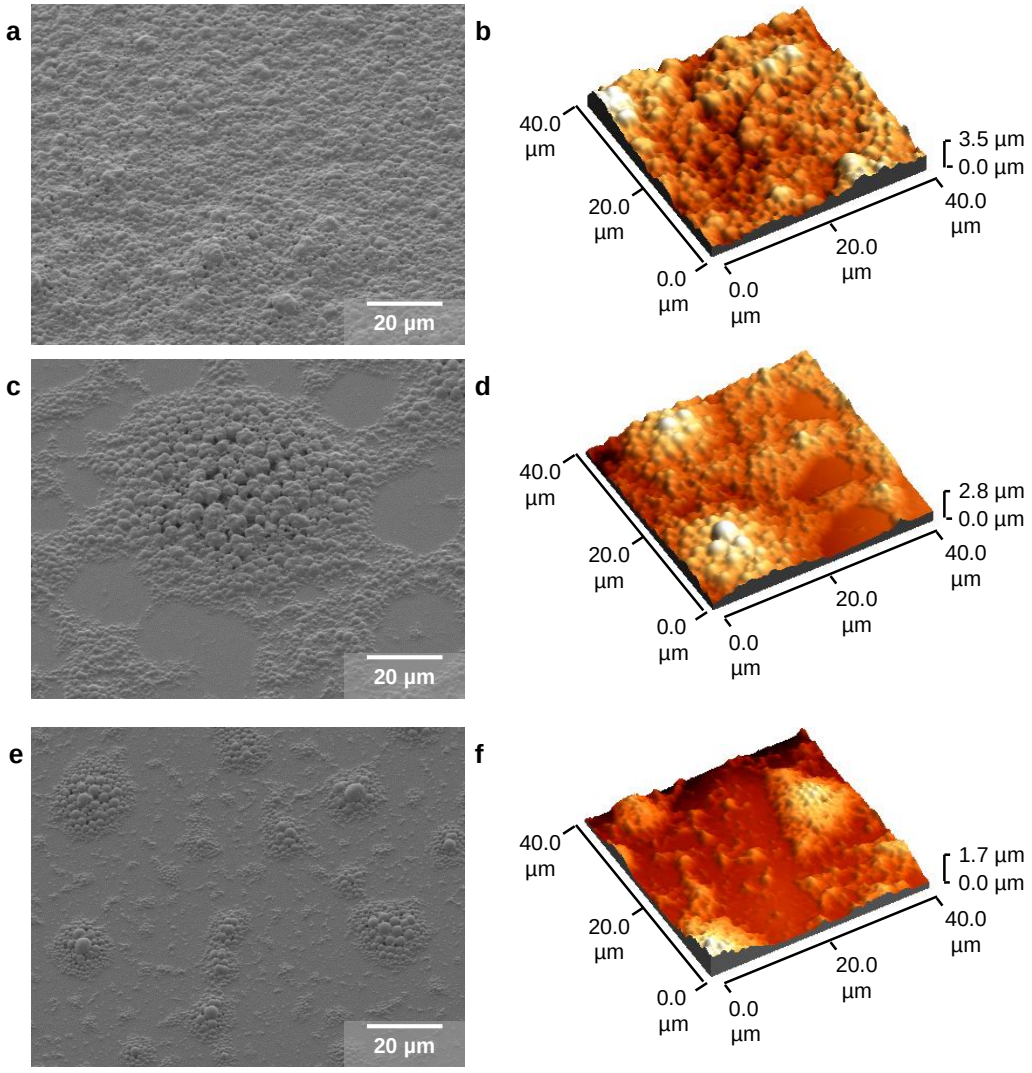

Figure 2.1. SEM and tapping-mode AFM images of (a, b) PDMS/glue$_{1:1}$; (c, d) PDMS/glue$_{3:1}$; (e, f) PDMS/glue$_{5:1}$.

The structural difference between the continuous glue$_{1:1}$ coating and the patchy glue$_{3:1}$ and glue$_{5:1}$ coatings becomes relevant when PDMS/glue structures are stretched. Although glue coatings form compliant layers on PDMS due to the rubbery nature of PVAc (the main component of white glue), the Young's modulus of glue (0.6 GPa for Elmer's glue[20]; 0.75 GPa for pure PVAc[21]) is higher than that of PDMS (1 – 2 MPa)[22]. All three PDMS/glue structures could be stretched to 60% elongation without visible delamination; however, optical microscope images reveal that stretching causes the formation of zigzag microscale cracks in the glue$_{1:1}$ coating due to the high Young's modulus of the continuous glue coating (Figure S2.4a). The random peaks and valleys of

the rough glue$_{1:1}$ surface provide numerous sites for strain localization, which initiates the microcracks that relieve the strain. These cracks increase in number as the elongation increases from 20% to 60%. In contrast, glue$_{3:1}$ and glue$_{5:1}$ coatings do not exhibit cracks (Figure S2.4b, c); instead, the regions between the PVAc glue islands likely absorb the strain and allow the PVAc clustered globules to behave like rigid islands.

2.3.2. Density of Microclusters Affects Crack Propagation in Gold Films on PDMS/Glue

We used an e-beam evaporator to coat PDMS/glue surfaces with a 30-Å-thick layer of titanium as an adhesion promoter followed by a 250-Å-thick layer of gold. SEM micrographs show that the metal uniformly coats the surface, yielding a gold-coated surface with glue globules with dimensions that are similar to the uncoated glue films (Figure S2.5). Despite the differences in topography of PDMS/glue surfaces, the sheet resistance values (R_s) of these gold films are similar to 250-Å-thick gold films deposited on glass (Table 2.1).

Table 2.1. Sheet resistance (R_s) of 250-Å-thick-gold films on glass and PDMS/glue substrates.

Substrate	R_s (Ω/□)
Glass	1.8 ± 0.1
PDMS/glue$_{1:1}$	2.5 ± 0.2
PDMS/glue$_{3:1}$	2.4 ± 0.2
PDMS/glue$_{5:1}$	1.9 ± 0.2

The topography of the glue layer has a pronounced effect on how cracks initiate and propagate in the overlying gold film of PDMS/glue/gold structures when these structures are subjected to linear strain. We collected optical microscope images of PDMS/glue$_{1:1}$/gold, PDMS/glue$_{3:1}$/gold, and PDMS/glue$_{5:1}$/gold structures at intervals of 5% strain and present images taken at 5, 25, and 60% strain in Figure 2.2. For all three

glue concentrations, the cracks become more numerous as the strain increases. The initiation of new cracks as the strain increases can be attributed to the topography of the PVAc glue globules, which provide sites for strain localization and crack nucleation. The manner in which the number of cracks increases with strain, therefore, is related to the coverage of PVAc glue globules on the PDMS surface. The higher coverage of PVAc glue globules on PDMS/glue$_{1:1}$ (100% coverage) and PDMS/glue$_{3:1}$ (44% coverage) leads to an increased number of cracks compared to PDMS/glue$_{5:1}$ (17% coverage), which is particularly apparent in the optical images taken at 60% strain (Figure 2.2c, f, i). Despite this difference, the cracking patterns of gold on all three glue formulations are distinct from those of gold films deposited on smooth PDMS without a glue layer (PDMS/gold). Smooth PDMS provides far fewer defect sites on the surface for strain localization and crack nucleation. The paucity of crack nucleation events results in the appearance of relatively few cracks when the sample is stretched to 5% (Figure 2.3a), but these cracks propagate through the field of view of a 10x microscope objective (that is, at least 1000 μm) to relieve strain. Although the number of cracks increases with further elongation to 30% (Figure 2.3b), the appearance of long, straight cracks is maintained. In contrast, the rapid increase in the density of small cracks of PDMS/glue/gold structures effectively relieves strain, and as the sample is elongated the cracks encounter and interact with one another. A crack approaching another crack enters a relaxed zone where the strain has already been relieved. Consequently, the crack stops propagating, resulting in a film comprised of numerous small cracks rather than long straight cracks.

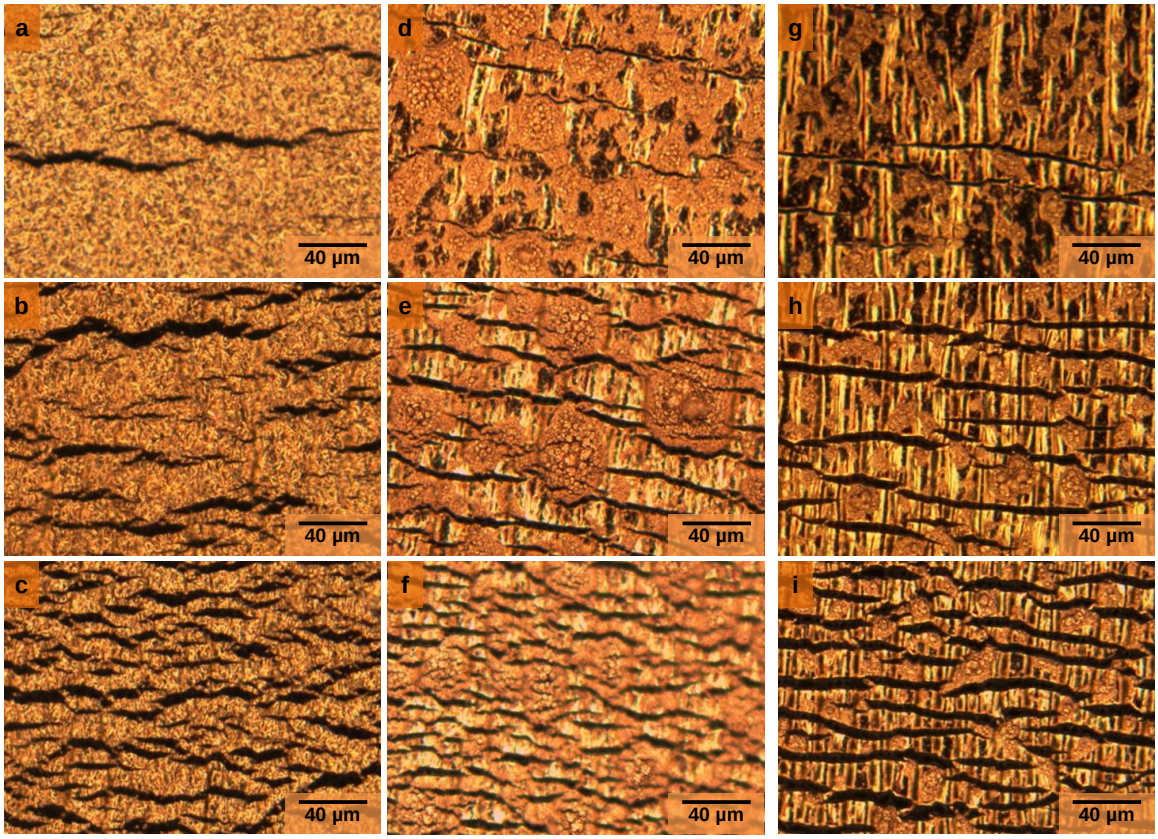

Figure 2.2. Evolution of cracks on PDMS/glue/gold structures with stretching. Optical images captured at 5% (top row), 25% (middle row), and 60% (bottom row) strain for (a-c) PDMS/glue1:1/gold; (d-f) PDMS/glue3:1/gold; (g-i) PDMS/glue5:1/gold.

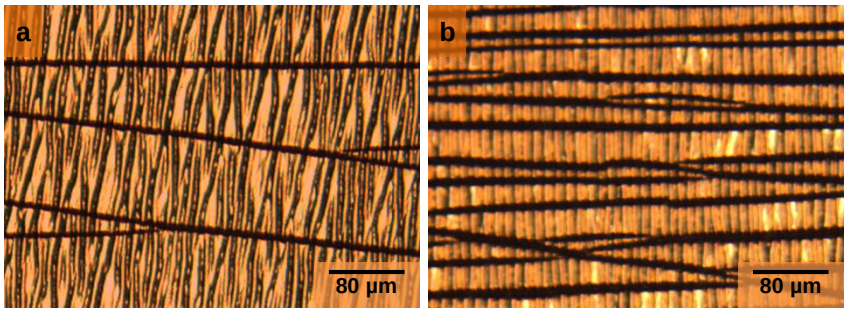

Figure 2.3. Evolution of cracks on PDMS /gold structures with stretching. Optical images captured at (a) 5% strain and (b) 30% strain.

The difference in cracking patterns between PDMS/glue$_{1:1}$/gold, PDMS/glue$_{3:1}$/gold, PDMS/glue$_{5:1}$/gold, and PDMS/gold structures can be qualitatively, and to some extent quantitatively, correlated to resistance measurements of these structures as a function of linear strain. Figure 2.4 displays the change in resistance of PDMS/glue/gold structures

with stretching. R/R_0 of gold films deposited on smooth PDMS without a glue layer (inset in Figure 2.4) increases rapidly with stretching and reaches 360 at 25% elongation. We (and others)[10],[11] attribute the resistance increase to the long, straight cracks that propagate through the film and severely impede conductivity. The use of a glue layer, however, both dramatically lowers the change in resistance and increases the elongation at failure. Resistance data recorded for PDMS/glue$_{1:1}$/gold, PDMS/glue$_{3:1}$/gold, and PDMS/glue$_{5:1}$/gold show that increasing the coverage of glue globules on the PDMS surface reduces the change in resistance that occurs with stretching. The highest glue coverage of 100% in PDMS/glue$_{1:1}$/gold structures ultimately causes the smallest change in resistance (R/R_0 = 23 at 65%), whereas the lowest glue coverage of ~ 17% in PDMS/glue$_{5:1}$/gold structures causes a change in resistance that is ten times higher (R/R_0 = 243 at 70%). Thus, the most "defective" surface – i.e., the surface with the greatest number of defect sites for strain localization – causes the lowest increase in R. This defect site density also influences R/R_0 values at strain intervals up to the point of failure. At 5% strain, the emergence of cracks causes the resistance of the three PDMS/glue/gold structures to increase similarly ($R/R_0 < 3$). The microscope images of Figure 2.2a, d, and g show that the gold films bear cracks of various lengths, the longest of these being ~ 100 μm. On PDMS/glue$_{3:1}$/gold and PDMS/glue$_{5:1}$/gold, the cracks appear to initiate and terminate at the edges of the isolated glue globule clusters; this guiding of how the cracks propagate results in cracks that are rather straight. In contrast, the cracks on PDMS/glue$_{1:1}$/gold take on a more irregular, jagged shape due to the consistently rough topography of this surface. This surface is also punctuated by a few cracks that are 8-10 μm in width, whereas the cracks on PDMS/glue$_{3:1}$/gold and PDMS/glue$_{5:1}$/gold are uniformly narrow (< 5 μm in width). At 25% strain, R/R_0 increases to ~ 30 for PDMS/glue$_{3:1}$/gold and PDMS/glue$_{5:1}$/gold. The microscope images in Figure 2.2e and h show the appearance of new cracks to relieve the strain; at the same time, there is an appreciable and uniform widening of the cracks to ~ 5-7 μm. Furthermore, there is a considerable lengthening of cracks on PDMS/glue$_{5:1}$/gold to > 200 μm. This crack propagation visible in SEM micrographs of films stretched to 30% elongation relates to the low density of topographical features on this surface to localize the strain and initiate cracks, which leads to fewer interactions between cracks that limit

crack propagation (Figure S2.6b, c). We postulate that the lengthening and widening of the cracks on PDMS/glue$_{3:1}$/gold and PDMS/glue$_{5:1}$/gold contributes to the increase in resistance. This idea is supported by the microscope image of PDMS/glue$_{1:1}$/gold at 25% elongation (Figure 2.2b), which retains a low R/R_0 value of 6. This gold film exhibits an increase in the number of cracks, similar to PDMS/glue$_{3:1}$/gold and PDMS/glue$_{5:1}$/gold, without any appreciable lengthening of the cracks. Although there is widening of the cracks, the surface is dominated by short, irregular cracks separated by regions of uncracked gold that constitute the conduction pathway. The irregularity of cracks in gold films on PDMS/glue$_{1:1}$ is further evidenced in SEM micrographs of the film stretched to 30% (Figure S2.6a). At 60% strain, the three sample types are all dissimilar: The resistance of PDMS/glue$_{1:1}$/gold remains rather low ($R/R_0 = 20$), the resistance of PDMS/glue$_{3:1}$/gold increases to $R/R_0 = 107$, and the resistance of PDMS/glue$_{5:1}$/gold increases dramatically to $R/R_0 = 171$. Differences in the crack dimensions account for the observed differences in resistance change. Although the most conductive structure, PDMS/glue$_{1:1}$/gold, develops new, small cracks to relieve the strain, the structure preserves ~ 30-μm-wide strips of gold between the cracks that undoubtedly help maintain conductivity (Figure 2.2c). The preservation of these gold strips can be attributed to the numerous cracks in the gold film that interact with one another, limiting the propagation length: A propagating crack has a high probability of entering into the relaxed zone near another crack where strain is relieved, thus halting propagation. Similarly, PDMS/glue$_{3:1}$/gold also develops small, new cracks; however, the continuous gold strips separating the cracks are narrower (~ 10-15 μm), which increases the resistance (Figure 2.2f). PDMS/glue$_{5:1}$/gold is distinguished from the other two structure types by long cracks that become wider in response to the strain (Figure 2.2i). At 60% strain, these cracks can reach ~ 250 μm in length, with a typical width of ~ 50 μm. These long, wide cracks dominate the gold structure, leaving a limited conductive pathway through the film. Notwithstanding the differences in resistance changes in response to strain, PDMS/glue$_{1:1}$/gold, PDMS/glue$_{3:1}$/gold, and PDMS/glue$_{5:1}$/gold do remain conductive to 65-70% elongation, and ultimately fail due to fracture through the PDMS/glue/gold stack. This fracture is likely due to the extension of cracks from the gold layer into the PDMS

substrate caused by the large mismatch in elastic properties between metal, glue, and PDMS.[23]

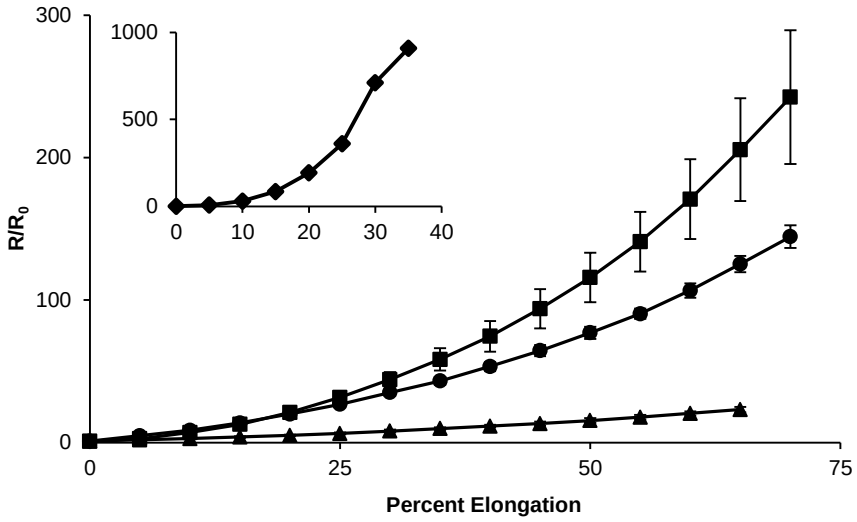

Figure 2.4. Plot of normalized resistance as a function of linear strain for PDMS/glue$_{1:1}$/gold (triangles), PDMS/glue$_{3:1}$/gold (circles), PDMS/glue$_{5:1}$/gold (squares), and PDMS/gold (inset).

2.3.3. Application of Stretchable Gold Films on PDMS/Glue as Device Interconnects

The high conductivity of PDMS/glue$_{1:1}$/gold that persists with stretching to 65% elongation makes these films suitable as interconnects in stretchable electronic devices. As a demonstration, we constructed circuits consisting of 1.5 cm x 2.5 cm stretchable gold interconnects connected in series with a source-measure unit and a green LED (Figure 2.5a). The LED demonstrates a voltage drop of 2.2 V when biased with a current of 20 mA. We applied the 20 mA current bias to the circuit, and measured the total voltage drop (V_T) as the interconnect was stretched from 0% - 50% strain. The stretchable gold interconnect acts as a variable resistor (R_{var}) whose resistance rises with increased applied strain. As the interconnect is stretched, the voltage required to drive the LED increases due to the increasing voltage drop across the gold film. V_T as a function of interconnect elongation is plotted in Figure 2.5b for interconnects fabricated from PDMS/glue$_{1:1}$/gold and PDMS/glue$_{3:1}$/gold. At 0% strain, V_T is 2.4 V for both

PDMS/glue$_{1:1}$/gold and PDMS/glue$_{3:1}$/gold. For the PDMS/glue$_{1:1}$/gold interconnect, V_T increases with increasing strain, until it reaches 5.0 V at 50% strain. In contrast, V_T increases more quickly for the PDMS/glue$_{3:1}$/gold interconnect, and reaches 6.5 V at 50% elongation. The steeper slope of the V_T versus percent elongation for PDMS/glue$_{3:1}$/gold is consistent with the plots of R/R_0 versus elongation presented in Figure 2.4.

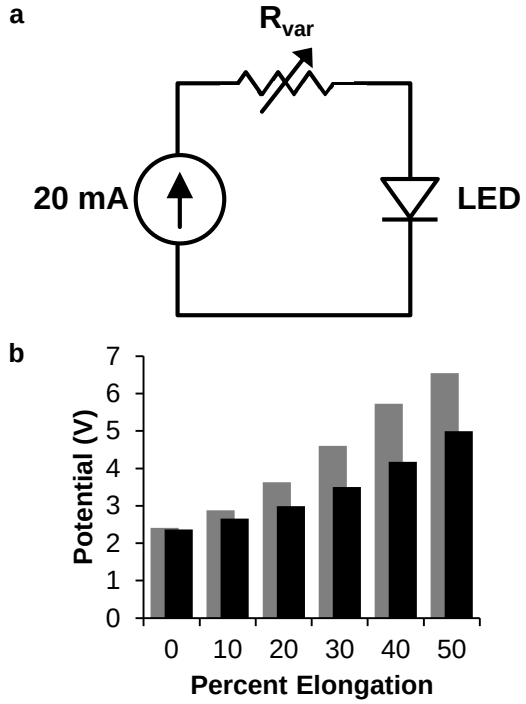

Figure 2.5. Demonstration of PDMS/glue$_{1:1}$/gold and PDMS/glue$_{3:1}$/gold as stretchable interconnects. (a) Circuit diagram (b) Plot of V_T as a function of percent elongation for PDMS/glue$_{1:1}$/gold (black bars) and PDMS/glue$_{3:1}$/gold (grey bars).

2.3.4. Demonstration of Stretchable Gold Films on PDMS/Glue as Human Motion Strain Sensors

The greater change in resistance with stretching exhibited by PDMS/glue$_{3:1}$/gold compared to PDMS/glue$_{1:1}$/gold indicates that the former structures are more sensitive to changes in strain, which makes them potentially useful as soft strain sensors. Strain sensors detect mechanical deformation through a change in electrical resistance. Metal foils patterned on a flexible plastic backing are a common gauge type. The gauge is mounted on the object to be monitored, and deformation of the object translates into a

change in electrical resistance of the gauge. The sensitivity of the gauge to mechanical deformation is quantified as the gauge factor (GF), which relates the fractional change in resistance to the mechanical strain:

$$GF = \frac{\Delta R/R_0}{\varepsilon}$$

Conventional metal foil strain sensors have a GF of 2 to 5, and can stretch to a maximum of 5% before electrical failure.[24] Biomechanics, physiology, kinesiology, and robotics applications, however, require soft strain sensors that can conform easily to the curves of the human body or over robotic joints to allow unimpeded motion, while at the same time being capable of detecting large strains.[6] Metals deposited on elastomers – a soft version of the classic metal strain gauge – are a possible solution. The limited stretchability of gold films on PDMS hinders their use as human motion strain sensors. In contrast, PDMS/glue$_{3:1}$/gold structures are highly stretchable, compatible with the soft nature of the human body, and sensitive to changes in strain. We fabricated a simple PDMS/glue$_{3:1}$/gold strain sensor as a proof-of-concept by attaching a 1.5 cm x 3.5 cm PDMS/glue$_{3:1}$/gold structure to an adhesive bandage and attaching electrical contacts using conductive silicone paste. The bandage was then adhered along the length of a thumb (Figure 2.6a). We applied a voltage of 0.5 V and recorded the change in resistance as the thumb was bent (Figure 2.6b) and straightened repetitively. Bending the thumb fully resulted in a tenfold increase in resistance (Figure 2.6c); the resistance returned to the initial value upon straightening of the thumb. The initial resistance was recovered after six cycles of the bending/straightening process. Furthermore, gold films on PDMS/glue$_{3:1}$ demonstrate excellent durability exhibiting negligible changes in resistance after 100 strain cycles of 15% (Figure S2.7). While gold films deposited on PDMS/glue$_{5:1}$ exhibit higher sensitivity to strain than those deposited on PDMS/glue$_{3:1}$ (Figure 2.4) the higher standard deviation in normalized resistance exhibited by the former prohibits their use as reproducible strain sensors. The action of these thumb-mounted strain sensors can also be visualized using a series of LEDs interfaced by an Arduino singleboard microcontroller (Video S1 in the supporting information). When the thumb is bent, the analog output voltage drop (0-5 V) is converted to a digital number (0-

1023) via the Arduino's analog-to-digital converter. The digital value controls the number of LEDs that light up on the breadboard: As the strain increases, more LEDs light up. Based on the data presented in Figure 2.4, the tenfold increase in resistance produced by bending the thumb corresponds to a strain of approximately 15%; this data furthermore shows that these structures are capable of detecting much larger strains caused by human or robotic motion. Figure 2.4 also indicates that the output of these strain sensors is nonlinear in resistance versus strain, similar to semiconductor strain sensors. The GF thus is not a constant as the strain takes place; rather, it increases from 0.96 at 5% strain to 2.01 at 70% strain.

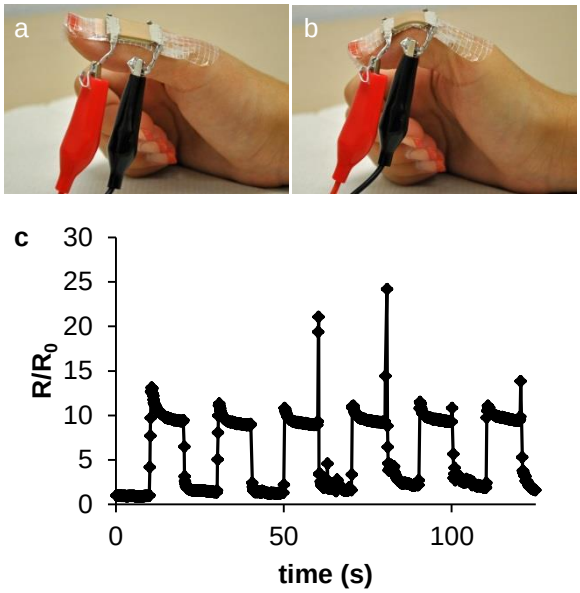

Figure 2.6. Demonstration of PDMS/glue$_{3:1}$/gold as a wearable strain sensor. Photograph of the sensor mounted on a human thumb in (a) straightened (unstrained) and (b) bent (strained) positions. (c) Plot of normalized resistance as a function of time corresponding to six bending/straightening cycles.

2.4. Conclusions

We have demonstrated a simple, low-cost, and green approach to fabricate microstructured PDMS surfaces that produce highly stretchable and conductive gold films. The PVAc glue used to create the microstructure is low cost, commercially available and can be deposited from aqueous solution to avoid the use of harmful organic solvents. By controlling the concentration of the PVAc globules in the emulsion we can tune the change in resistance in the gold films deposited on the surface when they are subjected to strain. High concentrations of glue (PDMS/glue$_{1:1}$) result in small changes in resistance making these wires ideal as stretchable interconnects. Gold films deposited onto films fabricated using more dilute glue solutions, such as PDMS/glue$_{3:1}$, have higher sensitivities, which make them potentially useful as soft, stretchable versions of conventional metal foil strain sensors. These soft sensors are highly conformable and can detect strains up to 70%, which makes them good candidates for low-cost motion detection across both human and robotic joints.

2.5. References

[1] M. Ying, A. P. Bonifas, N. Lu, Y. Su, R. Li, H. Cheng, A. Ameen, Y. Huang, J. A. Rogers, *Nanotechnology* **2012**, *23*, 344004.

[2] S. Xu, Y. Zhang, L. Jia, K. E. Mathewson, K. I. Jang, J. Kim, H. Fu, X. Huang, P. Chava, R. Wang, S. Bhole, L. Wang, Y. J. Na, Y. Guan, M. Flavin, Z. Han, Y. Huang, J. A. Rogers, *Science* **2014**, *344*, 70-74.

[3] D. H. Kim, N. S. Lu, R. Ghaffari, Y. S. Kim, S. P. Lee, L. Z. Xu, J. A. Wu, R. H. Kim, J. Z. Song, Z. J. Liu, J. Viventi, B. de Graff, B. Elolampi, M. Mansour, M. J. Slepian, S. Hwang, J. D. Moss, S. M. Won, Y. G. Huang, B. Litt, J. A. Rogers, *Nature Materials* **2011**, *10*, 316-323.

[4] J. D. Cutnell, K. W. Johnson, *Physics*, John Wiley & Sons, Incorporated, **2000**.

[5] T. Sekitani, H. Nakajima, H. Maeda, T. Fukushima, T. Aida, K. Hata, T. Someya, *Nature. Materials* **2009**, *8*, 494-499.

[6] N. Lu, C. Lu, S. Yang, J. Rogers, *Advanced Functional Materials* **2012**, *22*, 4044-4050.

[7] M. Niklaus, H. R. Shea, *Acta Materialia* **2011**, *59*, 830-840.

[8] K. S. Kim, Y. Zhao, H. Jang, S. Y. Lee, J. M. Kim, J. H. Ahn, P. Kim, J. Y. Choi, B. H. Hong, *Nature* **2009**, *457*, 706-710.

[9] D. J. Lipomi, J. A. Lee, M. Vosgueritchian, B. C. K. Tee, J. A. Bolander, Z. Bao, *Chemistry of Materials* **2012**, *24*, 373-382.

[10] S. P. Lacour, S. Wagner, Z. Huang, Z. Suo, *Applied Physics Letters* **2003**, *82*, 2404.

[11] S. P. Lacour, J. Jones, S. Wagner, L. Teng, S. Zhigang, *Proceedings of the IEEE* **2005**, *93*, 1459-1467.

[12] S. P. Lacour, D. Chan, S. Wagner, T. Li, Z. Suo, *Applied Physics Letters* **2006**, *88*, 204103.

[13] O. Graudejus, P. Görrn, S. Wagner, *ACS Applied Materials & Interfaces* **2010**, *2*, 1927-1933.

[14] J. Jones, S. P. Lacour, S. Wagner, Z. Suo, *Journal of Vacuum Science & Technology A* **2004**, *22*, 1723-1725.

[15] P. Gorrn, W. Cao, S. Wagner, *Soft Matter* **2011**, *7*, 7177-7180.

[16] D. Brosteaux, F. Axisa, M. Gonzalez, J. Vanfleteren, *Electron Device Letters, IEEE* **2007**, *28*, 552-554.

[17] P. Mandlik, S. P. Lacour, J. W. Li, S. Y. Chou, S. Wagner, *Electron Device Letters, IEEE* **2006**, *27*, 650-652.

[18] A. P. Robinson, I. Minev, I. M. Graz, S. p. P. Lacour, *Langmuir* **2011**, *27*, 4279-4284.

[19] N. Lambricht, T. Pardoen, S. Yunus, *Acta Materialia* **2013**, *61*, 540-547.

[20] U. Khan, P. May, H. Porwal, K. Nawaz, J. N. Coleman, *ACS Applied Materials & Interfaces* **2013**, *5*, 1423-1428.

[21] Y. M. Tseytlin, *Structural Synthesis in Precision Elasticity*, Springer, **2007**.

[22] K. M. Choi, J. A. Rogers, *Journal of the American Chemical Society* **2003**, *125*, 4060-4061.

[23] N. J. Douville, Z. Li, S. Takayama, M. D. Thouless, *Soft Matter* **2011**, *7*, 6493-6500.

[24] A. L. Window, *Strain Gauge Technology*, Springer **1992**.

2.6. Supporting Information

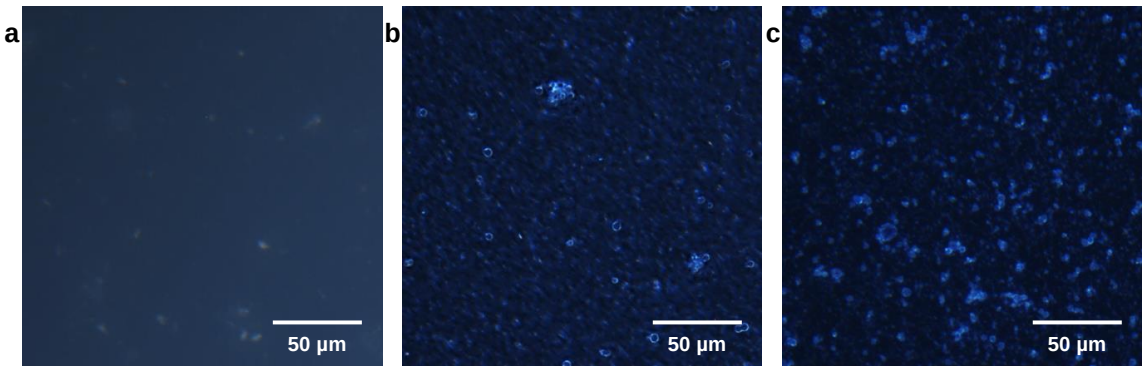

Figure S2.1. Optical micrographs of glue emulsions in water (a) 1:1 water:glue (b) 3:1 water:glue (c) 5:1 water:glue.

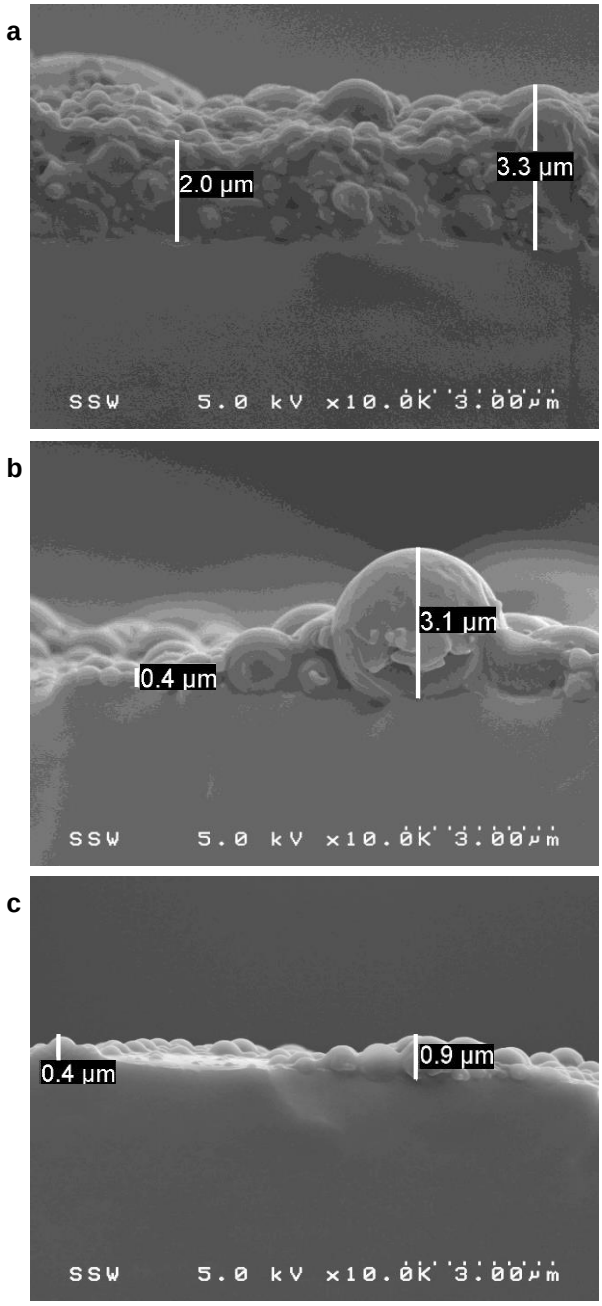

Figure S2.2. SEM cross sections of (a) PDMS/glue$_{1:1}$ (b) PDMS/glue$_{3:1}$ (c) PDMS/glue$_{5:1}$.

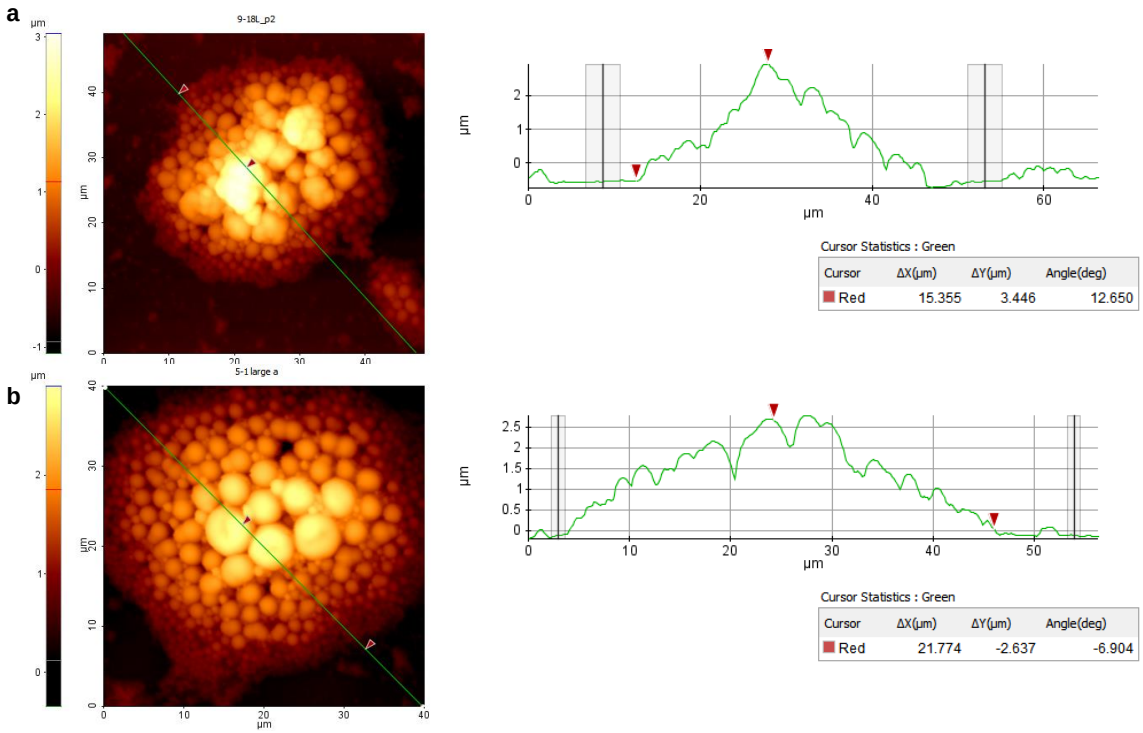

Figure S2.3. AFM image and line trace of large glue cluster on (a) PDMS/glue$_{3:1}$ (b) PDMS/glue$_{5:1.}$

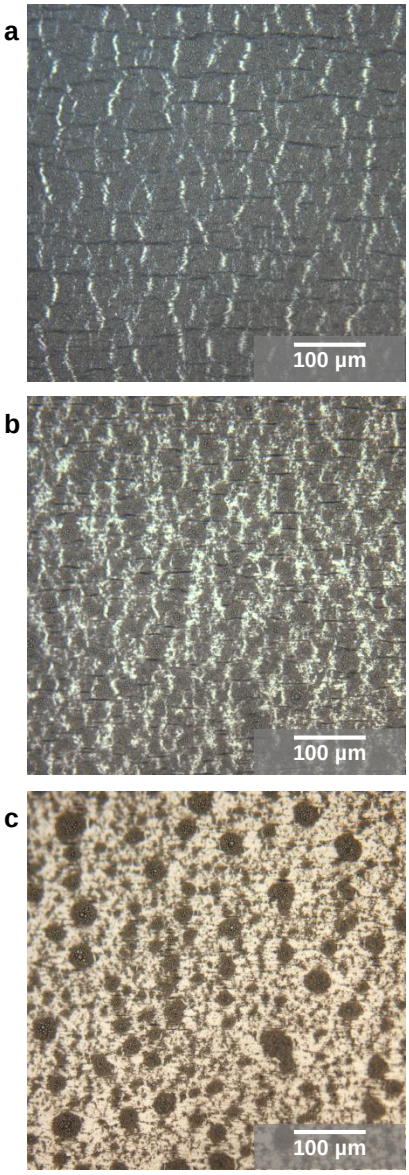

Figure S2.4. Optical micrographs of (a) PDMS/glue$_{1:1}$ (b) PDMS/glue$_{3:1}$ (c) PDMS/glue$_{5:1}$ stretched to 60% elongation.

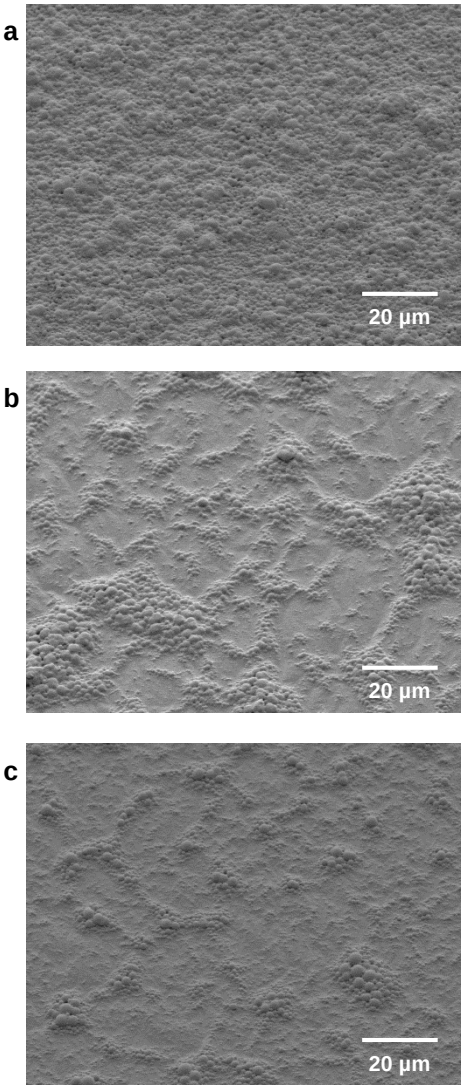

Figure S2.5. SEM images of 250-Å-thick gold with 30-Å-thick titanium adhesion layer on (a) PDMS/glue$_{1:1}$ (b) PDMS/glue$_{3:1}$ (c) PDMS/glue$_{5:1}$.

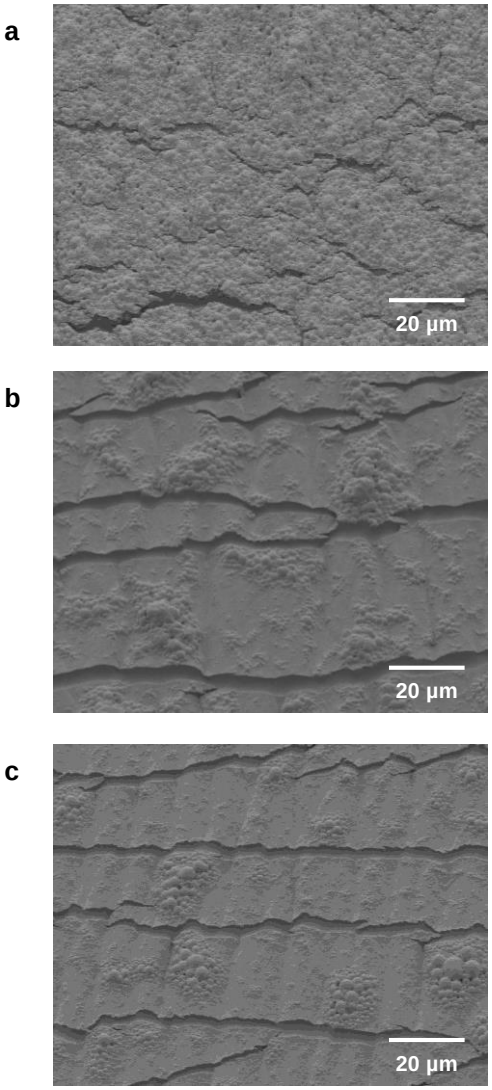

Figure S2.6. SEM images of 250-Å-thick gold with 30-Å-thick titanium adhesion layer on (a) PDMS/glue$_{1:1}$ (b) PDMS/glue$_{3:1}$ (c) PDMS/glue$_{5:1}$ stretched to 30% elongation.

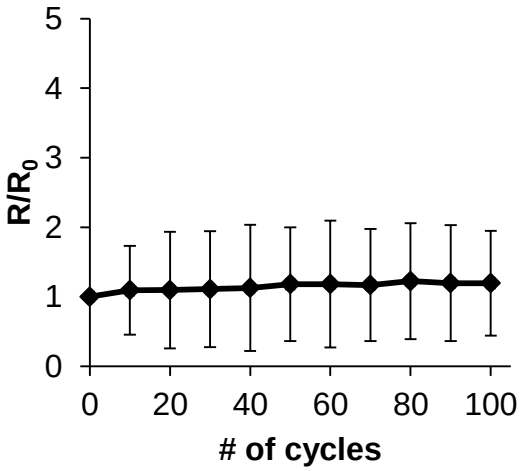

Figure S2.7. Plot of normalized resistance as a function of number of cycles of 15% strain for PDMS/glue$_{3:1}$/gold.

Code for Arduino LED Control

Adapted from:
http://arduinobasics.blogspot.ca/2011/05/arduino-uno-flex-sensor-and-leds.html

```
const int flexPin = A0;

void setup(){
  for (int i=4; i<14; i++){
    pinMode(i, OUTPUT);
  }
  Serial.begin(9600);
}

void loop(){

  int flexReading = map (analogRead(flexPin), 0, 1023, 13, 4);
  int LEDnum = constrain(flexReading, 4, 13);

  for (int x=4; x<LEDnum; x++){
  digitalWrite (x, HIGH);
  }

  for (int x=LEDnum; x<13; x++){
    digitalWrite (x, LOW);
  }
}
```

3. Chapter 3

Highly Stretchable Gold Films on Elastomeric Substrates Coated with Poly(Vinyl Alcohol) Interlayers

3.1 Introduction

Stretchable metal wires are required for the fabrication of stretchable interconnects and as electrodes in stretchable devices. While free-standing metal films have elongations at break of a few percent, increased elongations can be achieved by depositing metal films on a compliant substrate.[1],[2],[3] Researchers have developed methods for rendering metal films stretchable by laying metal wires out in new geometries such as arches[4] or serpentines[5],[6],[7],[8] in order to transform stretching strains into more favourable planarization or bending and twisting strains. These approaches rely on photolithography to generate sophisticated patterns of metal and the processes are very costly. A lithography-free approach to creating favorable geometries in metal films involves prestraining the elastomeric substrate prior to metal deposition. When the prestrain is released, compressive strain is exerted on the metal film forcing it to buckle. These buckles in the metal film have mechanics similar to those of an accordion bellows: Under applied tensile strain the buckles planarize to accommodate the strain. Samples that are prestrained uniaxially support stretching along the axis of prestrain up to 100%[3] and samples that are radially prestretched can support biaxial elongations up to 40%[9].

Rather than alter the geometry of metal films to render them stretchable, a recent approach has aimed to achieve *controlled* crack propagation in strained metal films via the introduction of a microstructured topography.[10],[11],[12] In the previous Chapter, we demonstrated a low-cost, green method to introduce a compliant microstructured topography onto poly(dimethyl siloxane) (PDMS) by spin coating aqueous emulsions of PVAc white glue onto PDMS. The resultant microstructured topography of glue globule clusters creates multiple nucleation sites for cracks to form rather than the single necking sites that are typically observed in buckled gold films deposited on smooth PDMS.[1] The presence of multiple necking sites provides in situ strain relief to the metal film: Gold ligaments neighbouring cracks experience strain relief such that when new cracks enter this relaxation zone they cease to propagate. The result is a network of small isolated cracks that do not exhibit significant growth upon increased strain application allowing gold films to remain conductive to high strains (up to 75%). This Chapter builds upon the concept of achieving altered crack propagation in metal films through the use of a

smooth, homogeneous polymer interlayer. In this Chapter we demonstrate that high stretchability of gold films can also be realized through the introduction of a uniform film of poly(vinyl alcohol) (PVA) treated with water condensate. We show that treatment with water condensate is crucial to achieving high stretchability in gold films on PDMS/PVA due to two effects: Treatment with water condensate swells the PVA interlayer and produces a wrinkled topography providing multiple sites for crack nucleation; simultaneously, the crystallinity of PVA interlayer is reduced by water molecules disrupting inter- and intramolecular hydrogen bonding which increases the elongation at break of the polymer interlayer and retards crack formation.

PVA is prepared by the hydrolysis of the acetate groups on PVAc to produce hydroxyl groups on the polymer backbone. The introduction of hydroxyl groups renders PVA water-soluble whereas PVAc is not soluble at all in water and PVAc glue forms an emulsion in water. The small size of the hydroxyl groups allows the polymer chains to adopt a zigzag conformation and pack tightly resulting in PVA films with a high degree of crystallinity. In comparison, PVAc chains form an amorphous polymer due to the larger acetate group on PVAc preventing the formation of tightly packed films. The ability of PVA to form intra- and intermolecular hydrogen bonds results in a high Young's modulus of 2.26 GPa[13] compared to that of Elmer's glue (0.6 GPa)[14] and pure PVAc (0.75 GPa)[15]. These properties of high crystallinity and high Young's modulus contribute to the low elongation at break of PVA films (0-3%) compared to PVAc (60-100%). The large number of hydroxyl groups on PVA also contributes to its ability to absorb water. It is well known in the literature that the mechanical properties of PVA films are highly dependent on the amount of water present in the polymer because water acts as a plasticizer in PVA films by disrupting intermolecular and intramolecular hydrogen bonding.[13],[16] Water exists in three states in PVA films: (1) *non-freezing water*, which is water that is hydrogen bonded to the hydroxyl groups of PVA and does not exhibit any detectable phase transitions over the normal range of temperatures associated with bulk water; (2) *freezable bound water,* which has some interaction with the polymer chains but to a lesser extent than *non-freezing water* and whose phase transitions are shifted with respect to bulk water; and (3) *free water* which occupies the

free volume of the polymer and exhibits similar thermal phase transitions to bulk water.[17] Water present in PVA in the form of *non-freezing water* is the most effective plasticizer of PVA as it disrupts hydrogen bonding within the polymer.[16] PVA films exhibit lower degrees of crystallinity when the content of water is higher which in turn affects the glass transition temperature (T_g), Young's modulus, elongation at break and tensile strength. Konidari et al. demonstrated that by changing the relative humidity (RH) at which PVA films are equilibrated from 0% RH to 86% RH, the Young's modulus of the films could be tuned from 2.26 GPa to 0.10 GPa.[13]

Research into several polymer systems has shown that the stretchability of polymer films on elastomers can be altered by changing the Young's modulus of the polymer. For instance, PEDOT:PSS can be made more stretchable through the addition of surfactants and additives which plasticize the PEDOT:PSS film.[18] It has also been shown that Young's modulus affects the onset of crack formation in polymer films; in poly(3-alkylthiophene) (P3AT) films, the polymers with higher moduli exhibited cracking at lower elongations. This chapter exploits the tunability of the mechanical properties of PVA and demonstrates the effects of Young's modulus and polymer interlayer crystallinity on the stretchability of overlying metal films. We demonstrate that when metal films are deposited on elastomers with PVA polymer interlayers, the stretchability of the interlayer dictates crack propagation through the metal film. Under dry conditions, the PVA interlayer is crystalline and cracks at low strain causing gold films lose conductivity at strains > 15%. When the metallized PVA interlayer is treated with water condensate two synergistic effects provide conditions for enhanced stretchability of gold films: First, a wrinkled topography forms due to swelling of the PVA interlayer; the wrinkled topography provides multiple strain localization sites analogously to those occurring in the microstructured PVAc layer presented in Chapter 2. Second, treatment of PDMS/PVA/gold with water condensate softens the PVA interlayer due to water molecules disrupting inter- and intramolecular hydrogen bonding thus increasing the elongation at break of the polymer. Gold films on PDMS/PVA treated with humidity exhibit smaller cracks than analogous films on dry PDMS/PVA due to plasticization of

the PVA film by water and the formation of wrinkles that halt crack propagation which allows the overlying gold films to remain conductive up to 75% elongation.

3.2. Experimental Section

3.2.1. Materials

All materials and chemicals were purchased commercially and used as received. Poly(dimethylsiloxane) (PDMS) (Sylgard 184) was obtained from Dow Corning (Midland, MI). All other chemicals were obtained from Sigma-Aldrich and were used as received.

3.2.2. Preparation of PDMS Substrates

PDMS (Dow Corning Sylgard 184) was prepared by mixing prepolymer with curing agent in a 10:1 w:w ratio and stirring, followed by degassing. The prepolymer mixture was cured against a polystyrene Petri dish at 60°C to obtain smooth substrates. PDMS substrates were treated with air plasma for 40 seconds at an air pressure of 10 psig (flow rate of 32 mL/min).

3.2.3. Deposition of PVA and Gold Layers on PDMS

Poly(vinyl alcohol) (PVA) solutions were prepared in water (25 mg/mL) and heated in a microwave in 10 second intervals until dissolved. Oxidized PDMS substrates were spin coated with the PVA solution at 1000 rpm for 1 minute followed by 2000 rpm for 1 minute to yield PVA films on PDMS (PDMS/PVA). 250-Å-thick gold films were deposited onto the PDMS/PVA substrates at a rate of 1 Å/s by e-beam metal evaporation under high vacuum (10^{-6} mbar).

3.2.4. Humidity Treatment of Gold Films on PDMS/PVA

Gold-coated PDMS/PVA samples with polymer interlayers were exposed to humidity levels of 80-90% with a humidifier in an enclosed glovebox container. The humidifier was turned on for 20 minutes to increase the humidity level in the container and the

samples were exposed to 80-90% humidity for one hour total. Following exposure samples were allowed to dry overnight in ambient atmosphere, annealed samples were dried overnight in a vacuum oven at 120°C. Humidity treatment in a controlled environment chamber was performed in an environmental test chamber (MCBH-1.2-.33-H/AC, Cincinnati Sub-Zero, Cincinnati, OH) at 85% RH for 3 days and 95% RH for 5 days. For immersion testing 18 MΩ water was employed and samples were either immersed in water for 1 hour or 0.5 mL of water was pipetted onto the surface and left for 5 minutes before rolling it off.

3.2.5. Characterization

Optical characterization was performed using an Olympus BX51 microscope equipped with an Olympus Q-Color3 digital camera. A micro-vice stretcher (S. T. Japan, USA, Inc) was mounted to the microscope stage and samples were clamped in the stretcher to obtain microscope images of stretched samples. Scanning electron microscopy was carried out on a Hitachi S-4500 scanning electron microscope at Surface Science Western, London, Canada. Samples were stretched manually and secured with copper tape to the specimen stage. SEM cross sections of the PVA film were obtained by spin coating PVA on a silicon wafer followed by freeze-fracture in liquid nitrogen to obtain a clean cleavage. Prior to SEM imaging, all samples were coated with 3-5 nm Au using a Hummer VI sputtering system. Atomic force microscopy was carried out at Surface Science Western, London, Canada. The surface was imaged using the dynamic force mode of a Park Systems XE-100 AFM. A silicon cantilever with a nominal spring constant of 40 N/m, resonant frequency of 300 kHz and tip radius of 10 nm was used. Images were collected from three spots on each sample in an area of 40 μm × 40 μm. For electrical characterization under strain, samples were clamped in a micro-vice stretcher (S.T. Japan, USA, Inc.) and stretched in 5% increments while the resistance was measured with a Keithley 2601A Sourcemeter. Gallium-indium eutectic (EGaIn) (~0.01 mL) was deposited by syringe at each end of the wire to facilitate contact to the metal films. A minimum of three samples was tested and an average is reported.

3.3. Results and Discussion

3.3.1. Preparation of PDMS Substrates

PDMS substrates were prepared by mixing the pre-polymer and curing agent in a 10:1 w/w ratio, casting in a Petri dish and curing to obtain smooth PDMS substrates.

3.3.2. E-beam Deposition of Gold on PDMS/PVA Substrates

In the previous chapter we demonstrated that poly(vinyl acetate) (PVAc) glue forms an emulsion in water which creates a rough topography when spin coated on the surface of PDMS. Poly(vinyl alcohol) (PVA) is made by hydrolysis of PVAc and unlike PVAc, it is soluble in hot water due to the abundance of OH groups on the polymer chain. Water-solubility allows for the deposition of homogeneous films of PVA to be produced on PDMS in contrast to the microstructured topographies obtained from spin coating solutions of aqueous polymer emulsions. We used plasma oxidation to generate oxidized functional groups at the surface of PDMS substrates prior to PVA deposition to improve the wettability of the aqueous PVA solution. Oxidation decreases the water contact angle on PDMS from $112 \pm 8°$ to $< 20°$. We prepared a solution of 25 mg/mL of PVA in hot water by microwaving the mixture at 10 second intervals until the PVA was completely dissolved. We spin-coated the solutions of aqueous PVA on the oxidized substrates using an initial spin speed of 1000 rpm for 1 min followed by 2000 rpm for 1 minute to yield PVA films with a thickness of 118.1 ± 6.5 nm. Figure 3.1 depicts a representative image of a cross section of PVA on silicon wafer obtained by SEM.

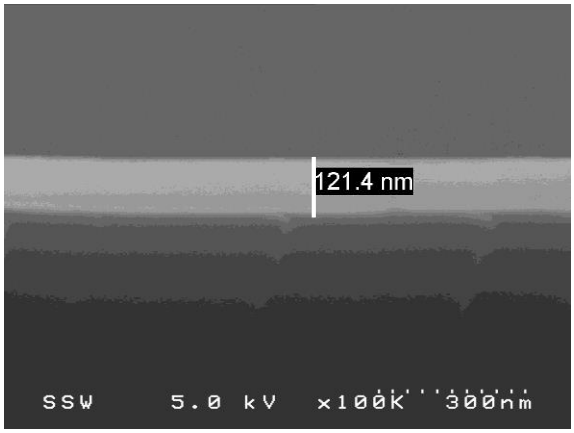

Figure 3.1. SEM cross section of a PVA film on silicon wafer**.**

Subsequently, we deposited 250-Å-thick gold films onto PDMS with PVA interlayers by e-beam deposition at a rate of 1 Å/s. The resulting gold films were metallic in appearance and conductive. As evidenced in the optical micrograph, 250-Å-thick gold films on PDMS/PVA substrates have a buckled topography (Figure 3.2a). It has been shown that buckles with wavelengths of 20-50 μm spontaneously form in gold films deposited on PDMS due to heating of the substrate during metallization followed by subsequent thermal contraction.[19] We hypothesize that the buckles we observe are also caused by the compressive stress that follows the thermal expansion of the PDMS/PVA during e-beam metal deposition. The buckles in gold films on PDMS/PVA are further visible in the SEM and AFM images in Figure 3.2b&c. The buckles have a period of 10-15 μm and peak-to-peak amplitude of 450-700 nm.

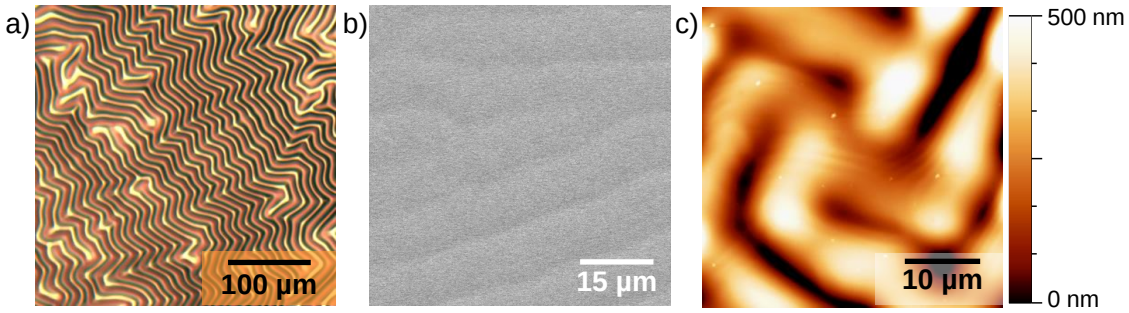

Figure 3.2. 250-Å-thick gold films on PDMS/PVA (a) optical micrograph; (b) SEM image; (c) AFM image.

3.3.3. Stretching Gold Films on PDMS/PVA

In the previous Chapter we demonstrated that introducing a microstructured PVAc polymer interlayer of intermediate Young's modulus between the compliant PDMS substrate and gold inhibits cracks from propagating the full width of the gold wire and allows gold films on PDMS/glue to maintain conductivity up to 60%. While PVA also possesses a higher Young's modulus than PDMS (2.26 GPa[13] vs 1.8 MPa[20]), PVA films are homogeneous and more crystalline than PVAc due to the small size of the hydroxyl group on the backbone resulting in a very low elongation at break. The high stiffness and high degree of crystallinity cause PVA films to fracture at low strains even when they are supported on a compliant substrate. Crack propagation in gold films on PDMS/PVA is similar to that of gold films on flat PDMS substrates; the lack of multiple sites for strain localization causes single necking points to form in the gold film causing uninterrupted crack propagation across the metal film. Figure 3.3a shows the density and size of cracks that form at 5% strain with cracks measuring ~ 9 μm in width. As the strain is increased to 15% more cracks form and the existing cracks widen to 11-17 μm (Figure 3.3b). At 15% strain the normalized resistance is 700 and electrical failure occurs at strains greater than 15% (Figure 3.3c). We postulate that this failure is due to lack of multiple strain localization sites in the gold films. While the presence of a rough microstructured topography in PDMS/glue films introduces multiple sites for strain localization no such sites exist on PDMS/PVA films which cause single necking points to occur; cracks propagate unhindered from these single necking points and traverse the full width of the gold film completely disrupting conductivity. This cracking mechanism is similar to the crack propagation that occurs in buckled gold films on flat PDMS. This result stresses the importance of having multiple strain localization sites in order to alter the cracking mechanism and produce multiple sites of crack nucleation.

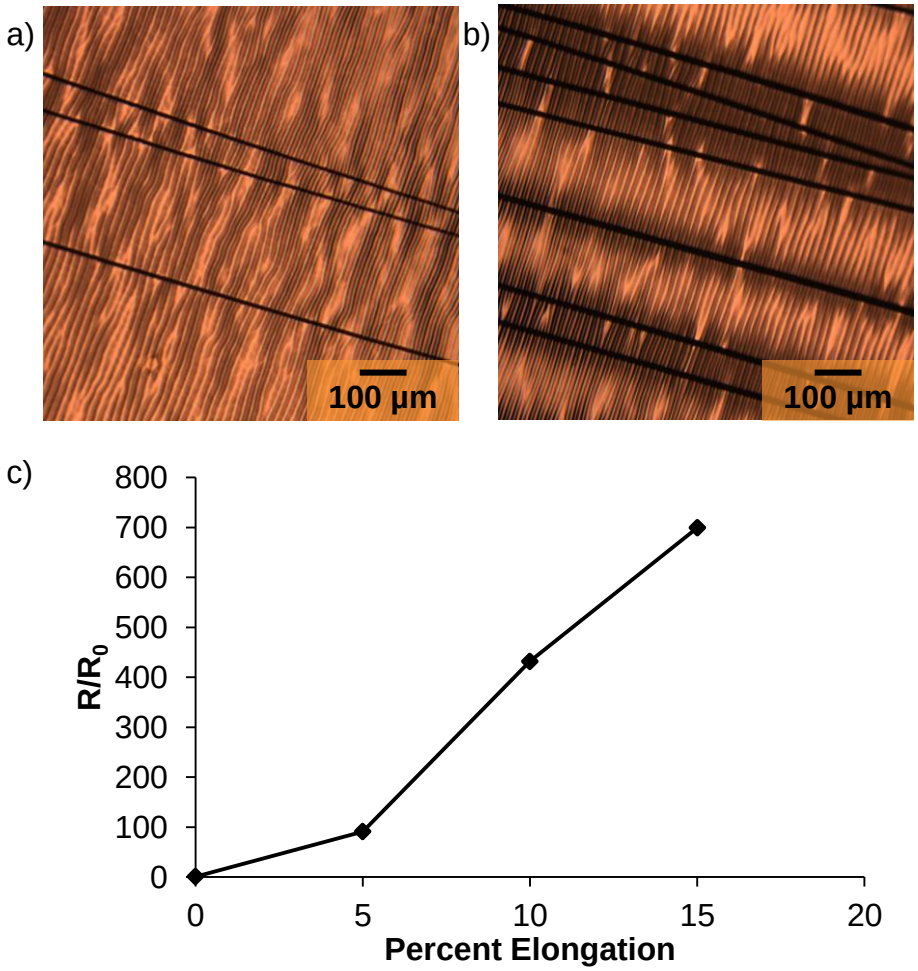

Figure 3.3. Optical micrographs of as-deposited films of 250-Å-thick Au on PDMS/PVA (a) stretched 5%; (b) stretched to 15%. (c) Plot of normalized resistance as a function of percent elongation.

3.3.4. Effect of Humidity Treatment on Morphology of Gold Films on PDMS/PVA

Previous research has shown that the Young's modulus of PVA can be decreased by exposing films to different relative humidity levels which alters the content of water present in the film. Water molecules permeate into amorphous regions of the PVA and disrupt the intramolecular and intermolecular hydrogen bonding in the polymer chains. This reduces the crystallinity of the PVA film and creates a plasticizing effect. We exposed samples of gold on PDMS/PVA to humidity using a humidifier in an enclosed container. The humidifier was kept on for 20 minutes and then turned off allowing the

humidity in the container to increase to 80-90% RH. The samples were kept in this increased humidity environment for one hour. After one hour, water condensation was visible on the surface of the gold films. The samples were left to dry under ambient conditions overnight. Optical microscopy reveals profound changes in the gold morphology following humidity treatment. Evidence of large and fine wrinkles are visible in both the optical microscopy and SEM images (**Figure 3.4**a, b). The smaller wrinkles have a height of 100-200 nm and are shown in the AFM image in Figure 3.4c. The larger wrinkles can measure up to 1 μm in height as shown in the AFM image and line trace profile (Figure 3.5). The surface morphology is transformed into a wrinkled morphology (**Figure 3.4**b) due to the PVA interlayer taking up water and swelling. This indicates that water molecules are able to permeate through the gold film likely at grain boundaries and reach the underlying PVA layer causing the PVA to swell and the gold/PVA to wrinkle. The swelling of the PVA does not produce sufficient strain in the gold film to cause cracks; the gold film deforms with the underlying PVA. We believe that the buckled morphology of the as-deposited gold provides sufficient surface area for planarization and wrinkling to occur as the water swells PVA without causing cracks due to excess strain on the gold film.

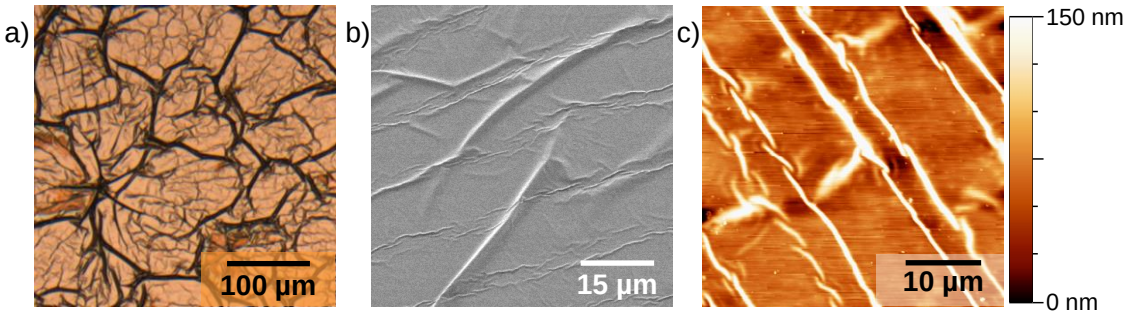

Figure 3.4. 250-Å-thick gold films on PDMS post-humidity treatment for 1 hour at 25°C and 80-90% RH (a) optical micrograph; (b) SEM image; (c) AFM image.

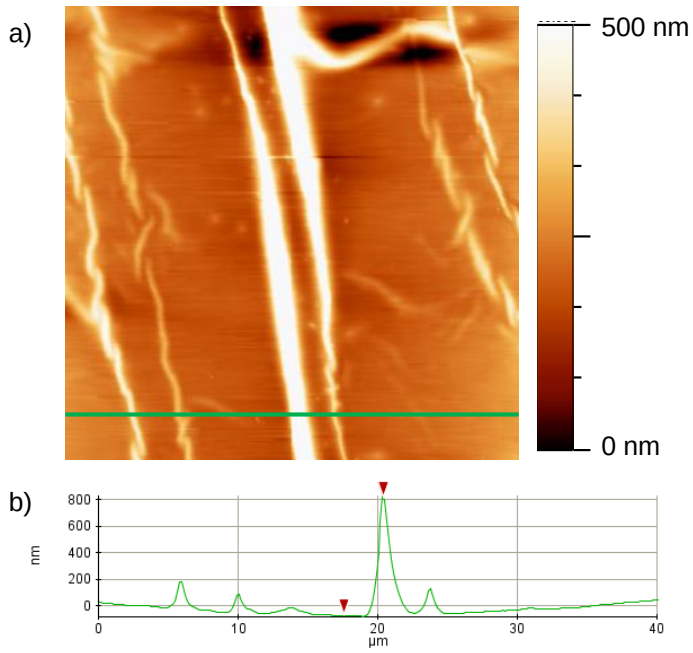

Figure 3.5. (a) AFM image of humidity treated gold on PDMS/PVA with green line showing trace of line profile. (b) Line profile of height across the sample.

3.3.5. Stretching Gold Films on Humidity Treated PDMS/PVA

Higher water content in PVA results in lower degrees of crystallinity, lower Young's modulus and a higher elongation at break, which coupled with the wrinkled topography, enables gold films on humidity treated PDMS/PVA to achieve higher elongations at failure. Upon stretching, cracks form in the Au/PVA layer perpendicular to the direction of applied strain however, optical microscopy reveals a dramatic change in the crack formation of humidity treated gold films on PDMS/PVA (Figure 3.6). At 10% strain, the number of cracks is more numerous than that observed for gold films on dry PDMS/PVA (Figure 3.6a). We hypothesize that the alteration in crack propagation compared to gold films deposited on dry PVA occurs due to two factors: First, humidity treatment makes the PVA film more stretchable by interrupting inter- and intramolecular hydrogen bonding in the PVA interlayer which lowers the Young's modulus and decreases the crystallinity of the PVA film. Second, the swelling of PVA causes wrinkles in the topography of the gold film creating a relief which provides multiple sites of strain localization and crack nucleation. Cracks formed on the humidity treated samples

measure 5-10 μm in width and unlike the cracks formed in gold films on dry PDMS/PVA, they do not propagate the full width of the gold wire; cracks entering a relaxed region of the gold film cease to propagate. The normalized resistance of gold films on humidity treated PDMS/PVA at 10% elongation is 20.9. As more strain is applied, the cracks become more numerous and widen reaching 10-15 μm in width at 50% elongation (Figure 3.6b). Overall, the conductive pathway is maintained and the average R/R_0 is 220 at 50% elongation. SEM imaging of the cracking pattern supports our hypothesis; in a sample stretched to 20% elongation, cracks appear localized around the wrinkles in the film (Figure 3.6c). Resistance measurements as a function of strain show that humidity treated gold films on PDMS/PVA remain conductive up to 75% elongation at which point the PDMS fractures in the micro-vice stretcher (Figure 3.6d). The slope of the line of best fit of resistance versus strain is 5.16 which is higher than the gold films prepared on microstructured glue interlayers in Chapter 2 indicating that gold films on humidity treated PDMS/PVA exhibit increased sensitivity to strain. Additionally, the change in resistance is very linear ($R^2 = 0.98$). The high sensitivity and linearity of these gold films make them promising candidates for strain sensors where a larger change in resistance upon application of strain is desirable.

Interestingly, even when samples are annealed at 120°C overnight they continue to exhibit increased elongations at failure compared to gold films on dry PVA (Figure 3.6d). It has been shown in the literature that water exists in multiple states in PVA films and that when the water molecules are strongly bound to the hydroxyl groups in PVA they do not exhibit the same thermal transitions as free water.[17] Wang et al. found that in water-plasticized PVA, the water-evaporation peak occurs at higher temperatures than bulk water indicating that the hydrogen bonding with PVA is delaying the evaporation of water from the polymer.[21] We hypothesize that the non-freezing water present in our humidity-treated PVA films remains in the PVA layer and continues to act as a plasticizer even after annealing at 120°C overnight due to hydrogen bonding to the hydroxyl groups on PVA. The slope of the line of best fit of normalized resistance versus strain is lower in annealed samples ($m = 3.18$) than in samples that were dried in ambient conditions. Previous research has shown that water does not inhabit intact crystallites of PVA and is

only found in the amorphous region of the polymer.[22],[23] Therefore we postulate that that heating the samples above the T_g of PVA facilitated the diffusion of water throughout the sample by rendering the polymer chains amorphous resulting in a softer polymer film due to incorporation of more water.

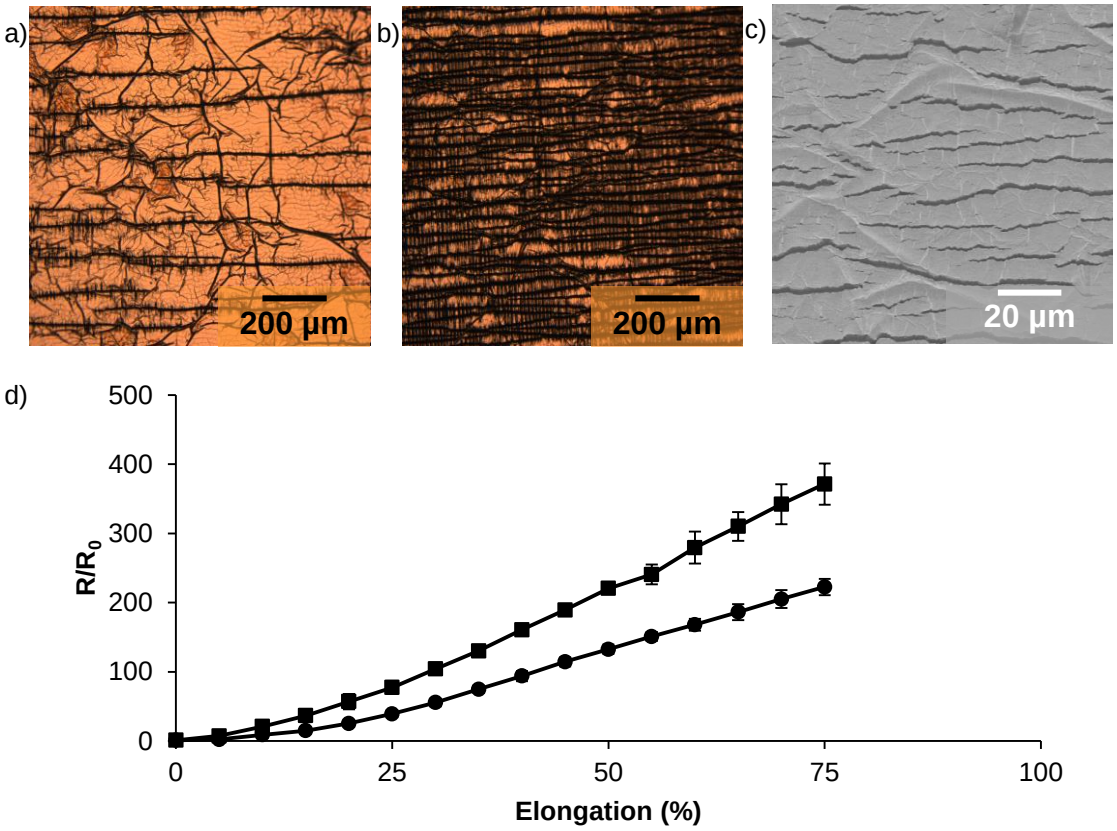

Figure 3.6. Characterization of 250-Å-thick Au film on PDMS/PVA exposed to 80-90% RH in an enclosed container for one hour dried overnight in ambient conditions. Optical micrographs of the sample (a) stretched to 10%; (b) stretched to 50%; (c) SEM image of the sample stretched to 20%; (d) electrical response as a function of strain for samples dried in ambient overnight (squares) and in vacuum oven overnight (circles).

3.3.6. Alternative Humidity Treatment Methods

We next investigated alternative methods to introduce water into the PVA film. We performed humidity treatment in a controlled environment chamber which prevents water condensation from forming on the samples while maintaining the setpoint humidity and temperature in the atmosphere of the chamber. We treated gold films on PDMS/PVA to

85% RH at 25°C for 3 days and found no increase in stretchability of gold films compared to as-deposited films on dry PVA. Similarly, humidity treatment at higher relative humidity and temperature of 95% RH and 35°C for 5 days did not produce an increased elongation at failure in gold films. While it is evident from optical microscopy images that the as-deposited gold films (Figure 3.7a, b) experience a change in morphology due to swelling of the PVA in increased humidity environments (Figure 3.7c, d) under the conditions reported the changes to the PVA/gold film are not sufficient to alter the cracking mechanism of the films. Indeed, large cracks that propagate the full width of the gold wire are visible when the sample is strained to 5% (Figure 3.7e, f). We hypothesize that the amount of water that is permeating into the PVA film in the controlled humidity chamber is not sufficient to impact the highly crystalline regions of the films and therefore these regions are failing at low elongations. Researchers have found that at room temperature, water molecules only penetrate the amorphous regions of PVA leaving the crystalline regions of the polymer, where chain packing is more dense, unaffected.[22],[23] Hodge et al. immersed PVA films in water and found that in excess amounts, water is able to destroy crystallinity by first permeating into the amorphous regions of the polymer and then attacking crystallites at the interface between the amorphous and crystalline region.[17] We hypothesize that films treated in the humidity chamber at 85% RH and 25°C do not absorb sufficient amounts of water to penetrate into the crystallites of the PVA film thereby only affecting the amorphous region. It interesting to note that the cracks in the sample treated for 5 days appear smaller in width than samples treated for 3 days (2-4 μm vs. 6-8 μm), therefore it is possible that longer exposure time in the controlled humidity chamber could produce the desired effect of plasticizing the PVA layer.

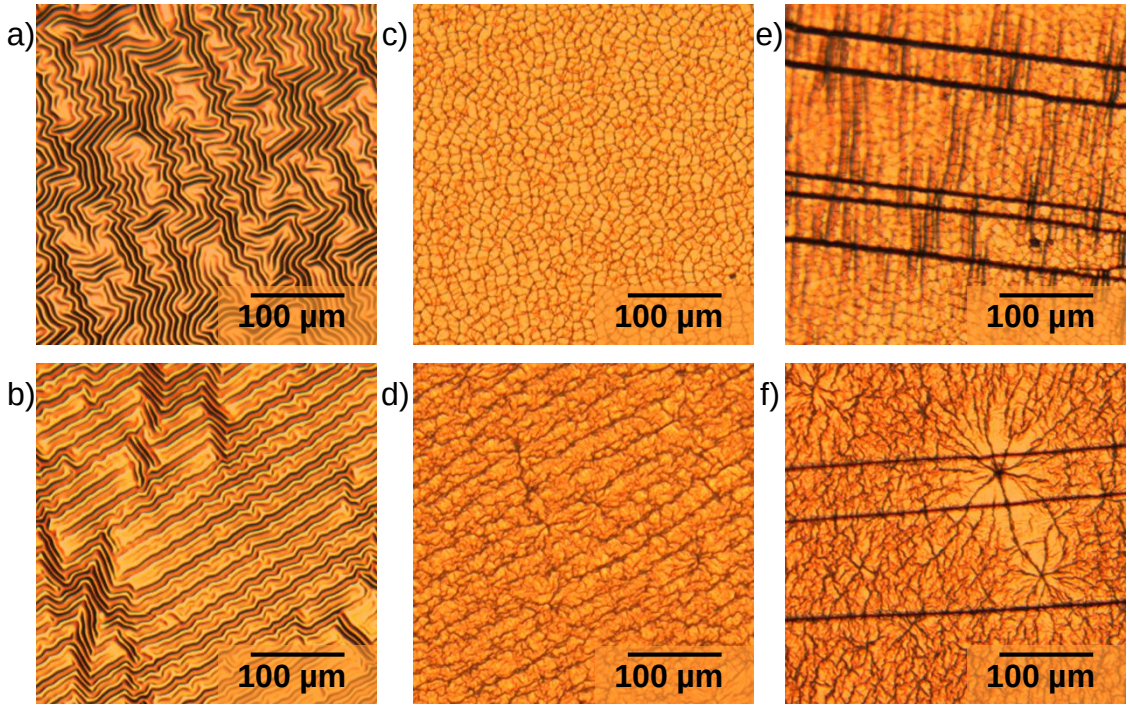

Figure 3.7. Optical micrographs of 250-Å-thick Au on PDMS/PVA: (a, b) as-deposited; (c) after humidity treatment for 72 hours at 85% RH and 25°C; (d) after humidity treatment for 5 days at 95% RH and 35°C; (e) after humidity treatment for 72 hours at 85% RH and 25°C stretched to 5% elongation; (f) after humidity treatment for 5 days at 95% RH and 35°C stretched to 5% elongation.

Exposure to 85-95% RH in the controlled environment chamber maintains the setpoint humidity level in the atmosphere of the chamber however the chamber is designed to prevent water from condensing on the surface of the samples. We hypothesize that water condensation on the samples is necessary to increase the amount of water that permeates into the PVA layer through the gold film in order to not only permeate into the amorphous regions of the polymer but also attack the crystalline regions at the interface between the amorphous regions and the crystalline regions.

We exposed gold films on PDMS/PVA to excess water by immersing the samples in water but found that immersion treatment was too harsh; the water-soluble PVA thin film starts to dissolve in water and gold lifts off of the substrate (Figure 3.8). We hypothesize that there is an ideal amount of water that must be introduced into the PVA film in order to act as a plasticizer and that it must be delivered in a way that is not too harsh to damage

the thin films of gold and PVA. A shift to chemically cross-linked films of PVA with gluteraldehyde may permit more vigorous exposure to water in order to swell the PVA film since cross-linked films of PVA create more robust films that are not soluble in water. Park et al. demonstrated that chemically crosslinked PVA had lower T_g values than uncrosslinked PVA films due to the crosslinking moieties attenuating some of the inter and intramolecular hydrogen bonding in the PVA film.[24] In all formulations tested, the wet PVA had decreased tensile strain and longer elongations than the analogous dry films indicating that even in cross-linked films, water can act as a plasticizer.

Figure 3.8. Photograph of 250-Å-thick Au on PDMS/PVA after submersion in water for 1 hour.

3.4. Conclusions

In conclusion, we have demonstrated that it is possible to tune the stretchability of gold films on elastomers by controlling the mechanical properties and topography of the PVA polymer interlayer. While inserting a crystalline, brittle polymer between PDMS and gold results in electrical failure of the gold film at strains greater than 15%, treatment with water condensate results in gold films that can stretch up to 75% before electrical failure occurs due to the dual effect of the creation of topographic wrinkles that act as multiple sites for strain localization and nucleation of microcracks and the softening of the PVA interlayer. We hypothesize that water condensation on the surface of gold films penetrates into the PVA layer, disrupts intermolecular hydrogen bonding and causes the polymer/gold layers to swell. We have found that the method used to introduce water into the PVA layer is of great importance: It is not sufficient to treat samples in a controlled humidity chamber at high humidity levels (85-95% RH); water condensation on the samples is necessary to swell the PVA and produce an altered cracking mechanism

in the overlying gold films under strain. Immersing the samples in water causes gold films to peel away from the PDMS substrate due to the solubility of PVA in water.

Future experiments will investigate the effect of temperature during humidity treatment on the morphology of gold and the change in resistance of gold films as a function of strain. Zielinski et al. demonstrated that the diffusivity of water in PVA increases when the temperature is raised from 90°C to 110°C.[25] We hypothesize that humidity treatment of gold films on PDMS/PVA at temperatures above the T_g will facilitate water diffusion into PVA due to increased mobility of the polymer chains rendering the polymer more amorphous.

We will also investigate the use of small molecule plasticizing agents: Previous research has found that glycerol and caprolactam are effective small molecules that can disrupt the intermolecular hydrogen bonding in PVA and act as plasticizing agents for thermal processing of PVA films.[21] The use of small molecule plasticizers can be done in combination with humidity treatment as a means to make the PVA layer less crystalline and more ductile. We will also develop methods to encapsulate gold films in order to make them more robust for applications as strain sensors. This Chapter demonstrates proof-of-concept that the mechanical properties of a polymer interlayer can affect the crack propagation in an overlying metal film. This opens the door to investigation of new polymer systems with plasticizing agents as interlayers between PDMS and gold for enhanced elongation at failure of gold films under strain.

3.5. References

[1] S. P. Lacour, S. Wagner, Z. Huang, Z. Suo, *Applied Physics Letters* **2003**, *82*, 2404.

[2] T. Li, Z. Huang, Z. Suo, S. P. Lacour, S. Wagner, *Applied Physics Letters* **2004**, *85*, 3435-3437.

[3] S. P. Lacour, J. Jones, S. Wagner, L. Teng, S. Zhigang, *Proceedings of the IEEE* **2005**, *93*, 1459-1467.

[4] Y. Sun, W. M. Choi, H. Jiang, Y. Y. Huang, J. A. Rogers, *Nature Nanotechnology* **2006**, *1*, 201-207.

[5] T. Li, Z. Suo, S. P. Lacour, S. Wagner, *Journal of Materials Research* **2005**, *20*, 3274-3277.

[6] D. S. Gray, J. Tien, C. S. Chen, *Advanced Materials* **2004**, *16*, 393-397.

[7] S. Xu, Y. Zhang, J. Cho, J. Lee, X. Huang, L. Jia, J. A. Fan, Y. Su, J. Su, H. Zhang, H. Cheng, B. Lu, C. Yu, C. Chuang, T.-i. Kim, T. Song, K. Shigeta, S. Kang, C. Dagdeviren, I. Petrov, P. V. Braun, Y. Huang, U. Paik, J. A. Rogers, *Nature Communications* **2013**, *4*, 1543.

[8] Z. Yihui, W. Shuodao, L. Xuetong, A. F. Jonathan, X. Sheng, S. Young Min, C. Ki-Joong, Y. Woon-Hong, L. Woosik, N. Sharaf Nafees, L. Bingwei, Y. Lan, H. Keh-Chih, A. R. John, H. Yonggang, *Advanced Functional Materials* **2014**, *24*, 2028-2037.

[9] P. Gorrn, W. Z. Cao, S. Wagner, *Soft Matter* **2011**, *7*, 7177-7180.

[10] A. P. Robinson, I. Minev, I. M. Graz, S. P. Lacour, *Langmuir : the ACS journal of surfaces and colloids* **2011**, *27*, 4279-4284.

[11] P. Mandlik, S. P. Lacour, J. W. Li, S. Y. Chou, S. Wagner, *Electron Device Letters, IEEE* **2006**, *27*, 650-652.

[12] N. Lambricht, T. Pardoen, S. Yunus, *Acta Materialia* **2013**, *61*, 540547.

[13] M. V. Konidari, K. G. Papadokostaki, M. Sanopoulou, *Journal of Applied Polymer Science* **2011**, *120*, 3381-3386.

[14] U. Khan, P. May, H. Porwal, K. Nawaz, J. N. Coleman, *ACS Applied Materials & Interfaces* **2013**, *5*, 1423-1428.

[15] Y. M. Tseytlin, *Structural Synthesis in Precision Elasticity*, Springer, **2007**.

[16] R. M. Hodge, T. J. Bastow, G. H. Edward, G. P. Simon, A. J. Hill, *Macromolecules* **1996**, *29*, 8137-8143.

[17] R. M. Hodge, G. H. Edward, G. P. Simon, *Polymer* **1996**, *37*, 1371-1376.

[18] M. Vosgueritchian, D. J. Lipomi, Z. Bao, *Advanced Functional Materials* **2012**, *22*, 421-428.

[19] N. Bowden, S. Brittain, A. G. Evans, J. W. Hutchinson, G. M. Whitesides, *Nature* **1998**, *393*, 146-149.

[20] K. M. Choi, J. A. Rogers, *Journal of the American Chemical Society* **2003**, *125*, 4060-4061.

[21] R. Wang, Q. Wang, L. Li, *Polymer International* **2003**, *52*, 1820-1826.

[22] N. A. Peppas, E. W. Merrill, *Journal of Applied Polymer Science* **1976**, *20*, 1457-1465.

[23] N. A. Peppas, *Makromolekulare Chemie-Macromolecular Chemistry and Physics* **1977**, *178*, 595-601.

[24] J. S. Park, J. W. Park, E. Ruckenstein, *Journal of Applied Polymer Science* **2001**, *82*, 1816-1823.

[25] J. M. Zielinski, M. Hamedi, I. M. Balashova, R. P. Danner, *Polymer International* **2014**, *63*, 221-227.

4. Chapter 4

Stretchable Light-Emitting Electrochemical Cells Using an Elastomeric Emissive Material

4.1. Introduction

Remarkable progress in stretchable electronics over the past few years has produced some amazing devices: Devices that can be laminated onto skin,[1] hemispherical arrays of photodetectors that mimic the human retina, [2] and arrays of light-emitting devices for use in flexible displays[3] are just a few examples. The methodology used to impart stretchability connects rigid circuit elements with stretchable conductive interconnects that absorb applied strain. [4] A different approach to stretchability is now emerging, in which the devices themselves are fabricated to be intrinsically stretchable. Here, we describe the use of a stretchable electroluminescent material to produce a light-emitting device that exhibits intrinsic stretchability at room temperature. These devices are well-suited to new applications in stretchable and conformable lighting that require uniform, diffuse light emission over large areas. We demonstrate devices with large emission areas (~ 20 – 175 mm^2) that tolerate linear strains up to 27% and repetitive cycles of 15% strain with minimal performance degradation relative to devices fabricated using a conventional electroluminescent material.

There are few examples of intrinsically stretchable devices – that is, systems in which the device itself operates under tensile strain. The two strategies that have been used to impart stretchability to these devices are identical to those used to fabricate stretchable device interconnects: Device materials can be either dispersed into an elastomeric matrix or deposited onto a pre-stretched elastomeric substrate. Kaltenbrunner et al. used the first strategy to produce a stretchable battery of gel materials encased in an elastomer that can withstand uniaxial strains up to 100%.[5] Yu et al. and Lipomi et al. used the second approach to fabricate stretchable supercapacitors and organic solar cells, respectively. [6,7] In these examples, the organic device materials were deposited on top of a pre-stretched poly(dimethylsiloxane) (PDMS) substrate. Releasing the pre-strain induces compressive forces on the films, producing sinusoidal buckles that can accommodate the subsequent application of a uniaxial tensile stress in the direction of the pre-strain. In this way, supercapacitors operate under applied uniaxial strains of 30%; organic solar cells, under applied uniaxial strains of ~20%. Despite these advances, there are no examples of

intrinsically stretchable light-emitting devices to enable the fabrication of large-area, illuminated, and conformable panels needed for lighting and biomedical applications.

Lights and signage that conform to curved surfaces have many potential uses in interior and exterior design, [8] and illuminated panels that conform to the human body can provide useful therapies that treat a variety of skin conditions,[9] accelerate wound healing,[10] activate chemotherapy drugs at tumour sites for cancer treatment, [11] and aid in pain management.[12] During the preparation of this manuscript, Yu et al. reported the fabrication of a light-emitting device consisting of a luminescent polymer laminated between two carbon nanotube electrodes supported on polyacrylate substrates.[13] Although these devices exhibit intrinsic stretchability, they only do so at temperatures greater than the Tg of the polyacrylate substrate (70°C), making them compatible with signage applications but limiting their use in applications involving contact with the human body.

The challenge with fabricating intrinsically stretchable conventional organic light-emitting devices (OLEDs) is the device complexity, which requires that elasticity be conferred to all of the thin-film layers of the device: emissive layer, anode, cathode, and hole and electron injection, transport, and blocking layers. Our approach to the fabrication of intrinsically stretchable light-emitting devices reduces the device complexity by using light-emitting electrochemical cells (LECs) instead of conventional OLEDs. LECs are a class of electroluminescent device that use a mixture of ionic and electronic conductors sandwiched between two metal electrodes to support all three processes of charge injection, charge transport, and emissive recombination. [14] LECs can be based on a conjugated polymer, such as poly(phenylene vinylene), blended with a solid electrolyte that provides mobile ions,[15] or on an ionic transition metal complex (iTMC), such as $Ru(bpy)_3^{2+}(PF_6^-)_2$, which is both an electronic and ionic conductor. We have focused on the latter LEC type, in which the application of a voltage bias reduces Ru^{2+} ions adjacent to the cathode and oxidizes Ru^{2+} ions adjacent to the anode. Electron hopping from one ruthenium complex ion to the next ultimately creates adjacent Ru^{+} and Ru^{3+} ions, which combine to form a ground-state Ru^{2+} species and an excited-state Ru^{2+} species. The latter emits visible light in the red part of the spectrum as it returns to its

spectroscopic ground state. The applied voltage bias also causes a redistribution of PF_6^- ions in the film. The key feature of LECs is the charge injection enhancement that occurs, which enables a simple device architecture because additional electron/hole injection, transport, and blocking layers are not required. To account for this enhancement, recent studies have provided support for an electrochemical model,[15-18] in which charge injection is promoted by doping of the material adjacent to the electrodes, and an electrodynamic model,[19-21] in which the decreased injection barrier is due to the accumulation of ions at the interface. Despite intense research, the mechanism that causes this charge injection enhancement remains controversial.[22]

Our concept for a stretchable LEC uses an elastomeric iTMC material sandwiched between two metallic electrodes to enable stretching at room temperature. To impart elasticity to the iTMC $Ru(dtb\text{-}bpy)_3(PF_6)_2$ (dtb-bpy = 4,4'-di-tert-butyl-2,2'-dipyridyl), we dispersed it in an elastomeric matrix of PDMS. Rubner et al. previously showed that films in which an ionic ruthenium complex is dispersed in ~25 vol % of a brittle polymer such as polymethylmethacrylate (PMMA), polycarbonate, or polystyrene exhibit fewer structural defects relative to films without polymer, which improves the device external quantum efficiency (EQE). [23]

4.2 Experimental Section

4.2.1. Materials

All materials and chemicals were purchased commercially and used as received. $Ru(dtb\text{-}bpy)_3(PF_6)_2$ was synthesized according to Bernhard et al.[34] PDMS substrates were prepared by casting PDMS prepolymer (Sylgard 184, Dow Chemical) against polystyrene Petri dishes and curing at 60 °C for 1 h.

4.2.2. Anode Preparation

ITO-coated glass substrates were employed for rigid devices; Au/PDMS substrates were employed for stretchable devices. ITO-coated glass substrates (15-25 Ω/square, Delta Technologies) were rinsed with acetone and then treated with UV ozone (Jelight Company, Inc., Model 42) for 5 min. Stretchable Au/PDMS anodes were prepared by depositing a 15 Å titanium adhesion layer followed by 200 Å of gold onto a PDMS substrate in an e-beam evaporator at 10^{-6} mbar at a rate of 1 Å/s. The substrates were then treated with an air plasma (Harrick Plasma) for 10 s.

4.2.3. Device Fabrication

LECs with $Ru(dtb\text{-}bpy)_3(PF_6)_2$/PDMS emissive layers were prepared using a 3:1 v/v mixture of a 40 mg/mL solution of $Ru(dtb\text{-}bpy)_3(PF_6)_2$ in dichloromethane and a 25 mg/mL solution of PDMS base (Sylgard 184) in dichloromethane. The solution was passed through a 0.2 μm pore size PTFE syringe filter, and then spin coated onto the anode at 1000 rpm for 30 s. The resulting film was annealed in an oven at 60°C overnight. LECs with $Ru(dtb\text{-}bpy)_3(PF_6)_2$/PMMA emissive layers were prepared using a 3:1 v/v mixture of a 40 mg/mL solution of $Ru(dtb\text{-}bpy)_3(PF_6)_2$ in acetonitrile and a 25 mg/mL solution of PMMA (Avg Mw = 996,000 g/mol) in acetonitrile. The solution was passed through a 0.45 μm pore size PTFE syringe filter, and then spin coated onto the anode at 1500 rpm for 30 s. The resulting film was annealed in a vacuum oven at 120°C overnight. The cathode, a 75 μL drop of eutectic gallium-indium (EGaIn), was then deposited on the surface of Ru/PDMS and Ru/PMMA films. Devices fabricated on ITO anodes had a copper wire contact inserted into the EGaIn drop, which was then sealed in an epoxy resin.

4.2.4. Device Characterization

Optical characterization of the thin films was performed using an Olympus BX51 microscope equipped with an Olympus Q-Color3 digital camera. The thickness of Ru/PDMS films was determined using atomic force microscopy in tapping mode. The measurements were carried out on a Digital Instruments Multimode atomic force microscope using a Veeco type FESP cantilever with a nominal tip radius of 8 nm and a nominal force constant of 2.8 N/m. LEC devices were tested using a Keithley 2601 source-measure unit to apply a voltage bias of 5 V DC and measure the current. Radiance was measured with a calibrated UDT S470 optometer attached to an integrating sphere.

4.2.5. Stretchability Measurements

Device stretching was done using a custom built stretching apparatus equipped with clamps to hold the device. The linear strain at failure was determined by stretching Ru/PDMS or Ru/PMMA devices (fabricated using Au/PDMS anodes) until light emission was no longer observed. Device performance of Ru/PDMS and Ru/PMMA devices subjected to repetitive linear strains of 15% was determined by first measuring the current and radiance of the unstretched device for 10 min. After applying 20 - 50 cycles of 15% strain, a new EGaIn cathode was deposited on a previously untested portion of the film and the current and radiance were measured over 10 min.

4.3. Results and Discussion

4.3.1. Optical Characterization of Ru/PDMS LECs

We fabricated 1500-Å-thick films of $Ru(dtb\text{-}bpy)_3(PF_6)_2$ containing ~ 25 vol % PDMS (Ru/PDMS) on an ITO (indium tin oxide) coated glass substrate by spin coating. Optical micrographs of the films show the improvement of film quality caused by the polymer matrix. Films without PDMS (Figure 4.1a) exhibit numerous pinhole defects, which are problematic because they present a pathway for current leakage when the film is used in a device. Optical microscopy reveals that although Ru/PDMS films (Figure 4.1b) have comparatively few pinhole defects, the films exhibit a morphology consistent with phase

separation of the ionic $Ru(dtb\text{-}bpy)_3(PF_6)_2$ and non-polar PDMS. Phase separation can increase the surface roughness of the films, which is detrimental to device performance because significant variation in film thickness produces higher field strengths in the thinner areas.[24, 25] We used tapping-mode AFM to determine the root-mean-square (RMS) roughness of Ru/PDMS films, and compared the RMS roughness value to that of Ru/PMMA films, which do not exhibit a morphology consistent with phase separation (Figure 4.1c). Phase separation in the Ru/PDMS film produces a RMS roughness of 4.54 nm, which is slightly higher than the RMS roughness of Ru/PMMA films (2.64 nm). Compared to RMS-roughness values reported in the literature for LECs,[24-26] both Ru/PDMS and Ru/PMMA films are suitable for LEC devices.

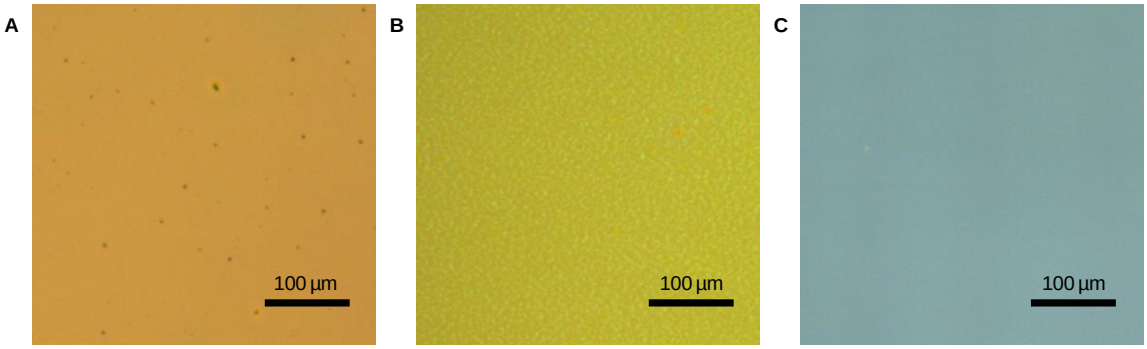

Figure 4.1. Improvement of the quality of $Ru(dtb\text{-}bpy)_3(PF_6)_2$ films using a PDMS matrix. (a) Optical micrograph of a $Ru(dtb\text{-}bpy)_3(PF_6)_2$ film on ITO-coated glass with no polymer matrix. The dark spots in the layer are defects. (b) Optical micrograph of a $Ru(dtb\text{-}bpy)_3(PF_6)_2$ film containing ~25% PDMS. (c) Optical micrograph of a $Ru(dtb\text{-}bpy)_3(PF_6)_2$ film containing ~25% PMMA.

4.3.2. Optoelectronic Characterization of Ru/PDMS LECs on the Rigid Device Test Structure

We fabricated LECs according to the rigid test structure in Figure 4.2a to demonstrate that using PDMS to disperse $Ru(dtb\text{-}bpy)_3(PF_6)_2$ yields LECs with EQEs that are similar to those of devices that use PMMA. The devices consisted of a Ru/PDMS film on a glass substrate bearing an ITO anode. The cathode was a drop of gallium-indium eutectic (EGaIn) ~5 mm in diameter deposited on the surface of the Ru/PDMS film and encased in an epoxy resin. The devices produced bright, uniform emission over the entire area

defined by the cathode when operated under a forward bias of 5 V in ambient conditions (Figure 4.2b). The evolution of current and radiance (Figure 4.2c) and EQE (Figure 4.2d) over 60 minutes of DC device operation show that the devices reach their maximum EQE of just under 1% at ~70 s, and then slowly decay over the testing period. We determined the EQE range and average EQE by depositing two EGaIn cathodes on each of seven Ru/PDMS layers on ITO to produce 14 devices. We operated these devices for 10 minutes under a 5 V bias to determine their steady-state EQEs, which ranged from 0.20 - 0.89% with an average EQE of 0.58%. Two devices were shorted, likely due to defects in the Ru/PDMS film from particle contamination during spin coating. Such defects can be avoided by fabrication in a cleanroom. The average EQE and distribution of EQEs for our devices compare well to those of similar devices with films of Ru(dtb-bpy)$_3$(PF$_6$)$_2$ and 25 vol % PMMA (Ru/PMMA) reported by Bernards et al. [27] These devices used an ITO anode and a gold film on a PDMS substrate laminated on the Ru/PMMA film as the cathode. The devices were operated in ambient conditions for 10 minutes under a 5 V bias, yielding EQEs that ranged from 0.4 - 0.9% with an average of 0.6%.

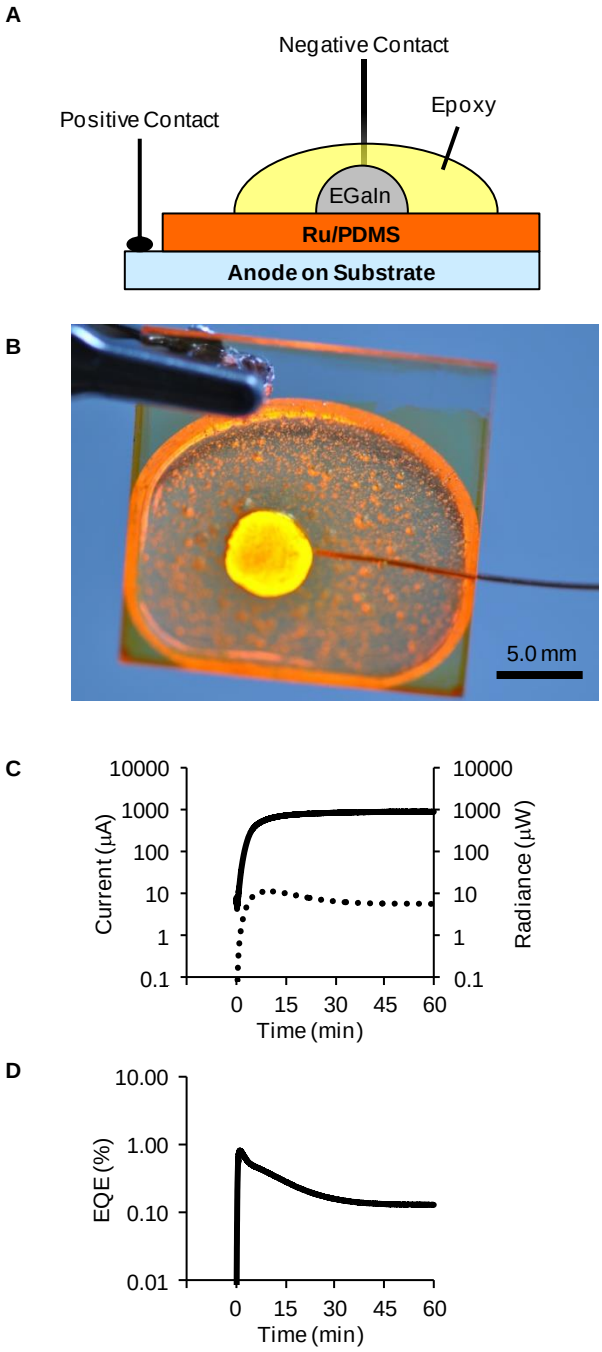

Figure 4.2. Fabrication and characterization of LECs with Ru/PDMS emissive layers. (a) Diagram of the Ru/PDMS device test structure fabricated on an ITO-coated glass anode. (b) Photograph of the device. (c) Temporal evolution of current (solid line) and radiance (dotted line) of a typical device operated under a 5 V bias in ambient conditions. (d) Temporal evolution of external quantum efficiency of a typical device operated under a 5V bias in ambient conditions.

4.3.3. Fabrication and Characterization of Stretchable LECs with a Ru/PDMS Emissive Layer

To test the intrinsic stretchability of the Ru/PDMS layer, we developed a test structure that replaces the rigid ITO anode on glass in Figure 4.2a with a stretchable, semitransparent gold anode on PDMS (Au/PDMS). ITO itself is incompatible with elastomeric substrates such as PDMS due to the high annealing temperatures (~300°C) needed to reach sufficient conductivity, and its brittle nature that severely limits device stretchability.[28] Thin gold films on PDMS, however, remain conductive when subjected to tensile strains of ~20 - 30%.[29] Pre-stretching the PDMS substrate before depositing the gold film boosts the elongation at electrical failure to 100% due to buckles that form in the Au/PDMS when the pre-strain is released. [30] Electrically, gold films possess a lower sheet resistance than ITO, making them especially well-suited to the fabrication of large-area OLEDs. [31] Helander et al. recently demonstrated that the low sheet resistance of thin gold anodes on glass and plastic substrates reduces the voltage drop across the device area, producing more uniform light emission relative to devices with ITO anodes.[32] For large-area emission, this advantage outweighs the lower transparency to visible light of thin gold films compared to ITO. On PDMS, we determined that there is an additional trade-off between optical transparency and stretchability. We fabricated 200-Å-thick gold films by e-beam evaporation on unstretched and pre-stretched (by 15%) PDMS substrates. Transmission spectra are given in Figure S4.1 in the Supporting Information. The transmission of gold films on the former substrates is 26% at 630 nm (the peak wavelength of the electroluminescence spectrum of $Ru(dtb\text{-}bpy)_3(PF_6)_2$); in contrast, the buckles induced in gold films upon releasing the pre-strain from the latter substrates decreases the transmission to 4.5%. Due to this extreme reduction in transmission, we used Au/PDMS anodes fabricated without pre-stretching to evaluate and compare the intrinsic stretchability of Ru/PDMS and Ru/PMMA films. We fabricated LECs by spin-coating either Ru/PDMS or Ru/PMMA films on semitransparent Au/PDMS anodes, and then completing the device by depositing free-standing EGaIn cathodes on top of the films. Although this cathode is not a realistic choice for practical devices, it is

useful to evaluate device stretchability because it deforms along with the device as it is stretched.

LECs with Ru/PDMS emissive layers operate when subjected to bending, twisting, and stretching. Figure 4.3a shows a device that is twisted and stretched into a complex shape to illustrate the deformation that these devices can tolerate. Figure 4.3b shows a device with ~175 mm^2 EGaIn cathode, demonstrating that uniform emission is maintained over large areas even when the devices are deformed. We quantified the stretchability of LECs with Ru/PDMS emissive layers by first determining the linear strain at which the devices fail to emit light. Ru/PDMS LECs show a clear advantage compared to LECs with Ru/PMMA emissive layers: Devices with Ru/PDMS layers sustained up to 27% tensile strain before failure, whereas those with Ru/PMMA layers were only viable up to 17% elongation. Figure S4.2 shows a photograph of a Ru/PDMS device in the unstretched state and stretched to 20%. Since gold films on PDMS typically lose conductivity due to cracking at ~20 - 30% elongation,[29] the likely source of failure of Ru/PMMA devices is damage to the Ru/PMMA films caused by stretching. The elongation at failure of Ru/PDMS devices, however, suggests that failure may be due to cracking of the gold anode rather than the Ru/PDMS emissive layer, although attempts to use scanning electron microscopy to determine the source of device failure were inconclusive.

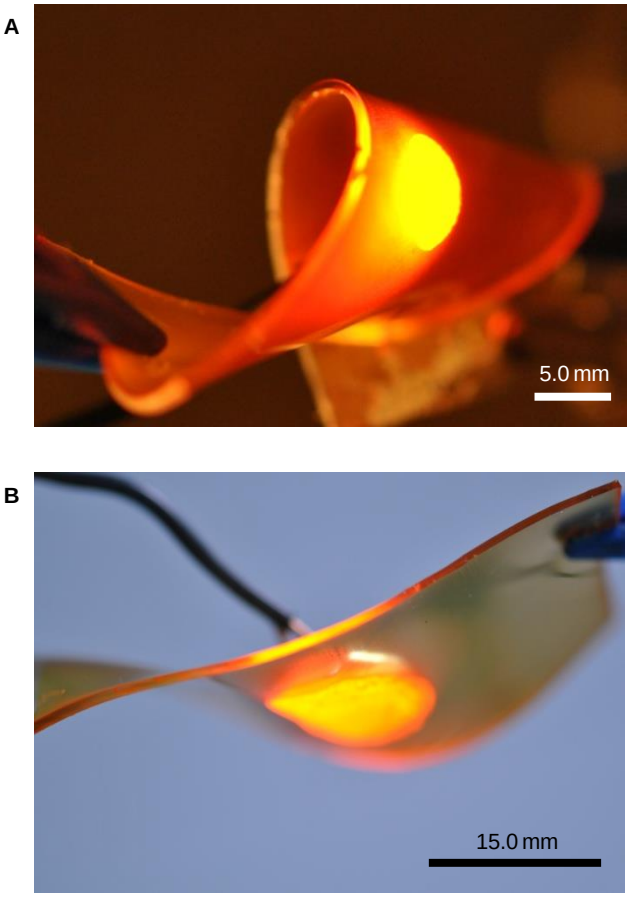

Figure 4.3. Intrinsically stretchable LECs fabricated from Ru/PDMS emissive layers, Au/PDMS stretchable anodes, and EGaIn cathodes. (a) Photograph of a twisted device. (b) Photograph of a large-area (~ 175 mm^2) device, demonstrating uniform emission during stretching.

4.3.4. Durability of Stretchable Ru/PDMS LECs in Comparison with Ru/PMMA LECs

The difference between the strain at failure of Ru/PDMS and Ru/PMMA devices is interesting, but a more compelling difference emerges when the devices undergo repetitive cycles of a small (15%) strain. After a set number of cycles, we relaxed the device, deposited an EGaIn cathode (5 mm in diameter) on a previously untested part of the film, and determined the current (Figure S4.3 in the Supporting Information), radiance (Figure 4.4a, b) and EQE (Figure 4.4c, d) under a 5 V bias for 10 min. EQEs of devices in the initial, unstretched state are lower than those measured for analogous devices fabricated using ITO/glass anodes. The average EQE of four Ru/PDMS devices

fabricated on Au/PDMS anodes is 0.16%, compared to 0.58% on ITO/glass, and the average EQE of four Ru/PMMA devices fabricated on Au/PDMS anodes is 0.40%, compared to 0.60% on ITO/glass. Although lower EQEs are expected due to the lower transparency of Au/PDMS compared to ITO/glass, which reduces the light output, this reduction is worse for Ru/PDMS devices than Ru/PMMA devices. Since Ru/PDMS and Ru/PMMA films perform nearly identically on ITO/glass, we hypothesize that the film quality of Ru/PDMS films on Au/PDMS is simply worse than that of Ru/PMMA films. Unfortunately, optical and scanning electron micrographs of both films do not reveal any major differences since defects in the gold film, such as microcracks, make it difficult to distinguish differences between the polymer films. Despite the different starting EQEs for Ru/PDMS and Ru/PMMA devices on Au/PDMS anodes, the decline of the radiance and, consequently, the EQE with stretching cycles clearly shows the increased device degradation that stretching provokes in Ru/PMMA devices compared to Ru/PDMS devices. After 20 cycles of stretching, Ru/PMMA devices fail to reach the peak radiance achieved by the unstretched device. Subsequent stretching cycles further reduce the peak radiance; after 50 strain cycles, it drops to two orders of magnitude lower than the unstretched device. In contrast, the peak radiance of Ru/PDMS devices remains relatively constant even after 50 strain cycles.

To quantify the device degradation, we used the method of Kalyuzhny et al., [33] which compares the total emitted energy, E_{tot}, of the device (determined from the integral of the radiant flux versus time curve) from the initial application of the voltage to the time at which the electroluminescent intensity drops to one fifth of its maximum value. Figure 4.4e shows a plot of E_{tot} vs the number of strain cycles for Ru/PDMS and Ru/PMMA devices. For both Ru/PDMS and Ru/PMMA devices, the initial set of 20 strain cycles reduces E_{tot}. For Ru/PDMS devices, E_{tot} decreases by one order of magnitude, whereas for Ru/PMMA devices, E_{tot} decreases by two orders of magnitude. The difference between the two devices becomes apparent with additional strain cycles. After the initial drop, E_{tot} for Ru/PDMS devices remains relatively constant at ~0.4 mJ with additional strain cycles. In contrast, E_{tot} for Ru/PMMA devices continues to decrease with additional strain cycles; by 50 strain cycles it falls by three orders of

magnitude to 6.6 μJ. Previous work by Lacour et al.[29] has shown that a network of microcracks develop in gold films supported on PDMS substrates when they are first stretched, along with out-of-plane deflection of the film along the crack margins due to film delamination. With additional strain cycles, the cracks do not increase in length or density and the microscale pattern of the gold film is maintained. The changes in the gold film with initial stretching can account for the initial drop in E_{tot} for Ru/PDMS devices. The initial introduction of microcracks and delaminated regions roughens the gold film, which likely distorts the Ru/PDMS layer, causing it to be inconsistent in thickness. Thin regions (likely where the gold film has delaminated) will produce current leakage, reducing the EQE and E_{tot}. With additional strain cycles, however, both the microstructure of the gold film and E_{tot} stabilize, indicating that Ru/PDMS films can sustain these strain cycles without degradation. The PDMS matrix has imparted stretchability to the LEC. Changes in the gold film after the initial stretching cycles may also account, in part, for the E_{tot} reduction in Ru/PMMA devices after initial stretching, although the continued decrease in E_{tot} with additional stretching cycles can only be attributed to damage to the Ru/PMMA film with stretching. The difference in LEC performance *after* stabilization of the Au/PDMS anode with initial stretching establishes that the elastomeric nature of the PDMS matrix increases the stretchability of LECs relative to those that use a brittle PMMA matrix.

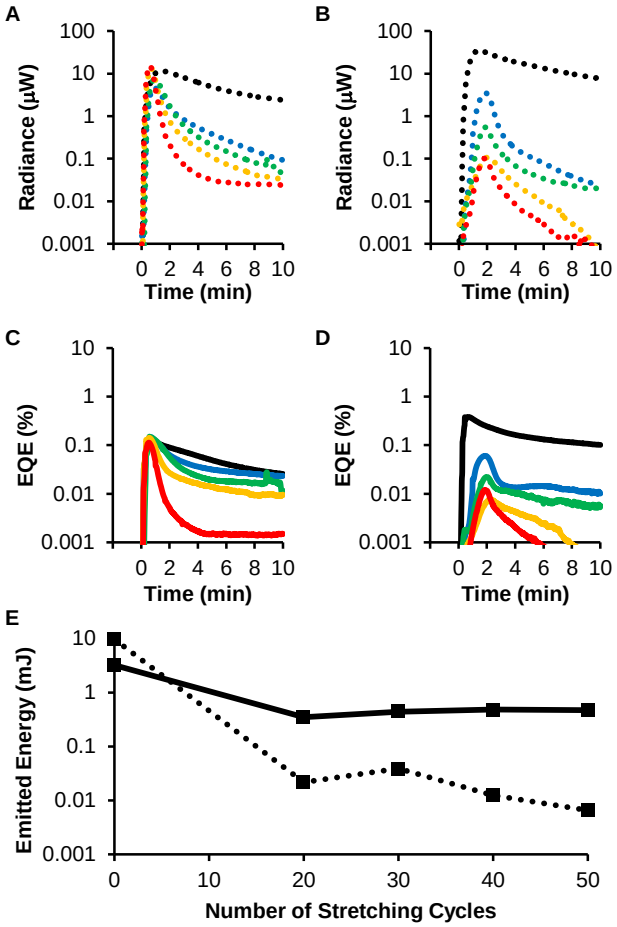

Figure 4.4. Performance comparison after repetitive, 15% elongation of LECs fabricated from Ru/PDMS and Ru/PMMA emissive layers, with Au/PDMS stretchable anodes and EGaIn cathodes. Parts a – d show traces corresponding to unstrained (black), 20 strain cycles (blue), 30 strain cycles (green), 40 strain cycles (yellow), 50 strain cycles (red). (a) Temporal evolution of radiance of Ru/PDMS devices operated under a 5 V bias. (b) Temporal evolution of radiance of Ru/PMMA devices operated under a 5 V bias. (c) Temporal evolution of EQE of Ru/PDMS devices operated under a 5 V bias. (d) Temporal evolution of EQE of Ru/PMMA devices operated under a 5 V bias. (e) Plot of total emitted energy (E_{tot}) vs the number of strain cycles for Ru/PDMS (solid line) and Ru/PMMA (dotted line) devices.

4.4. Conclusions

In conclusion, the approach to stretchable light-emitting devices presented here combines a simple LEC device architecture with an intrinsically stretchable light-emitting material. The design of these devices is well-suited to the fabrication of large-area, illuminated panels for use in signage and biomedical applications due to several device features: First, the device design supports the large-area emission necessary for these macroscopic applications. Second, heating is not required to stretch and deform the elastomeric devices, thus they are compatible with applications that involve wrapping the device around the human body. Third, the limited stress testing reported here indicates that the devices can withstand repetitive deformation, making them useful for applications where reusability is important and those that require dynamic conformational changes. Fourth, they withstand substantial deformation before device failure. Presently, practical use of these devices is limited by the semitransparent Au/PDMS anode and the EGaIn cathode used to support the proof-of-concept presented here. Replacing these electrodes with stretchable conductive films such as carbon nanotubes or metal nanowires, encapsulating the devices into an elastomeric package, and optimising the device performance are the next important steps toward useful devices.

4.5. References

[1] D. -H. Kim, N. Lu, R. Ma, Y. -S. Kim, R. -H. Kim, S. Wang, J. Wu, S. M. Won, H. Tao, A. Islam, K. J. Yu, T. Kim, R. Chowdhury, M. Ying, L. Xu, M. Li, H. -J. Chung, H. Keum, M. McCormick, P. Liu, Y. -W. Zhang, F. G. Omenetto, Y. Huang, T. Coleman, J. A. Rogers, *Science* **2011**, *333*, 838.

[2] H. C. Ko, M. P. Stoykovich, J. Song, V. Malyarchuk, W. M. Choi, C. -J. Yu, J. B. Geddes III, J. Xiao, S. Wang, Y. Huang, J. A. Rogers, *Nature* **2008**, *454*, 748.

[3] T. Sekitani, H. Nakajima, H. Maeda, T. Fukushima, T. Aida, K. Hata, T. Someya, *Nature Materials* **2009**, *8*, 494.

[4] J. A. Rogers, T. Someya, Y. Huang, *Science* **2010**, *327*, 1603.

[5] M. Kaltenbrunner, G. Kettlgruber, C. Siket, R. Schwodiauer, S. Bauer, *Advanced Materials* **2010**, *22*, 2065.

[6] C. Yu, C. Masarapu, J. Rong, B. Wei, H. Jiang, *Advanced Materials* **2009**, *21*, 4793.

[7] D. J. Lipomi, B. C. Tee, M. Vosgueritchian, Z. Bao, *Advanced Materials* **2011**, *23*, 1771.

[8] R. Sprengard, K. Bonrad, T. K. Daeubler, T. Frank, V. Hagemann, I. Koehler, J. Pommerehne, C. R. Ottermann, F. Voges, B. Vingerling, *Proceedings of SPIE* **2004**, *5519*, 173.

[9] B. L. Diffey, *Physics in Medicine and Biology* **1980**, *25*, 405.

[10] H. T. Whelan, R. L. Smits Jr., E. V. Buchman, N. T. Whelan, S. G. Turner, D. A. Margolis, V. Cevenini, H. Stinson, R. Ignatius, T. Martin, J. Cwiklinski, A. F. Philippi, W. R. Graf, B. Hodgson, L. Gould, M. Kane, G. C., J. Caviness, *Journal of Clinical Laser Medicine and Surgery* **2001**, *19*, 305.

[11] H. Bayley, F. Gasparro, R. Edelson, *Trends in Pharmacological Sciences* **1987**, *8*, 138.

[12] D. Hawkins, H. Abrahamse, *African Journal of Biomedical Research* **2007**, *10*, 99.

[13] Z. Yu, X. Niu, Z. Liu, Q. Pei, *Advanced Materials* **2011**, *23*, 3989.

[14] J. D. Slinker, J. Rivnay, J. S. Moskowitz, J. B. Parker, S. Bernhard, H. D. Abruña, G. G. Malliaras, *Journal of Materials Chemistry* **2007**, *17*, 2976.

[15] Q. Pei, G. Yu, C. Zhang, Y. Yang, A. J. Heeger, *Science* **1995**, *269*, 1086.

[16] Q. Pei, Y. Yang, G. Yu, C. Zhang, A. J. Heeger *Journal of the American Chemical Society* **1996**, *118*, 3922.

[17] P. Matyba, K. Maturova, M. Kemerink, N. D. Robinson, L. Edman *Nature Mater.* **2009**, *8*, 672.

[18] M. Lenes, G. Garcia-Belmonte, D. Tordera, A. Pertegas, J. Bisquert, H. J. Bolink *Advanced Functional Materials* **2011**, *21*, 1581.

[19] J. D. Slinker, J. A. DeFranco, M. J. Jaquith, W. R. Silveira, Y. -W. Zhong, J. M. Moran-Mirabal, H. G. Craighead, H. D. Abruña, J. A. Marohn, G. G. Malliaras, *Nature Materials* **2007**, *6*, 894.

[20] J. C. de Mello, N. Tessler, S. C. Graham, R. H. Friend *Physical Review B* **1998**, *57*, 12951.

[21] J. C. de Mello *Physical Review B* **2002**, *66*, 235210.

[22] D. R. Rodovsky, O. G. Reid, L. S. C. Pingree, D. S. Ginger *ACS Nano* **2010**, *4*, 2673.

[23] H. Rudmann, M. F. Rubner, *Journal of Applied Physics* **2001**, *90*, 4338.

[24] F. P. Wenzl, P. Pachler, C. Suess, A. Haase, E. J. W. List, P. Poelt, D. Somitsch, P. Knoll, U. Scherf, G. Leising *Advamced Functional Materials* **2004**, *14*, 441.

[25] F. P. Wenzl, P. Polt, A. Haase, S. Patil, U. Scherf, G. Leising *Solid State Ionics* **2005**, *176*, 1747.

[26] T. -H. Kwon, Y. H. Oh, I. -S. Shin, J. -I. Hong *Advanced Functional Materials* **2009**, *19*, 711.

[27] D. A. Bernards, T. Biegala, Z. A. Samuels, J. D. Slinker, G. G. Malliaras, S. Flores-Torres, H. D. Abruña, J. A. Rogers, *Applied Physics Letters* **2004**, *84*, 3675.

[28] F. Zhu, in *Organic Light-Emitting Materials and Devices* (Eds: Z. Li, H. Meng), CRC Press, Boca Raton, Florida **2007**, Ch. 6.

[29] S. P. Lacour, D. Chan, S. Wagner, T. Li, Z. Suo, *Applied Physics Letters* **2006**, *88*, 204103.

[30] J. Jones, S. P. Lacour, S. Wagner, Z. Suo, *Journal of Vacuum Science & Technology A* **2004**, *22*, 1723.

[31] S. Han, Y. Yuan, Z. H. Lu, *Journal of Applied Physics* **2006**, *100*, 074504.

[32] M. G. Helander, Z. -B. Wang, M. T. Greiner, Z. -W. Liu, J. Qiu, Z. -H. Lu, *Advanced Materials* **2010**, *22*, 2037.

[33] G. Kalyuzhny, M. Buda, J. McNeill, P. Barbara, A. J. Bard, *Journal of the American Chemical Society* **2003**, *125*, 6272.

[34] Bernhard, S. J. A. Barron, P. L. Houston, H. D. Abruña, J. L. Ruglovksy, X. Gao, G. G. Malliaras, *Journal of the American Chemical Society* **2002**, *124*, 13624.

4.6. Supporting Information

4.6.1. Supporting Figures

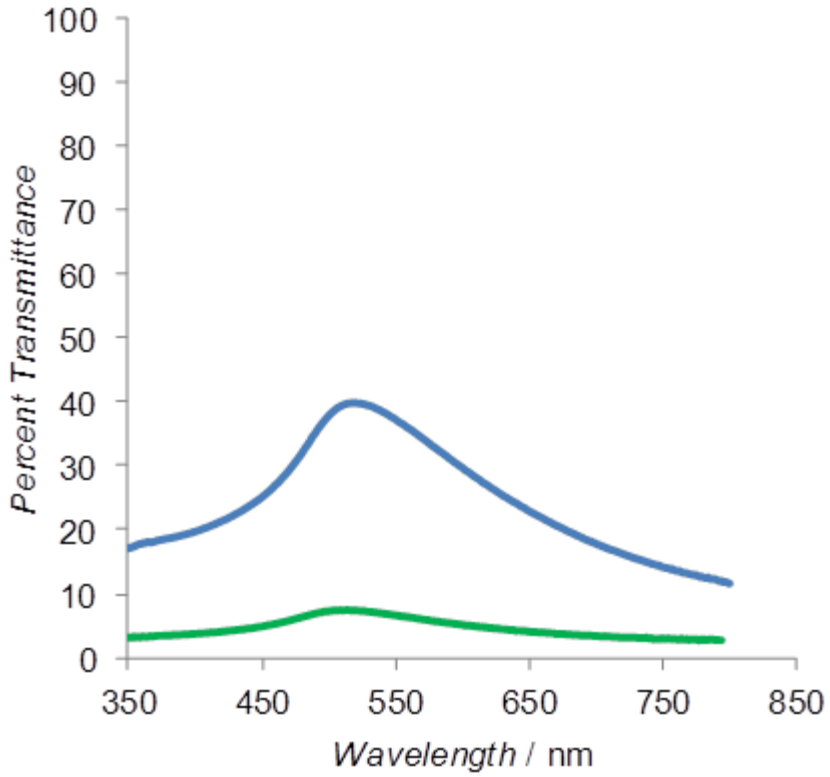

Figure S4.1. Transmittance of gold on PDMS. Percent Transmittance of 200 Å Au on unstrained PDMS (blue) and of 200 Å Au on pre-strained PDMS (15% pre-strain) after releasing the pre-strain to induce waves in the film (green).

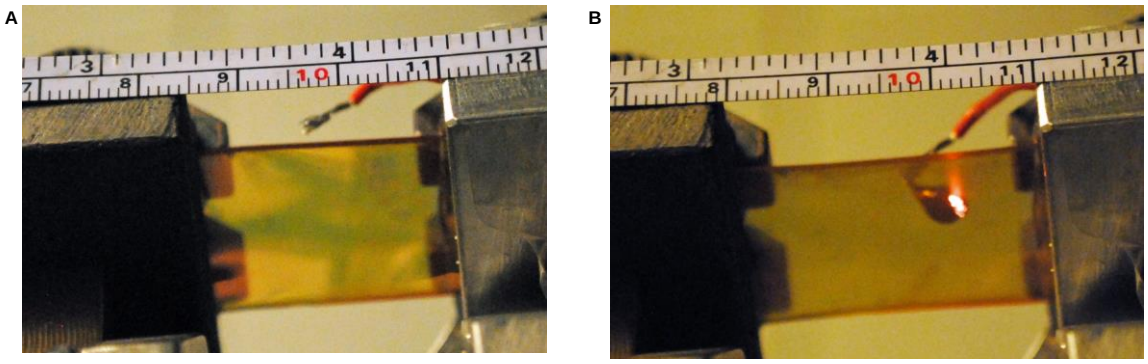

Figure S4.2. Photograph of a Ru/PDMS LEC with and without linear strain (a) Ru/PDMS LEC unstretched and in the off state; (b) Ru/PDMS LEC stretched to 20% elongation and operating under a 5V forward bias.

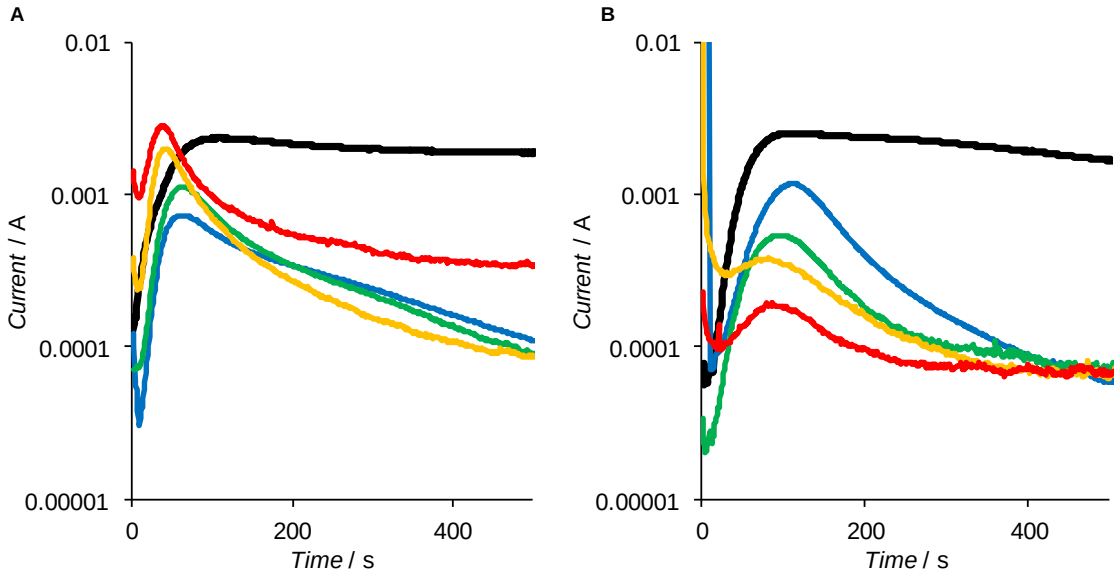

Figure S4.3. Performance comparison after repetitive, 15% elongation of LECs fabricated from Ru/PDMS and Ru/PMMA emissive layers, with Au/PDMS stretchable anodes and EGaIn cathodes. Parts (a) and (b) show traces corresponding to unstrained (black), 20 strain cycles (blue), 30 strain cycles (green), 40 strain cycles (yellow), 50 strain cycles (red). (a) Temporal evolution of current of Ru/PDMS devices operated under a 5 V bias. (b) Temporal evolution of current of Ru/PMMA devices operated under a 5 V bias.

5. Chapter 5

Light-Emitting Electrochemical Cells with IIR-g-PEO Elastomeric Matrices for Improved Mixing with Ionic Transition Metal Complex Emitters

5.1. Introduction

Stretchable light-emitting devices will have significant implications in wearable electronics that can deform and stretch with the movements of the human body for applications in clothing, wearable health-monitoring devices with digital read-outs, and even light-therapy treatments that can be laminated directly onto skin. Rogers and co-workers have demonstrated that rigid pixel islands of inorganic light-emitting diodes (ILEDs) can be connected by stretchable arc-shaped bridges to enable the fabrication of displays[1] and Someya et al. demonstrated that organic light-emitting diode (OLED) islands could be connected by stretchable nanotube interconnects[2]. In these approaches, the device islands themselves are rigid and do not experience strain, rather the strain is absorbed fully by the interconnect enabling the fabrication of an array of small pixels joined by stretchable interconnects. An alternative method to developing stretchable light-emitting devices focuses on the development of inherently stretchable materials to enable the fabrication of large-area stretchable pixels.

The field of large-area stretchable light-emitting devices has seen great advancements over the last 5 years. Pei and co-workers introduced the first intrinsically stretchable polymer light emitting electrochemical cell (PLEC) capable of deformations of up to 45% without damaging the electroluminescent properties; the drawback of this device was that the substrates had to be heated above the glass transition temperature to 70°C to deform the device, rendering them incompatible with applications on the human body where elasticity at room temperature is required.[3] In Chapter 4, we demonstrated the first example of a stretchable light-emitting electrochemical cell (LEC) capable emitting light up to 27% strain and sustaining 50 cycles of repetitive strains of 15% without affecting the peak radiance.[4] Following these initial reports, Pei and co-workers developed a room-temperature stretchable PLEC by modifying the elastomer used in their composite, realizing devices capable of withstanding strains up to 120% while still emitting light.[5] Pei and co-workers also demonstrated for the first time a stretchable polymer light-emitting device (PLED) which was capable of stretching up to 130%.[6]

In contrast to PLECs where the light-emitting properties are derived from the semiconducting polymers themselves, ionic transition metal complex (iTMC) LECs achieve light-emission from small ionic transition metal complex molecules. LECs based on iTMCs are unique in that they can be used as single component systems or they can be dispersed in non-conductive polymer matrices to impart different features to the resultant LECs: For instance, dispersing $Ru(dtb\text{-}bpy)_3(PF_6)_2$ in a rigid polymer matrix such as poly(methyl methacrylate) (PMMA), polycarbonate (PC) and poly(styrene) (PS) results in increased device stability and enhanced lifetimes of 900 – 1100 hours compared to pristine films which had lifetimes of 700 hours.[7] Lyons et al. found that dispersing the Ru-iTMC in a poly(ethylene oxide) (PEO) matrix results in faster turn-on times than pristine Ru-iTMC devices owing to the increased ion mobility of the counter ions through the PEO matrix.[8] In systems with electrolyte additive, PEO has been shown to enhance ion dissociation by coordinating to the cations of the salt while the anions have low interaction with the polymer and maintain their mobility leading to an acceleration of ion transport through the film.[9] In Chapter 4, we demonstrated that dispersing the Ru-iTMC in an elastomeric matrix enables the creation of stretchable LECs. The main drawback of using poly(dimethyl siloxane) (PDMS) as a matrix is its permeability to water and oxygen which react with the ionic transition metal complex and form quenching species.[10],[11] Therefore, there is a need to develop new stretchable polymer matrices for LECs with high impermeability to oxygen and moisture to enable the fabrication of high-stability, stretchable LECs.

An exciting candidate to replace PDMS as an elastomeric matrix in stretchable LECs is isobutylene-co-isoprene rubber (IIR). Uncured IIR has an elongation at break of ~ 800% and a Young's Modulus of 0.5 MPa combining elastic properties necessary for stretchable LEC fabrication with high oxygen and moisture impermeability.[12] We have demonstrated that IIR can be used as a barrier against corrosive vapors to protect electrical components such as indium tin oxide (ITO) and silver nanowires (AgNWs)[13] and as a barrier to oxygen and moisture to protect thin films of silver against oxidation[14]. Incorporation of IIR directly in the emissive layer may prevent oxygen and moisture from

permeating into the emissive layer and reacting with the iTMC thus providing greater stability to the LEC.

In this Chapter, we will show that commercial formulations of non-polar IIR exhibit poor mixing with the iTMC $Ru(dtb\text{-}bpy)_3(PF_6)_2$ resulting in macroscale phase separation visible by optical microscopy. Macroscale phase separation results in an emissive layer of inhomogeneous thickness which will result in different turn-on times for different regions in the emissive layer: Thinner regions with less insulating polymer will exhibit faster turn-on times since the counter ions have shorter distances to travel to reach the electrode and lower the barrier to charge injection. Conversely, thicker regions of the emissive layer or regions of reduced ion mobility due to higher insulating polymer content will exhibit longer turn-on times due to the longer migration distance and the slower mobility of the ions respectively. In LEC devices, improving the blend quality in order to achieve maximum interfacial surface area between constituents is desired in order to achieve homogeneous light-emission and maximize device performance.[15] In PLEC devices phase separation is a challenge that is inherent to the system; the non-polar semiconducting polymer of PLECs requires the addition of ionic electrolyte and polar polymer ion-transport polymers to provide the mobile ionic species necessary for the creation of electric double layers. In PLEC systems, researchers have developed methods to reduce phase separation of PLEC components through the addition of bifunctional (surfactant-like) additives[15] to promote mixing between the polymer and the electrolyte or by chemically modifying the semiconducting polymer with PEO side chains to enhance its mixing with the solid salt electrolyte.[16],[17] In order to render IIR and the Ru-iTMC compatible, we chose the latter approach and grafted PEO side chains onto the IIR backbone (IIR-g-PEO). Graft copolymers are intriguing materials because they combine the properties of the polymers of which they are comprised. In this case polar PEO chains which will promote mixing with the ionic ruthenium complex light-emitter are grafted onto the stretchable, water and oxygen impermeable IIR backbone. We hypothesize that incorporating PEO sidechains onto IIR will increase the miscibility with the ionic light-emitting species while still providing stretchability to the emissive layer due to the flexible IIR backbone. It is important to note, that a trade-off between

increased miscibility with the iTMC and decreased impermeability of the IIR-g-PEO as the PEO content is increased is expected. Addition of hydrophilic polymers to IIR can affect impermeability; copolymers of IIR with hydrophilic polymers have been used to form cell encapsulation membranes that allow oxygen exchange to occur.[18] Longer PEO side chains in the IIR-g-PEO graft copolymer will increase the free-volume which will render the material more permeable to oxygen and moisture. Additionally, increased PEO content in IIR-g-PEO graft copolymers have been found to form crystalline PEO domains[19] which reduces the elongation at break of the graft copolymer.[12] Therefore, the ideal formulation of IIR-g-PEO will possess an amount of PEO that is sufficient to provide adequate mixing with the iTMC yet maintain stretchability and high impermeability to moisture and oxygen.

IIR-g-PEO graft copolymers were first reported by Ikeda et al. where the PEO content was modified by altering the molecular weight of the PEO in the graft.[19] Gillies and co-workers reported a novel functionalization method for grafting PEO onto IIR with unprecedented control over PEO graft sites allowing for very high PEO content to be incorporated into the graft copolymer.[20] At high PEO content, they demonstrated that IIR-g-PEO surfaces were able to resist the adsorption of proteins for applications as antimicrobial coatings. We will show that IIR-g-PEO can be used as a polymer matrix in LECs allowing for increased miscibility with the Ru-iTMC at high PEO content. Emissive layers fabricated with IIR-g-PEO polymer matrices with PEO content greater than 34 wt% exhibited enhanced device stabilities: While LECs with PDMS polymer matrices decay to one fifth of the maximum radiance in 35 minutes when operated at a 0.5 mA bias, LECs with IIR-g-PEO (PEO content > 34 wt%) do not decay to one fifth of the maximum radiance even after 6 hours of testing at a 0.5 mA bias. Devices fabricated with IIR-g-PEO (34 wt% PEO) as the polymer matrix can sustain repeated cyclic strain without experiencing changes to the peak radiance demonstrating their potential as a stretchable emissive layer material.

5.2 Experimental Section

5.2.1. Materials

All materials and chemicals were purchased commercially and used as received. $Ru(dtb\text{-}bpy)_3(PF_6)_2$ was synthesized according to Bernhard et al.[21] LANXESS X_Butyl™ products (RB301, RB101-3, BB2030, CB1240, I4565P) were provided by Lanxess Inc. (London, Ontario) and used as received without further purification. IIR-g-PEO was provided by the Gillies group (UWO, London, Ontario) and prepared according to literature.[20] Poly(dimethylsiloxane) (PDMS) (Sylgard 184) was obtained from Dow Corning (Midland, MI).

5.2.2. Anode Preparation

ITO-coated glass substrates 1 $inch^2$ (15 – 25 Ω/square, Delta Technologies) were sonicated in DI H_2O 15 minutes, followed by sonication in IPA for 15 minutes then dried under a stream of nitrogen. ITO substrates were subsequently treated with UV-ozone (Jelight Company, Inc., Model 42) for 15 minutes. Stretchable Au/PDMS anodes were prepared by depositing a 15 Å-thick titanium adhesion layer followed by 200 Å of gold onto a PDMS substrate in an e-beam evaporator at 10^{-6} mbar at a rate of 1 Å/s. The substrates were then treated with an air plasma (Harrick Plasma) for 30 s at an air pressure of 10 psig (flow rate of 32 mL/min) at medium discharge setting.

5.2.3. LEC Device Fabrication

Emissive layer solutions were prepared with dry solvent and spin coated in inert atmosphere to minimize exposure to humidity and oxygen. Raw butyl rubber formulations (LANXESS X_Butyl™ RB301, RB101-3, BB2030, CB1240 and I4565P) were prepared in 1:1 CH_2Cl_2:$CHCl_3$ at a concentration of 25 mg/mL. PDMS (Sylgard 184 base), IIR-g-PEO(16wt% PEO), IIR-g-PEO(34 wt% PEO), IIR-g-PEO(69 wt% PEO) and PEO stock solutions were prepared in dry dichloromethane at a concentration of 25 mg/mL. $Ru(dtb\text{-}bpy)_3(PF_6)_2$ was prepared at a concentration of 40 mg/mL in the same solvent as the polymer matrix. LECs with Ru(dtb-

bpy)$_3$(PF$_6$)$_2$/polymer emissive layers were prepared using a 3:1 v/v mixture of Ru(dtb-bpy)$_3$(PF$_6$)$_2$ stock solution to polymer stock solution. The solutions were passed through a 1 µm pore size PTFE syringe filter followed by a 0.2 µm pore size PTFE syringe filter, and then spin coated onto the anode at 1000 rpm for 30 s. Solutions containing commercial grade IIR were only passed through the 1 µm pore size PTFE syringe filter prior to spin coating. The resulting films were annealed in an oven at 120°C overnight.

5.2.4. Emissive Layer Characterization

Optical characterization was performed using an Olympus BX51 microscope equipped with an Olympus Q-Color3 digital camera. Scanning electron microscopy was carried out on a Hitachi S-4500 scanning electron microscope at Surface Science Western, London, Canada. Prior to imaging, samples were coated with 3 – 5 nm Au using a Hummer VI sputtering system. Thickness of the emissive layer was determined by spin coating the emissive layer on silicon wafer instead of ITO/glass and freeze-fracturing the silicon to create a cross section. Atomic force microscopy was carried out using the dynamic force mode of a Park Systems XE-100 AFM at Surface Science Western, London, Canada. A silicon cantilever with a nominal spring constant of 40 N/m, resonant frequency of 300 kHz and tip radius of 10 nm was used. Images were collected from three spots on each sample in an area of 40 µm × 40 µm and processed using WSxM 5.0 Develop 1.0 software. Root-mean-square (RMS) roughness values from three different areas of a sample were averaged.

5.2.5. LEC Characterization

Drops of eutectic gallium indium (EGaIn) (50 µL) were pipetted onto the surface of the emissive layers to serve as cathodes. Two drops were deposited onto each emissive layer therefore two devices were tested per piece of ITO/glass. Prior to sealing EGaIn drops in epoxy, copper wire was inserted in the EGaIn drop to enable contact to the sourcemeter and copper tape (3M) was adhered to the ITO to create a contact to the anode. LECs were tested in inert atmosphere by applying 9 V bias with 0.1 A compliance (for voltage biased testing) or a 0.5 mA bias with 40 V compliance (for current biased testing) using a Keithley 2601 source-measure and measuring the voltage. Radiance was

measured in inert atmosphere with a calibrated UDT S470 optometer attached to an integrating sphere.

5.2.6. Stretchability Measurements

Device stretching was done using a micro-vice stretching apparatus (S.T. Japan Inc). Device performance of Ru/PDMS and Ru/IIR-g-PEO (34 wt% PEO), and Ru/IIR-g-PEO (69 wt% PEO) devices subjected to repetitive linear strains of 15% was determined by first measuring the current and radiance of the unstretched device for 5 min. After applying 10 – 50 cycles of 15% strain, a new EGaIn cathode was deposited on a previously untested portion of the film and the current and radiance were measured over 5 min.

5.3. Results and Discussion

In order for IIR to be used as a polymer matrix in the emissive layer of LECs, homogeneous films of the IIR with the Ru-iTMC must first be obtained. Ru(dtb-bpy)$_3$(PF$_6$)$_2$ was chosen as the iTMC due to its facile synthesis and previous use in the literature as an iTMC material dispersed in both brittle polymers and elastomers for the fabrication of rigid[7],[8] and stretchable LECs[4]. Film homogeneity is an important criterion of emissive layer thin films since macroscale phase separation results in an emissive layer of inhomogeneous thickness which will result in different turn-on times and different ionic conductivities throughout the emissive layer. In PLEC devices, it has been shown that the best device performances occur when an interpenetrated morphology is formed between the constituents of the emissive layer as this maximizes the interfacial surface area resulting in fast ion-transport and a continuous network of electronic transport of injected electrons and holes.[15]

We fabricated emissive layers with IIR polymer matrices and compared the morphology and degree of phase separation to established Ru/PDMS emissive layers (Chapter 4). Emissive layers were fabricated on silicon wafer to allow for thickness measurements to be obtained. Film homogeneity was investigated by optical microscopy and scanning electron microscopy (SEM), and the RMS roughness was measured by

tapping-mode atomic force microscopy (AFM). The Ru/PDMS emissive layers developed in Chapter 4 produce homogeneous films with low RMS surface roughness (RMS roughness = 3.4 ± 2.5 nm) (Figure 5.1a-c).

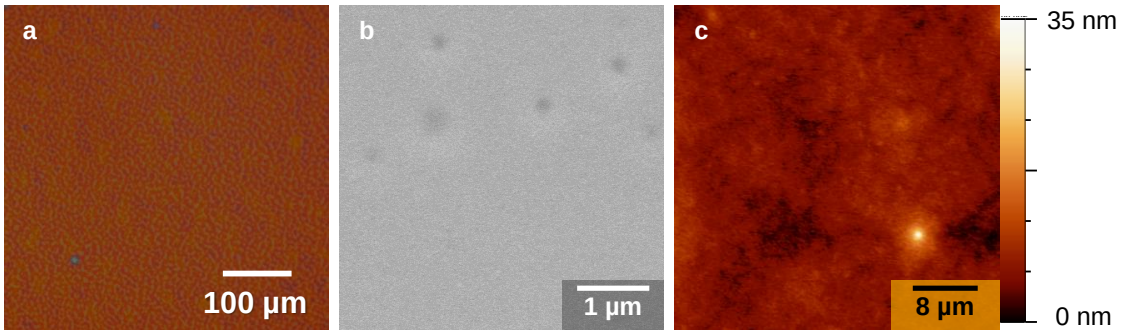

Figure 5.1. (a) Optical micrograph of Ru/PDMS; (b) SEM image of Ru/PDMS; (c) AFM image of Ru/PDMS.

5.3.1. Incorporation of Commercial IIR Formulations in Emissive Layers

The first butyl rubber compounds that we tested as elastomeric matrices for the Ru-iTMC were raw, commercial formulations of butyl rubber. LANXESS X_Butyl™ RB301 is a commercial grade butyl rubber comprised of 1.85 mol% isoprene used in tire innerliners. LANXESS X_Butyl™ RB101-3 is used primarily as a base in chewing gum and it contains 1.75 mol% isoprene. The chemical structure of butyl rubber is shown in Figure 5.2. LANXESS X_Butyl™ RB301 and LANXESS X_Butyl™ RB101-3 have limited solubility in dichloromethane, therefore a 1:1 v/v mixture of CH_2Cl_2:$CHCl_3$ was used to solubilize 25 mg/mL of butyl rubber. The ruthenium iTMC was also dissolved in 1:1 CH_2Cl_2:$CHCl_3$ and the two solutions were mixed in a 3:1 v/v Ru-iTMC:IIR ratio. The mixture was spun onto clean silicon wafer and characterized by optical microscopy, SEM and AFM.

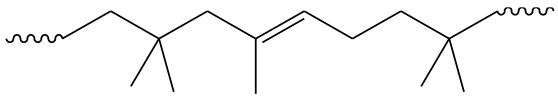

Figure 5.2. Chemical structure of LANXESS X_Butyl™ RB301 and RB101-3 where RB301 contains 1.85 mol% isoprene functionality and RB101-3 contains 1.75 mol% isoprene functionality.

As evidenced in the optical microscopy and SEM images, thin films of Ru/RB301 and Ru/RB101-3 exhibit large-scale phase separation due to the poor miscibility of the nonpolar raw butyl rubber backbone with the iTMC. Ru/RB301 appears to have large domains of phase separation on the order of several microns (Figure 5.3a, b). The AFM image shows the great variation in height within the film (Figure 5.3c) resulting a variation in maximum height of 697.29 ± 60.84 nm and high RMS surface roughness values of 213.0 ± 30.0 nm which are two orders of magnitude larger than Ru/PDMS emissive layers. Ru/RB101-3 also exhibits phase separation in the film with variation in maximum height of 671.38 ± 26.49 nm (Figure 5.3d-f) and high RMS roughness of 192.7 ± 30.7 nm which is the same as Ru/RB301 thin films within error. Compared to the homogeneous thin film of Ru/PDMS (RMS roughness = 3.4 ± 2.5 nm) which have variations in maximum height of 34.86 ± 2.56 nm, it is evident that these films are not suitable for use in LECs.

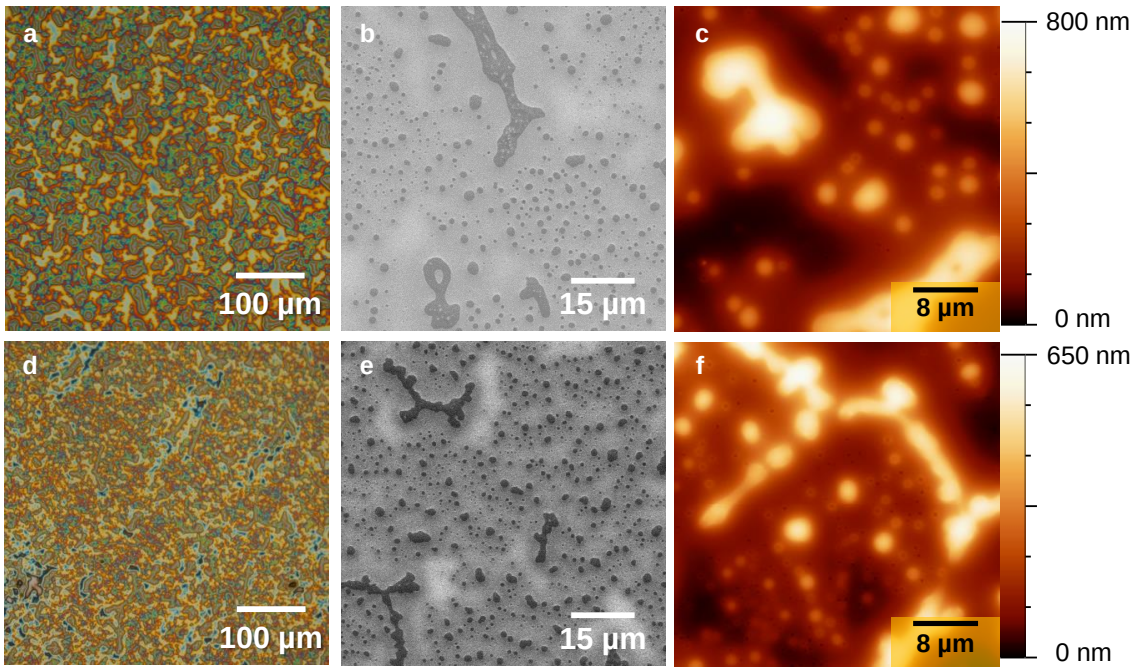

Figure 5.3. (a) Optical micrograph of Ru/RB301; (b) SEM image of Ru/RB301; (c) AFM image of Ru/RB301; (d) Optical micrograph of Ru/RB101-3; (e) SEM image of Ru/RB101-3; (f) AFM image of Ru/RB101-3.

We investigated the use of halogenated butyl rubber derivatives to determine if the presence of more polar groups on the rubber backbone would facilitate mixing with the Ru-iTMC. LANXESS X_Butyl™ BB2030 is a butyl rubber polymer created by bromination of the isoprene functionality resulting in 1.8 mol% bromine incorporation (Figure 5.4a). Similarly, LANXESS X_Butyl™ CB1240 is a chlorinated butyl rubber containing 1.25 mol% chlorine (Figure 5.4b). Halogenated rubber derivatives also have limited solubility in CH_2Cl_2 and therefore the 1:1 v/v mixture of CH_2Cl_2:$CHCl_3$ was used to prepare solutions of BB2030, CB1240 and the Ru-iTMC. The halogenated rubber species were mixed with $Ru(dtb\text{-}bpy)_3(PF_6)_2$ in a 3:1 v/v Ru:polymer ratio and spin coated onto silicon wafer substrates to determine the impact of halogenated rubber on the miscibility with the Ru-iTMC.

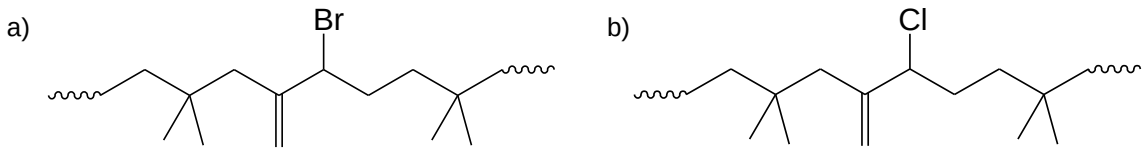

Figure 5.4. (a) Chemical structure of LANXESS X_Butyl™ BB2030. (b) Chemical structure of LANXESS X_Butyl™ CB1240.

The incorporation of polarizable halogen functional groups on the rubber backbone was not sufficient to overcome the phase separation between the non-polar butyl rubber chains and the iTMC, likely due to the low mol% of halogen functionalization. Ru/BB2030 films show phase separation in the optical micrograph (Figure 5.5a) and in the SEM image (Figure 5.5b). There are large variations in height (Figure 5.5c) resulting in a high RMS roughness of 111.5 ± 19.4 nm and variation in maximum height of 663.7 ± 86.0 nm showing no improvement over films prepared with RB301 and RB101-3. Similarly, films of CB1240 also exhibit phase separation in the optical, SEM and AFM images (Figure 5.5d-f) with a high surface roughness of 118.7 ± 23.4 nm and variation in maximum height of 657.4 ± 74.1 nm. The high degree of phase separation in emissive layer films with halogenated rubber makes BB2030 and CB1240 poor polymer matrices for the Ru-iTMC and they were not pursued further in the fabrication of LECs.

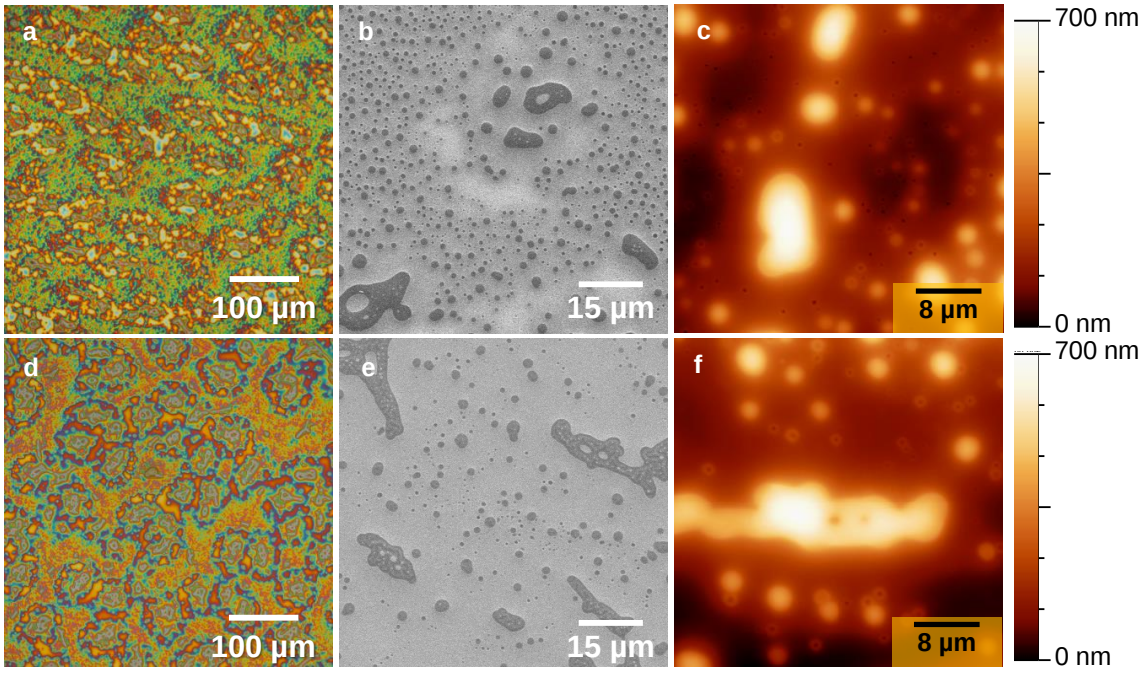

Figure 5.5. (a) Optical micrograph of Ru/BB2030. (b) SEM image of Ru/BB2030. (c) AFM image of Ru/BB2030. (d) Optical micrograph of Ru/CB1240. (e) SEM image of Ru/CB1240. (f) AFM image of Ru/CB1240.

We attempted to achieve better mixing of the Ru-iTMC with butyl rubber through the use of a butyl rubber ionomer species (LANXESS X_Butyl™ I4565) as the polymer matrix whose structure is given in Figure 5.6. Ionomers are a class of polymer containing ionic groups on the polymer backbone which form ionic aggregates in solution.[22] However, given the low ionic content (0.4 mol%) even this modification to the rubber backbone proved insufficient to facilitate mixing between the polymer and the iTMC. Again, phase separation was visible (Figure 5.7a-c) and the RMS surface roughness was 117.8 ± 34.4 nm with variation in maximum height of 686.3 ± 122.1 nm.

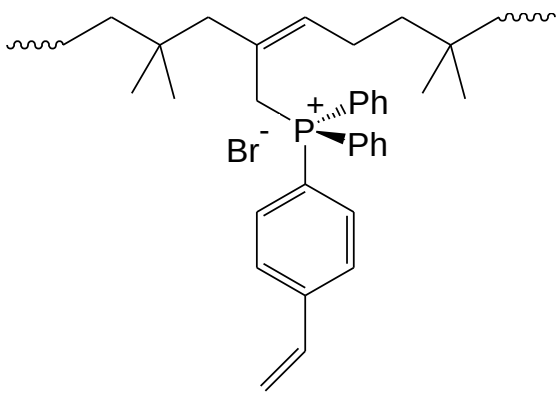

Figure 5.6. Chemical structure of LANXESS X_Butyl™ I4565P.

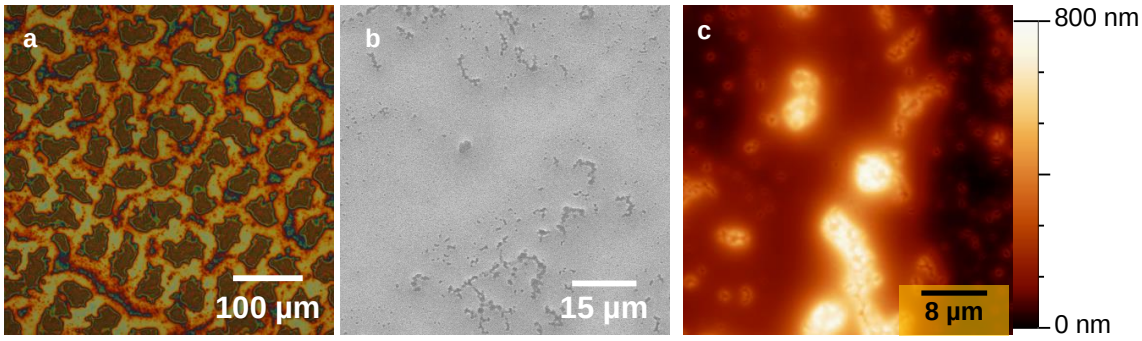

Figure 5.7. (a) Optical micrograph of Ru/I4565P. (b) SEM image of Ru/I4565P. (c) AFM image of Ru/I4565P.

Table 5.1 summarizes the RMS roughness values and variation in maximum height of Ru-iTMC emissive layers with commercial grade IIR compared to Ru/PDMS emissive layers. There is no commercial grade butyl rubber that can be used as a polymer matrix in LECs due to poor miscibility between the hydrophobic butyl rubber chains and the ionic emissive material. It is possible that these rubber materials may be compatible with iTMCs containing more hydrophobic ligands. Other iTMC materials with ligands containing alkyl sidechains to promote mixing with the raw IIR materials may enable deposition from organic solvents in which the LANXESS X_Butyl™ materials are more soluble such as chloroform, THF and toluene. This may be investigated as a future avenue for stretchable LECs.

Table 5.1. RMS roughness and maximum variation in height of Ru-iTMC emissive layers with commercial grade IIR compared to Ru/PDMS emissive layers.

Emissive Layer	RMS Roughness (nm)	Maximum Variation in Height (nm)
Ru/PDMS	3.4 ± 2.5	34.9 ± 2.6
Ru/RB301	213.0 ± 30.0	697.3 ± 60.8
Ru/RB101-3	192.7 ± 30.7	671.4 ± 26.5
Ru/BB2030	111.5 ± 19.4	663.7 ± 86.0
Ru/CB1240	118.7 ± 23.4	657.4 ± 74.1
Ru/I4565P	117.8 ± 34.4	686.3 ± 122.1

5.3.2. Optical Characterization of LECs with IIR-g-PEO

Gillies and co-workers synthesized a graft co-polymer of poly(ethylene oxide) (PEO) and IIR for use as an antimicrobial coating to resist protein adsorption.[23] Graft copolymers of PEO and IIR are interesting candidates for polymer materials in LECs because they combine the stretchable backbone of IIR with the polar polymer chains of PEO to facilitate mixing with the Ru-iTMC. Graft copolymers of IIR with tunable amounts of PEO were prepared through the incorporation of different molecular weights PEO onto the sidechains[20] (Figure 5.8). Low molecular weight PEO (750 g/mol) grafted onto the butyl rubber backbone results in ~ 16 wt% PEO in the graft copolymer (IIR-g-PEO16) . By increasing the molecular weight of PEO from 750 g/mol to 2000 g/mol and 5000 g/mol, 34 wt% PEO and 69 wt% PEO graft copolymers were achieved (IIR-g-PEO34 and IIR-g-PEO69 respectively).

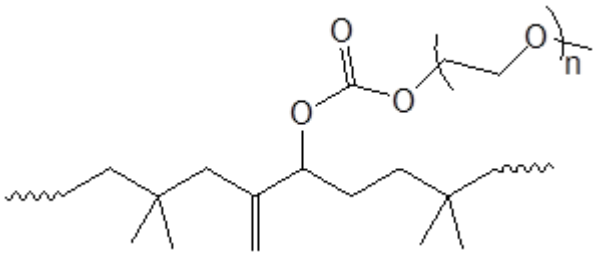

Figure 5.8. Chemical structure of IIR-g-PEO.

First, we determined the impact of PEO content on mixing of the iTMC with the graft copolymer. We prepared emissive layer films by spin coating a 3:1 v/v mixture of $Ru(dtb\text{-}bpy)_3(PF_6)_2$ in CH_2Cl_2 (40 mg/mL) with IIR-g-PEO graft polymers (25 mg/mL) from CH_2Cl_2 onto silicon wafer at 1000 rpm for 30 seconds. Emissive layers containing Ru/IIR-g-PEO16 exhibit phase separation in the optical micrograph of the thin film (Figure 5.9a) indicating that the amount of PEO in the graft copolymer is not sufficient to render the polymer miscible with the iTMC. The graft copolymer is still 84% IIR by weight and the butyl rubber backbone dictates the overall properties of the graft polymer. SEM and AFM images (Figure 5.9b, c) show that films of Ru/IIR-g-PEO16 exhibit depressions in the emissive layer with maximum variation in height of 919.2 ± 78.2 nm due to phase separation between the hydrophobic polymer and the iTMC. These emissive layer films have RMS roughness values of 104.1 ± 9.4 nm which is similar to emissive layers prepared with commercial butyl rubber grades. Previous work has found that films of IIR-g-PEO16 spin coated onto silicon wafer from CH_2Cl_2 exhibited micrometer scale patterns with RMS roughness values of 4.9 nm.[20] Therefore our findings show that dissolving an ionic species into the graft copolymer exacerbates the phase separation within the polymer segments leading to films with high surface roughness and holes. These holes in the emissive layer will undoubtedly lead to current leakage and inhomogeneous electric fields and therefore these films are not useful in the fabrication of LECs.

Emissive layers formed by mixing the iTMC with the graft polymer with longer PEO sidechains, IIR-g-PEO34, appear homogeneous in the optical micrograph (Figure 5.9d). The SEM and AFM images of the film reveal a granular nanometer-scale morphology

(Figure 5.9e, f). RMS roughness of the Ru/IIR-g-PEO34 is 44.7 ± 1.7 nm, which is half that exhibited by films made with commercial grade IIR formulations. The maximum variation in height is also significantly lowered to 390.5 ± 41.8 nm. The RMS roughness of the graft copolymer mixed with iTMC is still higher than that of IIR-g-PEO34 films alone (RMS roughness < 2 nm) indicating that increased phase separation is occurring due to the presence of the ionic transition metal complex. Films made with even higher PEO content, Ru/IIR-g-PEO69 also appear homogenous in the optical micrograph (Figure 5.9g). Ru/IIR-g-PEO69 also exhibit a granular nanometer-scale morphology (Figure 5.9h,i) however the feature size is smaller than that of Ru/IIR-g-PEO34 films, presumably due to the higher PEO content which results in more homogeneous mixing of the iTMC with the graft copolymer. The increased film homogeneity is also reflected in the decreased RMS roughness values of 13.4 ± 1.8 nm which is still an order of magnitude larger than previously reported films of IIR-g-PEO69 alone (RMS roughness < 2 nm). The variation in height is significantly reduced to 190.3 ± 3.3 nm compared to blends fabricated with commercial grades of IIR. Table 5.2 summarizes the RMS roughness values of emissive layers with IIR-g-PEO matrices.

Table 5.2. RMS roughness and maximum variation in height of Ru-iTMC emissive layers with IIR-g-PEO matrices compared to Ru/PDMS emissive layers.

Emissive Layer	RMS Roughness (nm)	Maximum Variation in Height (nm)
Ru/PDMS	3.4 ± 2.5	34.9 ± 2.6
Ru/IIR-g-PEO16	104.1 ± 9.4	919.2 ± 78.2
Ru/IIR-g-PEO34	44.7 ± 1.7	390.5 ± 41.8
Ru/IIR-g-PEO69	13.4 ± 1.8	190.3 ± 3.3

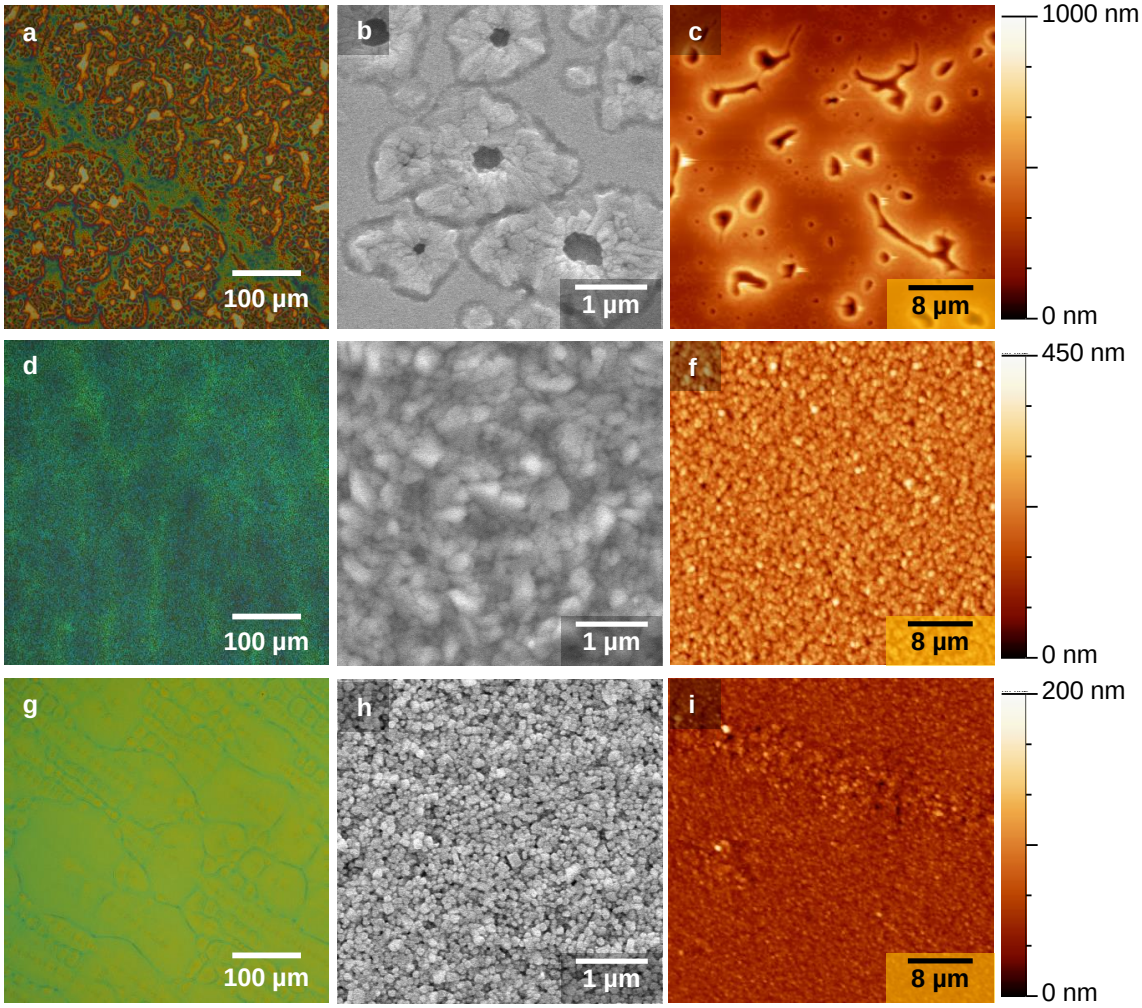

Figure 5.9. (a) Optical micrograph of Ru/IIR-g-PEO16. (b) SEM image of Ru/IIR-g-PEO16. (c) AFM image of Ru/IIR-g-PEO16. (d) Optical micrograph of Ru/IIR-g-PEO34. (e) SEM image of Ru/IIR-g-PEO34. (f) AFM image of Ru/IIR-g-PEO34. (g) Optical micrograph of Ru/IIR-g-PEO69. (h) SEM image of Ru/IIR-g-PEO69. (i) AFM image of Ru/IIR-g-PEO69.

We postulate that the granular morphology exhibited in Ru/IIR-g-PEO34 and Ru/IIR-g-PEO69 is an effect of graft copolymer self-assembly attempting to minimize unfavorable interactions of the nonpolar butyl rubber backbone with the ionic ruthenium transition metal complex. Films of Ru/IIR-g-PEO34 and Ru/IIR-g-PEO69 have excellent homogeneity and low RMS roughness making them excellent candidates for use as emissive layers in LECs. We will investigate the performance of IIR-g-PEO graft copolymers as polymer matrices in LECs and determine the effect of PEO content in the graft copolymer on turn-on time and lifetime in the following sections.

5.3.3. Optoelectronic Characterization of Ru/IIR-g-PEO LECs on the Rigid Device Test Structure

We fabricated LECs according to the rigid test structure in Figure 5.10a in order to compare the optoelectronic properties of different weight percentages of PEO in the graft copolymer of the emissive layer. Reference Ru/PDMS devices were used for comparison as the established stretchable elastomeric emissive layer used in iTMC LECs. The devices consisted of a Ru/elastomer film on a glass substrate bearing an ITO anode. Solutions of the emissive layer were spin coated in inert atmosphere onto the anode followed by annealing at 120°C overnight. The cathode was a 50 µL drop of gallium-indium eutectic (EGaIn) deposited on the surface of the Ru/elastomer film and encased in an epoxy resin. Ru/IIR-g-PEO devices produced bright, uniform emission over the entire area defined by the cathode when operated under a forward bias of 9 V in ambient conditions (Figure 5.10b, c).

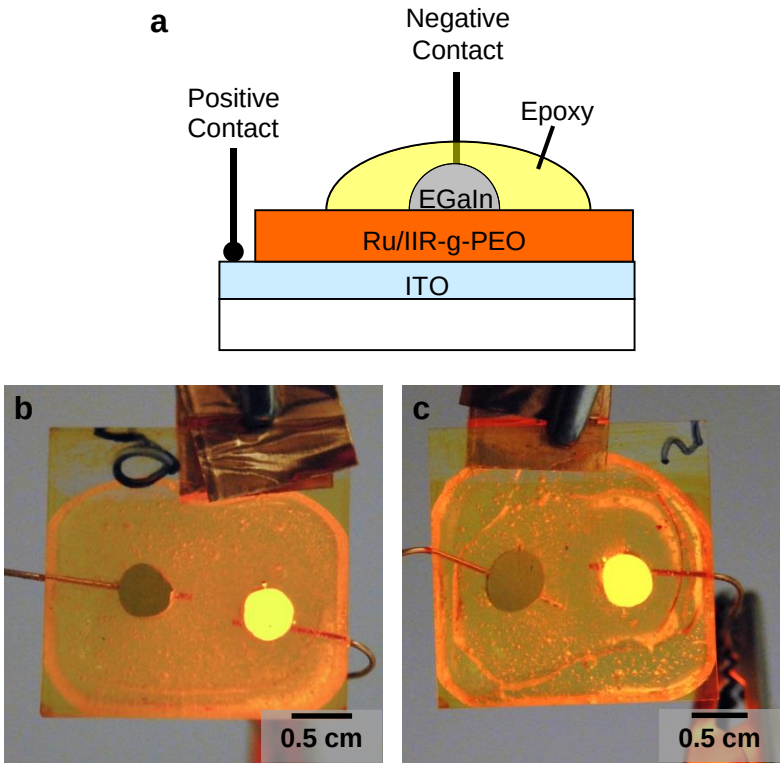

Figure 5.10. (a) Diagram of the Ru/IIR-g-PEO device test structure fabricated on an ITO-coated glass anode with EGaIn cathode. (b) Photograph of the Ru/IIR-g-PEO34 device operated at 9 V. (c) Photograph of the Ru/IIR-g-PEO69 device operated at 9 V.

One contributor to device instability is quenching of the exciton.[24] When a voltage is applied to the LEC, ions migrate to form electric double layers at the electrodes and electrons and holes are injected into the emissive layer. As the p- and n-doped regions grow, it becomes more probable that an exciton will interact with the proximal neighbouring doped regions and that exciton quenching will occur. At higher voltages, the growth of the n- and p-doped regions occurs at a more accelerated rate which causes exciton quenching to occur sooner than in devices operated at lower voltages. In order to determine the effects of the polymer matrix on LEC stability, we chose a bias of 9 V to accelerate device degradation. It is possible to achieve longer lifetimes than those reported herein by driving devices at a lower voltage or using a pulsed voltage.[7]

The evolution of radiance (Figure 5.11a, c) and EQE (Figure 5.11b, d) over 60 minutes of DC device operation at 9 V show that devices reach their maximum radiance of ~ 10 µW and ~ 8 µW for Ru/IIR-g-PEO34 and Ru/IIR-g-PEO69 devices respectively and

then slowly decay over the testing period. There are two figures of merit to quantify the stability of LECs, $t_{1/2}$ which is the time it takes for the radiance to decay to one half of the maximum value and $t_{1/5}$ which is the time it takes for radiance to decay to one fifth of the maximum value. Notably, neither device with Ru/IIR-g-PEO in the emissive layer decayed to one fifth of the maximum radiance within the one hour testing period. Ru/IIR-g-PEO34 devices have a $t_{1/2}$ of 2195 ± 918 seconds and exhibit further decay to $35.64 \pm 3.89\%$ of the maximum radiance after one hour. Ru/IIR-g-PEO69 have a $t_{1/2}$ of 2373 ± 603 seconds and the devices decay further to $37.04 \pm 6.37\%$ in one hour. Conversely, devices fabricated with Ru/PDMS reach maximum radiances of ~ 14.5 μW and decay more quickly with $t_{1/2}$ of 348 ± 241 seconds and $t_{1/5}$ of ~ 35 minutes (Figure 5.11e, f). The EQEs of the Ru/PDMS devices are lower than those reported in Chapter 4 which could be due to the higher operating voltage or due to operation in inert atmosphere. Kalyuzhny et al. observed that LECs operated in ambient conditions exhibited EQEs 2x higher than analogous devices tested in inert atmosphere presumably due to more efficient charge injection in ambient conditions due to the presence of ambient moisture and/or oxygen.[25] Ru/IIR-g-PEO LECs exhibited EQEs on the same order of magnitude as Ru/PDMS LECs (Table 5.2). Operation of devices at lower voltage bias or with pulsed voltages may increase the EQEs of these devices. Additionally, higher EQEs may be attained by changing the iTMC to a more efficient emitter however their syntheses are more involved and the degree of phase separation will differ as the iTMC is altered.[26]

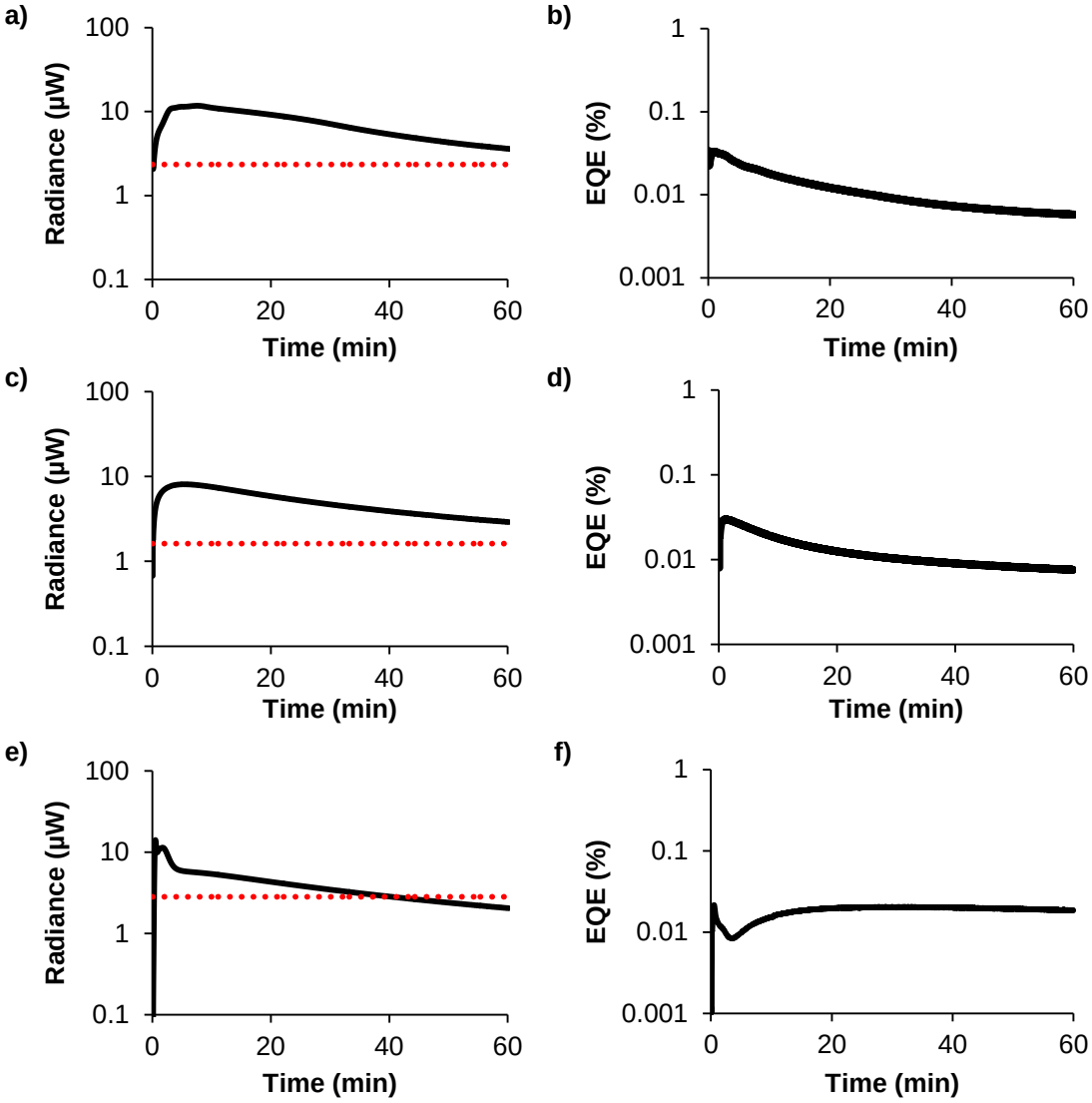

Figure 5.11. Temporal evolution of radiance (solid line) of a representative device operated with a 9 V bias in inert conditions (dotted red line = 1/5th of maximum radiance) (a) Ru/IIR-g-; (c) Ru/IIR-g-PEO69; (e) Ru/PDMS. Temporal evolution of external quantum efficiency of a representative device operated with a 9 V bias in inert conditions (b) Ru/IIR-g-PEO34; (d) Ru/IIR-g-PEO69; (f) Ru/PDMS.

Table 5.3. Summary of figures of merit for LECs operated at 9 V potential bias.

Emissive Layer	Max. Rad. (μW)	t_{on} (s)	EQE (%)	$t_{1/2}$(s)	$t_{1/5}$ (s)	Device Yield (%)
Ru/PDMS	14.47 ± 4.31	43.13 ± 23.64	0.021 ± 0.0032	348 ± 241	2128.38 ± 545.66	100
Ru/IIR-g-PEO34	10.89 ± 1.72	223.00 ± 43.96	0.033 ± 0.0042	2195 ± 918	N/A	62.5
Ru/IIR-g-PEO69	7.75 ± 2.14	202.14 ± 86.87	0.033 ± 0.0075	2373 ± 603	N/A	87.5

The thickness of the emissive layers was determined by freeze fracturing the emissive layer thin film on silicon wafer using liquid nitrogen to freeze the sample followed by SEM imaging of the cross section to determine the thickness of the emissive layer. The Ru/elastomer emissive layers all have a film thickness of ~ 300 nm (Figure 5.12), therefore any difference in turn-on time and lifetime will be due to the influence of the polymer film on the charge transport through the emissive layers and not due to the thickness of the films.

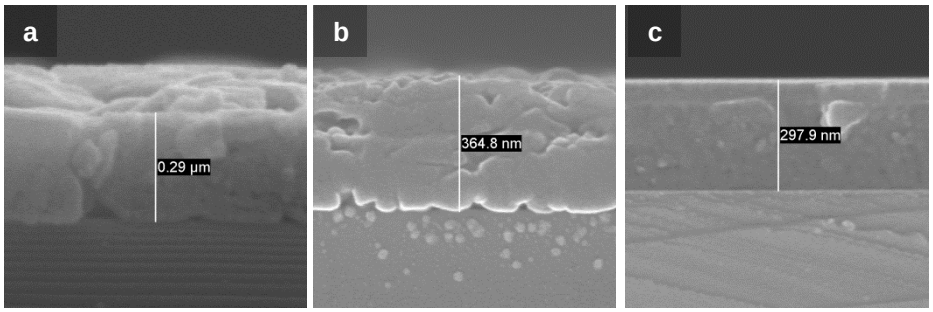

Figure 5.12. SEM cross sections of (a) Ru/IIR-g-PEO34; (b) Ru/IIR-g-PEO69; (c) Ru/PDMS.

To further probe the stability of LECs with IIR-g-PEO emissive layers we tested devices at 0.5 mA current bias in order to prevent overdriving LECs at too high of an operating voltage and to maximize the device lifetime. Similarly to devices tested at 9 V,

Ru/PDMS devices operated at 0.5 mA have $t_{1/2}$ values of 473 ± 212 seconds and decay to one fifth of the maximum radiance in ~ 15 minutes. The evolution of radiance (Figure 5.13a) over 60 minutes of DC device operation at 0.5 mA show that the Ru/PDMS emissive layer devices reach a maximum radiance of ~ 1 μW and then decay over the testing period. Under the applied current bias, devices require an initial ramp up voltage of 28 V and then they operate at a fairly steady voltage between 4 – 6 V for the remainder of the testing period. The EQE plot shows that EQEs of ~ 0.04% are attained and then EQE trails off similarly to the radiance (Figure 5.13b). To quantify the device degradation, we used the method of Kalyuzhny et al., which compares the total emitted energy, E_{tot}, of the device (determined from the integral of the radiant flux versus time curve) from the initial application of the voltage to the time at which the electroluminescent intensity drops to one fifth of its maximum value. Over the lifetime, devices emitted an average of 0.68 ± 0.47 mJ of energy.

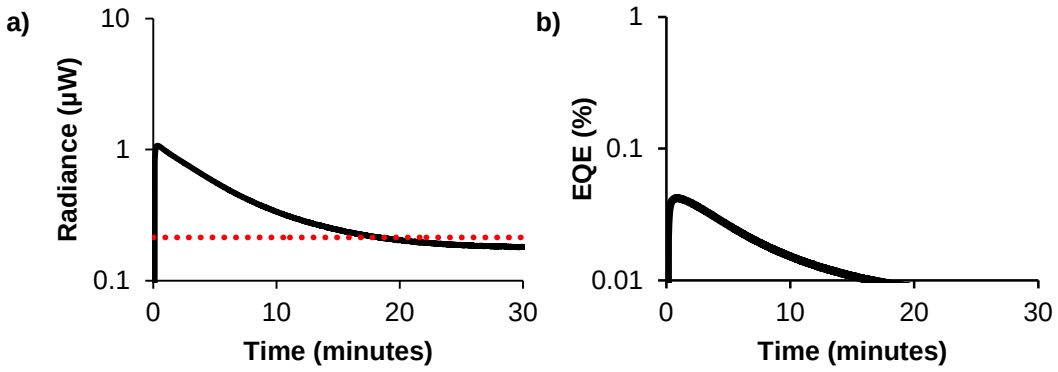

Figure 5.13. (a) Temporal evolution of radiance (solid line) of a typical Ru/PDMS device operated under a 0.5 mA bias in inert conditions, 1/5th of maximum radiance depicted as dotted red line. (b) Temporal evolution of external quantum efficiency of a typical device operated under a 0.5 mA bias in inert conditions.

Again, devices with IIR-g-PEO showed higher stability than Ru/PDMS devices; after one hour testing, neither Ru/IIR-g-PEO34 nor Ru/IIR-g-PEO69 devices had decayed to one fifth of the maximum radiance. The testing period was therefore extended to six hours. Ru/IIR-g-PEO34 devices turn-on in ~ 7 seconds reaching a maximum radiance of

~ 1 μW. The radiance curve remains quite steady and degrades to 54% of the maximum radiance after 6 hours (Figure 5.14a). Devices require an initial ramp up voltage of 14 V to produce the 0.5 mA current but then the required potential stabilizes between 3 - 4 V. The external quantum efficiency (EQE) reaches ~ 0.07% and similarly to the radiance curve, remains quite steady over the testing period (Figure 5.14b). Ru/IIR-g-PEO69 LECs turn on in ~ 5 seconds to a maximum radiance of ~ 2 μW. The decay of LECs with higher weight percent PEO is more pronounced: devices have $t_{1/2}$ values of 5772 ± 1729 seconds and the radiance degrades to ~ 25% of the maximum radiance approaching one fifth of the maximum radiance (red dotted line) by the end of the six hour testing period (Figure 5.14c). Devices require an initial ramp up voltage of 7 V to produce the 0.5 mA current but then the required potential stabilizes at ~ 5 V. The external quantum efficiency (EQE) reaches ~ 0.08% and decays analogously to the radiance curve (Figure 5.14d). E_{tot} is a measure of total energy emitted over the lifetime and as neither IIR-g-PEO device decayed to one fifth of the maximum radiance after 6 hours we cannot calculate the E_{tot} values for IIR-g-PEO devices. We can however, provide values for the total energy emitted over the testing period of six hours which was 17.0 mJ for Ru/IIR-g-PEO34 LECs and 18.5 mJ for Ru/IIR-g-PEO69 LECs. Table 5.4 summarizes the results of the device operation of LECs with Ru/elastomer operated at 0.5 mA bias.

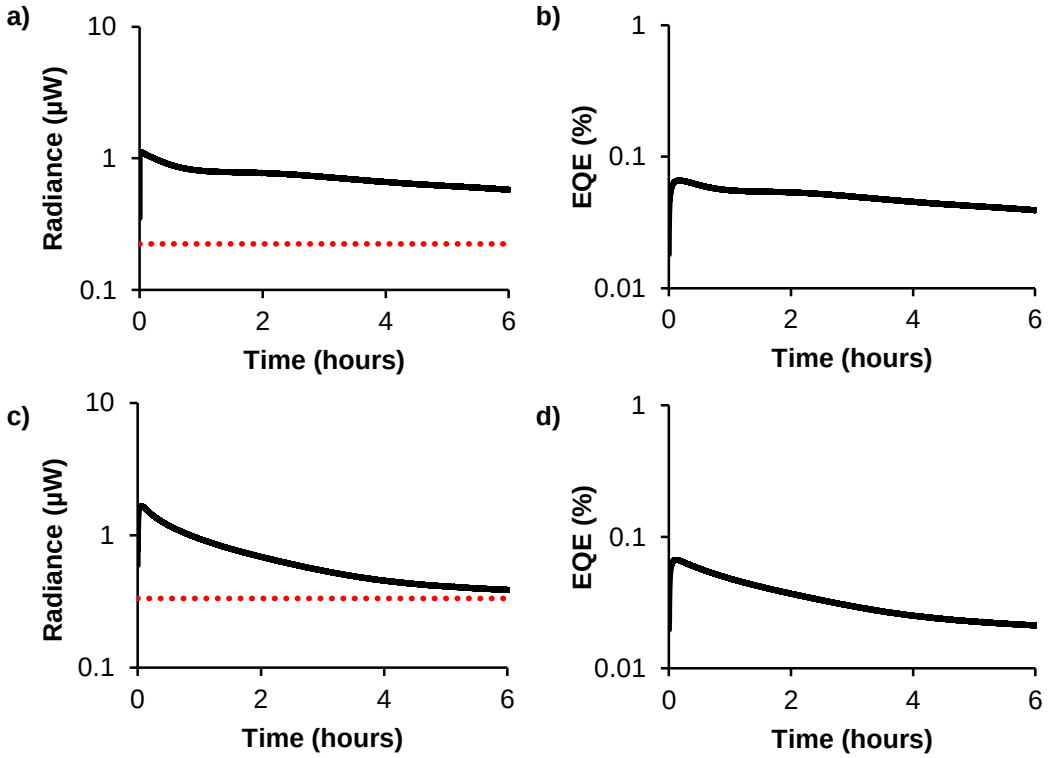

Figure 5.14. Temporal evolution of radiance (solid line) of a typical device operated under a 0.5 mA bias in inert conditions, 1/5th of maximum radiance depicted as dotted red line for (a) Ru/IIR-g-PEO34; (c) Ru/IIR-g-PEO69. Temporal evolution of external quantum efficiency of a typical device operated under a 0.5 mA bias in inert conditions (b) Ru/IIR-g-PEO34; (d) Ru/IIR-g-PEO69.

Table 5.4. Summary of figures of merit for LECs operated at 0.5 mA current bias.

Emissive Layer	**Max. Rad. (μW)**	**t_{on} (s)**	**EQE (%)**	**$t_{1/2}$ (s)**	**$t_{1/5}$ (s)**	**Device Yield (%)**
Ru/PDMS	1.01 ± 0.047	12.00 ± 4.08	0.04 ± 0.005	473 ± 212	924.00 ± 297.35	50
Ru/IIR-g-PEO34	1.16	7.00	0.071	N/A	N/A	25
Ru/IIR-g-PEO 69	2.00 ± 0.32	4.67 ± 1.15	0.083 ± 0.014	5772 ± 1729	N/A	37.5

5.3.4. Optoelectronic Characterization of Ru/IIR-g-PEO LECs on a Stretchable Device Test Structure

To test the durability of Ru/IIR-g-PEO emissive layers upon subjection to repeated stretching cycles, we used the same stretchable test structure from Chapter 4 that replaces the rigid ITO anode on glass with a stretchable, semitransparent gold anode on PDMS (Au/PDMS).[4] We fabricated LECs by spin-coating either Ru/IIR-g-PEO34, Ru/IIR-g-PEO69 or Ru/PDMS films on semitransparent Au/PDMS anodes, and then completing the device by depositing free-standing EGaIn cathodes on top of the films. Free-standing EGaIn drops are useful to evaluate device stretchability because they deform along with the device as it is stretched.[4],[27] Devices were subjected to 15% strain cycles and after a set number of cycles, we relaxed the device, deposited an EGaIn cathode (5 mm in diameter) on a previously untested part of the film, and determined the current, radiance (Figure 5.15a-c) and EQE under a 9 V bias for 5 minutes. As demonstrated in Chapter 4, Ru/PDMS LECs can sustain repeated cyclic strains of 15% and the peak radiance remains relatively constant even after 50 strain cycles when operated at 5 V. This effect is reproducible at 9 V operation; the peak radiance remains relatively constant and degradation occurs more quickly with subsequent strain cycles due to the cracking of the gold anode upon stretching. Ru/IIR-g-PEO34 LECs behave similarly to Ru/PDMS LECs subjected to cyclic strain; the peak radiance remains relatively constant even after 50 strain cycles. Ru/IIR-g-PEO69 LECs only emit light in the nW range after just 10 cycles of strain have been applied indicating that damage to the emissive layer is more severe in the graft copolymer with higher PEO weight content. Gillies and co-workers have demonstrated that IIR-g-PEO films have increased Young's Modulus and decreased elongation at break as the amount of PEO in the polymer is increased.[12] We hypothesize that the higher PEO content in IIR-g-PEO69 results in more crystalline films which are more susceptible to cracking than the less crystalline IIR-g-PEO34. For both Ru/PDMS and Ru/IIR-g-PEO34 devices, the initial set of 10 strain cycles reduces E_{tot} by approximately one order of magnitude. As additional strain cycles are applied Etot remains fairly constant at ~ 0.12 mJ and ~ 0.13 mJ for Ru/PDMS and Ru/IIR-g-PEO34 devices respectively (Figure 5.15d). As rationalized in Chapter 4, changes in the gold

film with initial stretching can account for the initial drop in E_{tot}. The initial introduction of microcracks and delaminated regions roughens the gold film, which likely distorts the elastomeric emissive layer producing inconsistent thicknesses which then results in current leakage through thinned or damaged areas effectively reducing the EQE and E_{tot}. With additional strain cycles, however, both the microstructure of the gold film and E_{tot} stabilize, indicating that Ru/PDMS and Ru/IIR-g-PEO34 films can sustain these strain cycles without further degradation. Future work will compare the durability of Ru/PDMS and Ru/IIR-g-PEO34 emissive layers on anode materials that do not crack, such as embedded films of nanowires or nanotubes in order to eliminate the effects of the cracked anode on device performance under cyclic strain. Additionally, deposition of Ru/IIR-g-PEO34 on composite anodes will allow for the determination of the elongation at failure of the emissive layer.

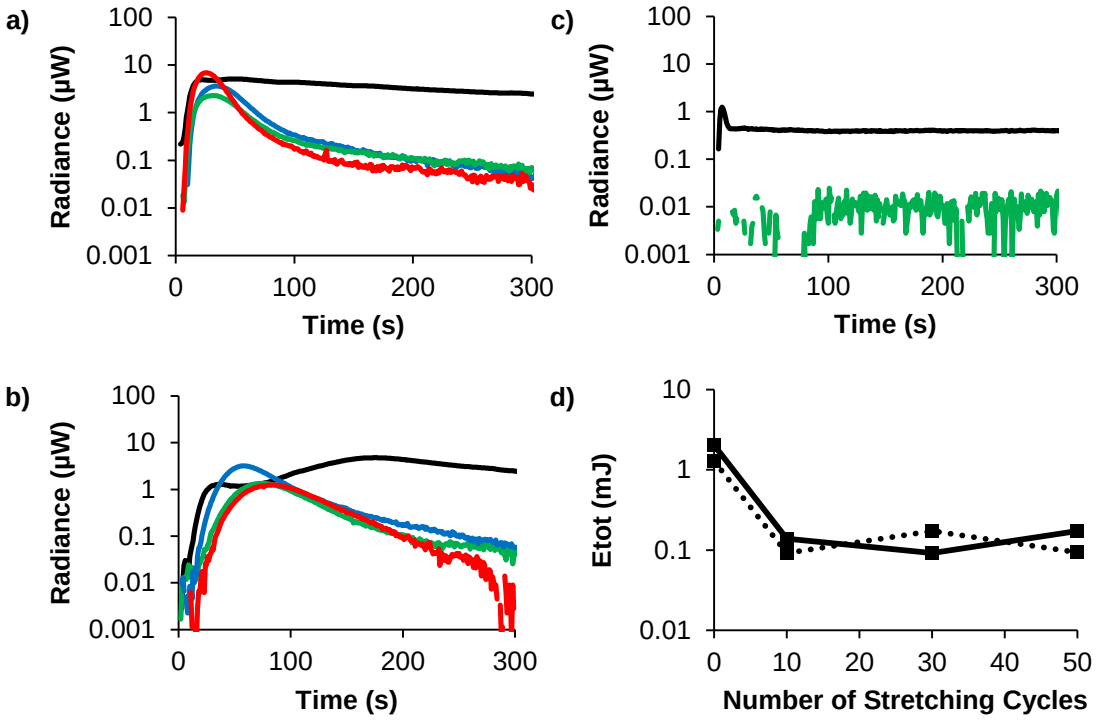

Figure 5.15. Performance comparison after repetitive, 15% elongation of LECs fabricated from Ru/PDMS, Ru/IIR-g-PEO34, and Ru/IIR-g-PEO69 with Au/PDMS stretchable anodes and EGaIn cathodes. Parts a – c show traces corresponding to temporal evolution of radiance of unstrained (black), 10 strain cycles (green), 30 strain cycles (blue), 50 strain cycles (red) of (a) Ru/PDMS devices operated under a 9 V bias;

(b) Ru/IIR-g-PEO34 devices operated under a 9 V bias; (c) Ru/IIR-g-PEO69 devices operated under a 9 V bias. (d) Plot of total emitted energy (E_{tot}) vs the number of strain cycles for Ru/PDMS (solid line) and Ru/IIR-g-PEO34 (dotted line) devices.

5.4. Conclusions

We have demonstrated that commercial grades of IIR are too nonpolar to mix well with the Ru-iTMC, therefore a chemically modified IIR with PEO sidechains grafted onto the backbone was used to achieve improved mixing of the two components. Low molecular weight PEO side chains on the graft copolymer IIR-g-PEO16 did not improve the mixing with the Ru-iTMC. While both IIR-g-PEO34 and IIR-g-PEO69 mix well with the Ru-iTMC, LECs fabricated from Ru/IIR-g-PEO34 exhibited higher stability than both Ru/IIR-g-PEO69 and Ru/PDMS with the radiance decreasing to only 54% of the peak radiance after 6 hours of operation at 0.5 mA. Additionally, Ru/IIR-g-PEO34 devices were more durable than Ru/IIR-g-PEO69 devices maintaining fairly constant peak radiance values even after 50 cycles of repetitive strain of 15% were applied while Ru/IIR-g-PEO69 devices only emit light in the nW range after only 10 cycles of 15% strain were applied. These results indicate that of the three graft copolymers incorporated in the emissive layer, IIR-g-PEO34 exhibits the best properties in terms of light-emission stability in the rigid device architecture and durability when subjected to repetitive strain in the stretchable device architecture. Future work will investigate the ultimate stretchability of the Ru/IIR-g-PEO emissive layers on composite electrodes which do not crack under applied strain in order to compare the elongation at failure of these LECs to that of Ru/PDMS LECs. Comparison of LECs operated under ambient and inert conditions will provide insight into whether incorporation of IIR-g-PEO into LECs provides protection from environmental moisture to the iTMC emitter. Gillies and coworkers recently reported arborescent hyperbranched copolymers of PEO and IIR which resist protein adsorption at PEO contents greater than 20%.[12] It would be interesting to compare light-emitting layers comprised of linear and arborescent graft copolymers with similar PEO content to determine the effect of branching on emissive layer thin film morphology and LEC operation.

5.5. References

[1] S.-I. I. Park, Y. Xiong, R.-H. H. Kim, P. Elvikis, M. Meitl, D.-H. H. Kim, J. Wu, J. Yoon, C.-J. J. Yu, Z. Liu, Y. Huang, K.-c. C. Hwang, P. Ferreira, X. Li, K. Choquette, J. A. Rogers, *Science* **2009**, *325*, 977-981.

[2] T. Sekitani, H. Nakajima, H. Maeda, T. Fukushima, T. Aida, K. Hata, T. Someya, *Nature Materials* **2009**, *8*, 494-499.

[3] Z. Yu, X. Niu, Z. Liu, Q. Pei, *Advanced Materials* **2011**, *23*, 3989-3994.

[4] H. L. Filiatrault, G. C. Porteous, R. S. Carmichael, G. J. Davidson, T. B. Carmichael, *Advanced Materials* **2012**, *24*, 2673-2678.

[5] J. Liang, L. Li, X. Niu, Z. Yu, Q. Pei, *Nature Photonics* **2013**, *7*, 817-824.

[6] J. Liang, L. Li, K. Tong, Z. Ren, W. Hu, X. Niu, Y. Chen, Q. Pei, *ACS Nano* **2014**, *8*, 1590-1600.

[7] H. Rudmann, M. F. Rubner, *Journal of Applied Physics* **2001**, *90*, 4338-4345.

[8] C. H. Lyons, E. D. Abbas, J. K. Lee, M. F. Rubner, *Journal of the American Chemical Society* **1998**, *120*, 12100-12107.

[9] F. P. Wenzl, P. Pachler, C. Suess, A. Haase, E. J. W. List, P. Poelt, D. Somitsch, P. Knoll, U. Scherf, G. Leising, *Advanced Functional Materials* **2004**, *14*, 441-450.

[10] D. L. Pile, A. J. Bard, *Chemistry of Materials* **2005**, *17*, 4212-4217.

[11] J. D. Slinker, J.-S. Kim, S. Flores-Torres, J. H. Delcamp, H. D. Abruna, R. H. Friend, G. G. Malliaras, *Journal of Materials Chemistry* **2007**, *17*, 76-81.

[12] S. Karamdoust, P. Crewdson, M. Ingratta, E. R. Gillies, *Polymer International* **2014**, doi: 10.1002/pi.4795.

[13] L. Ferrari, G. J. E. Davidson, T. B. Carmichael, PCT/CA2013/001043, **June 26 2014**.

[14] A. Vohra, T. B. Carmichael, *Unpublished work* **2014**.

[15] Y. Cao, G. Yu, A. J. Heeger, C. Y. Yang, *Applied Physics Letters* **1996**, *68*, 3218-3220.

[16] F. Habrard, T. Ouisse, O. Stephan, M. Armand, M. Stark, S. Huant, E. Dubard, J. Chevrier, *Journal of Applied Physics* **2004**, *96*, 7219-7224.

[17] F. Habrard, T. Ouisse, O. Stephan, *Journal of Physical Chemistry B* **2006**, *110*, 15049-15051.

[18] I. S. Isayeva, B. T. Kasibhatla, K. S. Rosenthal, J. P. Kennedy, *Biomaterials* **2003**, *24*, 3483-3491.

[19] Y. Ikeda, K. Kodama, K. Kajiwara, S. Kohjiya, *Journal of Polymer Science Part B: Polymer Physics* **1995**, *33*, 387-394.

[20] C. V. Bonduelle, S. Karamdoust, E. R. Gillies, *Macromolecules* **2011**, *44*, 6405-6415.

[21] S. Bernhard, J. A. Barron, P. L. Houston, H. D. Abruña, J. L. Ruglovksy, X. Gao, G. G. Malliaras, *Journal of the American Chemical Society* **2002**, *124*, 13624-13628.

[22] A. Eisenberg, J. S. Kim, *Introduction to Ionomers*, Wiley, **1998**.

[23] C. V. Bonduelle, E. R. Gillies, *Macromolecules* **2010**, *43*, 9230-9233.

[24] S. van Reenen, T. Akatsuka, D. Tordera, M. Kemerink, H. J. Bolink, *Journal of the American Chemical Society* **2013**, *135*, 886-891.

[25] G. Kalyuzhny, M. Buda, J. McNeill, P. Barbara, A. J. Bard, *Journal of the American Chemical Society* **2003**, *125*, 6272-6283.

[26] R. D. Costa, E. Orti, H. J. Bolink, F. Monti, G. Accorsi, N. Armaroli, *Angewandte Chemie-International Edition* **2012**, *51*, 8178-8211.

[27] D. J. Lipomi, B. C. Tee, M. Vosgueritchian, Z. Bao, *Advanced Materials* **2011**, *23*, 1771-1775.

6. Chapter 6

Methods to Enable the Fabrication of Conductive Metal Films on Butyl Rubber Substrates

6.1. Introduction

Stretchable and conformable electronics are emerging as an important new area of research due to applications in stretchable displays, wearable devices, and biocompatible devices such as artificial nerves and skin. Poly(dimethyl siloxane) (PDMS) is the most common substrate used in stretchable electronics owing to its biocompatibility, transparency, and commercial availability. The main drawback of using PDMS as a substrate in stretchable electronics is its permeability to moisture and oxygen, which irreversibly degrade the organic materials used in organic electronic devices and thus curtail the device lifetime. In the field of flexible electronics, a successful strategy to minimize device degradation has been to deposit multilayers of organic materials to smooth out the substrate and reduce pinhole defects, followed by deposition of thin inorganic layers which reduce moisture and oxygen permeation. Vitex Systems Inc. has developed a barrier coating named Barix which is comprised of alternating layers of polyacrylate and ceramic thin films. 3 micron-thick Barix films on poly(ethylenenaphthalate) (PEN) substrates deliver water permeability rates of 10^{-6} g m^{-2} day^{-1} which is on the order of magnitude required for organic light-emitting devices.[1] Seo et al. examined the effect of bending on organic-inorganic multilayer moisture barriers and found that moisture barrier properties are maintained up to the critical bending radius of 0.5 cm at which point cracking of the inorganic aluminum oxide layer creates a diffusion pathway for moisture to permeate through the film.[2] The cracking of inorganic layers at low bending radii demonstrates the challenge with adapting these multilayer organic-inorganic barrier layers to stretchable electronics: the barrier layers need to be stretchable to allow for mechanical deformation of devices and continued moisture resistance under strain. As yet, this is an unsolved problem.

Our approach to solving the permeability challenges associated with stretchable organic electronic devices is to employ isobutylene-co-isoprene rubber (IIR) as the substrate. There are many potential advantages to using IIR in stretchable electronic devices: IIR is notable for its high gas and water impermeability.[3] IIR is peroxide curable and additives can be added to increase the impermeability of the IIR: IIR filled with carbon black (B-IIR) has a permeation rate of 138.6 ± 9.9 cc-mm/(m^2-day), white

IIR (W-IIR) filled with calcinated clay has a permeation rate of 104.2 ± 8.8 cc-mm/(m^2-day) and unfilled transparent IIR (T-IIR) has permeation rates of 216 ± 4 cc-mm/(m^2-day)[3]. In addition to its high water and moisture impermeability, IIR is biocompatible, chemically resistant, and it possesses the mechanical properties required for stretchable electronics. To date, there are no literature examples of the use of isobutylene-co-isoprene rubber as a substrate in stretchable electronic devices. Uncrosslinked poly(isobutylene) (PIB) edge sealants demonstrate the effectiveness of the PIB chains in decreasing lateral diffusion of oxygen and moisture into the device. In polymer electrochromic devices sandwiched between two glass slides, sealing with PIB allows devices to continue to exhibit switching between on/off states even under accelerated degradation conditions of 50°C and 80% relative humidity (RH) while analogous devices sealed with epoxy no longer switched after 1500 h in ambient conditions.[4] Sheets of cross-linked white-filled IIR (W-IIR) laminated against ITO/glass protect ITO from exposure to HCl vapor: after 10 hours of exposure no change in sheet resistance is observed while PDMS protection resulted in an increase in sheet resistance to 4x the initial value.[5] These experiments demonstrate the effectiveness of IIR in protecting electrical components from environmental degradation. IIR is a promising substrate upon which to build stretchable electronics due to the combination of stretchability and high gas and moisture impermeability which circumvents the need to develop additional stretchable barrier layers.

The first step towards building stretchable electronic devices on IIR is the fabrication of stretchable metal films on IIR that remain conductive under tensile strain. Metal films are an essential part of stretchable electronic devices, where they are used as interconnects[6],[7] and electrodes[8],[9]. Previous work has focused on the deposition of conductive gold films on PDMS by e-beam metal deposition. Lacour et al. demonstrated that 100 nm thick layers of gold with 5 nm thick chromium adhesion interlayers deposited on PDMS by e-beam deposition retain electrical conductivity up to 22% elongation.[10] In this chapter we show that direct e-beam evaporation of gold onto IIR produces an Au/IIR composite layer on the surface that is not electrically conductive. We describe the use of a polymer protection layer to shield the rubber during the e-beam deposition process

providing a stable platform upon which gold can nucleate and grow into a conductive metal film. Additionally, when microstructured PVAc glue interlayers or PVA interlayers are employed it is possible to obtain stretchable gold films that remain conductive up to 120% elongation.

6.2 Experimental Section

6.2.1. Materials

All materials and chemicals were purchased commercially and used as received. Poly(dimethylsiloxane) (PDMS) (Sylgard 184) was obtained from Dow Corning (Midland, MI). PEDOT:PSS (Clevios™ P) was purchased from Heraeus Precious Metals GmbH & Co. KG (Leverkusen, Germany). Poly(vinyl alcohol) (PVA) M_w = 89,000 - 98,000 with degree of hydrolysis > 99% was obtained from Sigma Aldrich (St-Louis, Missouri). Glue-All was obtained from Elmer's Products, Inc (Westerville, Ohio). IIR substrates were molded at LANXESS, Inc (London, Canada). 3"-diameter polished silicon wafers were obtained from University Wafer (Boston, MA). Aluminum sheets were obtained from Essex Metals (Oldcastle, Ontario, Canada).

6.2.2. Preparation of IIR and PDMS Substrates

Smooth IIR substrates were prepared by molding the desired IIR formulation between two master substrates coated with PDMS according to Provisional Patent WO201409117 A1.[11] The master substrates used were silicon wafers and aluminum sheets. The PDMS coating provides a smooth layer that releases easily from cured IIR formulations. Polished silicon wafers were cleaned in Piranha solution at 140°C (a 3:1 (v/v) mixture of 98% H_2SO_4 and 30% H_2O_2) for 5 min, followed by rinsing with deionized water and drying with a stream of nitrogen. *Caution: piranha solution reacts violently with most organic materials and must be handled with extreme care.* Aluminum sheets were cleaned by swabbing with isopropanol followed by UV-ozone treatment (Jelight, Model 42A) for 5 min. Poly(dimethylsiloxane) (PDMS) prepolymer (Sylgard 184) was spin coated on the master substrate at 1500 rpm for 20 s then 2500 rpm for 30 s. The PDMS coating was cured in an oven at 60°C overnight. Smooth IIR substrates were

prepared by molding the IIR formulation between two PDMS-coated masters. Cure times and temperatures varied with each IIR formulation. The formulation for white-filled IIR (W-IIR) consisted of BB2030 as the base rubber, a calcinated clay filler and a zinc cure system. The ingredients are listed in Table 6.1 in the units of per hundred parts rubber (Phr). The formulation was cured for 9 minutes at 160°C. Black-filled IIR (B-IIR) was comprised of the base rubber BB2030, a carbon black filler and a sulfur cure system (Table 6.2). B-IIR was cured for 14 minutes at 160°C. Transparent IIR (T-IIR) consisted of chemically modified BB2030 to generate the diphenylphosphinostyrene (DPPS) ionomer and a peroxide cure system was used (Table 6.3). T-IIR was cured for 8 minutes at 175°C. After curing was complete, the PDMS-coated silicon wafers were removed to yield smooth, uniform IIR substrates. IIR substrates (~0.5 mm thick) were then cut to size (2.5 cm x 2.5 cm) and cleaned by sonication in acetone and isopropanol for 10 min each in a Branson sonicator (Model 3510). PDMS substrates were fabricated by casting liquid pre-polymer against flat polystyrene Petri dishes and curing in a 60°C oven for one hour then cut to size (2.5 cm x 2.5 cm) with a scalpel.

Table 6.1. Ingredient list for the W-IIR formulation.

Ingredient	**Phr**
BB2030	100
Calcinated Clay Satintone	80
Polyethylene AC-617A	2
Vulkacit LDA	0.2
ZnO	3

Table 6.2. Ingredient list for the B-IIR formulation.

Ingredient	Phr
BB2030	100
CB N660	50
Stearic acid	1
Vulkacit DM/C	1
Sulfur	0.5
Zinc Oxide	3

Table 6.3. Ingredient list for the T-IIR formulation.

Ingredient	Phr
BB2030	100
DPPS	5.1
Trigonox 101-45-PD-AM	0.3

6.2.3. Oxidation of IIR and PDMS Substrates

Substrates were mounted to an aluminum mesh on glass prior to oxidation to minimize the formation of gas between the substrate and the glass due to outgassing during e-beam metal deposition. Cleaned IIR substrates were treated with a mixture of air and oxygen plasma for 15 minutes in a Harrick plasma cleaner (Model: PDC-001) at an air pressure of 10 psig (flow rate 32 mL/min) and O_2 pressure of 10 psig (flow rate of 10.6 mL/min) at medium discharge setting. The oxidized samples were then gently swabbed with isopropyl alcohol, and dried in a stream of nitrogen. Following oxidation, IIR substrates

treated with $SiCl_4$ were suspended face down over a glass Petri dish containing 0.1 mL of silicon tetrachloride for 30 s at room temperature under inert atmosphere. The samples were then soaked in distilled water for 10 min, and dried in a stream of nitrogen. PDMS sheets (1 mm thickness) were treated with air plasma for 30 seconds at an air pressure of 10 psig (flow rate of 32 mL/min) at medium discharge setting.

6.2.4. Protection Layer Deposition

PEDOT:PSS polymer interlayers on IIR were prepared by spin coating 1 mL of Clevios™ P PEDOT:PSS onto the surface of oxidized IIR substrates at 1000 rpm for 1 minute followed by 2000 rpm for 1 min. Glue interlayers on IIR were prepared by spin coating 1 mL of 1:1 water:glue v/v solution onto oxidized IIR at 1000 rpm for 1 minute followed by 2000 rpm for 1 minute. PVA interlayers were prepared by spin coating 25 mg/mL of PVA in DI H_2O onto oxidized IIR at 1000 rpm for 1 minute followed by 2000 rpm for 1 minute.

6.2.5. Metal Layer Deposition

Gold films with thicknesses of 250 Å and 500 Å were deposited on oxidized and polymer-protected samples by e-beam evaporation under high vacuum (10^{-6} mbar) at a rate of 1 Å/s. For glue interlayer samples, a 30-Å-thick Ti layer was deposited prior to gold deposition to promote adhesion to the glue interlayer.

6.2.6. Characterization

Optical characterization was performed using an Olympus BX51 microscope equipped with an Olympus Q-Color3 digital camera. A micro-vice stretcher (S. T. Japan, USA, Inc.) was mounted to the microscope stage and samples were clamped in the stretcher to obtain microscope images of stretched samples. Scanning electron microscopy (SEM) and focused ion-beam milling was performed on a Zeiss 1540XB FIB–SEM instrument at the Western Nanofabrication Facility, London, Canada. The sample surface was imaged with a 1 keV energy electron beam at a working distance of 4 mm. For cross-sectioning, the sample was mounted at the coincidence point between the FIB and SEM beams with the surface normal to the FIB column and at a 54° tilt to the

SEM column. Prior to FIB milling a 1x5 micron band of platinum was deposited in situ by electron beam decomposition to produce a sacrificial protective layer over the film. A trench was milled through the film to expose a cross-section using a 50 pA focused beam of 30 keV energy gallium ions. The cross section was imaged and the film thickness measured with the SEM at 36° tilt to the exposed cross-section. Scanning electron microscopy of stretched samples was carried out on a Hitachi S-4500 scanning electron microscope at Surface Science Western, London, Canada. Samples were stretched manually and secured with copper tape to the specimen stage. Prior to imaging, samples were coated with 3-5 nm Au using a Hummer VI sputtering system. For electrical characterization under strain, samples were clamped in a micro-vice stretcher (S.T. Japan, USA, Inc.) and stretched in 5% increments while the resistance was measured with a Keithley 2601A Sourcemeter. Sheet resistances were measured with a Keithley 2601A Sourcemeter using the four-probe method. For electrical measurements, gallium-indium eutectic (EGaIn) (~ 0.05 mL) was deposited by syringe onto the metal films to facilitate contact unless otherwise stated.

6.3. Results and Discussion

6.3.1. Preparation of IIR and PDMS Substrates

We used three types of IIR: black-filled IIR (B-IIR), white-filled IIR (W-IIR) and transparent IIR (T-IIR), all of which are based on a bromo-substituted derivative of IIR. B-IIR contains carbon black and zinc oxide fillers with a sulfur cure system and stearic acid stabilizers. W-IIR contains calcinated clay and polyethylene fillers, a sulfur cure system and zinc oxide. T-IIR is cross-linked with a peroxide cure system and no additional fillers are added to the formulation.[11] Molding the IIR formulations against PDMS-coated masters provided smooth IIR sheets.

We prepared smooth PDMS substrates by mixing the pre-polymer and curing agent in a 10:1 w/w ratio, and then casting in a polystyrene Petri dish and curing in a 60°C oven for 1 h.

6.3.2. E-beam Deposition of Gold on IIR and PDMS Substrates

Deposition of gold films by e-beam evaporation causes critical damage to the IIR surface, and produces gold films that are not electrically conductive. This phenomenon does not occur on PDMS. Deposition of 500 Å of Au on native IIR substrates in an e-beam evaporator produces films on T-IIR, W-IIR and B-IIR that are not reflective or shiny (Figure 6.1 a-c); rather, the films have a matte appearance and are not conductive. Conversely, e-beam evaporation of 500 Å of Au on PDMS produces shiny, reflective films (Figure 6.1d) with a sheet resistance (R_s) of 0.723 ± 0.121 Ω/sq. We analyzed the grain structures of gold films deposited on IIR and PDMS by SEM to determine differences in film morphology. Gold films deposited on IIR substrates do not appear continuous, with gold grains separated by what appear to be voids which prevent electrical conduction through these films. Gold films deposited on B-IIR consist of small grains approximately 10 nm in diameter, separated by voids up to 20 nm wide (Figure 6.1e); on W-IIR the grains are ~ 20 nm in diameter separated by voids up to 50 nm wide (Figure 6.1f); and on T-IIR the grains vary in diameter from 10 – 50 nm and are separated by voids up to 40 nm wide (Figure 6.1g). In contrast, gold films deposited on PDMS substrates consist of gold grains ~ 40 nm in size that are in contact with one another, with no visible voids separating the grains (Figure 6.1h).

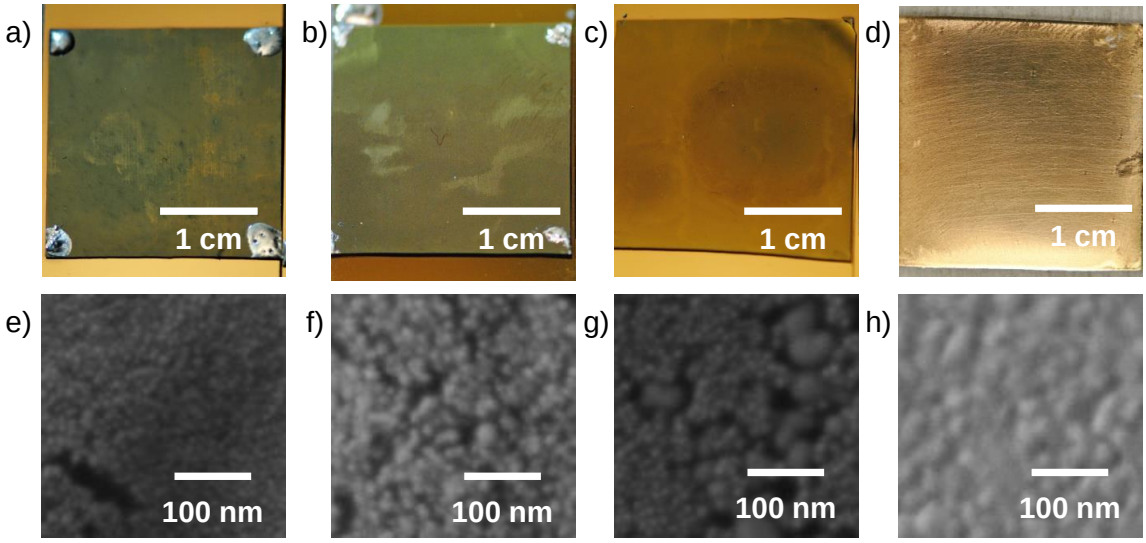

Figure 6.1. Photographs of gold (500 Å nominal thickness) on (a) B-IIR; (b) W-IIR; (c) T-IIR; (d) PDMS. SEM images of gold (500 Å nominal thickness) on (e) B-IIR; (f) W-IIR; (g) T-IIR (h) PDMS.

We measured the thickness of Au films on PDMS and W-IIR by coating the samples with platinum, using a focused ion beam to make a trench down through the underlying Au film and subsequently imaging the cross-section by SEM. The Au films deposited by e-beam evaporation had a nominal thickness of 500 Å. On PDMS, the measured cross-sectional thickness of the gold layer was 585.9 Å (Figure 6.2a) which agreed with the thickness of metal deposited as measured by the quartz crystal microbalance (QCM) in the e-beam evaporator. On W-IIR, however, the measured cross sectional thickness is 984.4 Å, which is almost twice the expected thickness (Figure 6.2b). We postulate that Au deposition on IIR results in the formation of a nonconductive Au/IIR composite layer caused by the penetration of Au into the IIR substrate during e-beam evaporation. A similar effect occurs when gold is thermally evaporated onto Nylon-11. At elevated temperatures of 46°C the formation of a nanocomposite is observed, however when analogous deposition occurred at room temperature gold films were localized on the surface of the nylon-11 film.[12] While we are not able to control the temperature of the sample plate during our e-beam depositions, this result indicates that formation of conductive gold films may be possible through cooling of the sample plate during e-beam deposition.

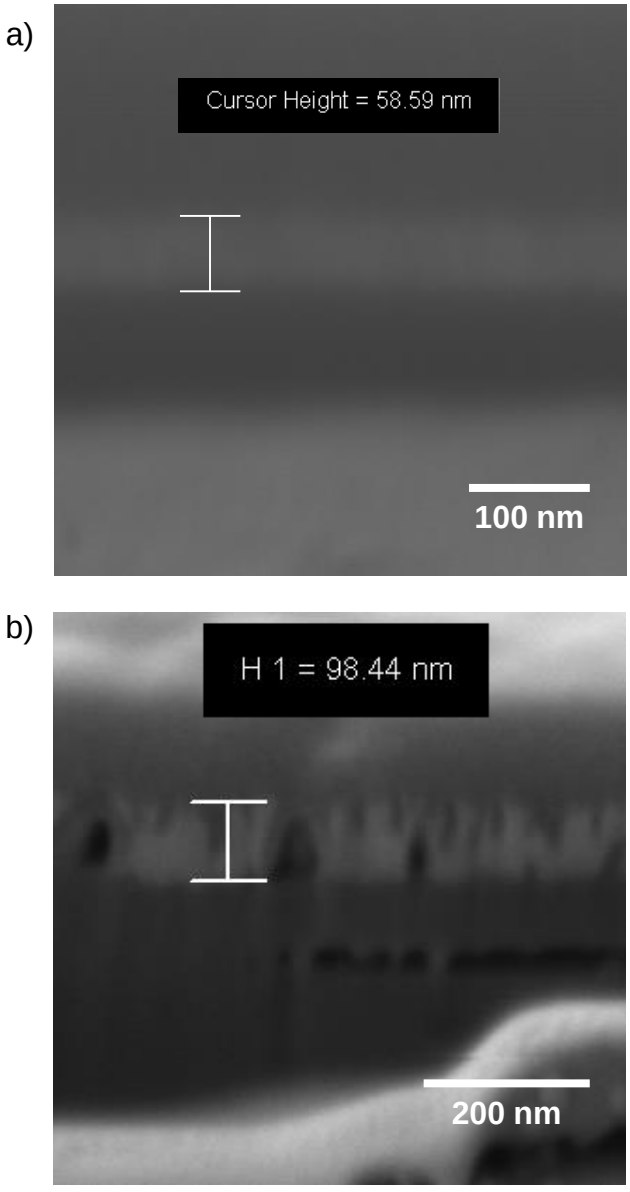

Figure 6.2. SEM cross-section images Au films with nominal thickness of 50 nm on: (a) PDMS; (b) W-IIR.

The formation of a composite gold/IIR material is further supported by UV-vis spectroscopy. Absorbance spectra of conductive gold films with 200 Å thickness on PDMS substrates show that the gold film absorbs yellow, red and orange light but not blue/green light causing a decrease in absorbance at 520-525 nm (Figure 6.3). Conversely, T-IIR substrates that had 200-Å-thick Au films deposited by e-beam deposition exhibit a maximum in the absorbance spectrum at 530 nm due to the surface plasmon resonance (SPR) of the isolated gold nanoparticles in the IIR matrix. Other gold

nanoparticle (AuNP) composite systems exhibit similar absorption spectra such as AuNPs functionalized with polysterene capping agents in a polystyrene matrix (SPR 523 nm)[13], gold nanoparticles synthesized *in-situ* in a PDMS matrix (SPR 530-534 nm)[14], and AuNPs in PEDOT:PSS (SPR 540 nm)[15].

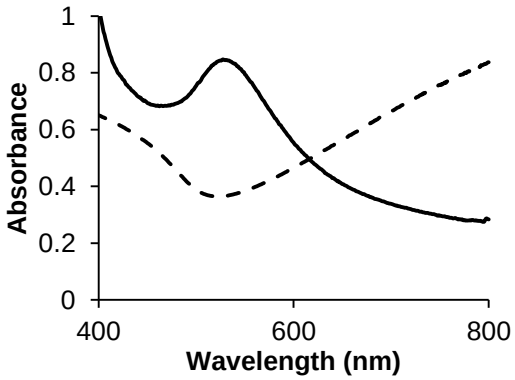

Figure 6.3. Absorption spectra of 200-Å-thick Au films on PDMS (dotted), and T-IIR (black).

While nanocomposite films of Au in elastomer have applications in surface-enhanced Raman spectroscopy[16], metal-enhanced fluorescence spectroscopy[17] or as biosensors[18] we require the formation of continuous, *conductive* metal films for applications in stretchable electronics. Therefore, we developed a method to circumvent the embedding of gold in IIR during e-beam metal deposition through the use of polymer interlayers to enable the fabrication of conductive metal films on IIR.

6.3.3. E-beam Deposition of Gold Films on PEDOT:PSS-protected IIR

In order to prevent gold atoms from embedding into the surface of the IIR during e-beam metal deposition we deposited a thin film of poly(3,4-ethylenedioxythiophene):poly(4-styrenesulphonic acid) (PEDOT:PSS) on the surface of the IIR prior to metal deposition to shield and protect the underlying IIR substrate and to provide a stable platform for gold to nucleate and grow into a conductive film. PEDOT:PSS is a conductive polymer that has previously been used to enable the evaporation of gold top electrodes onto self-assembled monolayers (SAMs) of alkane

dithiols on gold for the creation of molecular junctions with yields > 95% (in the absence of PEDOT:PSS electrical shorts were created from direct deposition of gold on the SAM).[19] PEDOT:PSS is an aqueous dispersion therefore it is compatible with spin coating on IIR as the water solvent does not swell or dissolve the IIR substrate.

Prior to PEDOT:PSS deposition, IIR substrates were cleaned via sonication in acetone and isopropanol followed by subsequent plasma oxidation to generate oxidized functional groups at the surface.[20] PEDOT:PSS was spin coated on the oxidized IIR surface at 1000 rpm for 1 min followed by 2000 rpm for 1 min to produce a uniform polymer film on the surface of IIR. Subsequently, gold films were deposited on PEDOT:PSS-protected IIR by e-beam metal deposition.

E-beam gold deposition on PEDOT:PSS-protected IIR results in **conductive**, shiny metallic gold films. The process can be applied to a range of IIR substrates (B-IIR, W-IIR, T-IIR). In the optical micrographs of 500-Å-thick Au films on native unprotected B-IIR, W-IIR and T-IIR, gold films appear grainy and discontinuous with some pinholes visible (Figure 6.4a-c). On PEDOT:PSS-protected IIR continuous gold films are produced. Waves are visible in the gold films on PEDOT:PSS-protected IIR due to thermal expansion of the substrate during e-beam gold deposition which produces compressive strain in the gold film upon relaxation due to cooling (Figure 6.4d-f); similar buckling patterns have been observed in gold films deposited on PDMS.[21] The PEDOT:PSS protection layer provides a stable platform upon which gold can nucleate and grow into a continuous film allowing for electrical conduction. Table 6.4 compares the sheet resistance of 500-Å-thick Au films on PDMS and on PEDOT:PSS-protected IIR. The sheet resistances of 500-Å-thick Au films on PEDOT:PSS-protected B-IIR, W-IIR and T-IIR similar to those on PDMS.

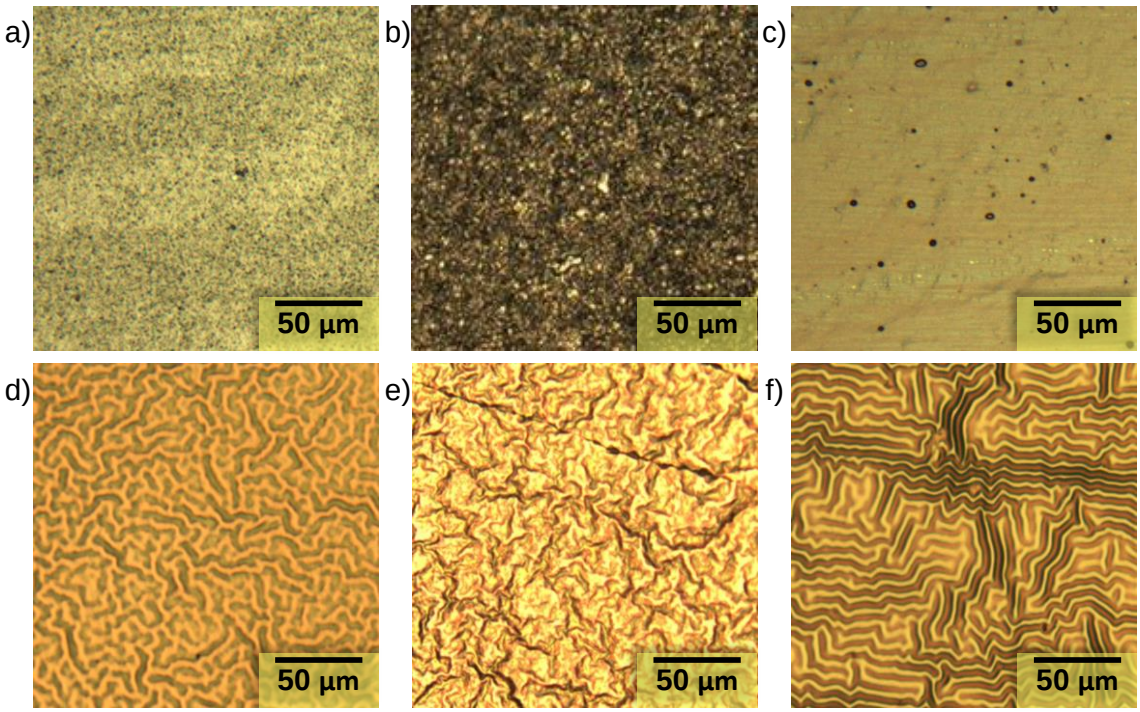

Figure 6.4. Optical micrographs of 500-Å-thick-Au films with a Ti adhesion layer (15-Å-thick) on: (a) B-IIR; (b) W-IIR; (c) T-IIR; (d) PEDOT:PSS-protected B-IIR; (e) PEDOT:PSS-protected W-IIR; (f) PEDOT:PSS-protected T-IIR.

Table 6.4. Sheet resistance of 500-Å-thick-Au films on various substrates.

Sample	Average Sheet Resistance (Ω/sq)
500-Å-thick Au/PDMS	0.723 ± 0.121
500-Å-thick /PEDOT/B-IIR	0.770 ± 0.344
500-Å-thick Au/PEDOT/W-IIR	2.75 ± 0.935
500-Å-thick Au/PEDOT/T-IIR	0.730 ± 0.256

PEDOT:PSS shields the underlying IIR substrates during e-beam metal deposition to afford conductive metal films on IIR substrates. Gold films deposited on PEDOT:PSS remain conductive up to 40% elongation at which point the cracks in the gold film disrupt

conductivity completely (Figure 6.5). In order for metal films to be used in stretchable electronics requiring large deformations such as strain sensors in applications requiring one-time large-area deformations such as deformation to non-planar conformations, stretching to higher elongations may be required. The following sections will build on the success of interlayers developed for highly stretchable gold films on PDMS (Chapters 2 and 3 of this dissertation) and apply the methods to IIR substrates for the preparation of highly stretchable, gold films on IIR.

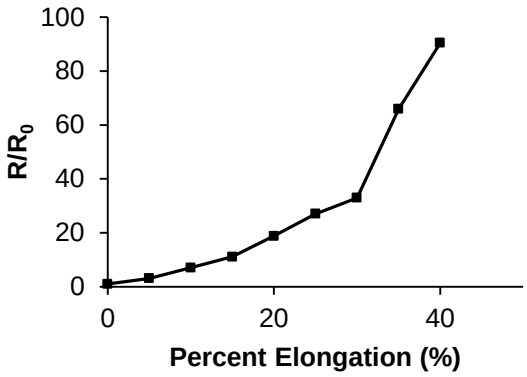

Figure 6.5. Electrical characterization of 250-Å-thick Au films on B-IIR/PEDOT:PSS as a function of strain.

6.3.4. Stretchable, Conductive Gold Films on IIR with Microstructured Glue Interlayers

In Chapter 2, we demonstrated the use of poly(vinylacetate) glue (PVAc) emulsions spin coated on PDMS to create microstructure reliefs which alter the cracking mechanism of overlying gold films. This approach enabled the fabrication of gold interconnects on PDMS/glue$_{1:1}$ stretchable to 65% strain with very small changes in resistance (R/R_0 of 23 at 65% elongation). The same approach can also be applied to IIR substrates to create highly stretchable gold interconnects. On IIR, the glue interlayer plays a dual role: In addition to providing a microstructured relief for favorable crack propagation, the glue interlayer provides effective shielding to the underlying IIR substrate during e-beam metal evaporation to enable the deposition of conductive gold films on IIR.

We spin coated glue emulsions (1:1 v/v water:glue) on oxidized T-IIR substrates treated with $SiCl_4$ to decrease the water contact angle of the surface and promote wetting of the glue emulsion (Section 1.2.2.3). Subsequently, we deposited a 30-Å-thick Ti adhesion layer and 250-Å-thick Au films by e-beam metal deposition. Deposition of gold on T-IIR/$glue_{1:1}$ produces continuous, conductive gold films (Figure 6.6a). The initial resistance of 250-Å-thick Au films on T-IIR/$glue_{1:1}$ with dimensions 1.5 cm x 2.5 cm is 2.09 ± 0.34 Ω. As the film is stretched, the rough topography of the glue interlayer provides multiple sites for strain nucleation and microcracks begin to form perpendicular to the direction of applied strain. At 25% elongation, cracks measure up to 65 μm in width but do not propagate the full width of the gold film (Figure 6.6b). A similar crack propagation mechanism as that observed in Chapter 2 is occurring in this system. Cracks interact with one another and when a crack enters a region of the film that has experienced prior relaxation the crack propagation is halted. The result is the formation of a large number of small cracks in gold films on T-IIR/$glue_{1:1}$ in contrast to the fewer number of long straight cracks that occur in gold films on PDMS which experience fewer crack nucleation sites and as a result develop longer cracks. As the strain increases to 60% the cracks widen to up to 100 μm in diameter and additional cracks are visible however, coalescence of cracks does not occur and the conductive pathway is maintained (Figure 6.6c).

Gold films deposited on T-IIR/$glue_{1:1}$ exhibit similar changes in resistance with stretching as gold films on PDMS/$glue_{1:1}$ supporting our hypothesis that the microstructured glue topography provides a similar mechanism for crack propagation on both substrates. The slope of the line of best fit for the change in resistance against elongation is 0.329 and 0.337 for 250-Å-thick gold films on T-IIR/$glue_{1:1}$ and PDMS/$glue_{1:1}$ respectively. The small change in resistance makes these gold films excellent candidates for device interconnects where small changes in resistance are desirable. At 25% elongation, the emergence of multiple short cracks measuring up to 65 μm in width causes the R/R_0 of gold films on T-IIR/$glue_{1:1}$ to increase to ~8.2. Although these cracks are quite large, they are not numerous and the gold ligament network that remains is quite large (ligaments are ~ 200 μm in width) leading to a small

increase in resistance. As strain in gold films on T-IIR/glue$_{1:1}$ is increased to 60% new cracks emerge, which combined with the widening of existing cracks, causes R/R_0 to increase to ~ 20.4 (Figure 6.6d). The entanglement of cracks prevents long-range propagation limiting the length of cracks to several hundred microns. Mechanical failure of the T-IIR substrate occurs between 45-65% strain which we hypothesize is due to extension of cracks from the gold layer into the T-IIR substrate caused by the large mismatch in elastic properties between metal, glue, and T-IIR.[22] The mechanical failure of PDMS/glue$_{1:1}$/gold stacks occurs at similar elongations of 60-65%. The glue$_{1:1}$ interlayer produces a similar change in resistance as a function of strain in gold films independently of which elastomeric substrate is used making it a versatile approach to producing ultrahigh stretchable gold films for use as interconnects on a variety of elastomeric substrates.

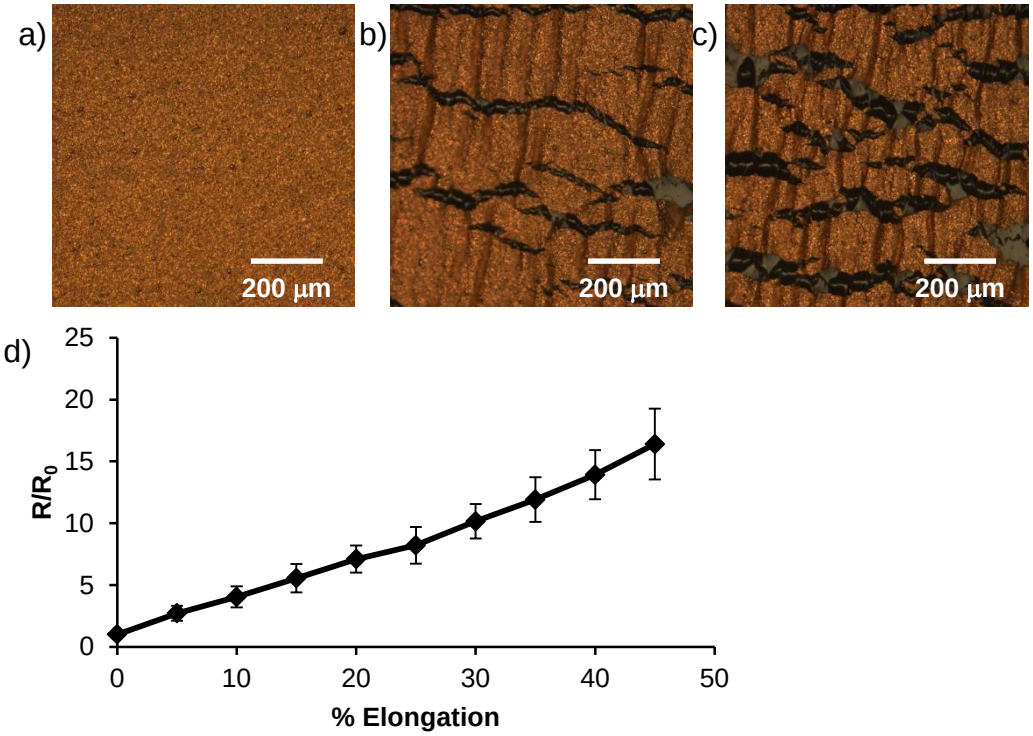

Figure 6.6. Optical images of 250-Å-thick Au films on T-IIR/glue$_{1:1}$: (a) unstretched; (b) stretched 25%; (c) stretched 60%. (d) Electrical characterization of 250-Å-thick Au films on T-IIR/glue$_{1:1}$ as a function of strain.

6.3.5. E-beam Deposition of Gold Films on PVA-protected IIR

Building upon the insights gained in Chapter 3, we investigated the use of PVA interlayers on IIR to determine whether PVA provided effective shielding to IIR substrates during e-beam metal deposition and whether the same ultrahigh stretchability of gold films on PVA interlayers was possible on IIR as that which was observed on PDMS. We prepared solutions of PVA in water and spin-coated the materials on the oxidized substrates using an initial spin speed of 1000 rpm for 1 min followed by 2000 rpm for 1 minute. We then deposited 250-Å-thick gold films onto IIR with PVA interlayers by e-beam deposition at a rate of 1 Å/s. As discussed in Chapter 3, PVA is a brittle material up to 42% relative humidity (RH); exposure to higher humidity levels increases the ductility of the material due to water molecules disrupting the hydrogen bonding within the PVA polymer which in turn softens the material and decreases its crystallinity.[23] We prepared gold films on IIR with PVA interlayers at humid ambient

conditions (RH 60% at 26°C). Protection of B-IIR, W-IIR and T-IIR with PVA interlayers enabled the fabrication of conductive gold films.

Optical microscopy shows that gold films deposited on B-IIR/PVA are continuous (Figure 6.7a). As these films were prepared under ambient humid conditions (60% RH) and not treated with water condensate post-metallization we do not expect to see a wrinkled surface topography as was observed in Chapter 3. Despite the lack of surface wrinkles, gold films on B-IIR/PVA exhibit multiple crack nucleation sites instead of the fewer continuous cracks that form on smooth gold films on PDMS indicating that the ambient humidity conditions of 60% RH at 26°C are sufficient to plasticize PVA and prevent brittle cracking under applied strain. This result shows promise that we may be able to isolate the effects of a compliant polymer interlayer from surface topography in order to produce smooth metal electrodes with ultrahigh stretchability. Upon application of strain, multiple short microcracks propagate perpendicular to the direction of applied strain and measure up to 25 μm in width and up to 500 μm in length at 25% elongation (Figure 6.7b). At 60% strain, the cracks widen to 35 μm and new cracks form, however a network of connected gold ligaments remains preserving the electrical pathway (Figure 6.7c). The preservation of the gold ligament network is further evidenced in the SEM images which reveal the homogeneous topography of the unstretched sample (Figure 6.7d) which cracks upon exposure to strain. The cracks, measuring ~ 15 μm in width at 30% strain, do not propagate the full width of the wire, allowing electrical conductivity to be maintained (Figure 6.7e). At high magnification, the underlying B-IIR substrate is visible in the cracked region between gold ligaments on PVA (Figure 6.7f). Figure 6.7g shows the change in resistance as a function of percent elongation of a representative 250-Å-thick Au films on B-IIR/PVA. The initial resistance of a wire cut to 1 cm x 2 cm is 8.5 Ω. The sample remained conductive up to 120% elongation at which point mechanical failure of the substrate occurred.

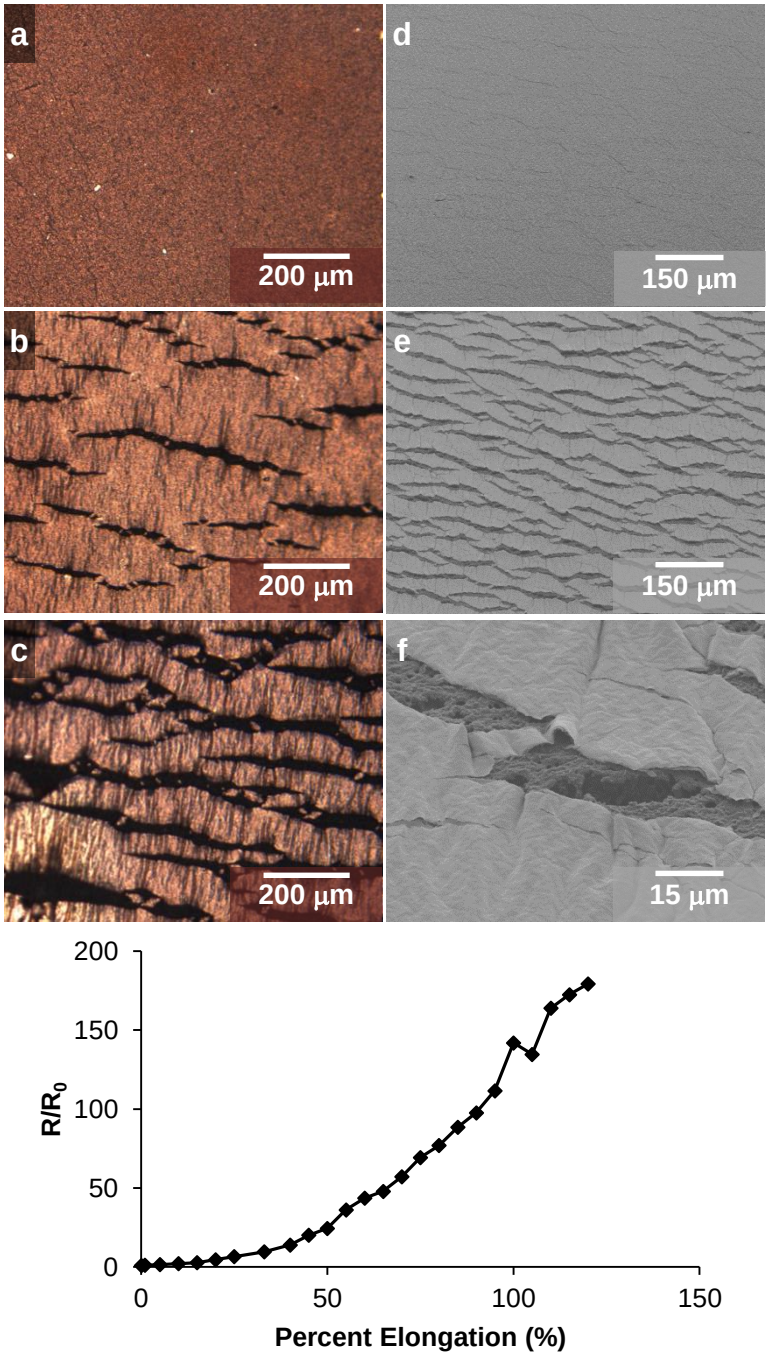

Figure 6.7. Optical micrographs of 250-Å-thick Au films on B-IIR/PVA a) unstretched; (b) stretched to 25%; (c) stretched to 60%. SEM images of 250-Å-thick Au films on B-IIR/PVA; (d) unstretched; (e, f) stretched to 30%. (g) Electrical characterization of 250-Å-thick Au films on B-IIR/PVA as a function of strain.

We hypothesize that the difference in mechanical failure of the T-IIR/glue$_{1:1}$/gold stacks and the B-IIR/PVA/gold stacks is due to differences in the crack propagation. In glue interlayer systems we hypothesize that cracks in the gold film propagate vertically into the substrate causing premature mechanical failure compared to native PDMS (elongation at break of 160%) and native T-IIR (elongation at break of 170%). In contrast, that cracks that propagate through gold films on IIR/PVA do not propagate vertically into substrate; the PVA/gold layers can be seen to delaminate from the IIR substrates and buckles are visible in the PVA/gold film in Figure 6.7e, f. This delamination allows higher elongations at failure to be obtained however it is undesirable for device electrodes which require smooth surfaces and excellent adhesion to the substrate in order to sustain cyclic deformations.

The PVA-protection layer can also be applied to T-IIR substrates prior to metal deposition to achieve conductive gold films on T-IIR. Upon application of ~30% strain, multiple cracks propagate through the gold film measuring ~ 15 μm in width (Figure 6.8a) causing an R/R_0 of 6.11. At high magnification, the underlying T-IIR substrate is visible and the PVA/gold film is visibly delaminating from the T-IIR substrate. Loading the stretched sample onto a tilted stage provides an edge-on view of the buckled, delaminated ligaments of gold (Figure 6.8c) whose amplitudes reach ~ 3.5 μm in height (Figure 6.8d). Metal films with poor adhesion to elastomeric substrates fail at strains of a few percent because they become free-standing and are no longer able to delocalize strain into the elastomeric substrate. [24] In contrast, gold films on T-IIR/PVA can stretch up to 65% elongation before failure occurs. Unlike weakly adhered metal films on elastomers, the gold films on T-IIR/PVA are not free-standing; the PVA/gold layers buckle and delaminate together therefore the metal film continues to reside on a polymer support platform which prevents single necking sites from propagating through the metal film and interrupting conductivity at low strains. We hypothesize that gold films on T-IIR/PVA fail sooner than analogous films on B-IIR/PVA due to insufficient adhesion to the smooth T-IIR surface which causes increased delamination of the PVA/gold film upon subjection to strain. It is possible that PVA films have superior adhesion to B-IIR substrates due to the increased roughness of B-IIR

substrates (RMS roughness of 13.56 ± 1.88 nm)[25] compared to T-IIR substrates (RMS roughness of 6.59 ± 0.51 nm) which provides increased mechanical interlock to the PVA film.

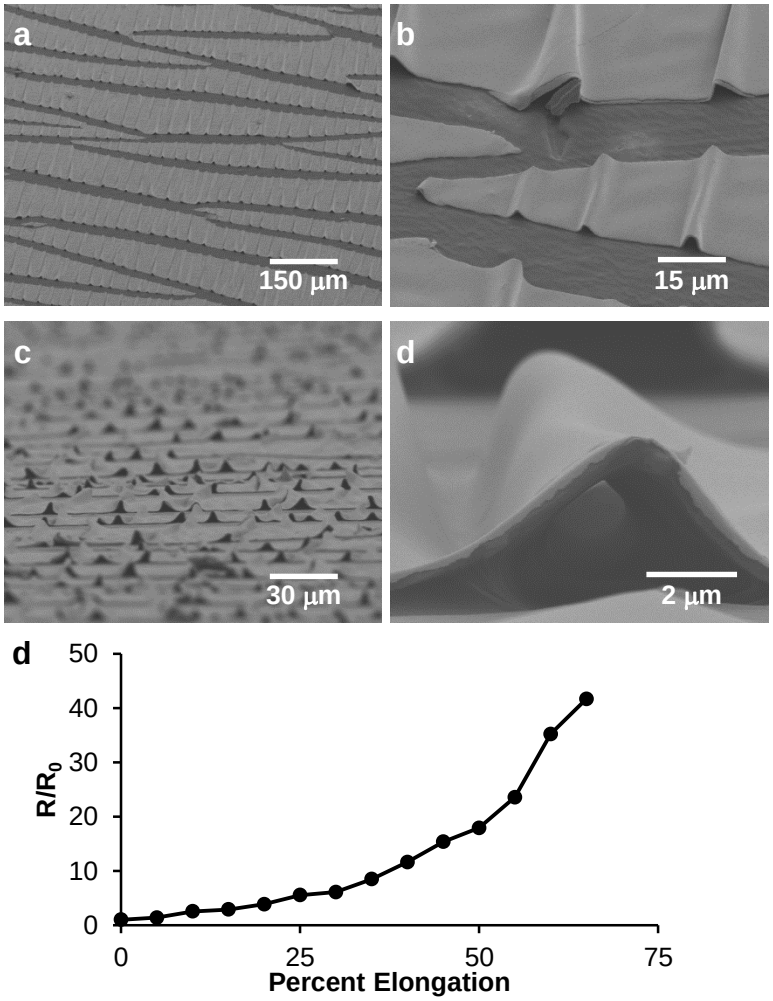

Figure 6.8. Scanning electron micrographs of 250-Å-thick Au films on T-IIR/PVA (a, b) stretched ~ 30%; (c, d) stretched ~ 30% and tilted 45°. (e) Electrical characterization of 250-Å-thick Au films on B-IIR/PVA as a function of strain.

6.4. Conclusions

We have demonstrated that direct e-beam metal deposition onto IIR results in the formation of a non-conductive Au/IIR composite material. We have developed polymer protection layers which provide stable platforms upon which gold films can nucleate and grow into conductive gold films. PEDOT:PSS polymer interlayers enable the fabrication of conductive gold films on W-IIR, B-IIR and T-IIR with similar sheet resistances to analogous gold films deposited on PDMS. Gold films on B-IIR/PEDOT:PSS can sustain elongations of 40% before electrical failure occurs. Gold films with higher stretchability can be produced through the use of microstructured glue interlayers enabling gold films to remain conductive up to 65% elongation at which point mechanical failure of the conductive stack occurs. These gold films have very low gauge factors (0.329) making these wires useful as stretchable interconnects. PVA polymer interlayers also enable the fabrication of stretchable gold films on IIR however more work is needed to improve the adhesion at the interface of PVA and IIR. Future work will investigate methods to improve the adhesion of PVA/gold to IIR substrates. It is possible that treatment with of the oxidized IIR substrate with $SiCl_4$ may introduce more terminal OH groups on the surface of the IIR in order to increase hydrogen bonding with the PVA interlayer and improve adhesion. Alternatively, we may investigate methods to chemically cross-link the PVA layer to the IIR substrate for improved adhesion. Development of elastomeric interlayers in lieu of polymeric interlayers will enable the production of smooth gold films for use as electrodes in stretchable light-emitting devices as elastomers are softer than polymers and are not prone to cracking.

6.5. References

[1] J. Lewis, *Materials today* **2006**, *9*, 38-45.

[2] S.-W. Seo, E. Jung, H. Chae, S. J. Seo, H. K. Chung, S. M. Cho, *Thin Solid Films* **2014**, *550*, 742-746.

[3] T. B. Carmichael, A. Vohra, L. Ferrari, N. Suhan, PCT/CA2013/001047, **2014**.

[4] Y. Kim, H. Kim, S. Graham, A. Dyer, J. R. Reynolds, *Solar Energy Materials and Solar Cells* **2012**, *100*, 120-125.

[5] L. Ferrari, G. J. E. Davidson, T. B. Carmichael, PCT/CA2013/001043, **26 June 2014**.

[6] D.-H. Kim, N. Lu, R. Ghaffari, Y.-S. Kim, S. P. Lee, L. Xu, J. Wu, R.-H. Kim, J. Song, Z. Liu, J. Viventi, B. de Graff, B. Elolampi, M. Mansour, M. J. Slepian, S. Hwang, J. D. Moss, S.-M. Won, Y. Huang, B. Litt, J. A. Rogers, *Nature Materials* **2011**, *10*, 316-323.

[7] S. P. Lacour, J. Jones, S. Wagner, T. Li, Z. Suo, *Proceedings of the IEEE* **2005**, *93*, 1459-1467.

[8] M. G. Helander, Z.-B. Wang, M. T. Greiner, Z.-W. Liu, J. Qiu, Z.-H. Lu, *Advanced Materials* **2010**, *22*, 2037-2040.

[9] H. L. Filiatrault, G. C. Porteous, R. S. Carmichael, G. J. E. Davidson, T. B. Carmichael, *Advanced Materials* **2012**, *24*, 2673-2678.

[10] S. P. Lacour, S. Wagner, Z. Y. Huang, Z. Suo, *Applied Physics Letters* **2003**, *82*, 2404.

[11] L. Ferrari, N. Suhan, T. B. Carmichael, C. Siegers, PCT/CA2013/001035, **26 June 2014**.

[12] K. Sayo, S. Deki, S. Hayashi, *The European Physical Journal D* **1999**, *9*, 429-432.

[13] M. K. Corbierre, N. S. Cameron, M. Sutton, S. G. J. Mochrie, L. B. Lurio, A. Rühm, B. R. Lennox, *Journal of the American Chemical Society* **2001**, *123*, 10411-10412.

[14] Q. Zhang, J.-J. Xu, Y. Liu, H.-Y. Chen, *Lab on a Chip* **2008**, *8*, 352-357.

[15] S. Sivaramakrishnan, P.-J. Chia, Y.-C. Yeo, L.-L. Chua, P. K. H. Ho, *Nature Materials* **2007**, *6*, 149-155.

[16] K. S. Giesfeldt, R. M. Connatser, M. A. De Jesús, P. Dutta, M. J. Sepaniak, *Journal of Raman Spectroscopy* **2005**, *36*, 1134-1142.

[17] S. Dutta Choudhury, R. Badugu, K. Ray, J. R. Lakowicz, *The Journal of Physical Chemistry C* **2012**, *116*, 5042-5048.

[18] P. Devi, A. Y. Mahmoud, S. Badilescu, M. Packirisamy, P. Jeevanandam, V.-V. Truong, in *Biosciences (BIOSCIENCESWORLD), 2010 International Conference on*, **2010**, pp. 1-5.

[19] H. B. Akkerman, P. W. M. Blom, D. M. de Leeuw, B. de Boer, *Nature* **2006**, *441*, 69-72.

[20] G. S. Ferguson, M. K. Chaudhury, H. A. Biebuyck, G. M. Whitesides, *Macromolecules* **1993**, *26*, 5870-5875.

[21] N. Bowden, S. Brittain, A. G. Evans, J. W. Hutchinson, G. M. Whitesides, *Nature* **1998**, *393*, 146-149.

[22] N. J. Douville, Z. Li, S. Takayama, M. D. Thouless, *Soft Matter* **2011**, *7*, 6493-6500.

[23] M. V. Konidari, K. G. Papadokostaki, M. Sanopoulou, *Journal of Applied Polymer Science* **2011**, *120*, 3381-3386.

[24] Y. Xiang, T. Li, Z. Suo, J. J. Vlassak, *Applied Physics Letters* **2005**, *87*, 161910.

[25] A. Vohra, H. L. Filiatrault, N. Suhan, C. Siegers, G. J. E. Davidson, L. Ferrari, T. B. Carmichael, *unpublished work* **2011**.

7. Chapter 7

Conclusions and Outlook

7.1 Conclusions

The research presented in this dissertation focused on solving some of the most important lingering challenges in the fabrication of stretchable electronic devices: how to make metal films on elastomeric substrates highly stretchable through the use of low-cost methods that do not rely on photolithography, how to enable the fabrication of large-area room-temperature stretchable light-emitting displays, and how to replace air and moisture permeable elastomers with more impermeable elastomeric substrates. This section will summarize the challenges that were undertaken and solved in each Chapter of this dissertation.

Stretchable metal films are required for stretchable interconnects, stretchable device electrodes and for stretchable circuits. Gold films deposited directly onto PDMS exhibit various morphologies depending on the deposition conditions and these morphologies impact the stretchability of the resultant metal films.[1] Gold films with buckled morphologies fail electrically at strains of ~22%[2] while gold films with microcracked morphologies can sustain strains up to 60% before electrical failure occurs[3] although it is very difficult to control the conditions required for the formation of microcracks.[1] Researchers have used sophisticated photolithography techniques to produce arc-shaped pop-ups[4],[5] and serpentines[6] in order to achieve highly stretchable metal interconnects however photolithography is a very expensive technique. We sought to improve the stretchability of gold films on PDMS and control crack propagation through the introduction of low-cost polymer interlayers which are deposited from solution using benchtop fabrication methods.

In Chapter 2, we demonstrated that white PVAc glue forms an emulsion in water which creates a microstructured relief when spin coated onto oxidized PDMS. The microstructured relief provides multiple sites for crack nucleation upon application of strain. The formation of small microcracks relieves the strain in the metal film and when cracks enter a relaxed region of the gold film crack growth is arrested. This phenomenon results in a gold film comprised of numerous small cracks instead of the continuous long cracks that form in buckled gold films on PDMS.[2] We demonstrate that by altering the

concentration of glue in the emulsion, we can control the morphology of the microstructured interlayer. As the concentration of glue is decreased, void regions are introduced in between the clusters of PVAc which reduces the number of crack nucleation sites and leads to the formation of longer cracks. By controlling the crack propagation in strained gold films through the concentration of glue in the emulsion, the change in resistance can be tuned to meet various applications. For interconnect applications which require small changes in resistance with applied strain the most concentrated glue emulsions (1:1 water:glue) are used for the interlayer. In contrast, for strain sensor applications, larger changes in resistance with applied strain are desired and therefore more dilute glue emulsions are employed in the interlayer.

In Chapter 3, we demonstrated that in addition to microstructure, the mechanical properties of the polymer interlayer contribute to crack propagation in strained gold films on elastomeric substrates. This effect was demonstrated with poly(vinyl alcohol) polymer interlayers as it has been shown that the Young's Modulus of PVA is dependent upon the amount of water contained in the PVA film.[7],[8] Water molecules disrupt hydrogen bonding within the PVA film leading to softer, less crystalline films that can sustain higher elongations at break. We demonstrated that gold films deposited on PDMS/PVA fail electrically at strains greater than 15% due to the continuous cracks that propagate perpendicular to the direction of applied strain. When gold films on PDMS/PVA are exposed to water condensate, the elongation at failure increased to 75%. We postulate that the increased elongation at failure is due to two effects: the softening of the PVA interlayer due to water disrupting hydrogen bonding within the polymer, and the formation of a wrinkled topography which occurs due to the swelling of the PVA layer upon treatment with water condensate. The wrinkles act as crack nucleation sites while the softer PVA layer is able to deform to greater strains before cracks nucleate. The combined effects lead to gold films with stretchability up to 70% elongation for use as device interconnects or strain sensors.

The second goal of the dissertation was to develop methods to fabricate large-area stretchable light-emitting devices. The first reports of stretchable light-emitting displays relied on rigid device islands joined by stretchable interconnects.[5] This approach allows

for a high density of small pixels which is ideal for display technologies. A second approach to achieving stretchable light-emitting devices is tailored towards applications requiring large-area light-emission for applications in lighting and signage. In order for large-area pixels to be developed, every layer of the device must be rendered stretchable. In Chapter 4, we report the first example of a large-area light-emitting device capable of emitting light when stretched at room-temperature. Room-temperature stretchability is critical for wearable electronics and in order for devices to be mounted directly to skin for various types of light-therapy treatments. We focused on the fabrication of light-emitting electrochemical cells (LECs) rather than organic light-emitting devices (OLEDs) since LECs require only a single layer emissive layer to support all functionality of charge injection, charge transport and emissive recombination. In order to achieve room-temperature stretchability we developed a stretchable semi-transparent gold film on PDMS for the anode. We dispersed the light-emitter, a ruthenium ionic transition-metal complex (iTMC), in an elastomeric matrix to impart stretchability to the emissive layer itself. Finally, the device was completed with a drop of gallium-indium eutectic liquid metal as the cathode. This device configuration allowed for the fabrication of large-area light-emitting devices that could emit light up to 27% elongation.[9]

Chapter 5 built upon the work reported in Chapter 4 with the aim of fabricating stretchable light-emitting devices with greater stability and longer lifetimes. PDMS is an elastomer that is highly permeable to oxygen and moisture. We sought to improve device lifetimes of LECs through the incorporation of the more impermeable elastomer isobutylene-co-isoprene (IIR). Commercial grades of IIR do not mix with the ruthenium iTMC therefore we incorporated IIR that was covalently modified with poly(ethylene oxide) (PEO) side chains on the polymer backbone. Emissive layers containing IIR-g-PEO with 34 wt% PEO and 69 wt% PEO exhibited improved mixing with the iTMC and only decay to 50% and 25% of the maximum radiance after six hours of operation at 0.5 mA respectively. Analogous devices with PDMS matrices decay to 20% of the maximum radiance in ~ 15 minutes. This supports the hypothesis that incorporation on IIR in the emissive layer is beneficial to device stability.

One of the major obstacles towards the commercialization of stretchable organic devices is the need for the development of stretchable encapsulating layers. Traditional rigid organic electronic devices are sealed with epoxy and glass to prevent the permeation of water and moisture into the active layers.[10] Flexible electronics developed on plastic use flexible multilayer stacks as barrier layers to protect the organic layers from moisture and oxygen however any cracking of the barrier layers due to tensile elongation would provide a pathway for oxygen and moisture diffusion into the device.[11] Rather than develop stretchable encapsulation layers, we aimed to replace the permeable PDMS substrate with an elastomer possessing higher impermeability to moisture and gas, isobutylene-co-isoprene rubber (IIR). A shift to IIR combines stretchability and oxygen and moisture barrier functionality into one material. The first step towards fabricating stretchable electronic devices on IIR is the fabrication of conductive metal films for use as device electrodes, interconnects and circuits. Through the course of this dissertation we discovered that direct deposition of gold films on IIR by e-beam metal evaporation produces non-conductive metal films due to partial embedding of gold atoms in IIR preventing the formation of a conductive pathway. Therefore, we established methods to enable the fabrication of conductive metal films on IIR.

In Chapter 6, we demonstrate that polymer interlayers can be deposited from aqueous solution onto cured IIR substrates to provide a stable platform upon which metal films can nucleate and grow into conductive metal films. Gold films deposited on PEDOT:PSS-protected IIR have similar sheet resistances to analogous gold films deposited onto PDMS. Building upon the work in Chapters 2 and 3, we also demonstrated that PVAc glue interlayers and PVA interlayers can be employed on IIR to achieve conductive metal films with ultrahigh stretchability. These developments bring the field of stretchable electronics one step closer to the realization of commercial stretchable electronic devices by potentially eliminating the need for stretchable barrier layers.

7.2. Outlook

Over the course of this dissertation we have gained new insights into the crack propagation mechanism of metal films, demonstrated for the first time that room-temperature stretchability of large-area light-emitting devices is possible, and developed methods to enable the fabrication of conductive metal films on IIR substrates. This research has opened the door to exciting research opportunities in the field of stretchable electronics, namely: the use of polymer interlayers for highly stretchable metal films on elastomeric substrates, the incorporation of elastomers in the emissive layers of LECs to enable the fabrication of large-area stretchable pixels, and the prospect of new elastomeric substrates with high moisture and gas impermeability to enable the fabrication of stretchable organic electronic devices that can operate in ambient conditions with long lifetimes. The following sections will explore new avenues that can be explored building upon the knowledge that was gained over the course of this dissertation.

7.2.1. Polymer Interlayers for Highly Stretchable Metal Films on Elastomers

In Chapters 2 and 3 we described the use of polymer interlayers between gold films and the PDMS substrate in order to achieve highly stretchable metal films. We discovered that the polymer interlayers employed provide multiple sites for crack nucleation due to presence of microstructured topologies. The polymer interlayer also required sufficient ductility otherwise cracks propagated through the metal film at low elongations causing electrical failure.

Future work will investigate the crack propagation of less expensive metal films, such as copper and aluminum, on elastomers with polymer interlayers to further reduce fabrication costs. Different metal films possess differences in grain size, coefficient of thermal expansion and ductility. Future work will aim to determine if either PVA or PVAc interlayers provide increased stretchability to copper, silver or aluminum films on elastomeric substrates in order to demonstrate the broad applicability of the approach.

The highly stretchable nature of gold films reported in Chapter 2 and 3 enables their application as device interconnects and as human motion strain sensors, however the rough topography precludes their incorporation as device electrodes where low surface roughness is required. Device electrodes require smooth surfaces since subsequent films of active layers are only ~ 100 nm thick, therefore any protrusions from the electrode that are greater than 100 nm threaten to pierce through the thin active layers and cause current leakage or short circuits. Future work will investigate candidates for smooth polymer interlayers, such as PVA films with plasticizing agents such as glycerol and caprolactam. Plasticizing agents incorporated in the polymer solution prior to thin film deposition will prevent intramolecular and intermolecular hydrogen bonding in the PVA film. This may eliminate the need for water condensate treatment which swells the polymer and produces a wrinkled topography in the gold film.

Elastomers are also intriguing candidates for use as interlayers as they are inherently stretchable and do not crack. Future work will examine the effect of stacked elastomers with different Young's Moduli on the crack propagation in overlying metal films. PVA and PVAc glue have higher Young's Moduli than PDMS but a lower Young's Modulus than gold. Therefore a gradient of Young's Modulus is present in the stack of the substrate, interlayer and gold film. The Young's Modulus of PDMS can be tuned by varying the ratio of base to cross-linking agent. We would like to investigate the effect of using PDMS substrates with a gradient of Young's Moduli on the crack propagation in overlying metal films by spin coating thin films of PDMS with different ratios of cross-linker to curing agent onto the substrate. Previous research has shown that the compliance of the substrate affects the stretchability of the overlying metal film: Substrates that are too compliant are unable to delocalize strain in the metal film leading to the formation of a single necking site causing the metal film to rupture and conductivity to be lost.[12] By depositing PDMS with a higher Young's Modulus onto a softer PDMS substrate we can achieve greater strain delocalization of the metal film while maintaining the soft substrate required for electronic skin-like application which require lamination to the skin for intimate contact with the body.

7.2.2. Elastomeric Matrices in LECs

In Chapter 4, we demonstrated for the first time that elastomers can be incorporated into iTMC LECs. Incorporation of PDMS enables the emissive layer to stretch to 27% before light-emission is no longer observed. We hypothesize that failure of the gold electrode limits the device stretchability.[9] Future work will involve depositing the Ru/PDMS emissive layer on more stretchable anodes such as the silver nanowire composite electrodes reported by Pei[13] and co-workers to determine the full potential of the stretchable emissive layer.

In Chapter 5, we report LECs with elastomeric IIR-g-PEO matrices which possess increased stability compared to Ru/PDMS analogues. We demonstrate that emissive layers fabricated with IIR-g-PEO matrices with 34 wt% PEO can undergo cyclic straining of 15% and still emit light. In order to probe the elongation at failure of the emissive layers with IIR-g-PEO emissive layers, these devices will also need to be deposited onto more stretchable anodes than PDMS/Au. Future work will compare the stretchability of LECs with IIR-g-PEO matrices to those containing PDMS. The Young's Modulus of IIR-g-PEO34 is 9 MPa[14] which is slightly higher than that of PDMS (1-2 MPa)[15] however its elongation at break is much larger (609% for IIR-g-PEO[14] vs. 160% for PDMS[15]) therefore we hypothesize that emissive layers with IIR-g-PEO34 will exhibit greater stretchability than those with PDMS. In Chapter 5 we also demonstrated that emissive layers with IIR-g-PEO34 matrices have higher stability than analogous devices with PDMS matrices in the emissive layer. All of the stability testing was carried out under inert conditions. Future work will compare the stability of LECs with IIR-g-PEO and PDMS emissive layers operated under ambient conditions to determine if IIR-g-PEO affords any protection to the emissive layer from reaction with ambient moisture and oxygen.

Finally, all of the experiments carried out in this dissertation incorporated the iTMC $Ru(dtb\text{-}bpy)_3(PF_6)_2$ in the emissive layer for ease of synthesis and in order to establish proof of concept. Future work will investigate the use of other iTMC materials with higher efficiencies that have been reported in literature.[16] Altering the iTMC material

will also enable the production of different coloured pixels and by altering the ligand sidechains on the iTMC it may be possible to achieve increased miscibility with the elastomeric matrix.

7.2.3. Butyl Rubber as a Substrate for Stretchable Electronic Devices

One of the greatest remaining challenges which prevent stretchable organic electronic devices from being brought to the market is the need for stretchable encapsulation and barrier layers to protect the sensitive organic components and air sensitive electrodes from ambient moisture and oxygen. Instead of developing stretchable encapsulating materials, we aim to resolve this challenge by moving away from the ubiquitously used PDMS substrate, which is highly permeable to moisture and oxygen, towards the more impermeable elastomer butyl rubber. In Chapter 6, we developed methods to enable the fabrication of conductive gold films on IIR through of use of polymer interlayers. Stretchable gold films on IIR with large changes in resistance upon application of strain have implications as human motion and robotic joint strain sensing while gold films on IIR with small changes in resistance upon application of strain have potential applications as device interconnects in a myriad of stretchable electronic devices.

The large strain that can be accommodated by gold films on IIR (up to 120%) opens the door to new strain sensing applications. The conformal nature of the IIR substrate enables its lamination to joints and other non-planar surfaces, both human and robotic. Physical therapists will be able to monitor the rehabilitation and range of motion in patients through strain sensors laminated to the body; the deposition of metal circuitry onto IIR-based strain sensors will enable the information to be transmitted wirelessly for live-feedback monitoring. Embedding the sensors into clothing will enable the fabrication of smart textiles that can monitor the postures and movements of athletes and correlate the results to performance. IIR-based sensors can be used to monitor moving parts in aquatic machinery as they are impermeable to water and the electronic components remain protected.

The ultimate goal of incorporating IIR into stretchable electronics is the realization of a fully elastomeric IIR stretchable device which protects organic active layers and enables operation of devices under ambient conditions. By combining the IIR emissive layer component developed in Chapter 5 with the stretchable interconnects and electrodes developed in Chapter 6 and components that other researchers of the Carmichael Group are developing such as composite silver nanowire films as transparent electrodes, it will be possible to realize a fully stretchable IIR light-emitting device with IIR in every layer of the device. We hypothesize that devices with IIR in every layer will have higher device stabilities than analogous PDMS devices due to the increased impermeability to water and oxygen of the IIR polymer.

Furthermore, the development of stretchable interconnects on IIR opens the door to a whole realm of stretchable device applications. Stretchable interconnects on IIR can be used to join rigid pixels of organic and inorganic light-emitting devices for the fabrication of high-resolution, water-proof displays that can be used as light-weight wristwatch displays for soldiers in combat. Interconnects on IIR can be used to connect solar cells and batteries for the creation of devices with self-charging capabilities for incorporation into clothing. Arrays of large-area stretchable solar cells can be fabricated on IIR with stretchable interconnects opening the door to weatherable solar cells that can be laminated onto roofs, bus stop shelters, domes, windows, etc. The development of sealing methods to bond IIR top substrates to IIR bottom substrates in order to prevent lateral diffusion of moisture and oxygen into devices presents the next challenge towards these types of devices becoming a commercial reality.

7.3. References

[1] O. Graudejus, P. Görrn, S. Wagner, *ACS Applied Materials & Interfaces* **2010**, *2*, 1927-1933.

[2] S. P. Lacour, S. Wagner, Z. Huang, S. Suo, *Applied Physics Letters* **2003**, *82*, 2404.

[3] P. Mandlik, S. P. Lacour, J. W. Li, S. Y. Chou, S. Wagner, *Electron Device Letters, IEEE* **2006**, *27*, 650-652.

[4] Y. Sun, W. M. Choi, H. Jiang, Y. Y. Huang, J. A. Rogers, *Nature Nanotechnology* **2006**, *1*, 201-207.

[5] D.-H. Kim, J. Xiao, J. Song, Y. Huang, J. A. Rogers, *Advanced Materials* **2010**, *22*, 2108-2124.

[6] D. Brosteaux, F. Axisa, M. Gonzalez, J. Vanfleteren, *Electron Device Letters, IEEE* **2007**, *28*, 552-554.

[7] R. M. Hodge, G. H. Edward, G. P. Simon, *Polymer* **1996**, *37*, 1371-1376.

[8] M. V. Konidari, K. G. Papadokostaki, *Journal of Applied Polymer Science* **2011**, *120*, 3381-3386.

[9] H. L. Filiatrault, G. C. Porteous, R. S. Carmichael, G. J. E. Davidson, T. B. Carmichael, *Advanced Materials* **2012**, *24*, 2673-2678.

[10] A. Asadpoordarvish, A. Sandstrom, S. Tang, J. Granstrom, L. Edman, *Applied Physics Letters* **2012**, *100*, 193508.

[11] S.-W. Seo, E. Jung, H. Chae, S. J. Seo, H. K. Chung, S. M. Cho, *Thin Solid Films* **2014**, *550*, 742-746.

[12] T. Li, Z. Suo, *International Journal of Solids and Structures* **2006**, *43*, 2351-2363.

[13] J. Liang, L. Li, X. Niu, Z. Yu, Q. Pei, *Nature Photonics* **2013**, *7*, 817-824.

[14] S. Karamdoust, P. Crewdson, M. Ingratta, E. R. Gillies, *Polymer International* **2014**, doi: 10.1002/pi.4795.

[15] K. M. Choi, J. A. Rogers, *Journal of the American Chemical Society* **2003**, *125*, 4060-4061.

[16] R. D. Costa, E. Orti, H. J. Bolink, F. Monti, G. Accorsi, N. Armaroli, *Angew. Chem.-Int. Edit.* **2012**, *51*, 8178-8211.

Appendix A

Copyright Permissions

JOHN WILEY AND SONS LICENSE TERMS AND CONDITIONS

Dec 29, 2014

This Agreement between Heather L Filiatrault ("You") and John Wiley and Sons ("John Wiley and Sons") consists of your order details and the terms and conditions provided by John Wiley and Sons and Copyright Clearance Center.

License Number	3466130368871
License date	Sep 11, 2014
Licensed Content Publisher	John Wiley and Sons
Licensed Content Publication	Advanced Materials
Licensed Content Title	Stretchable Light-Emitting Electrochemical Cells Using an Elastomeric Emissive Material
Licensed Content Author	Heather L. Filiatrault,Gyllian C. Porteous,R. Stephen Carmichael,Gregory J. E. Davidson,Tricia Breen Carmichael
Licensed Content Date	Mar 26, 2012
Pages	6
Type of use	Dissertation/Thesis
Requestor type	Author of this Wiley article
Format	Print and electronic
Portion	Full article
Will you be translating?	No
Title of your thesis / dissertation	New materials and methods for the fabrication of large-area stretchable electronics
Expected completion date	Nov 2014
Expected size (number of pages)	300
Billing Type	Invoice
Billing Address	[redacted]
Total	
Total	

Terms and Conditions

TERMS AND CONDITIONS

This copyrighted material is owned by or exclusively licensed to John Wiley & Sons, Inc. or one of its group companies (each a"Wiley Company") or handled on behalf of a society with which a Wiley Company has exclusive publishing rights in relation to a particular work (collectively "WILEY"). By clicking accept in connection with completing this licensing transaction, you agree that the following terms and conditions apply to this transaction (along with the billing and payment terms and conditions established by the Copyright Clearance Center Inc., ("CCC's Billing and Payment terms and conditions"), at the time that you opened your Rightslink account (these are available at any time at http://myaccount.copyright.com).

AIP PUBLISHING LLC LICENSE
TERMS AND CONDITIONS

Dec 29, 2014

All payments must be made in full to CCC. For payment instructions, please see information listed at the bottom of this form.

License Number	3538330669318
Order Date	Dec 29, 2014
Publisher	AIP Publishing LLC
Publication	Applied Physics Letters
Article Title	High ductility of a metal film adherent on a polymer substrate
Author	Yong Xiang,Teng Li,Zhigang Suo, et al.
Online Publication Date	Oct 12, 2005
Volume number	87
Issue number	16
Type of Use	Thesis/Dissertation
Requestor type	Student
Format	Print and electronic
Portion	Figure/Table
Number of figures/tables	1
Title of your thesis / dissertation	New Materials and Methods for the Fabrication of Large-Area Stretchable Electronics
Expected completion date	Feb 2015
Estimated size (number of pages)	250
Total	0.00 USD

Terms and Conditions

AIP Publishing LLC -- Terms and Conditions: Permissions Uses

AIP Publishing LLC ("AIPP"") hereby grants to you the non-exclusive right and license to use and/or distribute the Material according to the use specified in your order, on a one-time basis, for the specified term, with a maximum distribution equal to the number that you have ordered. Any links or other content accompanying the Material are not the subject of this license.

1. You agree to include the following copyright and permission notice with the reproduction of the Material:"Reprinted with permission from [FULL CITATION]. Copyright [PUBLICATION YEAR], AIP Publishing LLC." For an article, the copyright and permission notice must be printed on the first page of the article or book chapter. For photographs, covers, or tables, the copyright and permission notice may appear with the Material, in a footnote, or in the reference list.
2. If you have licensed reuse of a figure, photograph, cover, or table, it is your responsibility to ensure that the material is original to AIPP and does not contain the copyright of another entity, and that the copyright notice of the figure, photograph, cover, or table does not indicate that it was reprinted by AIPP, with permission, from another source. Under no circumstances does AIPP, purport or intend to grant permission to reuse material to which it does not hold copyright.
3. You may not alter or modify the Material in any manner. You may translate the Material into another language only if you have licensed translation rights. You may not use the Material for promotional purposes. AIPP reserves all rights not specifically granted herein.

Copyright Clearance Center RightsLink®

Home | Account Info | Help | Live Chat

IEEE Requesting permission to reuse content from an IEEE publication

Title:	Design and performance of thin metal film interconnects for skin-like electronic circuits
Author:	Lacour, S.P.; Jones, J.; Suo, Z.; Wagner, S.
Publication:	IEEE Electron Device Letters
Publisher:	IEEE
Date:	April 2004

Copyright © 2004, IEEE

Logged in as:
Heather Filiatrault
Account #:
3000832513
LOGOUT

Thesis / Dissertation Reuse

The IEEE does not require individuals working on a thesis to obtain a formal reuse license, however, you may print out this statement to be used as a permission grant:

Requirements to be followed when using any portion (e.g., figure, graph, table, or textual material) of an IEEE copyrighted paper in a thesis:

1) In the case of textual material (e.g., using short quotes or referring to the work within these papers) users must give full credit to the original source (author, paper, publication) followed by the IEEE copyright line © 2011 IEEE.
2) In the case of illustrations or tabular material, we require that the copyright line © [Year of original publication] IEEE appear prominently with each reprinted figure and/or table.
3) If a substantial portion of the original paper is to be used, and if you are not the senior author, also obtain the senior author's approval.

Requirements to be followed when using an entire IEEE copyrighted paper in a thesis:

1) The following IEEE copyright/ credit notice should be placed prominently in the references: © [year of original publication] IEEE. Reprinted, with permission, from [author names, paper title, IEEE publication title, and month/year of publication]
2) Only the accepted version of an IEEE copyrighted paper can be used when posting the paper or your thesis on-line.
3) In placing the thesis on the author's university website, please display the following message in a prominent place on the website: In reference to IEEE copyrighted material which is used with permission in this thesis, the IEEE does not endorse any of [university/educational entity's name goes here]'s products or services. Internal or personal use of this material is permitted. If interested in reprinting/republishing IEEE copyrighted material for advertising or promotional purposes or for creating new collective works for resale or redistribution, please go to http://www.ieee.org/publications_standards/publications/rights/rights_link.html to learn how to obtain a License from RightsLink.

If applicable, University Microfilms and/or ProQuest Library, or the Archives of Canada may supply single copies of the dissertation.

BACK | CLOSE WINDOW

Copyright © 2014 Copyright Clearance Center, Inc. All Rights Reserved. Privacy statement.
Comments? We would like to hear from you. E-mail us at customercare@copyright.com

JOHN WILEY AND SONS LICENSE TERMS AND CONDITIONS

Dec 29, 2014

This Agreement between Heather L Filiatrault ("You") and John Wiley and Sons ("John Wiley and Sons") consists of your license details and the terms and conditions provided by John Wiley and Sons and Copyright Clearance Center.

License Number	3538351428495
License date	Dec 29, 2014
Licensed Content Publisher	John Wiley and Sons
Licensed Content Publication	Advanced Materials
Licensed Content Title	Stretchable, Curvilinear Electronics Based on Inorganic Materials
Licensed Content Author	Dae-Hyeong Kim,Jianliang Xiao,Jizhou Song,Yonggang Huang,John A. Rogers
Licensed Content Date	Jan 25, 2010
Pages	17
Type of use	Dissertation/Thesis
Requestor type	University/Academic
Format	Print and electronic
Portion	Figure/table
Number of figures/tables	1
Original Wiley figure/table number(s)	Figure 2d
Will you be translating?	No
Title of your thesis / dissertation	New Materials and Methods for the Fabrication of Large-Area Stretchable Electronics
Expected completion date	Feb 2015
Expected size (number of pages)	250
Requestor Location	[redacted]
Billing Type	
Billing Address	

THE AMERICAN ASSOCIATION FOR THE ADVANCEMENT OF SCIENCE LICENSE TERMS AND CONDITIONS

Dec 29, 2014

This is a License Agreement between Heather L Filiatrault ("You") and The American Association for the Advancement of Science ("The American Association for the Advancement of Science") provided by Copyright Clearance Center ("CCC"). The license consists of your order details, the terms and conditions provided by The American Association for the Advancement of Science, and the payment terms and conditions.

All payments must be made in full to CCC. For payment instructions, please see information listed at the bottom of this form.

License Number	3538360662317
License date	Dec 29, 2014
Licensed content publisher	The American Association for the Advancement of Science
Licensed content publication	Science
Licensed content title	Printed Assemblies of Inorganic Light-Emitting Diodes for Deformable and Semitransparent Displays
Licensed content author	Sang-Il Park, Yujie Xiong, Rak-Hwan Kim, Paulius Elvikis, Matthew Meitl, Dae-Hyeong Kim, Jian Wu, Jongseung Yoon, Chang-Jae Yu, Zhuangjian Liu, Yonggang Huang, Keh-chih Hwang, Placid Ferreira, Xiuling Li, Kent Choquette, John A. Rogers
Licensed content date	Aug 21, 2009
Volume number	325
Issue number	5943
Type of Use	Thesis / Dissertation
Requestor type	Scientist/individual at a research institution
Format	Print and electronic
Portion	Figure
Number of figures/tables	1
Order reference number	None
Title of your thesis / dissertation	New Materials and Methods for the Fabrication of Large-Area Stretchable Electronics
Expected completion date	Feb 2015
Estimated size(pages)	250
Total	0.00 USD
Terms and Conditions	

American Association for the Advancement of Science TERMS AND CONDITIONS

Regarding your request, we are pleased to grant you non-exclusive, non-transferable permission, to republish the AAAS material identified above in your work identified above,

JOHN WILEY AND SONS LICENSE TERMS AND CONDITIONS

Dec 29, 2014

This Agreement between Heather L Filiatrault ("You") and John Wiley and Sons ("John Wiley and Sons") consists of your license details and the terms and conditions provided by John Wiley and Sons and Copyright Clearance Center.

License Number	3538370411264
License date	Dec 29, 2014
Licensed Content Publisher	John Wiley and Sons
Licensed Content Publication	Advanced Materials
Licensed Content Title	High-Conductivity Elastomeric Electronics
Licensed Content Author	D. S. Gray,J. Tien,C. S. Chen
Licensed Content Date	Feb 18, 2004
Pages	5
Type of use	Dissertation/Thesis
Requestor type	University/Academic
Format	Print and electronic
Portion	Figure/table
Number of figures/tables	1
Original Wiley figure/table number(s)	Figure 3
Will you be translating?	No
Title of your thesis / dissertation	New Materials and Methods for the Fabrication of Large-Area Stretchable Electronics
Expected completion date	Feb 2015
Expected size (number of pages)	250
Requestor Location	[redacted]
Billing Type	
Billing Address	

NATURE PUBLISHING GROUP LICENSE TERMS AND CONDITIONS

Dec 29, 2014

This is a License Agreement between Heather L Filiatrault ("You") and Nature Publishing Group ("Nature Publishing Group") provided by Copyright Clearance Center ("CCC"). The license consists of your order details, the terms and conditions provided by Nature Publishing Group, and the payment terms and conditions.

All payments must be made in full to CCC. For payment instructions, please see information listed at the bottom of this form.

License Number	3491140761644
License date	Oct 17, 2014
Order Content Publisher	Nature Publishing Group
Order Content Publication	Nature Communications
Order Content Title	Stretchable batteries with self-similar serpentine interconnects and integrated wireless recharging systems
Order Content Author	Sheng Xu, Yihui Zhang, Jiung Cho, Juhwan Lee, Xian Huang, Lin Jia
Order Content Date	Feb 26, 2013
Volume number	4
Type of Use	reuse in a dissertation / thesis
Requestor type	academic/educational
Format	print and electronic
Portion	figures/tables/illustrations
Number of figures/tables/illustrations	1
High-res required	no
Figures	Figure 1
Author of this NPG article	no
Your reference number	None
Title of your thesis / dissertation	New materials and methods for the fabrication of large-area stretchable electronics
Expected completion date	Nov 2014
Estimated size (number of pages)	300
Total	**0.00 USD**
Terms and Conditions	

Terms and Conditions for Permissions

Nature Publishing Group hereby grants you a non-exclusive license to reproduce this material for this purpose, and for no other use,subject to the conditions below:

1. NPG warrants that it has, to the best of its knowledge, the rights to license reuse of this material. However, you should ensure that the material you are requesting is original to Nature Publishing Group and does not carry the copyright of another entity (as credited in the published version). If the credit line on any part of the material you have requested indicates that it was reprinted or adapted by NPG with permission from another source, then you should also seek permission from that source to reuse the material.

RightsLink®

Home | Account Info | Help | Live Chat

Title: Microstructured Silicone Substrate for Printable and Stretchable Metallic Films

Author: Adam P. Robinson, Ivan Minev, Ingrid M. Graz, et al

Publication: Langmuir

Publisher: American Chemical Society

Date: Apr 1, 2011

Copyright © 2011, American Chemical Society

Logged in as:
Heather Filiatrault
Account #:
3000832513

LOGOUT

PERMISSION/LICENSE IS GRANTED FOR YOUR ORDER AT NO CHARGE

This type of permission/license, instead of the standard Terms & Conditions, is sent to you because no fee is being charged for your order. Please note the following:

- Permission is granted for your request in both print and electronic formats, and translations.
- If figures and/or tables were requested, they may be adapted or used in part.
- Please print this page for your records and send a copy of it to your publisher/graduate school.
- Appropriate credit for the requested material should be given as follows: "Reprinted (adapted) with permission from (COMPLETE REFERENCE CITATION). Copyright (YEAR) American Chemical Society." Insert appropriate information in place of the capitalized words.
- One-time permission is granted only for the use specified in your request. No additional uses are granted (such as derivative works or other editions). For any other uses, please submit a new request.

If credit is given to another source for the material you requested, permission must be obtained from that source.

BACK | CLOSE WINDOW

Copyright © 2014 Copyright Clearance Center, Inc. All Rights Reserved. Privacy statement.
Comments? We would like to hear from you. E-mail us at customercare@copyright.com

JOHN WILEY AND SONS LICENSE TERMS AND CONDITIONS

Dec 29, 2014

This Agreement between Heather L Filiatrault ("You") and John Wiley and Sons ("John Wiley and Sons") consists of your order details and the terms and conditions provided by John Wiley and Sons and Copyright Clearance Center.

License Number	3510360459887
License date	Nov 15, 2014
Licensed Content Publisher	John Wiley and Sons
Licensed Content Publication	Advanced Functional Materials
Licensed Content Title	Mechanical Properties of Conjugated Polymers and Polymer-Fullerene Composites as a Function of Molecular Structure
Licensed Content Author	Suchol Savagatrup,Aditya S. Makaram,Daniel J. Burke,Darren J. Lipomi
Licensed Content Date	Oct 14, 2013
Pages	13
Type of use	Dissertation/Thesis
Requestor type	University/Academic
Format	Print and electronic
Portion	Figure/table
Number of figures/tables	1
Original Wiley figure/table number(s)	Figure 6
Will you be translating?	No
Title of your thesis / dissertation	New materials and methods for the fabrication of large-area stretchable electronics
Expected completion date	Nov 2014
Expected size (number of pages)	300
Billing Type	Invoice
Billing Address	[redacted]
Total	
Total	

Terms and Conditions

TERMS AND CONDITIONS

This copyrighted material is owned by or exclusively licensed to John Wiley & Sons, Inc. or one of its group companies (each a"Wiley Company") or handled on behalf of a society with which a Wiley Company has exclusive publishing rights in relation to a particular work (collectively "WILEY"). By clicking "accept" in connection with completing this licensing

JOHN WILEY AND SONS LICENSE TERMS AND CONDITIONS

Dec 29, 2014

This Agreement between Heather L Filiatrault ("You") and John Wiley and Sons ("John Wiley and Sons") consists of your order details and the terms and conditions provided by John Wiley and Sons and Copyright Clearance Center.

License Number	3510471191322
License date	Nov 15, 2014
Licensed Content Publisher	John Wiley and Sons
Licensed Content Publication	Advanced Materials
Licensed Content Title	Autonomic Restoration of Electrical Conductivity
Licensed Content Author	Benjamin J. Blaiszik,Sharlotte L. B. Kramer,Martha E. Grady,David A. McIlroy,Jeffrey S. Moore,Nancy R. Sottos,Scott R. White
Licensed Content Date	Dec 20, 2011
Pages	4
Type of use	Dissertation/Thesis
Requestor type	University/Academic
Format	Print and electronic
Portion	Figure/table
Number of figures/tables	1
Original Wiley figure/table number(s)	Figure 1
Will you be translating?	No
Title of your thesis / dissertation	New materials and methods for the fabrication of large-area stretchable electronics
Expected completion date	Nov 2014
Expected size (number of pages)	300
Billing Type	Invoice
Billing Address	[redacted]
Total	
Total	

Terms and Conditions

TERMS AND CONDITIONS

This copyrighted material is owned by or exclusively licensed to John Wiley & Sons, Inc. or one of its group companies (each a"Wiley Company") or handled on behalf of a society with which a Wiley Company has exclusive publishing rights in relation to a particular work (collectively "WILEY"). By clicking accept in connection with completing this licensing

RightsLink®

Home | Account Info | Help | Live Chat

Title: A Unifying Model for the Operation of Light-Emitting Electrochemical Cells

Author: Stephan van Reenen, Piotr Matyba, Andrzej Dzwilewski, et al

Publication: Journal of the American Chemical Society

Publisher: American Chemical Society

Date: Oct 1, 2010

Copyright © 2010, American Chemical Society

Logged in as:
Heather Filiatrault
Account #:
3000832513

LOGOUT

PERMISSION/LICENSE IS GRANTED FOR YOUR ORDER AT NO CHARGE

This type of permission/license, instead of the standard Terms & Conditions, is sent to you because no fee is being charged for your order. Please note the following:

- Permission is granted for your request in both print and electronic formats, and translations.
- If figures and/or tables were requested, they may be adapted or used in part.
- Please print this page for your records and send a copy of it to your publisher/graduate school.
- Appropriate credit for the requested material should be given as follows: "Reprinted (adapted) with permission from (COMPLETE REFERENCE CITATION). Copyright (YEAR) American Chemical Society." Insert appropriate information in place of the capitalized words.
- One-time permission is granted only for the use specified in your request. No additional uses are granted (such as derivative works or other editions). For any other uses, please submit a new request.

If credit is given to another source for the material you requested, permission must be obtained from that source.

BACK | CLOSE WINDOW

Copyright © 2014 Copyright Clearance Center, Inc. All Rights Reserved. Privacy statement.
Comments? We would like to hear from you. E-mail us at customercare@copyright.com

Copyright Clearance Center RightsLink®

Home | Account Info | Help | Live Chat

nature publishing group

Title: Elastomeric polymer light-emitting devices and displays
Author: Jiajie Liang, Lu Li, Xiaofan Niu, Zhibin Yu, Qibing Pei
Publication: Nature Photonics
Publisher: Nature Publishing Group
Date: Sep 22, 2013
Copyright © 2013, Rights Managed by Nature Publishing Group

Logged in as:
Heather Filiatrault
Account #:
3000832513
LOGOUT

Order Completed

Thank you very much for your order.

This is a License Agreement between Heather L Filiatrault ("You") and Nature Publishing Group ("Nature Publishing Group"). The license consists of your order details, the terms and conditions provided by Nature Publishing Group, and the payment terms and conditions.

Get the printable license.

License Number	3538411363501
License date	Dec 29, 2014
Licensed content publisher	Nature Publishing Group
Licensed content publication	Nature Photonics
Licensed content title	Elastomeric polymer light-emitting devices and displays
Licensed content author	Jiajie Liang, Lu Li, Xiaofan Niu, Zhibin Yu, Qibing Pei
Licensed content date	Sep 22, 2013
Type of Use	reuse in a dissertation / thesis
Volume number	7
Issue number	10
Requestor type	academic/educational
Format	print and electronic
Portion	figures/tables/illustrations
Number of figures/tables/illustrations	1
High-res required	no
Figures	Figure 2
Author of this NPG article	no
Your reference number	None
Title of your thesis / dissertation	New Materials and Methods for the Fabrication of Large-Area Stretchable Electronics
Expected completion date	Feb 2015
Estimated size (number of pages)	250
Total	0.00 CAD

ORDER MORE... CLOSE WINDOW

Copyright © 2014 Copyright Clearance Center, Inc. All Rights Reserved. Privacy statement.
Comments? We would like to hear from you. E-mail us at customercare@copyright.com

ROYAL SOCIETY OF CHEMISTRY LICENSE TERMS AND CONDITIONS

Dec 29, 2014

This is a License Agreement between Heather L Filiatrault ("You") and Royal Society of Chemistry ("Royal Society of Chemistry") provided by Copyright Clearance Center ("CCC"). The license consists of your order details, the terms and conditions provided by Royal Society of Chemistry, and the payment terms and conditions.

All payments must be made in full to CCC. For payment instructions, please see information listed at the bottom of this form.

License Number	3537221165301
License date	Dec 27, 2014
Order Content Publisher	Royal Society of Chemistry
Order Content Publication	Journal of Materials Chemistry
Order Content Title	In situ identification of a luminescence quencher in an organic light-emitting device
Order Content Author	Jason D. Slinker,Ji-Seon Kim,Samuel Flores-Torres,Jared H. Delcamp,Héctor D. Abruña,Richard H. Friend,George G. Malliaras
Order Content Date	Nov 27, 2006
Volume number	17
Issue number	1
Type of Use	Thesis/Dissertation
Requestor type	academic/educational
Portion	figures/tables/images
Number of figures/tables/images	1
Format	print and electronic
Distribution quantity	50
Will you be translating?	no
Order reference number	None
Title of the thesis/dissertation	New Materials and Methods for the Fabrication of Large-Area Stretchable Electronics
Expected completion date	Feb 2015
Estimated size	200
Total	**0.00 USD**

Terms and Conditions

This License Agreement is between {Requestor Name} ("You") and The Royal Society of Chemistry ("RSC") provided by the Copyright Clearance Center ("CCC"). The license consists of your order details, the terms and conditions provided by the Royal Society of Chemistry, and the payment terms and conditions.

RSC / TERMS AND CONDITIONS

INTRODUCTION

The publisher for this copyrighted material is The Royal Society of Chemistry. By clicking "accept" in connection with completing this licensing transaction, you agree that the following terms and conditions apply to this transaction (along with the Billing and Payment terms and conditions established by CCC, at the time that you opened your RightsLink account and that are available at any time at .

LICENSE GRANTED

Vita Auctoris

Name: Heather Lynn Filiatrault

Place of Birth: Windsor, Ontario, Canada

Year of Birth: 1987

Education:

Ph.D. Chemistry

Department of Chemistry and Biochemistry, University of Windsor,
Windsor, Ontario, Canada. 2015.

B.Sc. Honours Chemistry with Thesis

Department of Chemistry and Biochemistry, University of Windsor,
Windsor, Ontario, Canada. 2009.

Honours and Awards:

2014 NanoOntario Poster Prize
NSERC CGS-D (2011-2014)
2013 3-Minute Thesis: Finalist & People's Choice Award Winner, University of Windsor
2012 NanoOntario Poster Prize
NSERC CGS-M (2010-2011)
Ontario Graduate Scholarship (2010-2011) (Declined)
Ontario Graduate Scholarship in Science and Technology (2009-2010)
University of Windsor Outstanding Scholars Award (2005-2007, 2008-2009)
University of Windsor Entrance Scholarship (2005)

Publications:

Heather L. Filiatrault, Gyllian C. Porteous, R. S. Carmichael, G. J. E. Davidson, T. B. Carmichael (2012) "Stretchable Light-Emitting Electrochemical Cells Using an Elastomeric Emissive Material" Advanced Materials. 24: 2673-2678.

Michael S. Miller, **Heather L. Filiatrault**, Gregory J. E. Davidson, Minmin Luo, and Tricia Breen Carmichael. (2010) "Selectively Metallized Polymeric Substrates by Microcontact Printing an Aluminum (III) Porphyrin Complex" Journal of the American Chemical Society. 132: 765- 772.

Conference and Poster Presentations (* denotes presenting author):

H.L. Filiatrault*, R.A. Boutette, R.S. Carmichael, T.B. Carmichael, (2014) Low-Cost, Highly Stretchable Gold Films on Elastomeric Substrates Coated with a Poly(vinyl acetate) Microstructured Relief, 5th NanoOntario Conference, Windsor, On, Canada, November 6-7 2014, Provincial Conference, Poster Presentation.

H.L. Filiatrault*, D.M.J. Mansour, R.A. Boutette, T.B. Carmichael, (2014) Highly Stretchable Gold Films on Elastomeric Substrates Coated with Polymer Interlayers, 97th Canadian Chemistry Conference, Vancouver, BC, Canada, June 1-5, 2014, National Conference, Oral Presentation.

H.L. Filiatrault*, G.C. Porteous, R.S. Carmichael, G.J.E. Davidson, T.B. Carmichael, (2012) Stretchable Light-Emitting Electrochemical Cells (LEECs), NanoOntario Conference, Waterloo, On, October 11-12, 2012, Provincial Conference, Poster Presentation.

H.L. Filiatrault*, G.C. Porteous, T.B. Carmichael, (2011) Stretchable Light-Emitting Electrochemical Cells (LEECs), MRS Fall Meeting, Boston, MA, USA, November 28-December 2, 2011, International Conference, Oral Presentation.

H.L. Filiatrault*, G.C. Porteous, P.J. Prochazka, T.B. Carmichael, (2011) Stretchable Organic Light-Emitting Devices (OLEDs) Based on a Tris(bipyridyl) Ruthenium Emissive Layer Blended in an Elastomeric Matrix, 94th Canadian Chemistry Conference, Montreal, Qc, June 5-9, 2011, National Conference, Oral Presentation.

T.B. Carmichael*, **H.L. Filiatrault**, G.C. Porteous, (2010) Stretchable Light-emitting Devices Using a Tris(2,2'-bipyridyl) Ruthenium Complex Dispersed in an Elastomeric Matrix, MRS Fall Meeting, Boston, MA, USA, November 29-December 3, 2010, International Conference, Poster Presentation.

H.L. Filiatrault*, G.C. Porteous, T.B. Carmichael, (2010) Stretchable Organic Light-Emitting Devices (OLEDs) Based on a Tris(bipyridyl) Ruthenium Emissive Layer Blended in an Elastomeric Matrix, 43rd Inorganic Discussion Weekend, Windsor, On, November 5-7, 2010, Provincial Conference, Poster Presentation.

H.L. Filiatrault*, T.B. Carmichael, (2010) Light-Emitting Devices Based on a Tris(bispyridyl) Ruthenium Emissive-Layer Blended in an Elastomeric Matrix, 93rd

Canadian Chemistry Conference and Exhibition, Toronto, On, May 29-June 2, 2010, National Conference, Poster Presentation.

H.L. Filiatrault, M.S. Miller and T.B. Carmichael*, (2009) Low-cost Fabrication of Flexible Devices Using Selective Electroless Metallization of Elastomeric and Polymeric Substrates, 92nd Canadian Chemistry Conference and Exhibition, Hamilton, On, May 30-June 3, 2009, National Conference, Oral Presentation.